

Cátia Vanessa de Matos Augusto

# MATHEMATICAL AND EXPERIMENTAL STUDY OF LOW-PRESSURE-VAPORIZATION PHENOMENA

PhD Thesis in the scientific area of Mechanical Engineering, specialty of Thermodynamics, supervised by Professor José Joaquim da Costa and Professor José Manuel Baranda Moreira da Silva Ribeiro, submitted to the University of Coimbra

Coimbra, 2013



UNIVERSIDADE DE COIMBRA



**Mathematical and experimental study of low-pressure-vaporization phenomena**

Copyright ©, Cátia Augusto, 2013

Printed by University of Coimbra, Coimbra

Published by Department of Mechanical Engineering of University of Coimbra

Coimbra, Portugal

ISBN978-972-8954-35-2





**Department of Mechanical Engineering  
Faculty of science and technology  
University of Coimbra**

PhD Thesis in Mechanical Engineering

Tese de doutoramento em Engenharia Mecânica apresentada à  
Universidade de Coimbra para obtenção do grau de Doutor

---

# **Mathematical and experimental study of low-pressure-vaporization phenomena**

---

Cátia Vanessa de Matos Augusto

***Supervisors/Orientadores:***

Professor Doutor José Joaquim da Costa

Professor Doutor José Manuel Baranda Moreira da Silva Ribeiro

***Financial Support:***

Ref. SFRH/BD/64486/2009

**FCT** Fundação para a Ciência e a Tecnologia  
MINISTÉRIO DA EDUCAÇÃO E CIÊNCIA

**PO PH**  
QUALIFICAR E CRESCER

**QR**  
QUADRO DE REFERÊNCIA  
ESTRATÉGICO  
NACIONAL  
PORTUGAL 2007-2013

  
UNIÃO EUROPEIA  
Fundo Social Europeu



**Coimbra, 2013**



# **Agradecimentos**

*Aos meus orientadores, Professor José Joaquim Costa e Professor José Manuel Baranda Ribeiro, agradeço todo o apoio prestado, tanto a nível científico como pessoal, durante o desenvolvimento deste trabalho. Não menos importante, o Professor Adélio Gaspar, orientador não oficial, mas que fez parte da equipa, de todos os momentos e passos percorridos. Agradeço-lhes a confiança depositada, a dedicação e o gosto demonstrado pelo meu trabalho, que, em alturas menos boas, me fizeram não perder o entusiasmo e seguir em frente.*

*À Reitoria da Universidade de Coimbra, na pessoa do Exmo. Senhor Vice-Reitor, Professor Doutor Henrique Madeira, pelo apoio e auxílio na direcção a seguir, numa altura crítica do meu percurso.*

*À Fundação para a Ciência e Tecnologia (FCT) no âmbito do QREN - POPH - Tipologia 4.1 - Formação Avançada, participado pelo Fundo Social Europeu e por fundos nacionais do Ministério da Educação e Ciência, pela bolsa de doutoramento SFRH/BD/64486/2009.*

*Ao Departamento de Engenharia Mecânica e à ADAI, pelas instalações e serviços concedidos para a realização deste trabalho.*

*Aos meus colegas e amigos Carla, Pedro, Sara, Professor Almerindo e Professor Gameiro, companheiros de muitas horas e de muitas partilhas. Em particular, ao meu amigo Professor Gameiro, por tudo, um muito obrigada.*

*A todos os meus amigos, que mais longe ou mais de perto, contribuíram com apoio moral, muitas vezes a chave para abrir e atravessar várias portas.*

*Aos meus mais recentes colegas de laboratório, pela companhia, pelas partilhas e desabafos.*

*À minha mãe e ao Rodrigo, a minha eterna gratidão por tudo o que fizeram e fazem por mim.*



*"Tudo aquilo que não me mata, torna-me mais forte.  
Se não me matou, mas apenas me derrubou, levanto-me mais forte"*

*Friedrich Wilhelm Nietzsche*



---

# Resumo

---

Em muitas áreas industriais, a melhoria/controlo da transferência de calor e de massa das etapas processuais é a solução para o aumento da rapidez e da eficiência dos seus processos. Nesse âmbito, o desenvolvimento de alternativas para a melhoria desses fenómenos revela-se de grande importância e é um desafio, tanto ao nível académico como industrial. Pretendendo ser um contributo neste contexto, o estudo detalhado do processo de vaporização a baixa pressão (VBP) de água livre e em meios porosos constitui a motivação chave da presente tese.

Nesse contexto, desenvolve-se, numa primeira fase do trabalho, um modelo matemático da VBP de água livre. O modelo visa uma primeira avaliação da evolução do processo e do efeito de algumas variáveis relevantes (volume da câmara, capacidade do sistema de despressurização e massa de água inicial). O modelo baseia-se em princípios físicos simples, porém permite verificar que a primeira fase do processo tem um peso significativo na duração total, contrariamente ao referido por outros autores. Foi construída uma instalação experimental para o estudo do processo de VBP, criando também a possibilidade de validar e melhorar o modelo matemático. Primeiramente, realiza-se um estudo experimental para a caracterização detalhada do processo de VBP de água livre, incluindo uma análise integrada das influências da temperatura e do volume inicial de água. São identificadas e caracterizadas as duas fases do processo, assim como os respectivos regimes. Verifica-se uma importante influência das condições iniciais na evolução do processo, bem como na massa total vaporizada. Para além do aperfeiçoamento do modelo matemático em termos físicos, é feita uma calibração com base nos resultados experimentais, onde são definidos e calibrados os seguintes parâmetros: tempos para o *flash point* e de transição de regime; coeficiente de vaporização; pressão de vapor à superfície livre e pressão da camada livre. Obtém-se, assim, um modelo mais realista, usado para a determinação de parâmetros difíceis de obter experimentalmente.

O processo de VBP é também estudado em diferentes tipos de meios porosos para avaliar os benefícios do seu uso na melhoria da taxa de vaporização. Experimentalmente, para além dos quatro meios porosos com propriedades diferentes, é também avaliado o efeito de diferentes temperaturas iniciais. Determinam-se as evoluções da massa total vaporizada, a taxa específica de vaporização e a energia removida. Conclui-se que o processo de VBP é fortemente dependente do volume de

água inicialmente contida nos meios porosos. Verifica-se ainda um aumento da taxa de vaporização e da capacidade de transferência de calor, o que justifica o uso dos meios porosos numa vasta gama de aplicações práticas.

É desenvolvido, calibrado e validado um modelo matemático do processo de VBP em meios porosos. O modelo permite colmatar algumas lacunas de modelos desenvolvidos nesta área por outros autores, e serve de ferramenta para futuros estudos, uma vez que, tal como para o caso de VBP de água livre, permite determinar parâmetros difíceis de obter experimentalmente.

A capacidade do processo de VBP, de água livre e em meios porosos, para melhorar a transferência de calor através de superfícies revestidas é também investigada. Verifica-se a aptidão do processo para esse efeito e, conseqüentemente, para acelerar o decréscimo da temperatura, particularmente quando se usam os meios porosos como revestimento.

O presente trabalho salienta a importância do processo em estudo para possíveis aplicações práticas, ao melhorar o desempenho na transferência de calor e de massa, podendo, assim, constituir a base para o desenvolvimento de novos produtos ou equipamentos.

O trabalho de investigação realizado no âmbito desta dissertação esteve condicionado por restrições decorrentes de obrigações legais, relacionadas com a protecção de propriedade industrial, a que a autora e a Universidade de Coimbra estiveram sujeitas. Essas restrições limitaram não só a liberdade de investigação e desenvolvimento, mas também, em determinadas situações, a própria justificação de algumas das opções tomadas.

*Palavras-chave:* Vaporização a baixa pressão; estudo experimental; água livre; modelo matemático; meios porosos; transferência de calor.

---

# Abstract

---

In many industrial areas, the improvement and control of the heat and mass transfer of the procedural stages are the solution to increase the speed and the efficiency of processes. In this domain, the development of alternatives to improve those phenomena is very important and is a challenge, both at academic and industrial levels. As a contribution for that, the detailed study of the low-pressure-vaporization (LPV) process in free water and in porous media constitutes the main goal of the present thesis.

In this context, a mathematical model of the LPV process of free water is developed, in the first stage of the work. The model aims at a first evaluation of the process evolution and the effect of some relevant variables (chamber volume, depressurization system capacity and initial water mass). The model is based on simple physical principles; however it reveals that the first stage of the process has a significant weight in the total duration, contrarily to reports by other authors. An experimental set-up was built to study the LPV process, enabling also the possibility to validate and improve the mathematical model. First, an experimental study is presented for a detailed characterization of the low-pressure-vaporization process of free water, including an integrated analysis of the influence of temperature and the initial volume of water. The two stages of the process are identified and characterized, as well as the respective regimes. The significant influence of the initial conditions on the process evolution is verified, as well as in the total mass vaporized. In addition to the physical improvement of the mathematical model, a calibration is performed based on experimental results, where the following parameters are defined and calibrated: time to the flash point and time to the regime transition; vaporization coefficient; free surface and free layer vapour pressures. A more realistic model is thus achieved, allowing the determination of parameters that are difficult to obtain experimentally.

The LPV process is also experimentally studied in different types of porous media to evaluate the benefits of its use in improving the vaporization rate. Experimentally, in addition to the four porous media with different properties, it is also evaluated the effect of different initial temperatures. The evolutions of the total mass vaporized, the specific rate of vaporization and the energy removed by this phenomenon are determined. It is verified that the LPV process is strongly dependent on the amount of water initially absorbed in the porous media. It is also observed an increase in the

vaporization rate and in the capacity of heat transfer, which justifies the use of porous media in a wide range of practical applications.

A mathematical model of the LPV process in porous media is also developed, calibrated and validated. The model solves some shortcomings of previous models developed by others authors in this field, and it is a tool for future studies, allowing to determine parameters that are difficult to obtain experimentally.

The capacity of the LPV process, both in free water and in porous media, to enhance the heat transfer rate across coated surfaces is investigated. It is verified the process ability for this proposal and consequently for the intensification of the temperature decrease, particularly when porous media are used as coatings.

The present work highlights the importance of the LPV process for possible practical applications, improving the performancec in heat and mass transfer, and thus empowering the development of new products or equipments.

The research conducted for this dissertation was subjected to constraints arising from legal obligations related to the protection of industrial property, to which the author and the University of Coimbra were subjected. These restrictions limited both the freedom of research and development and, in certain situations, the justification of some of the choices adopted.

**Keywords:** Low-pressure-vaporization; experimental study; free water; mathematical model; porous media; heat transfer.

---

# List of contents

---

	<b>Pag.</b>
Resumo	ix
Abstract	xi
List of figures	xvii
List of tables	xxiii
Nomenclature	xxv

## ***Part A - Scope and outline***

---

<b>II. Introduction</b>	<b>II.1</b>
-------------------------	-------------

---

II.1.Vaporization and low-pressure-vaporization .....	II.1
II.2.Vaporization in porous media .....	II.3
II.3.Motivation and Scope of the Thesis .....	II.4
II.4.Thesis Structure .....	II.6

---

<b>II. State of the Art</b>	<b>II.9</b>
-----------------------------	-------------

---

II.1.Synopsis of Literature of the vaporization .....	II.9
II.1.1 Vaporization phenomenon .....	II.9
II.1.2 Vaporization in porous media .....	II.10
II.1.3 Applicability's of the vaporization .....	II.11
II.2.Synopsis of Literature of the low-pressure-vaporization .....	II.12
II.2.1 Low-pressure-vaporization in products processing.....	II.13
II.2.2 Low-pressure-vaporization in drying.....	II.16
II.2.3 Low-pressure-vaporization in refrigeration .....	II.19
II.3.Conclusions .....	II.23

## **Part B - Low-pressure-vaporization of free water**

### **III. A mathematical model describing the two stages of low-pressure-vaporization of free water** **III.27**

---

III.1.Introduction.....	III.28
III.2.Modelling of the low-pressure-vaporization phenomena .....	III.29
III.2.1 Physical model.....	III.29
III.2.2 Mathematical model.....	III.31
III.2.3 Numerical solution procedure .....	III.36
III.2.4 Thickness of the diffusion layer.....	III.38
III.3.Results and discussion .....	III.39
III.4.Conclusions.....	III.43

### **IV. Detailed characterization of the low-pressure-vaporization of free water – features of the boiling regimes** **IV.45**

---

IV.1.Introduction .....	IV.46
IV.2.Experimental modelling .....	IV.48
IV.2.1 Features of the low-pressure-vaporization processes.....	IV.48
IV.2.2 Experimental set-up and methodology .....	IV.49
IV.3.Results and discussion.....	IV.51
IV.3.1 Influence of the initial conditions on the LPV evolution .....	IV.51
IV.3.2 Mass of the water vaporized in LPV .....	IV.57
IV.4.Conclusion .....	IV.60

### **V. Physical and experimental calibration of a mathematical model of the low-pressure-vaporization in free water** **V.63**

---

V.1.Introduction .....	V.64
V.2.Mathematical model of the low-pressure-vaporization in free water .....	V.66
V.3.Experimental calibration methodology.....	V.70
V.3.1 Experimental details .....	V.70

V.3.2 Calibration of the time to the flash point and of the time of first-to-second boiling regime .....	V.72
V.3.3 Determination of the vaporization coefficient and of vaporization layer volume .....	V.74
V.4.Validation and insights of the calibrated model .....	V.79
V.4.1 Model algorithm .....	V.79
V.4.2 Model insights .....	V.86
V.5.Conclusions.....	V.87

## ***Part C - Low-pressure-vaporization in porous media***

### **VI. Experimental study of the low-pressure-vaporization of water in different porous media VI.91**

---

VI.1.Introduction .....	VI.92
VI.2.Experimental details .....	VI.95
VI.2.1 Low-pressure-vaporization in porous media – physical model .....	VI.95
VI.2.2 Experimental set-up and methodology.....	VI.96
VI.2.3 Characterization of the porous media .....	VI.98
VI.3.Results and discussion.....	VI.100
VI.3.1 Influence of the initial conditions on the LPV in different PM.....	VI.100
VI.3.2 Mass of water vaporized on the LPV in porous media .....	VI.106
VI.3.3 Comparison of the LPV evolutions in porous media and of free water .....	VI.110
VI.4.Conclusions.....	VI.113

### **VII. Development, calibration and validation of a mathematical model for the low-pressure-vaporization of the water in porous media VII.115**

---

VII.1.Introduction .....	VII.117
VII.2.Experimental calibration methodology .....	VII.120
VII.3.Development and calibration of the mathematical model.....	VII.121
VII.4.Results and discussion.....	VII.133

VII.4.1 Features of development and calibration of the mathematical model	VII.133
VII.4.2 Validation of the mathematical model	VII.138
VII.5.Conclusions	VII.141

***Part D - Low-pressure-vaporization to enhance the heat transfer across surfaces***

**VIII. Experimental study of ability of the low-pressure-vaporization in porous media to enhance the heat transfer across surfaces VIII.145**

---

VIII.1.Introduction	VIII.147
VIII.2.Low-pressure-vaporization of a coated container – physical model	VIII.149
VIII.3.Experimental set-up and methodology	VIII.151
VIII.4.Results and discussion	VIII.152
VIII.4.1 Low-pressure-vaporization of a coated container with free water	VIII.153
VIII.4.2 Low-pressure-vaporization of a coated container with porous media	VIII.157
VIII.5.Conclusions	VIII.162

***Part D – Conclusions and forthcoming work***

**IX. Conclusions and forthcoming work IX.167**

---

IX.1.General overview and conclusions	IX.167
IX.2.Suggestions for forthcoming work	IX.170

**X. References X.171**

---

---

# List of Figures

---

	Pag.
<hr/>	
<b>III. A mathematical model describing the two stages of low-pressure-vaporization of free water</b>	
<hr/>	
<b>Figure III.1.</b> Schematic diagram of a low-pressure-vaporization system (adapted from (Saury et al., 2002)).	<b>III.30</b>
<b>Figure III.2.</b> Schematic diagram of the physical model.	<b>III.31</b>
<b>Figure III.3.</b> Flow chart of the simulation program.	<b>III.37</b>
<b>Figure III.4.</b> Tests for $\Delta z$ independence of the model, monitoring the influence on the threshold pressure level $P_{v,t}$ predicted in the first stage. The dashed line represents the $P_{v,t}$ level for $\Delta z = 0.025$ m.	<b>III.38</b>
<b>Figure III.5.</b> Evolution of the LPV parameters: (a) water temperature; (b) vapour partial and saturation pressures; (c) vapour generation rate; (d) total pressure in the vaporization chamber.	<b>III.40</b>
<b>Figure III.6.</b> Evolutions of: (a) the water temperature and (b) the vapour partial pressure for three different condenser temperatures.	<b>III.41</b>
<b>Figure III.7.</b> Evolutions of: (a) the water temperature and (b) the vapour partial pressure for three different masses of water.	<b>III.41</b>
<b>Figure III.8.</b> Evolution of: (a) the water temperature and of (b) the vapour partial pressure for two volume flow rates of the pump.	<b>III.42</b>
<b>Figure III.9.</b> Evolution of the water temperature: comparison between present simulation and the experimental results of (Cheng and Lin, 2007).	<b>III.43</b>
<hr/>	
<b>IV. Detailed characterization of the low-pressure-vaporization of free water - features of the boiling regimes</b>	
<hr/>	
<b>Figure IV.1.</b> Schematic diagram of the experimental set-up of the LPV process. (DS - depressurization system; DAS - data acquisition system; VC – vaporization chamber; C – container; W – water; DPS - Data processor and storage.	<b>IV.50</b>
<b>Figure IV.2.</b> Water temperature evolution for several initial water volumes and for (a) $T_{w,0}=22$ °C and (b) $T_{w,0}=34$ °C.	<b>IV.52</b>
<b>Figure IV.3.</b> Water temperature evolution for several initial water temperatures and two rather different initial volumes ( $V_{w,0} = 800$ and 10 ml).	<b>IV.52</b>
<b>Figure IV.4.</b> Total pressure evolution for several initial water volume for $T_{w,0} = 22$ °C.	<b>IV.54</b>
<b>Figure IV.5.</b> Total pressure evolution for several initial water temperature for (a) $V_{w,0} = 10$ ml and (b) $V_{w,0} = 800$ ml.	<b>IV.54</b>

**Figure IV.6.** Evolutions of the total pressure, saturation pressure and vapour pressure for (a)  $V_{w,0} = 10$  ml,  $T_{w,0} = 22$  °C; (b)  $V_{w,0} = 10$  ml,  $T_{w,0} = 34$  °C; (c)  $V_{w,0} = 200$  ml,  $T_{w,0} = 22$  °C; (d)  $V_{w,0} = 200$  ml,  $T_{w,0} = 34$  °C; (e)  $V_{w,0} = 800$  ml,  $T_{w,0} = 22$  °C; (f)  $V_{w,0} = 800$  ml,  $T_{w,0} = 34$  °C (The vertical line ( - - - - - ) indicates the FP point).

**IV.57**

**Figure IV.7.** Evolution of the mass of water vaporized for several initial water temperatures and for (a)  $V_{w,0} = 10$  ml; (b)  $V_{w,0} = 800$  ml.

**IV.58**

**Figure IV.8.** Plots and surface fittings of the variations with  $V_{w,0}$  and  $T_{w,0}$  of the total mass of water vaporized, for the sets of experiments in the lower and higher volume ranges, respectively: (a) container C1; (b) container C2.

**IV.59**

**Figure IV.9.** Water temperature evolution within the containers C1 and C2 for  $V_{w,0} = 100$  ml and two initial water temperatures ( $T_{w,0} = 22$  and  $34$  °C)

**IV.60**

**Figure IV.10.** Total pressure evolution for the two containers C1 and C2,  $V_{w,0} = 100$  ml and  $T_{w,0} = 34$  °C)

**IV.60**

## **V. Physical and experimental calibration of a mathematical model of the low-pressure-vaporization in free water**

---

**Figure V.1.** Schematic representation of the physical model during second stage of the LPV in free water.

**V.68**

**Figure V.2.** Schematic diagram of the experimental set-up of the LPV process. (DS - depressurization system; DAS - data acquisition system; VC – vaporization chamber; C – container; W – water; DPS - Data processor and storage.

**V.72**

**Figure V.3.** Illustration of the (a) determination of the time to flash point and (b) determination of the time of changing the first to second regime of the LPV.

**V.73**

**Figure V.4.** Evolution of the (a) time to flash point and (b) time of changing the first to second regime of the LPV and fittings respective for C1.

**V.73**

**Figure V.5.** Evolution of the vaporative coefficient for different initial water temperatures and volumes.

**V.75**

**Figure V.6.** Comparison between experimental and calibration model values for (a)  $V_{w,0} = 10$  ml,  $T_{w,0} = 21$  °C; (b)  $V_{w,0} = 50$  ml,  $T_{w,0} = 21$  °C; (c)  $V_{w,0} = 100$  ml,  $T_{w,0} = 22$  °C; (d)  $V_{w,0} = 800$  ml,  $T_{w,0} = 22$  °C.

**V.77**

**Figure V.7.** Evolution of the vaporization layer and free layer volumes for  $T_{w,0} = 21$  °C and for (a)  $V_{w,0} = 10$  ml and (b)  $V_{w,0} = 800$  ml

**V.79**

**Figure V.8.** Flow chart of the simulation program.

**V.81**

**Figure V.9.** Comparison between experimental and model results for different initial conditions of the volume range C1.

**V.83**

**Figure V.10.** Comparison between experimental and model results for different initial conditions of the volume range C2. **V.85**

**Figure V.11.** Evolution of the vapour pressure at free surface and free layer, and superheat degree for several initial conditions. **V.87**

## **VI. Experimental study of the low-pressure-vaporization of water in different porous media**

---

**Figure VI.1.** Schematic diagram of the vaporization phenomena in PM. **VI.96**

**Figure VI.2.** (a) Schematic diagram of the experimental set-up. (DS - depressurization system; DAS - data acquisition system; VC – vaporization chamber; C – container; W – water; DPS - Data processor and storage. (b) Detailed view of the PM1 with the thermocouple TC1 located inside. **VI.98**

**Figure VI.3.** Photographs of the porous media, taken with a microscope Nikon Optiphot HFX-DX with a Nikon Fx-35 DX camera (objective M Plan 2.5/0.075): (a) PM1; (b) PM2; (c) PM3 and (d) PM4. **VI.99**

**Figure VI.4.** Water temperature evolutions in different porous media and for different initial temperatures. **VI.101**

**Figure VI.5.** Water temperature evolutions for different initial water temperatures and in different porous media: (a) PM1; (b) PM2; (c) PM3 and (d) PM4. **VI.102**

**Figure VI.6.** Total pressure evolutions in the vaporization chamber for different initial water temperatures and two different porous materials: (a) PM1 and (b) PM2. **VI.104**

**Figure VI.7.** Comparison of the time evolutions of the total, the saturation and the vapour partial pressures during the LPV process, for the minimum and the maximum initial water temperatures, in each of the porous media tested. The dashed line indicates the flash point. **VI.106**

**Figure VI.8.** Evolution of the cumulative mass of vaporized water in the porous media PM1 and PM2, at two initial water temperatures,  $T_{w,0} = 18$  and  $35$  °C. **VI.108**

**Figure VI.9.** Evolutions of the specific rate of water vaporization in the porous media PM1 and PM2 for  $T_{w,0} = 35$  °C. **VI.108**

**Figure VI.10.** The schematically representation of the physical model of the vaporization in porous media. **VI.108**

**Figure VI.11.** Variation trend of the final mass of water vaporized with  $V_{w,0}$  and  $T_{w,0}$ . **VI.109**

**Figure VI.12.** (a) Specific rate of energy removal and (b) specific energy removed by vaporization for PM1 and PM2, starting with  $T_{w,0} = 35$  °C. **VI.110**

**Figure VI.13.** Time evolutions of (a) the water temperature and of (b) the total pressure for PM1 and free water. **VI.112**

**Figure VI.14.** Evolutions of (a) the water temperature and of (b) the total pressure for PM2 and free water. **VI.112**

**Figure VI.15.** Comparisons of the water vaporization rates: (a) in PM1 and in free water and (b) in PM2 and in free water. **VI.112**

## **VII. Development, calibration and validation of a mathematical model for the low-pressure-vaporization of the water in porous media**

---

**Figure VII.1.** Schematic diagram of the physical model of (a) the first stage, (b) the second stage and (c) detail of the second stage of the LPV in porous media. **VII.124**

**Figure VII.2.** Flow chart of the simulation program. **VII.132**

**Figure VII.3.** Time evolutions of the vaporization coefficient for the different porous media and two distinct initial temperatures. **VII.133**

**Figure VII.4.** Comparison between experimental and simulated values of the vaporization coefficient in different porous media and for  $T_{w,0}=18\text{ }^{\circ}\text{C}$ . **VII.135**

**Figure VII.5.** Evolution of the vaporization coefficients for two porous media and  $T_{w,0} = 27\text{ }^{\circ}\text{C}$ . **VII.135**

**Figure VII.6.** Evolutions of (a) the vapour pressure at the interface and (b) the free surface vapour pressure for four porous media and  $T_{w,0}=27^{\circ}\text{C}$ . **VII.136**

**Figure VII.7.** Evolutions of (a) the surface tension pressure and (b) the superheating degree for different porous media and  $T_{w,0} = 27\text{ }^{\circ}\text{C}$ . **VII.137**

**Figure VII.8.** Evolutions of the specific superheating degree for different porous media and  $T_{w,0} = 27\text{ }^{\circ}\text{C}$ . **VII.138**

**Figure VII.9.** Comparison between experimental and predicted results of the water temperature evolution for different initial conditions. **VII.139**

**Figure VII.10.** Comparison between experimental and modelled results for different PM and initial conditions. **VII.140**

## **VIII. Experimental study of ability of the low-pressure-vaporization in porous media to enhance the heat transfer across surfaces**

---

**Figure VIII.1.** Schematic diagram of the LPV phenomena in coated container. **VIII.150**

**Figure VIII.2.** Schematic diagram of the experimental set-up of the LPV process. (DS - depressurization system; DAS - data acquisition system; VC – vaporization chamber; DPS – Data processor and storage). **VIII.152**

- Figure VIII.3.** Evolution of the water temperature in coating, of the temperature in center and wall of the container, for two different free water volumes. **VIII.154**
- Figure VIII.4.** Evolution of the water temperature in coating, of the temperature in center and wall of the surface, for three different initial temperatures in  $V_{w,02}$ . **VIII.154**
- Figure VIII.5.** Water temperature evolution in coating free water (FW as coating) and bulk free water (FW) for (a)  $V_{w,01}=200$  ml and  $T_0 = 27$  °C; (b)  $V_{w,01}=200$  ml and  $T_0 = 34$  °C; (c)  $V_{w,02}=100$  ml and  $T_0 = 27$  °C; (d)  $V_{w,02}=100$  ml and  $T_0 = 34$  °C. **VIII.156**
- Figure VIII.6.** Total pressure evolution in vaporization chamber using coating free water (FW as coating) or bulk free water (FW) for  $V_{w,01}$  (a)  $T_0 = 27$  °C and (b)  $T_0 = 34$  °C. **VIII.156**
- Figure VIII.7.** Temperature evolution of the (a) water in coating (b) container wall and (c) container center using four different types of the PM as coating and  $T_0=34$  °C. **VIII.158**
- Figure VIII.8.** Evolution of the water temperature in coating, of the temperature in center and wall of the container for PM2 and PM4 and for three different initial temperatures. **VIII.159**
- Figure VIII.9.** Water temperature evolution for different types porous media used as coating (PM as coating) and as bulk porous media (PM) for  $T_0=27$  °C and  $T_0=34$  °C. **VIII.161**
- Figure VIII.10.** Total pressure evolution in VC for  $T_0=27$  °C and for (a) PM1; (b) PM2; (c) PM3 and (d) PM4 used as coating (PM as coating) and as bulk porous media (PM). **VIII.162**



---

# List of Tables

---

	<b>Pag.</b>
<b>Table II.1.</b> Research works developed by National University of Ireland.	<b>II.20</b>
<b>Table III.1.</b> Specific operating conditions of the low-pressure-vaporization process.	<b>III.35</b>
<b>Table IV.1.</b> Initial conditions used in the experimental tests.	<b>IV.51</b>
<b>Table V.1.</b> Initial conditions used in the experimental calibrated tests.	<b>V.71</b>
<b>Table V.2.</b> Parameters values of the Eq.(11)	<b>V.74</b>
<b>Table V.3.</b> Values of the coefficients of the Eq.(V.12), Eq.(V.13) and Eq.(V.14).	<b>V.76</b>
<b>Table V.4.</b> Coefficient values of the Eq.(V.20).	<b>V.78</b>
<b>Table VI.1.</b> Composition, thickness and water absorption capacity of the porous media.	<b>VI.99</b>
<b>Table VII.1.</b> Initial conditions of the experimental calibration tests.	<b>VII.120</b>
<b>Table VII.2.</b> Values of the coefficients for Eq.(VII.20), Eq.(VII.21), Eq.(VII.22) and Eq.(VII.23).	<b>VII.130</b>
<b>Table VIII.1.</b> Initial conditions used in the experimental tests.	<b>VII.152</b>



---

# Nomenclature

---

$A$  – surface area ( $\text{m}^2$ )

$A_i$  – inner surface area ( $\text{m}^2$ )

$A_1$  – surface area of container C1 ( $\text{m}^2$ )

$A_2$  – surface area of container C2 ( $\text{m}^2$ )

$c_p$  – specific heat capacity ( $\text{J kg}^{-1} \text{K}^{-1}$ )

$c_{p,PM}$  – mass-averaged initial specific heat of porous medium saturated with water ( $\text{J kg}^{-1} \text{K}^{-1}$ )

$C_{PM,0}$  – initial heat capacity of the porous medium ( $\text{J K}^{-1}$ )

$C_{PM,0}^*$  – normalized initial heat capacity of the porous medium (-)

$D$  – diffusion coefficient ( $\text{m}^2 \text{s}^{-1}$ )

$\partial T/\partial r$  – temperatures gradient in  $r$  direction ( $^{\circ}\text{C}/\text{m}$ )

$E_0$  – enthalpy of the initial mass of liquid water (kJ)

$E_v$  – energy removed by vaporization (J)

$E_v^*$  – specific energy removed by vaporization ( $= E_v/m_{w,0}$ ) ( $\text{J kg}^{-1}$ )

$\dot{E}_v$  – rate of energy removal by vaporization (W)

$\dot{E}_v^*$  – specific rate of energy removal ( $= \dot{E}_v/m_{w,0}$ ) ( $\text{W kg}^{-1}$ )

$h_{fg}$  – latent heat of water vaporization ( $\text{J kg}^{-1}$ )

$k$  – thermal conductivity ( $\text{W}/\text{m } ^{\circ}\text{C}$ )

$\dot{m}_a$  – rate of change of the mass of air ( $\text{kg s}^{-1}$ )

$m_{PM}$  – mass of the porous medium (kg)

$\dot{m}_v$  – rate of change of the water vapour mass ( $\text{kg s}^{-1}$ )

$\dot{m}_{v,cd}$  – mass flow rate of the condensed vapour ( $\text{kg s}^{-1}$ )

$\dot{m}_{v,DS}$  – mass flow rate of vapour extracted by the depressurization system ( $\text{kg s}^{-1}$ )

$\dot{m}_{v,i}$  – mass flow rate of vapour into CV2 (generated in CV1) ( $\text{kg s}^{-1}$ )

$\dot{m}_{v,o}$  – mass flow rate of vapour out of CV2 ( $\text{kg s}^{-1}$ )  
 $\dot{m}_{v,vp}$  – mass flow rate of vapour extracted by the vacuum pump ( $\text{kg s}^{-1}$ )  
 $m_t$  – total mass (kg)  
 $m_{t,0}$  – initial total mass (kg)  
 $m_w$  – mass of water (kg)  
 $m_{w,0}$  – initial mass of liquid water ( $=V_{w,0} \cdot \rho_w$ ) (kg)  
 $m_{w,v}$  – mass of water vaporized (kg) or (g)  
 $m_{w,v}^f$  – final mass of water vaporized (kg)  
 $\dot{m}_{w,v}$  – rate of water vaporization ( $= dm_{w,v} / dt$ ) ( $\text{kg s}^{-1}$ )  
 $\dot{m}_{w,v}^*$  – specific rate of water vaporization ( $= \dot{m}_{w,v} / m_{w,0}$ ) ( $\text{s}^{-1}$ )  
 $M_a$  – molecular weight of the air = 28.97 ( $\text{kg kmol}^{-1}$ )  
 $M_v$  – molecular weight of water vapour = 18.015 ( $\text{kg kmol}^{-1}$ )  
 $P$  – total pressure (Pa)  
 $P_a$  – partial pressure of the air (Pa)  
 $P_0$  – initial pressure (Pa)  
 $P_{\text{sat}}$  – saturation pressure (Pa)  
 $P_v$  – partial pressure of the water vapour (Pa)  
 $P_{v,FL}$  – free layer partial pressure of the water vapour (Pa)  
 $P_{v,FS}$  – free surface partial pressure of the water vapour (Pa)  
 $P_{v,i}$  – partial pressure of the water vapour at the interface (Pa)  
 $P_{v,p}$  – partial pressure of the water vapour within pores (Pa)  
 $P_{v,t}$  – threshold pressure level (Pa)  
 $P_w$  – pressure of the liquid water (Pa)  
 $R$  – universal ideal gas constant = 8314.5 ( $\text{J kmol}^{-1} \text{K}^{-1}$ )  
 $r_i$  – radius of container inner wall (m)  
 $r_0$  – radius of container center (m)  
 $r_p$  – porous radius (m)

$t$  – time (s)

$T^*$  – normalized initial temperature (-)

$T_0$  – initial temperature (°C)

$T_c$  – chamber temperature (K) or (°C)

$T_{cc}$  – temperature in container center (K) or (°C)

$T_{cd}$  – condenser temperature (K) or (°C)

$T_{cw}$  – temperature in container wall (K) or (°C)

$T_w$  – liquid water temperature (K) or (°C)

$T_{w,CM}$  – water temperature in the coating media (K) or (°C)

$T_{w,0}$  – initial water temperature (K) or (°C)

$T_{i,v}$  – temperature of the water vapour at the interface (K) or (°C)

$t_{FP}$  – time to the flash point (s)

$t_{RP}$  – reaction point (instant) (s)

$t_{RT}$  – time to the regime transition (s)

$V^*$  – initial volume normalized (-)

$\dot{V}_e$  – volume flow rate of the pump ( $m^3 s^{-1}$ )

$V_f$  – free volume of the vaporization chamber ( $m^3$ )

$V_{FL}$  – volume of the free layer ( $m^3$ )

$V_{PM,0}$  – initial volume occupied by the porous medium ( $m^3$ )

$V_{vc}$  – volume of the vaporization chamber ( $m^3$ )

$V_{VL}$  – Volume of the vaporization layer ( $m^3$ )

$V_{w,0}$  – initial volume of the water ( $m^3$ )

### ***Subscripts***

0 – initial condition

cd – condenser

f – free volume

i – coming into; liquid-vapour interface  
max – maximum value  
min – minimum value  
o – out  
v – water vapour  
vc – vaporization chamber  
vp – vacuum pump  
t – total  
w – liquid water  
 $z_0$  – free surface  
\* – specific quantity (per unit mass of initial water)

### ***Greek symbols***

$\gamma$  – surface tension ( $\text{N m}^{-1}$ )  
 $\Delta t$  – integration time step (s)  
 $\Delta z$  – thickness of diffusion layer (m)  
 $\varepsilon$  – vaporization coefficient (-)  
 $\varepsilon_{z_0}$  – vaporization coefficient in free surface (-)  
 $\varepsilon_{\text{PM}}$  – vaporization coefficient of the porous medium (-)  
 $\varepsilon_{i,\text{PM}}$  – vaporization coefficient at the liquid-vapour interface in the porous medium (-)  
 $\theta$  – contact angle ( $^\circ$ )  
 $\rho$  – density ( $\text{kg m}^{-3}$ )  
 $\rho_a$  – air density ( $\text{kg m}^{-3}$ )  
 $\rho_v$  – water vapour density ( $\text{kg m}^{-3}$ )  
 $\rho_w$  – water density ( $\text{kg m}^{-3}$ )  
 $\phi$  – superheating degree (Pa)

## **Acronyms**

C – Container

C1, C2 – container one and two, respectively

CV – Control volume

CV1, CV2 – Control volumes one and two, respectively

DS – Depressurization system

FL – Free layer

FP – Flash point

FW – Free water

LPV – Low-pressure-vaporization

LPV-FW – Low-pressure-vaporization of free water

LPV-PM – Low-pressure-vaporization of water in porous media

PM – Porous media

RP – Reaction point

VC – Vaporization chamber

VL – Vaporization layer



---

***Part A - Scope and outline***

---



## **I. Introduction**

---

This first chapter describes the objectives of the work developed. The low-pressure-vaporization (LPV) process is presented as a technology able to enhance heat and mass transfer in several industrial areas, and also as an alternative and/or a complement to the vaporization phenomenon in normal conditions. Relevant aspects of the low-pressure-vaporization in porous media are also addressed, a subject that was studied in detail in this work. Finally, the motivation, scope and structure of the thesis are addressed.

### **I.1. Vaporization and low-pressure-vaporization**

---

The vaporization of a component is a phenomenon of phase change from liquid to vapour. There are basically two types of vaporization: evaporation and boiling, according to the surrounding conditions. Evaporation is a slow phase-change from liquid to gaseous state which occurs at any temperature below the saturation temperature at a given pressure, whereas boiling occurs at the boiling temperature or above it. The main difference between evaporation and boiling is that the former only occurs at the liquid surface and the latter occurs below the surface, in the bulk of the liquid. For the liquid to evaporate, the molecules near the surface need to have sufficient kinetic energy to overcome the liquid phase intermolecular forces. Boiling, contrarily, is a rapid vaporization. The boiling point corresponds to the temperature at which its vapour pressure of the liquid equals the pressure of the surrounding. The phase changes from liquid to vapour (evaporation or boiling) are associated with the increase of the internal energy, occurring through energy exchanges with the environment. The evaporation is related with the increase in the molecular kinetic energy and the boiling is related with the latent heat of vaporization for specific temperatures and pressures, and thus associated with high energy and mass exchanges.

The low-pressure-vaporization (LPV) is defined as a process of rapid liquid-to-vapour phase change activated by a sudden pressure drop, in which both evaporation and boiling phenomena occur. Firstly, the sudden pressure drop provokes a high agitation and turbulence in the liquid, increasing its kinetic energy and thus stimulating a

higher vaporization rate than in the simple evaporation (evaporation at normal conditions). On the other hand, as the pressure continues decreasing, it causes the removal of vapour molecules that tend to accumulate above the liquid surface and thus inhibit further vaporization. Since the pressure drop is very fast, the liquid pressure soon reaches its saturation value, the boiling phenomenon starts, which origins the formation of the vapour bubbles inside the liquid bulk and a violent phase change is observed. At this point, a significant amount of the liquid sensible heat is required to power the phase-change: it is converted into latent heat of vaporization. Consequently, there is a temperature decrease of the liquid. The pressure decreases again, reaching a new lower level of pressure saturation in the liquid water. Thus, the low-pressure-vaporization is a continuous, yet very fast process of reaching the boiling point, generating high heat and mass transfer rates – a rapid cooling effect. The LPV involves several stages and regimes (Hahne and Barthau, 2000), being the boiling phenomenon the predominant one.

Saury et al. (2002) defined the LPV by *flash evaporation* as being the very quick phenomena caused by an abrupt pressure drop that transforms the initial supercooled liquid into superheated fluid. They wrote that initially the phenomenon is intense at the surface and forces the liquid to very heterogeneous temperature profiles, composed by superheated, saturated and subcooled zones. These authors referred that *flash evaporation* can involve vaporization rates 10 to 12 times higher than in simple vaporization.

Peng et al. (2002) studied the dynamic behaviour of bubble interface during boiling. They wrote that in different conditions the behaviour of the boiling and bubble dynamics will change. The physical mechanisms dominate the boiling, and thus primary forces may be different. Likewise, in Kim et al. (2007) it is shown that, during saturated nucleate pool boiling at sub-atmospheric pressure, the bubble radius obtained is larger than at atmospheric pressure and that it increases as the system pressure decreases, and the bubble departure is also larger. The low-pressure-vaporization is designated by Nutter and O’Neal (1997) as *flash boiling* since the principal phenomenon is boiling. The authors used steel spheres as a *passive enhancement technique* to the *flash boiling*, referring that this process can be used in different industrial areas to enhance the vaporization rate and the heat transfer, leading to a procedural temperature control.

Thus the low-pressure-vaporization process can be defined as an indirect technology to enhance the heat and mass transfer by sudden and continuous pressure drop, causing consecutive stages of violent boiling.

---

## I.2. Vaporization in porous media

---

Nowadays high capacity heat transfer techniques are quite required for industrial applications and scientific research. The vaporization in porous media has been studied as a passive technology to enhance heat and mass transfer in industrial processes. The passive technology employs special surface geometries, or fluid additives (Webb and Kim, 2005).

Webb and Kim (2005) wrote that the pores provide a high density of large cavities, which increases the nucleation sites, and so, the boiling enhancing. The nucleation is affected by the surface roughness; by capillary forces in meso and macrocopes; by the bubble growth kinetics and the boundary conditions, among others Yortsos and Stubos (2001) reported that the phase change in porous media occurs in the confines of the pore space, its structure being determinant for the phenomenon evolution, but it is driven by external boundaries conditions affecting the bubble growth. The phase equilibrium and growth kinetics are determined, respectively, by intermolecular forces between the fluids and the pore surface and by the transport of mass or heat within the pore structure and up to surface. The pores within the porous media are connected and the vapour formed in one pore activates the boiling in other pores. The same authors wrote that Gottzmann in 1971 theorized that essential vaporization occurs within the pores and the high performance is the result of pores entrapping large vapour-liquid interfaces, which reduces the superheating required for nucleation, and thus the pores have a much larger surface area for thin film or microlayer evaporation to occur than at a flat surface.

As referred before, the phase change at the liquid-vapour interface is of great importance in heat and mass transfer, in bubble formation and in the vaporization phenomena in general. The understanding of the liquid-vapour interface in the porous medium is essential to control the vaporization phenomena. The capillary pressure created within the pores as a function of their dimension is determinant to the liquid phase condition in the interface region, and modifies the thermodynamic equilibrium conditions for the liquid-vapour interface (Udell, 1983). Several interfacial vaporization models have been proposed based on molecular kinetic analysis (Carey, 1992), where the driving force is the difference between the interfacial and bulk vapour pressures, these pressures being affected by properties of the porous medium itself as by boundary conditions. The Kelvin equation is normally used to represent the interfacial interaction during the vaporization (Carey, 1992; Zhang et al., 2001), which is a function of the

capillary radius, the surface tension and the density and temperature of the liquid. The porous medium creates a non flat liquid-vapour interface which may take different forms, changing the thermodynamic equilibrium, as shown by Zhang et al.(2001) and by Udell (1983). For example, Zhang et al.(2001) described that for a concave interface the saturated liquid gets into the metastable superheated state due to the capillary effect which decreases the liquid pressure. The metastable superheated liquid becomes unstable by disturbances, such as nucleation sites, and vaporizes to saturated vapour which moves into a bulk vapour where vapour pressure is decreasing, turning up into superheated vapour. Thus, a positive pressure difference between liquid and vapour bulk promotes the vaporization. In this stage the two phases are in thermal equilibrium, i.e., with equal chemical potential. Therefore, if there are conditions at the interface for establishing consecutive thermal equilibriums, greater will be the vaporization rate. The relation between vapour pressure and liquid pressure within porous media may be represented by the Young-Laplace equation (Webb and Kim, 2005).

As referred before, the vaporization within pores is affected by the pore structure (pore scale and bead size), as well as by the bubble growth and coalescence and by the surface tension. By itself the surface tension has direct influence on the bubble shape, on the interface formation and on the bubble growth. The number of nucleation points increases due to the decrease of surface tension. The bubble growth is also dependent on the porous media structure and the boundary conditions.

The vaporization in porous media can be a big contribution to increase the vaporization rate and, consequently, the rate of heat removal by vaporization in different devices or surfaces in industrial processes. The porous media can be also used as a coating, enhancing the heat exchanges, as described by Webb and Kim (2005).

### **I.3. Motivation and Scope of the Thesis**

---

Nowadays, with a fierce increase of competitiveness in the industrial world and the demanding requirements of modern life, the search for the perfect solution leads to another perspective of the utilization of processes previously studied as mere scientific works. Many of them are presently being considered as high potential technologies in several industrial areas. In this way, over the recent years, many works have been carried out to enhance the heat and mass transfer, making industrial procedures more rapid, more efficient and more sustainable. The recent studies have been focused on the improvement of conventional technologies, or on technologies used with other functions,

in order to create new technologies able to perform the benefits indicated before. Emerging from this motivation, the main goal of this thesis is to study the low-pressure-vaporization process as a technology capable of enhancing the heat and mass transfer, contributing to the improvement of several industrial procedures, such as the drying and refrigeration processes, the processing/treatment of specific products (e.g. in wine and water production) or the temperature control of equipments and structures in industrial or quotidian environments.

For that purpose, the low-pressure-vaporization process is both mathematically and experimentally studied. At first, a preliminary mathematical model was developed to describe the LPV process in free water, in order to understand the process and its principal problems, the variables that influence its evolution and to make comparisons with experimental results in the literature.

Simultaneously, an experimental set-up was developed to study the LPV evolution in free water for different initial conditions, such as the initial water temperature and volume. The evolutions of the water temperature and of the total pressure in the chamber were measured in all experiments. From this study, it is possible to detail and characterize all stages and regimes of the LPV and the corresponding variations of the relevant parameters, such as vaporization rate, total amount of water vaporized, and how there are influenced by changing the initial conditions. From the experimental results and with an improved understanding of the LPV process, it was made the calibration and validation of the mathematical model of the LPV in free water. The development of this model aims to make the preliminary model more complete and physically more realistic.

The low-pressure-vaporization of the water was also studied in four different porous media. An experimental campaign was carried out to assess the LPV evolution for different initial temperature of the each porous medium. The comparison of several evolutions (e.g. temperature, vaporization rate, specific water vaporized, among others) was made for LPV in free water and in porous media. Simultaneously, a mathematical model which describes the LPV in different porous media was developed, calibrated and validated. From this model it is possible to analyse parameters which can not be determined experimentally.

A final objective of this thesis consisted of determining the effects of free water and of porous media as coatings of a container during the low-pressure-vaporization. The work described in each chapter has the main objective of contributing for a better

knowledge of the low-pressure-vaporization, and for this knowledge to be used or adapted to improve several industrial applications, as described throughout this thesis.

## **I.4. Thesis Structure**

---

This introductory chapter (Chapter I) contextualizes the work developed in the study of the low-pressure-vaporization as a technology to enhance heat and mass transfer for different industrial applications.

Chapter II consists of a concise review of the state-of-the-art of both the vaporization phenomena and the low-pressure-vaporization process. Reference works devoted to the study of the vaporization phenomena, of the vaporization in porous media and several research works of practical applications are summarized. A short synopsis of literature is presented about the low-pressure-vaporization and its application for the processing of products, for drying and for refrigeration processes. These two initial chapters are enclosed in Part A – *Scope and outline*.

The core of the thesis is divided in Parts B, C and D, each one composed by chapters. A great part of the work presented in some chapters is already published or submitted for publication in scientific international journals.

Part B – *Low-pressure-vaporization in free water* begins with Chapter III where a preliminary mathematical model describing the two stages of the LPV in free water is described. The corresponding research work is published in *Journal of Food Engineering* (<http://dx.doi.org/10.1016/j.jfoodeng.2012.05.013>). Chapter IV consists of a detailed characterization of low-pressure-vaporization of water based on an experimental study. The experimental set-up used throughout the work is described. The two stages of the LPV and the distinct boiling regimes in the second stage are identified and characterized. An integrated analysis of the influence of the initial conditions on the LPV process is made. The work of this chapter was submitted for publication in *International Journal of Thermal Science* and it is under review. In Chapter V, the physical calibration and validation of the mathematical model of the LPV in free water (developed in Chapter III) are presented. The experimental calibration with definition of the several LPV parameters and the improved physical model of the LPV in free water are described.

Part C – *Low-pressure-vaporization in porous media* is divided into two chapters. Chapter VI consists of an experimental study of the low-pressure-vaporization of water in different porous media where the performance comparison between LPV in free water

and in porous media is also made. This chapter is published in *International Journal of Heat and Mass Transfer* (<http://dx.doi.org/10.1016/j.ijheatmasstransfer.2013.06.037>). In Chapter VII, the development, calibration and validation of a mathematical model of the low-pressure-vaporization of the four different types of the porous media are shown.

Part D – *Low-pressure-vaporization in coated container* consists of one chapter (Chapter VIII) where an experimental study of the low-pressure-vaporization of water on container coated with porous media and free water was made. The performances of four different types of porous media and two different volumes of free water as container coatings to enhance heat and mass transfer are compared.

Chapter IX is Part E, where the relevant conclusions of this work are presented and some recommendations for future work are proposed.



---

## II. State of the Art

---

This chapter describes the contemporary literature of vaporization and low-pressure-vaporization. In a first phase, it is given an overview of the works on vaporization and vaporization in porous media. A second phase of literature reviewing describes the works published about the specific studies on low-pressure-vaporization and its main applications for industrial processes.

---

### II.1. Synopsis of Literature of the vaporization

---

The present section describes some works of relevant interest for the comprehension of the vaporization phenomenon as evaporation and boiling, and the particular case of vaporization in porous media. Its sub-section relates several works of practical applicability concerning evaporation and boiling, and both in porous media.

#### II.1.1 Vaporization phenomenon

The vaporization may be a natural phenomenon as described by Erbil (2012), according to whom, when the atmosphere around a liquid is not saturated with its vapour, evaporation occurs. However, small drops also evaporate in saturated vapour conditions, as the vapour pressure inside the drops increases. Thus, in these conditions, vaporization is designated by evaporation and may be considered as a diffusion process (Erbil, 2012). This author wrote a review about the evaporation of pure liquid sessile and spherical droplets suspended from thin fibres, referring that evaporation plays an important role in many engineering applications such as: spray drying, fuel injection into combustion engines, medical care, controlling of the deposition of particles on solid surfaces, rapid cooling and others. This author also described minutely the theory of drop evaporation (large and small spherical drops, self-cooling on the drop surface, sessile drops on solid surfaces and other important aspects), considering it as an extremely complex phenomenon. Cioulachtjian et al. (2010) focused their study in the experimental analysis of water drop evaporation under moist air or saturated vapour conditions. This study aims to give new physical elements for the modelling of drops

evaporation under the influence of surrounding gases. Their work is considered an important contribution because the wettability phenomena play an important role in several scientific and industrial areas. They concluded that the surroundings have great influence on the dynamic of drop evaporation, namely in the drop's initial volume, evaporation rate and contact angle.

On the other hand, the boiling phenomenon as another type of vaporization has been studied for decades and referred to be a phase-change transport process, characterized by small temperature differences and high heat flux. It is extensively employed in several energy conversions. Several authors (Peng et al., 2002; Wen and Wang, 2002; Das et al., 2007; Rops et al., 2009) specifically focused their studies in the boiling dynamic and in the nucleate boiling. For instance, Wen and Wang (2002) studied the effects of surface wettability on nucleate pool boiling heat transfer in surfactant solutions, concluding that it is an important parameter for this phenomena. In another work, Peng et al. (2002) studied the dynamic behaviour of bubble interface during boiling. They reinforced the complexity of the phenomenon and the need of more studies for its understanding in several environments. During the experimental activity of these authors some new phenomena were visually observed, such as the interfacial transport phenomena, including bubble interaction. The interfacial effects and the transport phenomena associated with surface tension were theoretically analysed to reveal the marked influence on bubble interfacial shape and dynamic behaviour; and the bubble dynamics including nucleation, bubble motion and coalescence. Several theoretical models and methods were proposed to describe the dynamic characteristics and explain the physics of the interfacial phenomena.

### **II.1.2 Vaporization in porous media**

The phase change in porous media is a concept that has been investigated for decades, shimmering its position in heat and mass transfer in several areas of the industry and science. Several authors (Udell, 1983; Prat, 1998; Yortsos and Stubos, 2001; Fang et al., 2004) have written about the phase change in porous media in which they have shown new knowledge and reinforced its importance. Yortsos and Stubos (2001) wrote a review where they explicated the aspects of thermodynamic and kinetics in phase changing, describing their applications and considering the boiling in porous media as a phenomenon at various scales of interest, sharing the position exposed in several works referred in their review.

Authors as Prat (1998) and Udell (1983) experimentally studied and developed transport phenomena models in porous media, such as heat transfer and the capillary effects. For example, Udell (1983) made a hydrodynamic analysis of the flows resulting of phase change, relating all happenings to the capillary pressure. In the same way, this author made a thermodynamic analysis in which the effect of chemical potential and its changes were explicated. A description of the phenomena from the illustration of *Van der wall's equation* was made, which introduced a significant improvement in the understanding of vaporization in porous media.

Other authors (Mantle et al., 2003; Wang and Peng, 2004; Wang et al., 2004; Phan et al., 2009; Li et al., 2011) focused their studies in more detailed concepts of vaporization in porous media. Wang and Peng (2004) performed an experimental investigation from which they observed nucleation and bubble dynamics in the boiling phenomena inside porous structures. They concluded that the dynamical bubble behaviour depended on the pore structure, and also that the effects of pore scale, liquid replenishment and interfacial phenomena were the most important factors for describing boiling dynamic and heat transfer. In a more recent work, Li et al. (2011) combine a series of parameters analysis that directly influence a practical applicability concerning the use of porous media or porous structures. In this work, the authors made a comparison between liquid replenishing impacts on critical heat flux and the heat transfer coefficient of nucleate pool boiling on multiscale modulated porous structures. They concluded, for instance, that modulated porous structures could dramatically increase the critical heat flux and heat transfer coefficient by delaying the beginning of hydrodynamic instability and enhancing the pumping for the liquid vertical and horizontal replenishments.

### **II.1.3 Applicability of vaporization**

As referred in previous sections, in present days, the vaporization phenomena, both free vaporization and in porous media, can be used in a series of practical applications. Several authors (Figueiredo and Costa, 2004; Meng and Hu, 2005; Zhao et al., 2008; Chen, 2011) studied the vaporization phenomena as way of temperature control, both in buildings as in thermal protection of flames. Jugjai and Polmart (2003) focused their work in the enhancement of evaporation and combustion of liquid fuels using porous media, concluding that the applications of this type of combination is

suggested for future use in burners. Webb. and Kim (2005) referred in their book that the boiling phenomenon is an important enhancement both for heat as for mass transfer processes, minutely describing the use of the *enhancement techniques* (passive and active techniques). According to the referred authors, the most significant advances in enhanced heat transfer technologies have been made in special surfaces that promote high performance of nucleate boiling, increasing the heat and mass transfer coefficients. One of these surfaces is the porous one, where the pores provide a high density area with large cavities with the function of increasing the nucleation sites. Authors as Jo et al. (2011) studied the nucleate boiling heat transfer in different types of wetting surfaces in order to contribute for a better knowledge of enhanced boiling heat transfer. Covering hydrophilic, hydrophobic and heterogeneous wetting surfaces, a detailed study and discussion were made both on the bubble dynamics formed, as on boiling heat transfer parameter versus heat flux.

## II.2. Synopsis of Literature of the low-pressure-vaporization

---

As referred in the first chapter, low-pressure-vaporization (LPV) is a rapid phase change process that improves the vaporization in normal conditions. Several works have focused their research both in the study of the physical phenomena of low-pressure-vaporization, as in the study of its application in different industrial areas.

From the 1970s to present day, several studies have addressed low-pressure-vaporization, firstly focused on specific aspects such as the bubble growth dynamic in nucleate boiling (Stralen et al., 1975), effects of superheated water (Barták, 1990) and effects of volume (Sulfredge et al., 1996), under low pressure conditions.

More recently, in the 2000s, more complete models and experimental studies began to be developed for LPV characterization as a whole. The parameters that could be important for future applications of LPV were also analysed. Aoki, (2000) developed the *water flash evaporator* device used in space shuttles as a heat sink. The author compared experimental and analytical results of the maximum heat transfer coefficient and the saturation temperature of vapour for vaporization under low pressure conditions, showing that the analytical model had a good behaviour in the studies. Hahne and Barthau (2000) made a good work where they showed and illustrated the different stages of pressure in the adiabatic LPV process in different initial system conditions. Saury D. and co-authors wrote two important experimental works providing an analytical contribution for a better knowledge of LPV (Saury et al., 2002, 2005). In Saury et al.

(2002) the evolution of several parameters of low-pressure-vaporization were analysed in a water film. This is the case of flashing time and evaporated mass (analytical and experimental comparison). The experiments were realized for different initial superheat values and with the visualization of different stages of the LPV. The conclusions identified that the initial temperature and superheat have a direct influence in the LPV kinetic, showing the proportionality between final mass evaporated and the superheat. In addition, in Saury et al. (2005), studied the influence of the liquid height and the depressurization rate in different parameters of the LPV process, such as violence of the phenomena, flashing time and mass evaporated. Kim et al. (2007) wrote a technical note to compare the bubble growth in nucleate pool boiling under atmospheric and sub-atmospheric pressure. The authors concluded that the bubble growth rate at sub-atmospheric pressure is significantly different, showing a higher growth rate.

As referred in the previous section, some authors combine the vaporization phenomenon with different techniques to enhance heat and mass transfer. Already in the 1990s, Nutter and O'Neal (1997) proposed an experimental investigation using steel spheres as a passive technique for boiling enhancement of HCFC-22 under low pressure. The authors used a range of several parameters such as diameter, height and volume of the vessel where the process occurred; refrigerant amount; initial pressure and orifice diameter (which provokes high and low vacuum flow). The results of this work showed that using steel spheres the total mass evaporated increased from an average 21% to 81%.

Therefore, the next sub-sections will describe several practical applications of low-pressure-vaporization as way of enhancing heat and mass transfer.

### **II.2.1 Low-pressure-vaporization in products processing**

One of the application areas where vaporization at low pressure has been more extensively studied is processing of products. For instance, in the desalination process, in the wine and fruit juice production, and in the extraction of flavours and oils from fruits.

Osamu Miyatake and co-authors, of the Kyushu University, developed in 1981 a *spray flash evaporation technique* where a fluid is injected directly into a low pressure vapour zone inside the flash chamber through a tubular nozzle and the fluid vaporizes to regain equilibrium and steam is formed (Miyatake et al., 1981). The authors have explored this technology along the years (Osamu and Toshiyuki, 1992; Miyatake et al., 1993; Osamu Miyatake, 1994). They began to apply this technology to desalination

processes in 2001 (Miyatake and Tagawa, 2001; Miyatake et al., 2001; Liar et al., 2002). In Miyatake et al. (2001) studied the transient characteristics and performance of a novel desalination system based on heat storage and spray flashing evaporation for producing fresh water from the generated steam from industrial and domestic uses. In this study the characteristics of spray flash were described, which determines its efficiency. It ranged from 0.73 to 0.96 according the fluid used and the initial superheat value. The variation in the amount of generated steam was experimentally and analytically determined with good agreement. The authors concluded that the hybrid system studied showed good results for steam generation and seawater desalination and that the system can be predicted with sufficient accuracy, facilitating the design of a practical system.

In the year 2005, two Indian institutes published two isolated works (Muthunayagam et al., 2005a; Muthunayagam et al., 2005b) for fresh water production from vaporization at low pressure of saline water. In Muthunayagam et al. (2005a) modelling and experiments were done with saline water vaporization at low temperature and low pressure. Its flash chamber was a column with three planes of water injection where the experiments were realized with a water temperature between 26-32°C. The modelling considers the vapour diffusion model at the droplet surface to calculate the net evaporation, which takes into account the temperature reduction of the droplet during the process. The global droplet temperature is modelled from the heat balance at the droplet-vapour interface. The results showed a good agreement between experimental and model results and a 4% yield is observed at the lower range of low-pressures and the upper range of temperatures.

Yasuyuki Ikegami, from the Institute of Ocean Energy in Japan, has dedicated much of her work to the study of *spray flash* desalination. In 2006, Yasuyuki Ikegami and co-authors published an experimental study of the process where the influence of the direction of injection was studied (Ikegami et al., 2006). Later, with other authors made studies of *flash evaporation* for the desalination process considering other application (Mutair and Ikegami, 2009, 2010, 2012). In Mutair and Ikegami (2010), the authors made an experimental work of *flash evaporation* from superheat water jets as a promising method of desalination suitable for low-populated and remote areas capable of producing 15.2 tons of fresh water per day. The authors studied several aspects, such as the mass evaporated under the influence of experimental variable: nozzle diameter, flow velocity, initial temperature and superheating degree. A modelling of the temperature variation was made at the centreline of the jet draws. It was concluded that

the *flash evaporation* showed efficiency at low degrees of temperature and superheat; the intensity of flash evaporation was found to increase as the initial water temperature and the superheat degree did; the highest evaporation rate was attained at a downstream distance that decreased linearly or exponentially with an increase in the initial temperature or superheat degree. The same authors published the Mutair and Ikegami (2012) where they also studied the *flashing evaporation* but here considering other applications of the this process, namely, in paper processing, wine concentration and refrigeration. The work was focused on modelling the heat transfer in superheated water drops. The results showed that the evaporation in superheated water was dominated by the heat conduction within the liquid, and the effective thermal conductivity was 10 times bigger than the molecular thermal conductivity.

The LPV process can also be applied in wine producing, specifically in wine concentration, grapes refrigeration, wine quality improvement and grape juice production. In this way, a France laboratory has been working in *flash evaporation* within the wine production (Sebastian and Nadeau, 2002; Bouchama et al., 2003; Tiat et al., 2008, 2010; Sebastian et al., 2010). In Sebastian & Nadeau (2002) developed a model of the vintage mono-stage flash evaporated and validated with experimental results. They investigated the effects of the condenser, vacuum pump and pressure drop inside the flash chamber, analysing the physical phenomena that determine the process and how to extend it to industrial applications. In 2010, two good works were published (Sebastian et al., 2010; Tiat et al., 2010) with significant improvements to Sebastian & Nadeau (2002). The works aim to optimize the design of the two-stage flash evaporators for the wine industry (for flash-cooling or concentration), modelling the process (Tiat et al., 2010), where, a heat and mass transfer model, a dimensional model, an environmental model, an economical model were made, as well as a multi-objective optimization with sensitivity analysis (Sebastian et al., 2010).

The Purdue University in USA has produced an isolated work in this area (Paranjpe et al., 2012) studying the effect of the *flash vacuum expansion* process on grape juice yield and quality. These authors referred that this process has a substantial potential to aid juice expression and improve extraction of potentially healthy components from fruits and vegetables. They concluded that *flash vacuum expansion* has a potential for extracting more phytochemicals from grapes; lower temperatures and lower pressures promoted higher extraction of polyphenolics; improved yield, anthocyanin content, and anthocyanin extraction as compared with other processes for juice production. The present process has the capacity of producing darker coloured

juice with the same anthocyanin. In 2001, other authors P. Brat et al. (2001) had already studied this process, but with a flash chamber significantly lower. Their aim was the preparation of passion fruit purée, which was obtained with higher consistency and viscosity.

Other French laboratories have used low-pressure-vaporization for other interesting applications – essential oil extraction from the fast *Controlled Pressure Drop* process, initially designated by *Controlled Sudden Decompression* (DIC). It was developed along the years by several laboratories, initially to be used in drying processes, as showed later in sub-section II.2.2. This process is based in subjecting the product to a rapid transition from high steam pressure to low pressure. Over the years, the researchers have worked in this area publishing several papers, for instance, on the optimization of operating conditions of essential oil extraction from rosemary (Rezzoug et al., 2005); on the evaluation of the pressure drop rate effect on the isolation of cananga oil (Kristiawan et al., 2008); on modifying the structure of raw coffee beans in order to obtain better quality in roasting and consequently in flavour, aroma and colour (Kamal et al., 2008) on the evaluation of the impact of texturing using the DIC as prior process to solvent extraction of anthocyanins from Malaysian Roselle.

### **II.2.2 Low-pressure-vaporization in drying**

The drying process is another important application of low-pressure-vaporization. It has been studied by several authors in different laboratories of the world since the early 1990s, as described by Louka and Allaf (2002) and Elustondo et al. (2001).

In the years 2001 and 2002, researches of an Argentine laboratory wrote two significant works. In the first, they demonstrated the development of a mathematical model of moisture evaporation from foodstuffs under low-pressure with superheated steam (Elustondo et al., 2001). The model developed considered that the water removed is carried out by evaporation in a moving boundary making vapour flow thought the dry layer built as drying proceeds, being the physical model divided in: dry layer, composed by dry material; interface or moving boundary, through which the water concentration gradient is established; and wet zone, where no evaporation occurs, hence water content is that of the original fresh sample. The diffusion is considered as the phenomenon that describes the movement of the water from wet core to the interface, considering not only the water content, but the porosity and other parameters changing with drying. In this model, the liquid diffusion was combined with the thermal

resistance of the material. As a conclusion, the authors found that low pressure superheated steam drying is an attractive technique for making good quality products, better than when they are dried with hot air. In the second work, Elustondo et al. (2002) studied the drying rate as a function of pressure, which showed that maximum drying rate and pressure can be rewritten in a unique linear function.

In 2006, an Ukrainian group of researchers wrote an interesting work on agriculture materials drying at low temperatures and low pressures (Bazyrna et al., 2006), considering the process as ecologically pure for drying plants and a power-saving technology for agricultural production, processing and preservation. From this study, several important parameters were obtained, such as duration of processing, final product humidity, polynomial relation for mass changes versus times for different products, and others, which may be used to model low-pressure-drying of several agriculture materials.

In 2007, a Japanese researcher group wrote two similar works on the study of the old drying process – fluidized bed, which began to be studied in the 1980s, but now under low-pressure conditions. They studied the drying characteristics of porous material immersed in a bed of fluidized glass beads (Tatemoto, Yano, et al., 2007) and immersed in a bed of fluidized hygroscopic porous particles (Tatemoto, Tsunekawa, et al., 2007) under low pressure. In both studies, a theoretical and experimental analysis on the comparison of drying characteristics was made, and the effect the several operations conditions evaluated and in second studied was compared the results with the results of the first work. It was conclude that hygroscopic porous particles fluidized has some advantages as high drying rate and low sample temperature.

Other authors focused their works on the study of drying in specific products. This is the case of some laboratories in Thailand which have studied the drying of banana combined with low-pressure-vaporization, with and without superheat steam, and with far-infrared radiation (Nimmol et al., 2007a, 2007b; Swasdisevi et al., 2009) – the last one being a novel drying technology for heat-sensitive products, where the far-infrared radiation is used as a source of energy supplied to both the drying medium and drying product. In Nimmol et al. (2007a) the effect of the various operating parameters is studied on the drying kinetics and dried product quality in the drying of banana slides, combining low pressure superheat steam with far-infrared radiation. The results showed that this process require shorter drying time than other drying process without superheat steam when it was conducted at 90°C, but a longer time conducted to lower temperatures. In terms of quality, the banana slices showed more crispness. In

Swasdisevi et al. (2009) a mathematical model was developed for drying banana slides with far-infrared combined with low pressure, which allowed the prediction of changes in the moisture content and temperature in a model of banana. The model results were compared with experimental results and it was verified that the model did not describe very well the experimental results, specifically for the first period of drying.

As referred in sub-section II.2.1., some French Laboratories, mainly *The Laboratoire Maitrise des Technologies Agro-Industrielles in Université de la Rochelle*, developed in 1992, the *Controlled Sudden Decompression* process for drying by Allaf and other authors. They have developed several works in this area along of years (Louka and Allaf, 2002, 2004; Sanya et al., 2003; Iguedjtal et al., 2008). In Louka and Allaf (2002), two parameters related to *Controlled Sudden Decompression* process for drying potatoes are examined: initial pressure and the decompression duration. In this work the authors demonstrated the importance of instantaneous decompression and the reduction by 4 times in the duration of the final drying state. The same authors in Louka and Allaf (2004) studied more details of the *Controlled Sudden Decompression* process for its optimization in specific products. They evaluated the expansion ratio and the colour improvement in dried potatoes, carrots and onion. Allaf and other authors, in 2012, wrote a comparative study of various drying processes of strawberries (Maritza et al., 2012). They compared *hot air drying*, *freeze drying* and *swell drying* with DIC before the second stage. It was concluded that DIC treatment has a greater impact on kinetics and performance when it is compared to classical *hot air drying*. The pressure drop leads to a great expansion of the structure, while the short thermal treatment time can preserve the quality. In this way, the new modified texture makes the trapped water accessible for improving the diffusion, especially in the second stage of drying after the product shrinkage, as well as in the rehydration process; the water holding capacity can be much higher.

In 2012, a research group of the Federal University of Santa Catarina in Brazil, wrote a work proposing a convective multi-flash drying process for producing dehydrated crispy fruits (Zotarelli et al., 2012). The authors have studied the drying process along the years, but only recently using the *flash drying* (low-pressure-drying). In the referred work, they heated the product (banana or mango) to 60°C using hot air, which was followed by low pressure pulse. The process was made cyclically. The authors concluded that a convective multi-flash drying process product dehydrated fruits with moisture content, water activity and mechanical properties similar to commercial

freeze-dried fruits; the product colour is preserved due to moderate temperatures and completed in shorter times.

Another recent application of LPV is in fresh cement paste drying. Over the years, the plastic shrinkage cracks, accelerating the deterioration and increasing maintenance costs and reducing the service life, which has been a great problem in the durability of structures. Several tests have been made to simulate the plastic shrinkage cracks as they mainly occur due to a high rate of water evaporation from the concrete surface. Thus, recently researches have proposed a drying simulation based on vaporization at low pressure once this process causes a rapid rate of evaporation in the while weight loss is measured and imposes a one-dimensional moisture flow through the thickness and facilitates parameter estimation from the mass transfer data (Bakhshi and Mobasher, 2011; Bakhshi et al., 2012).

### II.2.3 Low-pressure-vaporization in refrigeration

The use of refrigeration machines for food conservation is widespread all over society and indispensable according to the current standards of living. However, conventional refrigeration methods, such as air blast and boxed cooling, are characterized by long process times. They have being largely used for decades now and its technology is a drawback in many cases. This feature has motivated the search of alternative refrigeration methods. Among these, the technologies based in vaporization at low pressure are considered a promising technique, mainly in the area of fast food processing, presenting numerous advantages over conventional cooling, namely the time required and a smaller energy consumption (Mc Donald and Sun, 2000; Zheng and Sun, 2004; Sun and Zheng, 2006). This improvement in quality and safety increases the refrigeration products shelf life: a feature that has encouraged studies to apply this technology to various food sectors. In fact, low-refrigeration-rate processes are referred to be inefficient in killing microbial spores that survive to cooking and from which toxins can be produced.

The application of LPV in the refrigeration process has been studied in several Laboratories over the years, but some departments of the *National University of Ireland* have been pioneer and holder of the highest number of publications in this area. In this way, table II.1 resumes the published works over the years by several authors from the *National University of Ireland* of the LPV in the refrigeration process. As can be analysed from table II.1 all the papers published by this group of authors evaluate the application

of *vacuum cooling technology* only on cooked beef products, except for the review papers. In each publication presents improvements to the previous work.

Noteworthy works are, for example, Drummond and Sun (2008a) and Drummond and Sun (2008b), which introduced a new technology: immersion in water combined with *vacuum cooling (immersion vacuum cooling)* to avoid undesirable effects on yield and quality previously observed in *vacuum cooling*, such as moisture loss, cooling time and microbiological safety. In Drummond and Sun (2008a), the authors developed a mathematical model which used *vacuum cooling* for a solid immersed in liquid. Thus, they developed a finite difference model for the heat and mass transfer mathematical model during the *immersion vacuum cooling* of cooked beef, describing the temperatures in beef and in the surrounding liquid, as well as the mass loss evolution. The authors concluded that mass loss are higher in a first period when evaporation is mainly controlled by heat transfer, suggesting that mechanical agitation in the surrounding liquid reduced the times and uneven cooling did not occur. In Drummond and Sun (2008b) an experimental work of *immersion vacuum cooling* of cooked beef was made, comparing this with other technologies (air blast and *vacuum cooling*), in regard of food safety recommendations. The authors concluded that *immersion vacuum cooling* has shorter cooling times than air blast, but longer than *vacuum cooling*. The size sample was significantly affected by the use of *immersion vacuum cooling* technology. According to the model, there wasn't significant growth of bacteria in cooling growth for *Clostridium perfringens* in beef.

**Table II.1.** Research works developed by *National University of Ireland*.

Reference	Title	Main topics overed/comments
(Mc Donald and Sun, 2000)	<i>Vacuum cooling</i> technology for the food processing industry: a review.	In this paper review the various types of food described, in particular fruit and vegetables, were submitted to <i>vacuum cooling</i> technology. The authors highlighted the advantages and disadvantages of this technology for each food.
(Mc Donald and Sun, 2001b)	The formation of pores and their effects in a cooked beef product on efficiency of <i>vacuum cooling</i> .	In this experimental work, apparent density, true density, porosity, shrinkage and moisture content were investigated in cooked beef. The effect of several processing conditions, packaging, cooking and <i>vacuum cooling</i> were examined in referred properties.
(McDonald et al., 2001)	The effect of injection level on the quality of a rapid vacuum cooled cooked beef product.	This paper evaluated the effected of the injection of brine in cooked beef during the <i>vacuum cooling</i> compared with the immersion in water.

Reference	Title	Main topics overed/comments
(Mc Donald and Sun, 2001a)	Effect of evacuation rate on the <i>vacuum cooling</i> process of a cooked beef product.	This work analysed the evacuation rate during <i>vacuum cooling</i> on mass, temperature, speed and final product yield in a cooked beef.
(Wang and Sun, 2002a)	Modelling <i>vacuum cooling</i> process of cooked meat - part 1: analysis of <i>vacuum cooling</i> system.	The authors of this paper developed a model to analyse the performance of <i>vacuum cooling</i> . The model considered the mass conservation of air and vapour in the vacuum chamber.
(Wang and Sun, 2002b)	Modelling <i>vacuum cooling</i> process of cooked meat - part 2: mass and heat transfer of cooked meat under vacuum pressure.	The study modelled the three-dimensional and transient mass and heat transfer using the finite element method of cooked meat in <i>vacuum cooling</i> .
(Mc Donald et al., 2002)	Effect of <i>vacuum cooling</i> on the thermophysical properties of a cooked beef product.	In this paper, thermal conductivity, specific heat capacity, thermal diffusivity, porosity and other thermophysical properties were evaluated in cooked beef using <i>vacuum cooling</i> and air blast, ware immersion and slow air.
(Houska et al., 2003)	Experimental study of <i>vacuum cooling</i> of cooked beef in soup.	In this experimental work, the temperature, pressure and mass loses evolution were measured in order to evaluate whether time is a meat size dependent parameter.
(Sun and Hu, 2003)	CFD simulation of coupled heat and mass transfer through porous foods during <i>vacuum cooling</i> process.	A numerical simulation was developed in this paper using a computational fluid dynamics code for heat and mass transfer during <i>vacuum cooling</i> , allowing the prediction of temperature distribution, weight loss and moisture content of the meat.
(Zheng and Sun, 2004)	<i>Vacuum cooling</i> for the food industry - a review of recent research advances.	In this review, the research works used <i>vacuum cooling</i> to evaluate the cooling rate, yield, product quality and factors that improve efficiency and product quality.
(Sun and Wang, 2004)	Experimental investigation of performance of <i>vacuum cooling</i> for commercial large cooked meat joints.	<i>Vacuum cooling</i> of twenty commercial large cooked meat were experimentally analysed. Samples were studied with 5-8kh and initial temperature at 74°C.
(Wang and Sun, 2004)	Effect of operating conditions of a vacuum cooler on cooling performance for large cooked meat joints.	This work analysed the effect of operation conditions of <i>vacuum cooling</i> in its performance for large cooked meat from a mathematical model. Chamber free volume, pumping speed and condenser temperature are the operation conditions studied.
(Sun and Zheng, 2006)	<i>Vacuum cooling</i> technology for the agri-food industry: Past, present and future.	This paper reviews the principles and equipment of the <i>vacuum cooling</i> technology, its advantages and disadvantages and mainly applications in the agri-food industry to the time the paper was written. Futures prospects of development in technology were also studied.

Reference	Title	Main topics covered/comments
(Drummond and Sun, 2008a)	Temperature evolution and mass losses during immersion <i>vacuum cooling</i> of cooked beef joints - A finite difference model.	This paper developed a finite difference model to describe temperature evolution and mass losses in the immersion of cooked beef during <i>vacuum cooling</i> . The model was experimentally validated.
(Drummond and Sun, 2008b)	Immersion <i>vacuum cooling</i> of cooked beef - Safety and process considerations regarding beef joint size.	The experimental work realized in this paper compared the immersion <i>vacuum cooling</i> technology with air blast and <i>vacuum cooling</i> technologies in regard of food safety. It was used a cooling growth model for <i>C. perfringens</i> in beef broth, available from the USDA website (Pathogen Modelling Program – PMP version 7.0, USDA).
(Drummond et al., 2009)	Application of immersion <i>vacuum cooling</i> to water-cooked beef joints – Quality and safety assessment.	The study compared immersion <i>vacuum cooling</i> , air blast and <i>vacuum cooling</i> technologies on cooling times and quality parameters as sensory and microbial analysis.
(Drummond and Sun, 2012)	Evaluation of the immersion <i>vacuum cooling</i> of cooked beef joints - mathematical simulation of variations in beef size and porosity and pressure reduction rates.	This work evaluated the influence of variations in product (beef size and porosity) and process parameters (vacuum chamber pressure reduction rate) on time, mass loss, pressure and temperature distributions during immersion <i>vacuum cooling</i> of large cooked beef from a validated mathematical model.
(Zhang et al., 2013)	<i>Vacuum cooling</i> in bulk of beef pieces of different sizes and shape – Evaluation and comparison to conventional cooling methods.	<i>Vacuum cooling</i> to chill cooked beef dices, strips and mince in bulk were investigated in this study. Time and some product quality properties were evaluated and compared to those obtained after conventional cooling methods (air blast, cold room and plate cooling). Cooling time, mass losses, nutritional content and physical properties, as well as colour and instrumental shear force were compared.

Other laboratories have also developed some work in this area along the years. For example, the *Institute the Refrigeration and Cryogenics* in *Shanghai Jiao Tong University* published some studies in this area since 2006 (Jin and Xu, 2006a, 2006b; Jin, 2007). In Jin and Xu (2006a) and Jin and Xu (2006b), the authors developed a moisture movement model to describe temperatures in meat under a *vacuum cooling* process without water, considering the one-dimensional radial heat and mass transfer. This model arises due to movement of vapour in pores provoked by pressure differences. In Jin (2007) an experimental work was carried out to evaluate the

temperatures evolution of product and chamber during *vacuum cooling*, as well as the pressure evolution and evaporation rate.

Another researcher group, in *Czech Technical University in Prague*, developed in 1996 the first mathematical model for *vacuum cooling* of liquids (Houska et al., 1996), being improved later by (Dostal and Petera, 2004). These authors referred that the model developed by (Houska et al., 1996) is not complete and, claiming that their model respected standard conventions in the modern transport phenomena and the physics of the *vacuum cooling*. Some of these authors collaborated with some authors from the *National University of Ireland* in the works described in table II.1.

There are still some isolated work in other laboratories around the world, such as in *Pamukkale University* in Turkey (Ozturk and Ozturk, 2009) and in *National Taipei University of technology* in Taiwan (Cheng and Lin, 2007), among others. The first, Ozturk and Ozturk (2009), focused their work on studying the effect of pressure in *vacuum cooling* of iceberg lettuce, concluding that *vacuum cooling* is 13 times faster than the conventional method. The second work Cheng and Lin (2007), made an interesting morphological visualization of water in *vacuum cooling* and freezing, showing the different stages of it through the process.

### **II.3. Conclusions**

---

In a brief conclusion about the present state of the art, it is demonstrated that vaporization has been studied along years as a phenomenon able to improve the quality of several industrial procedures, being enhanced from its combination with others techniques, such as the application of low pressure and the use of porous media.

In the present state of the art, it is demonstrated that the low-pressure-vaporization process has been applied along the decades to different areas where, in all cases, the principal aim is to improve heat and mass transfer to the several process stages. For example, it was showed that in wine production, low-pressure-vaporization is used both for increasing the vaporization rate (to control the mass transfer) as to refrigeration (to control the heat and mass transfer). In the same way, it is essential for desalination, drying, as oil extraction in order to control the main mass transfer and to increase or decrease the vaporization rate. The refrigeration process based in LPV is important to evaluate the mass and heat transfer, as well as to control temperature.

In this way, as referred in the previous chapter, the present work aims to minutely study the low-pressure-vaporization process as a technique able to enhance the heat and mass transfer in order to improve the quality and the efficiency of several industrial processes.

---

***Part B - Low-pressure-vaporization of free water***

---



---

### **III. A mathematical model describing the two stages of low-pressure-vaporization of free water**

---

This chapter reports the development and application of a mathematical model for the prediction of the low-pressure-vaporization (LPV) process of free water. The study is focused on defining clearly the two stages of the LPV process (before and after the so-called flash point (FP)) and on evaluating their contribution for the overall transient evolution of the relevant parameters.

The physical domain was divided into two control volumes: the first one contains the mass of free water, ideally assumed at a uniform temperature; the second one includes the volume of the vaporization chamber above the water free surface, the condenser and the vacuum pump. The governing differential equations of the model were solved by the Euler method using the *EES-Engineering Equation Solver*.

The results obtained show that the mathematical model describes the complete process of low-pressure-vaporization of free water, giving evidence to the weight of the first stage on the process transient evolution.

*Keywords:* Low-pressure-vaporization; flash point; water vaporization modelling; two stages

### III.1. Introduction

---

The low-pressure-vaporization (LPV) of water is accompanied by evaporation from the free surface and by bulk vaporization whenever pressure decreases to a value well below the saturation pressure. The great amount of energy required by the water vaporization – the latent heat of phase change – is taken from the mass of water itself. The low-pressure-vaporization occurs in two distinct stages as pressure is gradually decreased: an initial period, with just evaporation at the free surface, while the air is being removed from its surroundings, and a second stage that suddenly begins when pressure drops below the saturation value and the water starts boiling (flash point). This second stage may be called *flash boiling* and it is responsible for the majority of the vapour production.

The LPV process has been differently defined and characterized by several authors according to its applications. Saury et al.(2002) studied this process, although calling it *flash evaporation*, and analyzed the flashing time and the vaporized mass of a water film. They evidenced the importance of this phenomenon for several applications and showed that the vaporization flow rate by *flash evaporation* is more significant than during simple vaporization. Likewise, Aoki (2000) made a detailed analysis of water *flash evaporation* under low-pressure, by studying the maximum heat flux and the maximum heat transfer coefficient, and emphasizing their relevance to the global phenomenon.

Several authors (Lai et al., 2004; Huang and Lai, 2010) focus their studies specifically on the development of technologies to enhance the water vaporization. The LPV could be a promising technique for this aim. Muthunayagam et al.(2005b) have used the low-pressure-vaporization of saline water for the production of fresh water, and they achieved a yield between 3% and 4%.

Another relevant application the LPV can be in the field of refrigeration, mainly in the area of food processing, presenting numerous advantages over conventional technologies, namely on the process duration and on a smaller energy consumption (Mc Donald and Sun, 2000; Sun and Zheng, 2006). Moreover, the improvement of the quality and safety of products by this method increases their shelf life, a feature that has encouraged studies towards the use of this technology to various food sectors. For instance, this process has been widely used in the fruit and vegetable industry, such as lettuce and sweet corn, and extensively studied for cooked beef (Mc Donald and Sun, 2000, 2001a; Mc Donald et al., 2002; Sun and Wang, 2004; Jin, 2007). Wang and Sun

(2004) evaluated the effect of the operating conditions on low-pressure refrigeration of cooked meat, concluding that the process evolution depends on three important parameters: the chamber free volume, the pumping speed and the condenser temperature.

The phenomenon of LPV of water has also been employed in the drying technology. Drying of fruits, vegetables and agriculture materials is operated using the LPV phenomenon integrated with other technologies (Bazyma et al., 2006; Nimmol et al., 2007a). For example, Nimmol et al. (2007a) described a technology combining the LPV phenomenon with superheated steam and far-infrared radiation for drying banana – a product that is rather sensitive to heat. They argue that the traditional technology – hot air drying – is a very energy-intensive operation and leads to great degradation of the product quality due to elevated drying temperature and the presence of oxygen in the drying system. As a result, this study showed a final product with more crispness, especially at higher temperatures.

As in other multiparametric processes, the study and optimization of LPV benefits from numerical simulations. Several researchers developed mathematical models and conducted numerical studies to simulate the phenomena of the LPV (Aoki, 2000; Dostal and Petera, 2004; Muthunayagam et al., 2005a; Jin and Xu, 2006b). Jin and Xu (2006a) and Aoki (2000) developed detailed and complete mathematical models to simulate the LPV of water. Nevertheless, these models could not distinguish between the two characteristic stages of the LPV process. The first stage, however, may have a significant importance in the overall transient evolution of the process and so it can not be ignored. The present chapter aims to give a step forward in the numerical modelling of the LPV phenomena of free water, proposing a model that differentiates the two characteristic stages of the process. This model describes minutely all transport phenomena as well as the physics of the process.

## **III.2. Modelling of the low-pressure-vaporization phenomena**

---

### **III.2.1 Physical model**

The LPV system considered for this study is schematically shown in Figure III.1. As typically, it comprises three major components: a vaporization chamber (VC); a vacuum pump (VP) and a vapour condenser (CD). The low-pressure required in the

vaporization chamber that contains the water is achieved with the vacuum pump. In the initial stage, while the total pressure within the chamber is above the saturation pressure of water, the evaporation at the free surface is ruled by the diffusion of the water vapour in the still air existing in the chamber (Cioulachtjian et al., 2010). Although the energy necessary for the vaporization is taken from the water itself, its temperature will not decrease significantly in this period, because the amount of water vapour produced in this stage is relatively small.

When the total pressure within the vaporization chamber reaches the water saturation pressure, the vapour production starts being governed by the boiling process and the diffusion component becomes irrelevant. This moment is designated the flash point. As the pressure of the water vapour drops below the saturation pressure by the action of the vacuum pump, the liquid water vaporizes to compensate that drop. Consequently, the water temperature (and likely the saturation pressure) starts to decrease substantially. At this stage the rate of pressure reduction can be significantly enhanced by capturing part of the generated water vapour in a condenser.

As it is clear from this description, the initial stage of the LPV has a minor importance in the parameters evolution and for this reason is usually skipped in the simulations of the process. However, the initial stage is known to have a non negligible importance in the total process duration (Saury et al., 2002; Cheng and Lin, 2007).

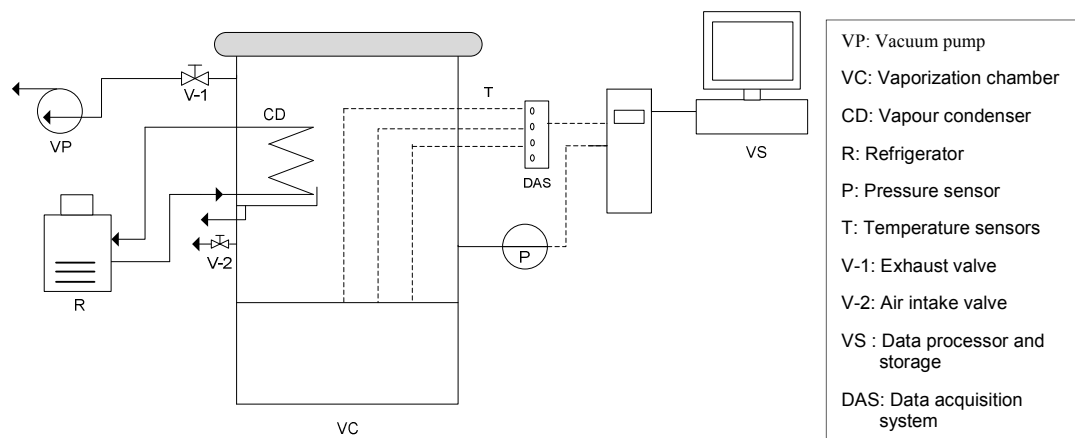


**Figure III.1.** Schematic diagram of a low-pressure-vaporization system (adapted from (Saury et al., 2002)).

### III.2.2 Mathematical model

For modelling purposes, the LPV system was divided into two control volumes (CV) as shown in Figure III.2. The first one comprises the mass of water (1.5 kg, see Table III.1). The water is considered ideally mixed with a uniform temperature throughout its volume. The CV2 defines the region of the vaporization chamber above the water free surface. The properties of the air and of the water vapour in this region are taken as homogeneous. Within this CV are included the condenser and the vacuum pump, both acting as mass sinks. As in the preceding one, the properties of the air-vapour mixture throughout this volume are considered uniform. Both control volumes are considered adiabatic and assumed to be in equilibrium with each other. This means assuming that there is thermodynamic equilibrium between gaseous and liquid phases, so that the two phases are instantaneously at the same temperature.

The temperature of liquid water determines the saturation pressure within CV2. However, the temperature of the water depends on the mass of the water vaporized and it will be determined by applying coupled mass and energy balances to CV1. The vapour pressure within the CV2 is, in turn, used to estimate the evaporation rate, which, during the first stage of the process, depends directly on the vapour pressure gradient across the diffusion layer. So, whenever the vapour pressure in CV2 drops below the saturation pressure, the water from the CV1 vaporizes aiming to raise the vapour pressure towards equilibrium with the saturation value. As referred before, it is this vaporization process that takes out the energy from the liquid phase and produces its temperature decrease.

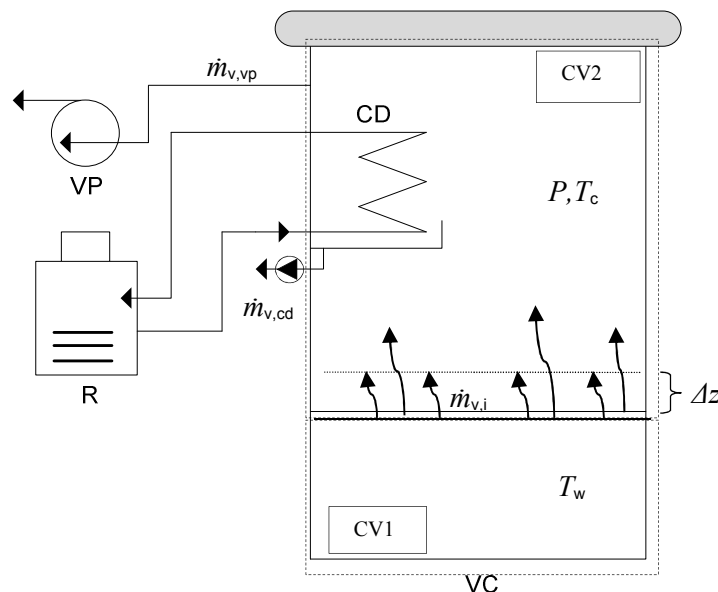


Figure III.2. Schematic diagram of the physical model.

The total pressure  $P$  in the vaporization chamber (CV2) is the sum of the partial pressures of the air and of the water vapour, respectively  $P_a$  and  $P_v$ :

$$P = P_a + P_v. \quad (\text{III.1})$$

Assuming that the air and the water vapour behave as ideal gases, the rate of variation of the partial pressure of air is defined by:

$$\frac{dP_a}{dt} = \frac{\dot{m}_a RT_c}{M_a V_f}, \quad (\text{III.2})$$

where  $R$  is the universal ideal gas constant,  $M_a$  is the molar weight of the air and  $V_f$  is the free volume of the vaporization chamber  $V_f = V_{vc} - V_{m_w}$  (essentially, the space that matches with the CV2).

The rate of change of the mass of air ( $\dot{m}_a$ ) in the chamber corresponds to the mass flow rate of air extracted by the vacuum pump and can be given by the Eq.(III.3):

$$\dot{m}_a = \frac{dm_a}{dt} = -\dot{V}_e \rho_a. \quad (\text{III.3})$$

Where  $\dot{V}_e$ , the volume flow rate of the pump, is considered constant and taken equal to the value shown in Table III.1 and  $\rho_a$ , the density of air, is given by:

$$\rho_a = \frac{P_a M_a}{R T_c}. \quad (\text{III.4})$$

Thus, replacing Eq.(III.3) and (III.4) in Eq.(III.2), the rate of variation of the partial pressure of air is given by:

$$\frac{dP_a}{dt} = -\frac{\dot{V}_e P_a}{V_f}. \quad (\text{III.5})$$

Similarly, the variation rate of the vapour partial pressure is calculated by:

$$\frac{dP_v}{dt} = \frac{\dot{m}_v RT_c}{M_v V_f}, \quad (\text{III.6})$$

where  $M_v$  is the molar mass of the vapour and  $\dot{m}_v$  is the rate of change of the mass of water vapour in the chamber, CV2, given by:

$$\dot{m}_v = \frac{dm_v}{dt} = \dot{m}_{v,i} - \dot{m}_{v,o} \quad (\text{III.7})$$

The mass flow rate of outgoing vapour ( $\dot{m}_{v,o}$ ) is given by:

$$\dot{m}_{v,o} = \dot{m}_{v,cd} + \dot{m}_{v,vp} \quad (\text{III.8})$$

where  $\dot{m}_{v,cd}$  is the mass flow rate of water vapour removed by the condenser and  $\dot{m}_{v,vp}$  is the mass flow rate of vapour extracted by the vacuum pump, calculated by:

$$\dot{m}_{v,vp} = \dot{V}_e \cdot \rho_v \quad (\text{III.9})$$

Given the typical values of the pump volume flow rate and of the vapour density, the mass flow rate of the vapour taken out from the system by the pump is small, and its value determines the vaporization rate. It is normally found that the use of only one typical vacuum pump is not enough to meet the purposes intended for a high vaporization rate. This problem is usually solved with the inclusion of a condenser in the system which will act as an additional vapour sink. In this model, it is assumed that the condenser imposes a constant condensation temperature ( $T_{cd}$ ) and therefore will reduce the vapour pressure in CV2 towards the corresponding saturation pressure. It should be noted, however, that at the beginning of each integration step, due to vaporization from CV1, the vapour pressure within CV2 will be higher than the saturation pressure at the condenser temperature. The mass flow rate of vapour removed from the system by the condenser can thus be approximated by

$$\dot{m}_{v,cd} = \frac{d}{dt} \left[ \frac{(P_v - P_{v,cd}) M_v V_f}{R \cdot T_{cd}} \right] \quad (\text{III.10})$$

where  $P_{v,cd}$  is equal to the saturation pressure of water at the condenser temperature ( $T_{cd}$ ) and the vapour density is given by

$$\rho_v = \frac{P_v M_v}{R T_c}. \quad (\text{III.11})$$

As stated before, the pressure reduction in CV2 is responsible for the vaporization of water in CV1. Before the flash point, i.e., while the total pressure in CV1 is still above the saturation pressure of the water, due to a still significant fraction of air existing in the gaseous mixture contained in CV2, the vaporization occurs mainly by diffusion at the water free-surface. In that case, the vapour generation rate ( $\dot{m}_{v,i}$ ) is a function of the vapour partial pressure in the vaporization chamber (CV2) and the water temperature. After Fick's law of diffusion, it may be expressed by (Mills, 1995):

$$\dot{m}_{v,i} = -AD \frac{M_v}{RT_w} \frac{\partial P_v}{\partial z}, \quad (\text{III.12})$$

where  $A$  is the free-surface area and  $\partial P_v / \partial z$  is the vapour pressure gradient at the water surface. The diffusion coefficient of water vapour in the air,  $D$ , is given by the Fuller-Schettler-Giddings equation (Quick et al., 2009):

$$D = \frac{1 \times 10^{-7} T_c^{1.75} \left( \frac{1}{M_a} + \frac{1}{M_v} \right)^{\frac{1}{2}}}{P_v \cdot \left( 20.1^{\frac{1}{3}} + 12.7^{\frac{1}{3}} \right)^2}. \quad (\text{III.13})$$

In the second stage of the process (after the *flash point*), the rate of vapour generation is mostly determined by the difference between the saturation pressure, at the liquid water temperature, and the vapour pressure in CV2, and it may be represented by:

$$\dot{m}_{v,i} = \frac{\partial}{\partial t} \left[ \frac{(P_{\text{sat}} - P_v) V_f M_v}{RT_c} \right], \quad (\text{III.14})$$

and the saturation pressure of the water  $P_{\text{sat}}$  is estimated by the Antoine equation (Poling et al., 2001):

$$P_{\text{sat}} = e^{\left(23.209 - \frac{3816.44}{T_w - 46.44}\right)} \quad (\text{III.15})$$

The time evolution of the water temperature is estimated after an energy balance to the CV1 one, expressed by:

$$m_w c_p \frac{dT_w}{dt} = -\dot{m}_{v,i} h_{fg}, \quad (\text{III.16})$$

where  $c_p$  is the specific heat capacity and  $h_{fg}$  is latent heat of vaporization of the water. The mass of water ( $m_w$ ) is assumed as being constant because the amount of vaporized water is small comparatively with the initial mass. Other authors, like Wang and Sun (2002a), adopted the same simplification. All the thermophysical properties of water considered in the equations shown above are varying with the thermodynamic conditions of the system. The initial conditions considered for the system are listed in Table III.1.

**Table III.1.** Specific operating conditions of the low-pressure-vaporization process.

<b>Low-pressure-vaporization conditions</b>		
Volume flow rate of the pump	$\dot{V}_e$ ( $\text{m}^3 \text{s}^{-1}$ )	0.0033
Volume of the vaporization chamber	$V_{vc}$ ( $\text{m}^3$ )	0.017
Initial mass of water	$m_w$ (kg)	1.5
Initial chamber temperature	$T_{c,0}$ ( $^{\circ}\text{C}$ )	25
Initial water temperature	$T_{w,0}$ ( $^{\circ}\text{C}$ )	25
Condenser temperature	$T_{cd}$ ( $^{\circ}\text{C}$ )	1
Initial vapour partial pressure	$P_{v,0}$ (Pa)	$0.5 P_{\text{sat},0}$
Initial total pressure	$P_0$ (Pa)	101325

### III.2.3 Numerical solution procedure

The model equations were solved using the *EES-Engineering Equation Solver* (Klein, 2004), a computer program to numerically solve algebraic equations that has many built-in mathematical and thermophysical properties functions.

The algorithm to solve the equations used in this model is schematically represented in Figure III.3. In the present configuration, the temperature is used as the stop criterion: when the water temperature ( $T_w$ ) is equal to the condenser temperature ( $T_{cd}$ ), the simulation stops. The differential equations were solved using the Euler method in an iterative procedure as sketched in the flowchart of Figure III.3. The calculation is made in two stages according to the value of the chamber pressure. When the total pressure equals the saturation pressure (flash point), the second stage of the process begins. The main difference between the first and second stages is the way how the rate of vapour generation is calculated (see Section III.2.2). The free-surface area is  $0.015 \text{ m}^2$  and water height is  $0.1 \text{ m}$ , and the diffusion layer thickness  $\Delta z$  was assigned a value of  $0.025 \text{ m}$  after a preliminary study described next.

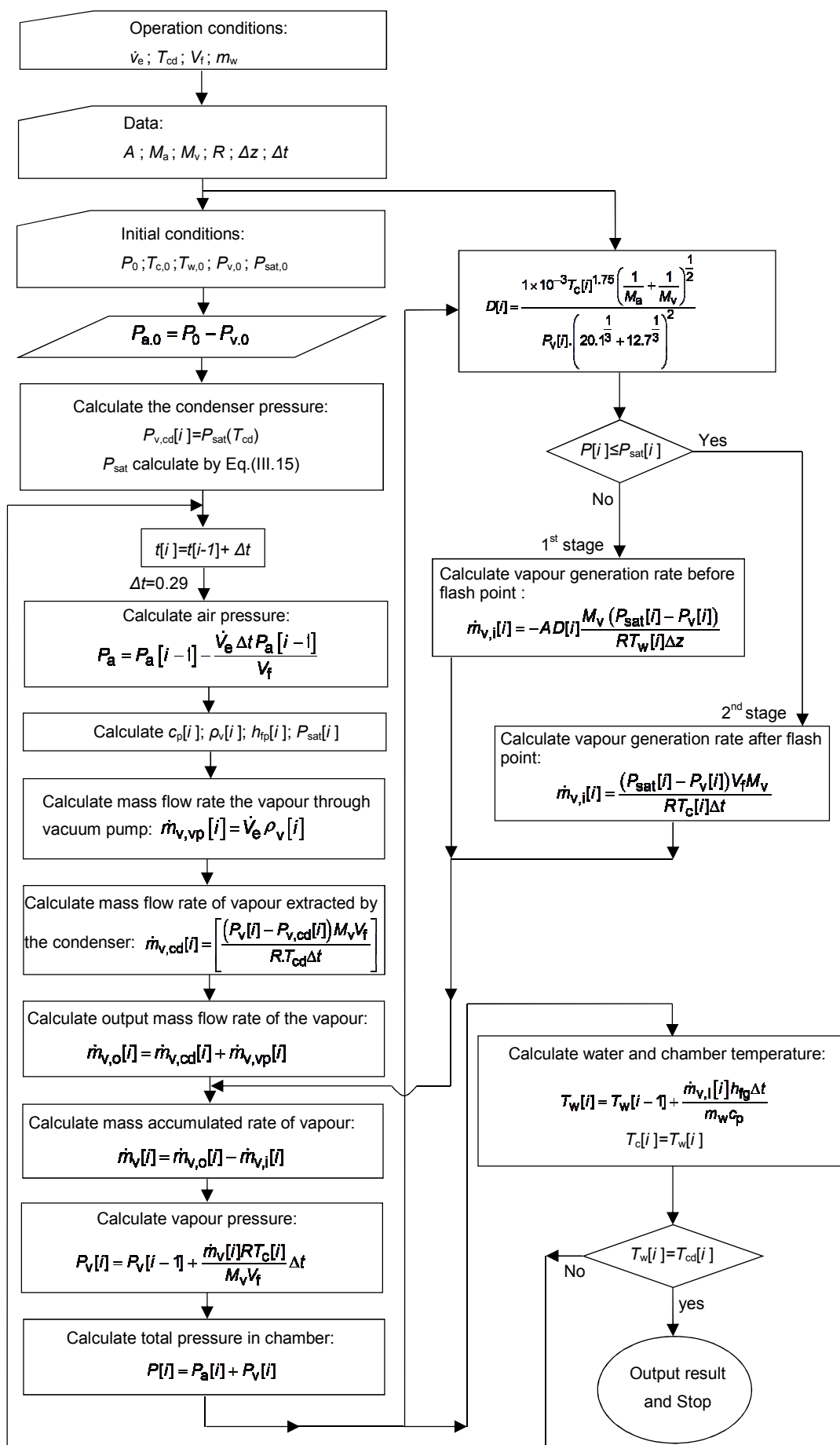
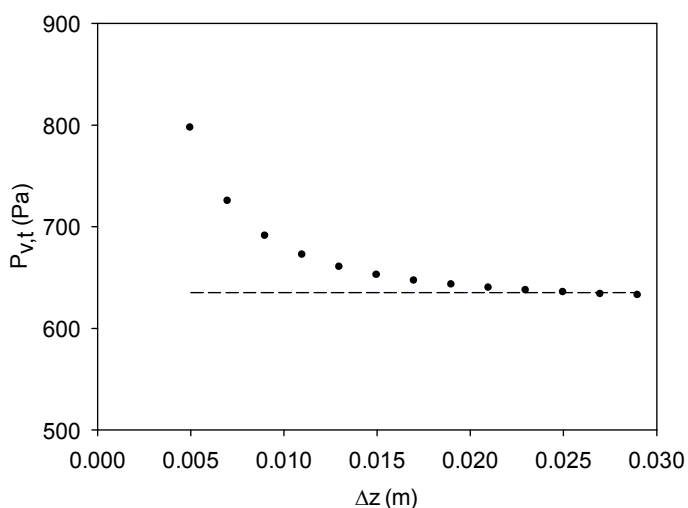


Figure III.3. Flow chart of the simulation program.

### III.2.4 Thickness of the diffusion layer

For the numerical solution of Eq.(III.12), the pressure gradient is approached by finite differences, which is equivalent to a piecewise linear representation:  $\Delta P/\Delta z$ . The driving potential  $\Delta P$  is taken as the difference between  $P_{\text{sat}}$ , which is determined by the liquid water temperature, and the vapour partial pressure  $P_v$  in CV2, which in the first stage will rapidly drop to a threshold level,  $P_{v,t}$ , closely below the saturation pressure at the condenser temperature (e.g.,  $\sim 659$  Pa, for  $T_{\text{cd}} = 1$  °C). A sensitivity analysis was performed regarding the influence of the diffusion layer thickness,  $\Delta z$ , on that threshold pressure level  $P_{v,t}$ . The results presented in Figure III.4 show an asymptotic decrease of that influence on the model output, which reaches independence at about  $\Delta z = 0.025$  m, a value that was assumed to be adequate for the thickness of the diffusion layer and thus used in all subsequent calculations.



**Figure III.4.** Tests for  $\Delta z$  independence of the model, monitoring the influence on the threshold pressure level  $P_{v,t}$  predicted in the first stage. The dashed line represents the  $P_{v,t}$  level for  $\Delta z = 0.025$  m.

### III.3. Results and discussion

The most innovative aspect of the present model consists of the representation of both stages of the LPV process (before and after the flash point). The results of the model are analysed in terms of their physical realism by conducting a parametric study and a comparison with to published experimental data.

Figure III.5(a) presents the predicted time evolution of the water temperature considering the operating conditions listed in Table III.1, with a clear definition of each of the two stages. After the flash point, the water temperature drops sharply, resulting in a decrease of approximately 24 °C in 150 s. Other authors (Dostal and Petera, 2004) obtained similar results, although using other initial and operating conditions. The great difference in the present results is the presence of the first stage that lasts for about 18 s. It is possible to see that this stage has an expressive contribution to the total process duration, in spite of its almost insignificant effect on the water temperature decrease. This was expected because in this stage the vaporization rate is governed by diffusion transport phenomena.

Figure III.5(b) shows the time variations of the vapour partial pressure and of the saturation pressure of the free water. As observed for the temperature, the two distinct stages of the vaporization process are evident. When the process starts, the vapour partial pressure  $P_v$  decreases sharply due to the combined effect of the vacuum pump and the condenser, stabilizing at a threshold value  $P_{v,t}$  slightly below the saturation pressure at the condenser temperature ( $P_{v,cd} = 659$  Pa). At this stage, the vaporization rate is very low, as it is governed by diffusion only. Simultaneously, the total pressure  $P$  in the chamber decreases due essentially to the removal of air. When  $P$  drops below the saturation pressure of the liquid water, the spontaneous onset of boiling (the flash point) is observed, producing step changes of both the vapour partial pressure  $P_v$  (see Figure III.5(b) and the vaporization rate  $\dot{m}_{v,i}$  (from  $1.7 \times 10^{-5}$  to  $1.2 \times 10^{-3}$  kg s<sup>-1</sup>, see Figure III.5(c). This results in a sudden increase of the total pressure  $P$  in the chamber, as it can be seen in Figure III.5(d). The order of magnitude of such changes is typical of this kind of process; however the precise values depend on the system characteristics.

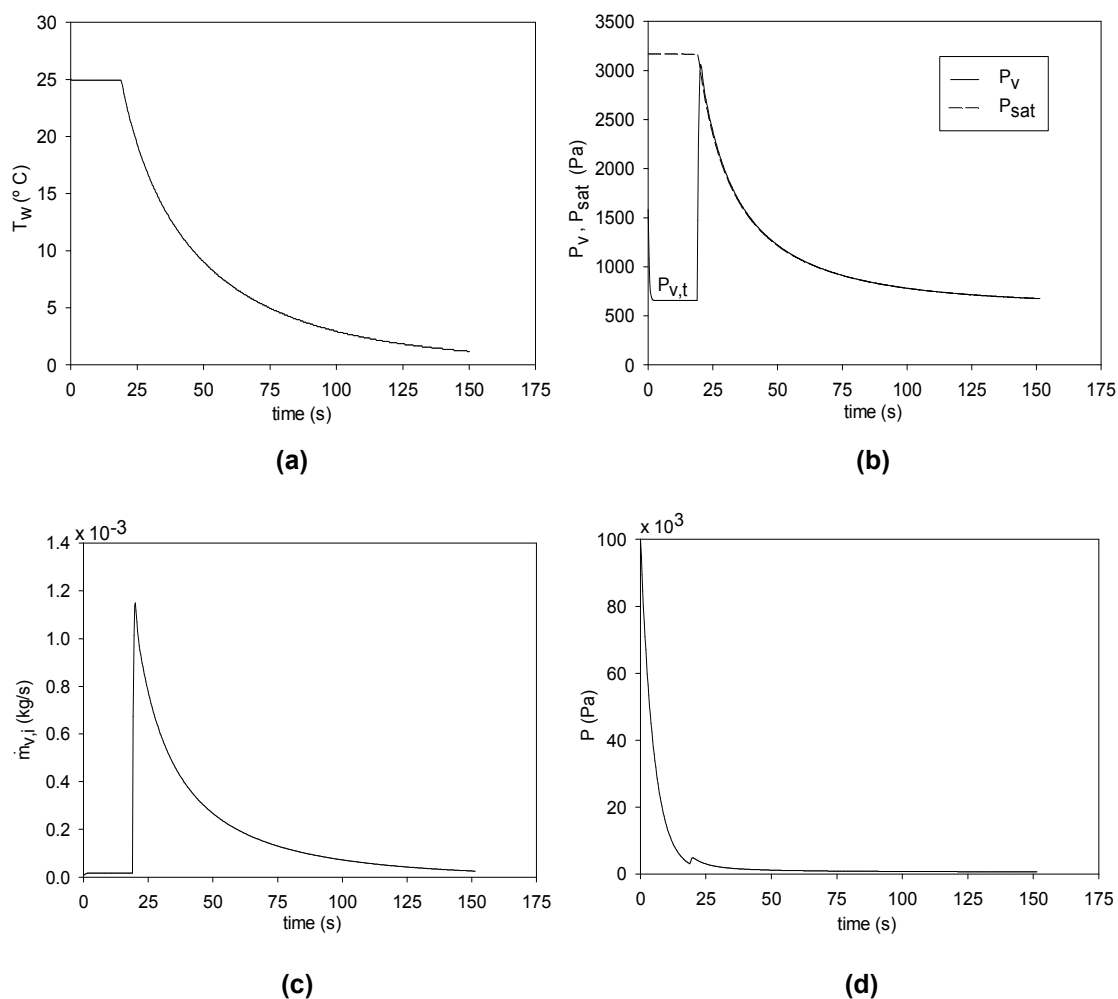


**Figure III.5.** Evolution of the LPV parameters: **(a)** water temperature; **(b)** vapour partial and saturation pressures; **(c)** vapour generation rate; **(d)** total pressure in the vaporization chamber.

A parametric study was then performed to analyse the effects of varying the condenser temperature  $T_{cd}$ , the mass of water  $m_w$  and the vacuum pump flow rate  $\dot{V}_e$  on the time variation of both the water temperature  $T_w$  and the vapour pressure  $P_v$ ; the results are plotted in Figures III.6 to III.8.

It is seen that although not having a significant influence on the time to the flash point  $t_{FP}$ , the temperature of the condenser  $T_{cd}$  has a relevant effect on the final temperature of the water, as evidenced in Figures III.6. This results from the fact that the vapour partial pressure  $P_v$  in the vacuum chamber tends asymptotically to the value of the saturation pressure at the condenser temperature ( $P_{v,cd}$ ). It is seen that the lower the condenser temperature, the higher the vaporization rate and likewise the water temperature decrease. It is possible to conclude that high vaporization rates are not

possible to achieve without a condenser (or a similar effect), since the vapour partial pressure in the chamber would then be only ruled by the vacuum pump.

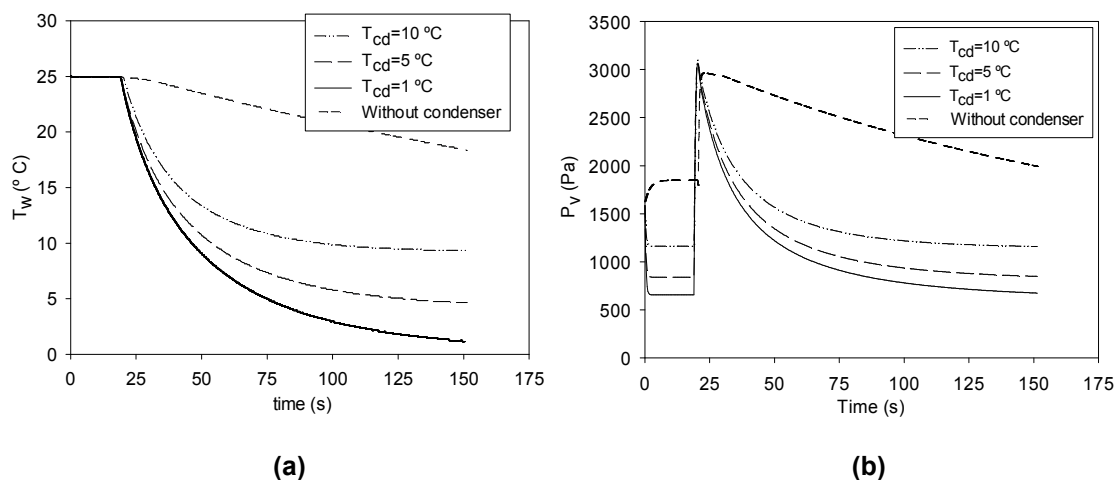


**Figure III.6.** Evolutions of: **(a)** the water temperature and **(b)** the vapour partial pressure for three different condenser temperatures.

On the other hand, Figures III.7 shows that the final values of the water temperature and of the vapour partial pressure, as well as the time to the flash point depend greatly on the mass of free water. As expected, the lower the heat capacity of the contained water, the lower will be the achieved temperature of the water after a given period (e.g., 150 s). However, as the curves for  $m_w = 0.5$  and 1.5 kg already suggest,  $T_w$  would always tend to  $T_{cd}$ , if  $t \rightarrow \infty$ . The different values obtained for the time to the flash point  $t_{FP}$  depend only on the free volume within the vaporization chamber and thus on the initial volume of air that must be removed.

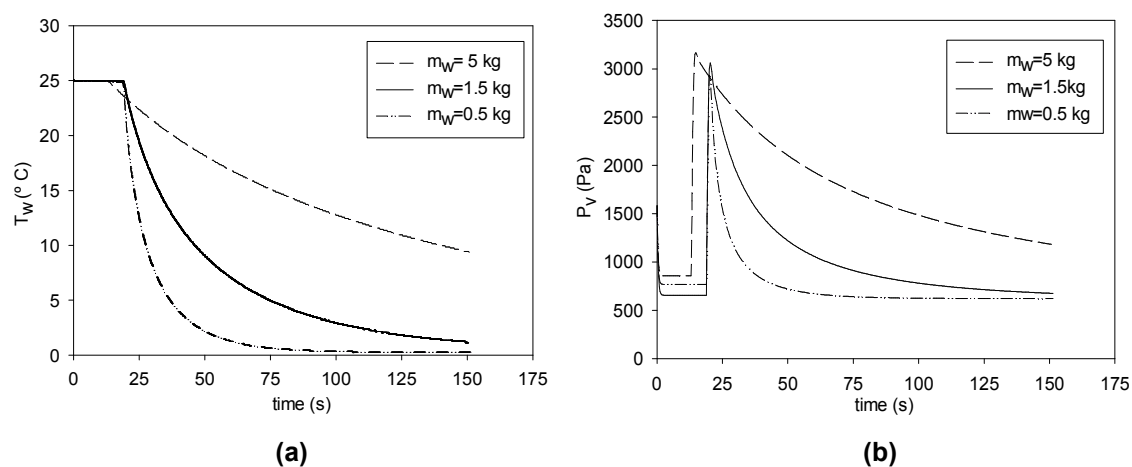


**Figure III.7.** Evolutions of: **(a)** the water temperature and **(b)** the vapour partial pressure for three different masses of water.

The effects of the volume flow rate of the vacuum pump on the time variations of the water temperature and of the vapour partial pressure can be observed in the graphics of Figures III.8. The pump flow rate has an important effect on the time to the flash point and consequently a relevant influence on the global evolution of all parameters of the LPV process (water temperature, vapour pressure and vaporization rate).

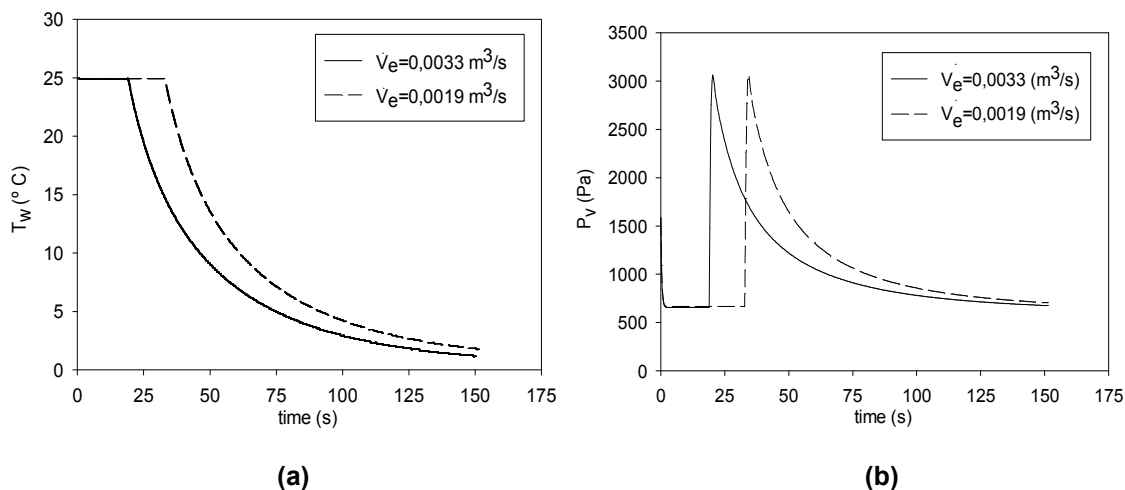


**Figure III.8.** Evolution of: (a) the water temperature and of (b) the vapour partial pressure for two volume flow rates of the pump.

Finally, a validation study was performed taking as a reference the experimental results of Cheng and Lin (2007). Since some characteristic data of the experimental set-up were not provided by these authors – namely the volume flow rate of the pump ( $\dot{V}_e$ ) and the free volume of the vaporization chamber ( $V_f$ ) – and as the value of  $\dot{V}_e$  is determinant for the duration of the first stage, the following strategy was adopted to somehow overcome the lack of those data. Using the same mass of water ( $m_w=0.6\text{kg}$ ) and the same temperature of the condenser mentioned by Cheng and Lin (2007), and considering the same free volume  $V_f$  ( $=0.0164 \text{ m}^3$ ) as in the previous calculations, a series of runs was performed changing the pump volume flow rate in order to search for the value of  $\dot{V}_e$  that allows predicting the same flash point time (about 130 s) as reported by Cheng and Lin (2007). With these data, the water temperature evolution predicted by the present model shows a good agreement with the experimental results as it can be seen in Figure III.9.

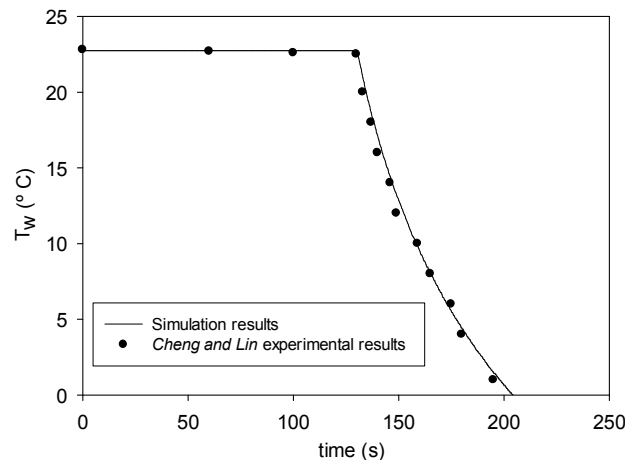


**Figure III.9.** Evolution of the water temperature: comparison between present simulation and the experimental results of (Cheng and Lin, 2007).

### III.4. Conclusions

In this work a mathematical model for the prediction of the process of low-pressure-vaporization (LPV) of free water was described with its two characteristic stages.

The results show that the mathematical model developed is able to describe the experimental results for LPV processes available in the literature. The present results indicate that the mass of water contained in the vaporization chamber experiences a temperature decrease of 24 degrees in about 150 s and that the first stage of the LPV process has an expressive contribution for the overall transient process. It is possible to conclude that the process is ruled by the time evolution of the water vapour partial pressure in the chamber, which in turn is governed by the vacuum pump flow rate and mainly by the condenser operating temperature.

The parametric analysis performed in this study allowed to conclude that the flow rate of the vacuum pump has a significant influence on the time to the flash point and that the condenser temperature affects mainly the final conditions (temperature and vapour pressure) as well as the total mass of vaporized water. The initial mass of water has influence on the time to the flash point as well as on the final temperature. Thus, it is possible to conclude that the first stage of process should not be neglected when modelling the LPV of water, since it accounts for a non negligible portion of the overall process duration.



---

## IV. Detailed characterization of the low-pressure-vaporization of free water – features of the boiling regimes

---

This chapter reports an experimental study for the detailed characterization of the low-pressure-vaporization (LPV) process of free water. For that purpose, an integrated analysis of the influences of the initial temperature  $T_{w,0}$  and volume  $V_{w,0}$  of the liquid water on the LPV process is made. The time evolutions of the water temperature and of the total pressure within the LPV chamber, for different initial conditions, were experimentally measured. The two stages of the LPV process and the respective regimes were identified and characterized, enhancing the current knowledge of the phenomena.

The experimental set-up comprises two main components: the vaporization chamber (VC) and the depressurization system (DS). Part of the VC volume is occupied by an open container for the water, which is insulated from the VC walls. Two different containers were used having different surface areas and heights, both with a negligible heat capacity. The results obtained show that the process parameters studied,  $T_{w,0}$  and  $V_{w,0}$ , have great influence on the superheating degree, and consequently on the LPV evolution, as well as on the total mass of the water vaporized. The identification and characterization of distinct boiling regimes in the second LPV stage allow a physically based optimization of the processes, such as enhanced heat removal or water vaporization existing in several industrial areas.

*Keywords:* Low-pressure-vaporization; boiling regimes; superheating degree; reaction point

## IV.1.Introduction

---

When a liquid initially in equilibrium is submitted to a sudden pressure drop that takes it below the saturation value, it becomes a metastable phase, and begins to vaporize both through its free surface and in the bulk volume in order to restore the initial equilibrium state, towards the new value of the saturation pressure (at the new temperature value) (Mutair and Ikegami, 2012). This set of associated phenomena (sudden pressure decrease and bulk vaporization) is known as low-pressure-vaporization (LPV). In a LPV process, the great amount of energy required by the vaporization – the latent heat of phase change – is taken from the liquid itself. Thus, the LPV process usually leads to vaporization rates much higher than in natural atmospheric vaporization.

This characteristic makes the LPV suitable for a wide variety of applications. Saury et al. (2002) studied this process (calling it *flash evaporation*), and analysed the flashing time and the vaporized mass of a water film. They showed that the vaporization rate during the *flash evaporation* is an order of magnitude higher than during simple vaporization and evidenced the importance of this process for several applications. Mutair and Ikegami (2012) proposed a model for heat transfer in water superheated drops resulting from flashing water jets, putting also in evidence the great interest of this process for several applications. Bouchama et al. (2003) evidenced the importance of a detailed study of the different stages of the LPV process. They developed a model for the design and the optimization of a two-stage flash evaporator focusing on thermodynamic aspects.

The LPV process has been widely studied to be implemented in industries of the distinct areas. Several authors (Wang and Catton, 2001; El-Dessouky et al., 2004; Muthunayagam et al., 2005b; Gude and Nirmalakhandan, 2009; Mutair and Ikegami, 2010) refer to the LPV as a promising technique to enhance the water vaporization and the heat removal for several industrial process. For example, Muthunayagam et al. (2005b) used the low-pressure-vaporization of saline water for the production of potable water, and they achieved a significantly good yield. Gude and Nirmalakhandan (2009) focused their study on the development of a prototype for a new phase-change desalination process to produce potable water from impaired or saline waters. In contrast to traditional phase-change processes, this can be operated in the range of 45–50°C. Thus, it could be driven by low-grade thermal energy sources such as solar energy or process waste heat.

Other authors (He and Li, 2003; Bazyma et al., 2006; Nimmol et al., 2007a; Pimpaporn et al., 2007a; Kingcam et al., 2008; Li et al., 2012) found relevant roles for LPV, when used in combination with other technologies to dry and refrigerate fruits, vegetables and other agriculture products. For example, Nimmol et al. (2007a) combined the superheated steam and far-infrared radiation with LPV process for drying banana – a product that is rather sensitive to heat. The traditional technology – hot air drying – is a very energy-intensive operation with high drying temperature, and the presence of oxygen leads to often degradation of the product quality. This study showed a final product with more crispness, especially at higher temperatures.

In wine industry, the use of LPV allows the wine concentration, to improve its quality, as several authors show in their works (Sebastian and Nadeau, 2002; Bouchama et al., 2003; Tiat et al., 2008, 2010; Paranjpe et al., 2012). Paranjpe et al. (2012) specifically compared the LPV and the enzymatic processing routes as means of increasing juice yield and quality, obtaining very good results with the LPV in two types of grapes.

Space shuttle industry is another area where the low-pressure-vaporization is studied. Aoki (2000) performed a detailed analysis of water *flash evaporation* under low-pressure, by studying the maximum heat flux, and emphasizing their relevance to space shuttle technology.

In most of the previously referred applications, LPV has been used with the aim at increasing the rate of water vaporization. As stated before, the vaporization of the liquid water requires significant amounts of energy. That energy can be taken from both the water and its surroundings, when the rate of vaporization is small, or just from the water when the rate of vaporization is high. In the later case, a significant decrease in the liquid water temperature can be observed. The field of practical applications of such sudden temperature drop is very wide and the process deserves to be studied in more detail in order to identify the most relevant physical phenomena and process parameters. In fact, most researchers analysed the influence of several parameters, but considering just the two stages (pre and pos-flash point) (Hahne and Barthau, 2000; Saury et al., 2002, 2005; Augusto et al., 2012).

The work of the present chapter is a step forward in the understanding of the second stage of the LPV processes, which is the most relevant for the practical applications. Based on a series of experiments, the effects of both the initial volume  $V_{w,0}$  and temperature  $T_{w,0}$  of the liquid water were analysed in an integrated way. The identification and characterization of distinct boiling regimes in the second LPV stage will

allow a physically based optimization of the processes (e.g., enhanced heat removal or water vaporization, existing in several industrial areas), namely the definition of the adequate stopping time.

## **IV.2.Experimental modelling**

---

### **IV.2.1 Features of the low-pressure-vaporization processes**

As referred above, the LPV is a complex physical phenomenon that results from a sharp pressure drop in a closed space where water (or any other liquid) is initially in equilibrium with its vapour at a pressure close to the atmospheric value. In these conditions, a sudden pressure drop will lead the system to a non-equilibrium situation from which it will tend to recover through a quick vaporization that will result into a very heterogeneous spatial distribution of the water temperature, with saturated, superheated and subcooled zones (Saury et al., 2002). These distinct zones with rather different temperatures are then responsible for significant buoyancy forces and highly turbulent water movements that greatly justify the observed high vaporization rates. As typically, the experimental set-up used in the present study to analyse the LPV process comprises two major components: a vaporization chamber (VC) and a depressurization system (DS). The pressure decrease that is required in the vaporization chamber is achieved with the depressurization system that includes a single stage vacuum pump as the main component. The process is known to occur in two distinct stages. In the initial stage, while the total pressure in the chamber is above the saturation pressure of water, the vaporization – only free surface evaporation – is ruled by the diffusion of the water vapour in the adjacent layer of still air (Cioulachtjian et al., 2010). The water temperature is not expected to decrease significantly during this stage because the amount of water evaporated is relatively small.

When the water vapour pressure reaches the saturation pressure by the action of the DS, the vapour production begins to be governed by the boiling process and it increases so significantly that the diffusion component (free surface evaporation) becomes comparatively irrelevant. Consequently, as the water container is insulated, the energy necessary for the vaporization is taken from the water itself and the water temperature (and the saturation pressure) starts to decrease substantially. This moment is named the flash point, and it defines the beginning of the second stage of the LPV

process, which is divided into two procedural regimes. However, as it will be referred in section IV.3, the flash point (i.e., the beginning of the sharp water temperature decrease) may occur also in other conditions.

## IV.2.2 Experimental set-up and methodology

The experimental set-up used to study the LPV process comprises two main components: the vaporization chamber (VC) and the depressurization system (DS), as sketched in Figure IV.1. The VC is a cylindrical stainless steel chamber with a volume of  $0.017 \text{ m}^3$  (diameter = 0.210m and height=0.500m). Part of the VC volume is occupied by an open container for the water, which is isolated from the VC walls. The DS consists of a vacuum pump with a volume flow rate capacity of  $0.0033 \text{ m}^3 \text{ s}^{-1}$ . The temperatures of the water in the container are measured by K-type thermocouples (accuracy:  $\pm 1.5 \text{ }^\circ\text{C}$ ; response time: 100 ms;  $\varnothing \approx 0.5\text{mm}$ ) and the chamber pressure (accuracy:  $\pm 2 \text{ mbar}$ ) is measured with an *Edwards™ ASG 1000 mbar* gauge. These sensors are connected through a *National Instruments™* data acquisition system to a personal computer where the signal is treated and saved using a *LabVIEW™ 8.6* based software.

As stated above, in this work will be studied the influences of the initial volume and temperature of the water on the LPV process evolution. The range of variation of these parameters was chosen considering the use of this phenomenon for practical applications. The initial values of these parameters are shown in Table IV.1 for the set of performed experiments. Two containers with negligible heat capacity, having different ratios of height to free surface area, were used. For the lower volume range (C1), the container used has a water free surface area of  $0.0027 \text{ m}^2$  and a height of 0.14 m. For the higher volume range (C2), the corresponding values are  $0.0058 \text{ m}^2$  and 0.3 m. At each experiment the time evolution of the water temperature  $T_w$  and of the total pressure  $P$  within the VC were measured. The saturation pressure is calculated from the water temperature evolution through the Antoine equation (Poling et al., 2001). The vapour partial pressure  $P_v$  is calculated from total pressure  $P$  by subtraction of the partial pressure of the air. The latter is obtained in a separate experiment with the same procedure protocol, without water in the VC, but with a solid occupancy volume equal to the initial volume of water to be used in the study. The experiment for each condition (cf. Table IV.1) was run in triplicate and the arithmetic mean at each instant was used as result. The coefficient of variation between experiments was lower than 10 % for  $T_w$ . For example, for  $V_{w,0} = 200 \text{ ml}$  and  $T_{w,0} = 22 \text{ }^\circ\text{C}$  (higher volume range), the coefficient of

variation is lower than 5.5 % and for  $V_{w,0} = 50 \text{ ml}$  and  $T_{w,0} = 22 \text{ °C}$  (lower volume range) the coefficient of variation below 8.4 %.

For all the performed experiments the water and the container were assumed to constitute an adiabatic system. Thus, once measured the water temperature ( $T_w$ ), it was possible to evaluate the vaporization rate at each instant through a simple energy balance. In those calculations the properties of the liquid, namely  $h_{fg}$ ,  $c_p$  and  $\rho_w$ , were assumed constant (evaluated at the initial temperature). It was also considered that the amount of water vaporized during the process is negligible compared with the value of the initial total mass. So, the mass (and the volume) of the liquid water was considered unchanged during each test. Based on these considerations, the mass of the water vaporized over the time is given by:

$$m_{w,v}(t) = \frac{m_w(t)c_p}{h_{fg}}(T_w(t - \Delta t) - T_w(t)) + m_{w,v}(t - \Delta t) \tag{IV.1}$$

Where  $m_w(t) = V_{w,0} \rho_w$ ,  $\rho_w$  and  $V_w$  being the water density and volume, respectively.

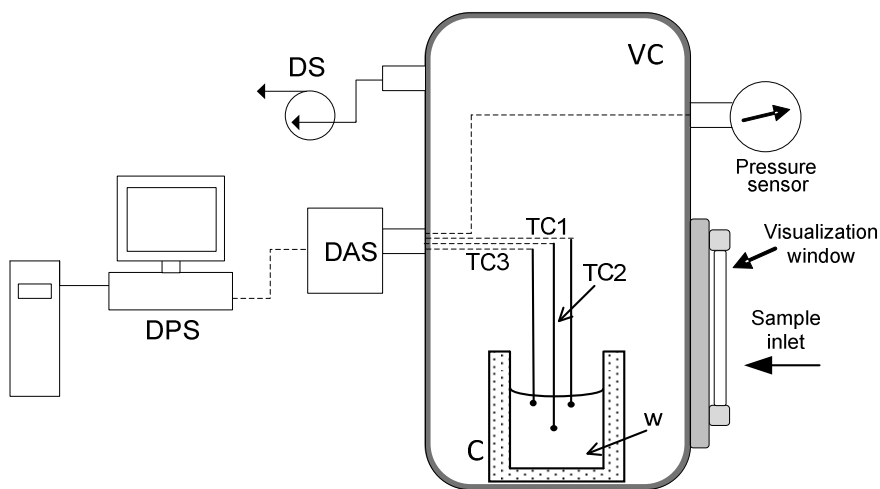


**Figure IV.1.** Schematic diagram of the experimental set-up of the LPV process. (DS - depressurization system; DAS - data acquisition system; VC – vaporization chamber; C – container; W – water; DPS - Data processor and storage; TC – Thermocouple.

**Table IV.1.** Initial conditions used in the experimental tests.

		C1				C2			
$T_{w,0}$ (°C)	$V_{w,0}$ (ml)	10	30	50	100	100	200	450	800
	22		√	√	√	√	√	√	√
27		√	-	-	-	-	-	-	√
34		√	√	√	√	√	√	√	√

### IV.3. Results and discussion

As referred above, to study minutely the LPV process, for the detailed characterization of the all process stages, it will be evaluated the influences of the initial values of the water temperature and volume on the LPV evolution was done through the comparison of the following process parameters: flash point time  $t_{FP}$ ; reaction point time  $t_{RP}$ ; time evolution of the water temperature  $T_w$ ; total pressure in the VC  $P$ ; saturation pressure  $P_{sat}$ ; partial vapour pressure within the VC  $P_v$  and final mass of the vaporized water  $m_{w,v}^f$ . The reaction point (RP) of the system is the beginning of the superheated phase, when an increase of the vapour partial pressure is observed, with the consequent changes of the total pressure.

#### IV.3.1 Influence of the initial conditions on the LPV evolution

As presented above, the LPV process is considered divided in two stages. In the first one, the vaporization occurs at the water free surface and is ruled by the diffusion of the water vapour in the just still air above it; it is commonly designated as evaporation. The amount of water vapour produced in this stage is relatively small. This initial stage is clearly apparent in Figures IV.2(a), (b) and IV.3, lasting from the initiation of the process up to the flash point – the beginning of the sharp temperature decrease.

Figures IV.2(a) and (b) show the time evolution of the water temperature for experiments with two different initial temperatures and with different initial volumes. As it might be expected, the smaller is the initial volume of water, the sharper is the temperature drop after the flash point. This effect is as more pronounced as higher is the initial temperature of the water. It can also be seen that while for the higher volumes (particularly for  $V_{w,0} = 800$  ml) the time evolution of the water temperature after the flash

point is approximately linear, that evolution tends to be exponential for the smaller volumes. It can also be concluded from the comparison of the Figures IV.2(a) and (b) that the differences in the temperature evolution fade away with the increase of the initial temperature.

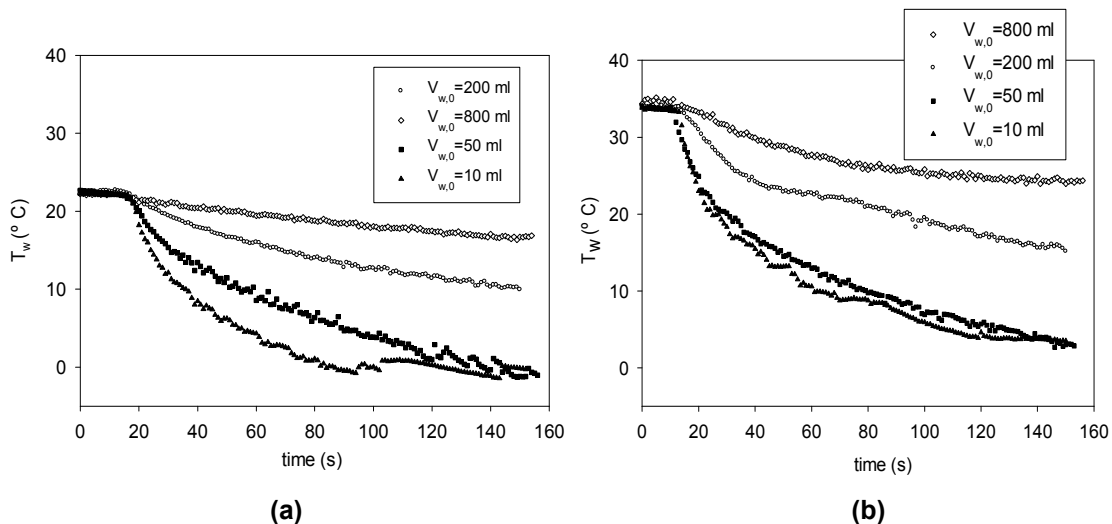


Figure IV.2. Water temperature evolution for several initial water volumes and for (a)  $T_{w,0} = 22$  °C and (b)  $T_{w,0} = 34$  °C.

Figure IV.3 shows the evolution of the water temperature for three different values of the initial temperature ( $T_{w,0} = 22, 27$  and  $34$  °C) and two different initial volumes of water ( $V_{w,0} = 10$  ml and  $V_{w,0} = 800$  ml). It is clearly seen that the initial volume has much more influence on the temperature evolution than the initial temperature.

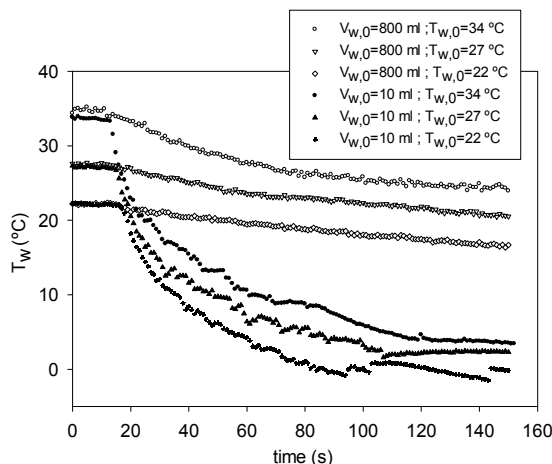


Figure IV.3. Water temperature evolution for several initial water temperatures and two rather different initial volumes ( $V_{w,0} = 800$  and  $10$  ml).

As referred before (see section IV.2.1 and Augusto et al. (2012)), the second stage of the LPV process begins at the flash point (FP). This second stage has been considered by several authors (Hahne and Barthau, 2000; Saury et al., 2002, 2005) divided into two different vaporization regimes. The first one begins exactly at the FP and is described as very violent. At this regime the free surface of the liquid is completely disrupted and the vapour bubble formation takes place throughout the whole volume of water. The second regime begins afterwards, when the total pressure reduction rate decreases, and it is characterized by vapour bubble formation underneath the liquid free surface. The LPV evolution, i.e. the transition from the first to the second stage and, particularly, from the first to the second regime in the latter, can be clearly seen in the total pressure temporal profiles presented in Figure IV.4. These results refer to the pressure time evolution for different initial water volumes and the same initial temperature. Point A in Figure IV.4 identifies the first stage of the process. The rate of the total pressure reduction is very high; however, the total pressure is still above the saturation pressure of water and the evaporation rate is small and ruled by the vapour diffusion in the still air above the free surface of the liquid.

At point B, the total pressure reaches the saturation pressure of the water. In normal conditions this point corresponds to the flash point (FP). From this point on, the second stage of the process takes place. The first regime of this second stage is characterized by an intense boiling throughout the whole water volume. The rate of vapour production is so high at this phase that an inversion in the total pressure reduction trend can be observed (at least for the bigger initial water volumes). The point at which this inversion is observed, point C, is called the reaction point (RP). For the smaller volumes of water ( $V_{w,0} = 10$  and  $50$  ml), point C marks not an inversion but a marked attenuation in the rate of total pressure decrease. For the larger initial volumes of water, point D signs a local maximum (LM) in the total pressure that follows the reaction point. For smaller initial volumes D corresponds to the point at which the rate of the total pressure decrease recovers values similar to those observed before the reaction point.

As a consequence of the quick water vaporization, the temperature of the liquid rapidly decreases, decreasing also the superheating degree. For that reason the rate of vapour production reduces substantially and becomes localized in a restrict zone underneath the liquid free surface. This marks the beginning of the second regime of the second stage designated by point E in Figure IV.4. Beyond a certain moment, point F in Figure IV.4, the total pressure becomes approximately constant and equilibrium between

the vapour generation and the rate of vapour removal by the depressurization system is reached (Hahne and Barthau, 2000).

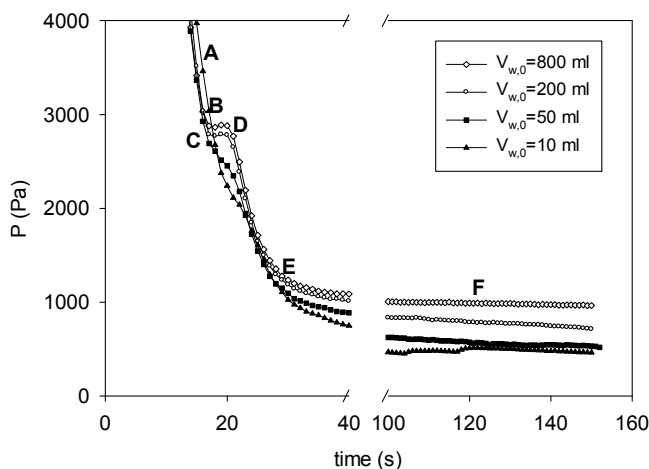


Figure IV.4. Total pressure evolution for several initial water volume for  $T_{w,0} = 22 \text{ }^\circ\text{C}$ .

The differences observed for the total pressure behaviour at the transition from the first to the second regime of vaporization in the second stage of the LPV process can be explained based on the amount of water that suddenly becomes superheated, due to the total pressure reduction beyond the saturation pressure. The bigger is the initial volume of the water, the bigger will be the amount of superheated water, as greater will be the vapour production and the change in the reduction trend.

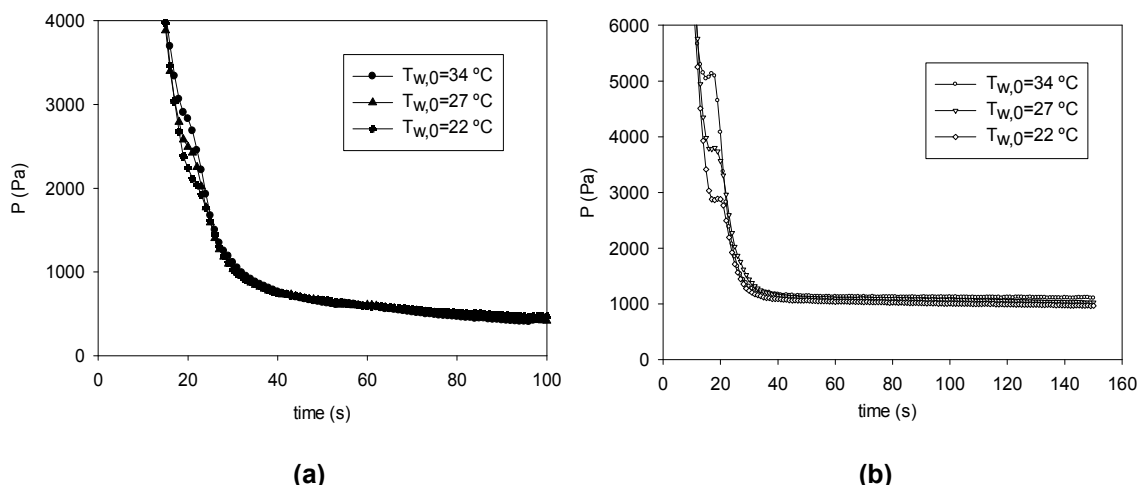


Figure IV.5. Total pressure evolution for several initial water temperature for (a)  $V_{w,0} = 10 \text{ ml}$  and (b)  $V_{w,0} = 800 \text{ ml}$ .

Figures IV.5a and b show that the initial water temperature has a great influence on the FP time (point B in Figure IV.4), in the RP time (point C in Figure IV.4) and on the LM (D in Figure IV.4). This effect increases with the initial volumes of the water (Figure IV.4b). Moreover, it can be seen that the initial water temperature does not greatly affect the final pressure of the LPV process (point F in Figure IV.4).

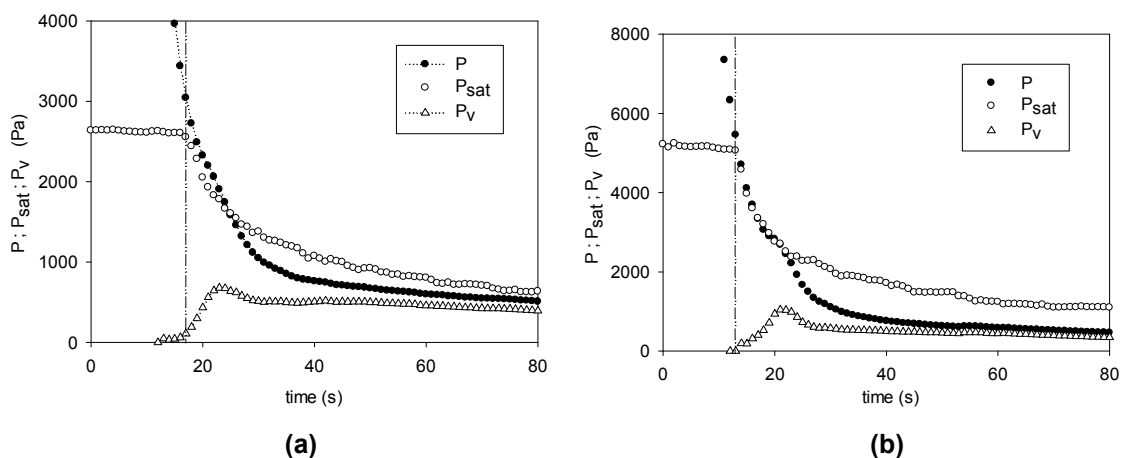
The occurrence in some circumstances of a pressure undershoot when the system evolves from the FP to the RP is being an interesting research topic for several authors throughout the years. For example, Barták (1990) studied the dependence of the characteristics of this undershoot on the initial water temperature. He concluded that the evolution of LPV, including the transition between regimes, as described above, may be influenced by many other parameters in addition to the initial water temperature. The author also refers that it is very difficult to find suitable functions to describe these complex dependencies (e.g., variation of the time to FP, or the time between the FP and the RP, or the time between the FP and LM, as a function of the water initial temperature).

As previously mentioned, in normal conditions, the FP (the beginning of the sharp decrease of the water temperature) corresponds to the instant at which the saturation pressure of the water is equal to the total pressure. However, as it is possible to see from Figure IV.6, the instant at which the sudden decrease in the water temperature starts may not match precisely the moment at which the total pressure reaches the saturation pressure. For example, in the case shown in Figure IV.6(c) the FP occurs before the total pressure reaches the saturation pressure of the water at that instant. The explanation for this behaviour is related with a non-homogeneous temperature distribution throughout the liquid phase. As shown in section IV.2.2, the thermocouples used to measure the water temperature are placed very close to the water free surface and, in part due to the evaporation during the first stage of the process the water underneath the free surface may become cooler than the rest of the bulk water. This means that a significant part of the water may be at a temperature slightly higher than the temperature measured by the thermocouples and that define the saturation pressure. The nucleation of the boiling may then occur locally, at the regions warmer than the upper layer of liquid. The vapour production associated with the beginning of the boiling process may then start before the total pressure reaches the saturation pressure, evaluated from the temperature given by the thermocouples. The greater is the total amount of the water, the greater will be the amount of water warmer than the upper layer of the liquid, as greater will be the overshoot in the vapour

production and the change in the ratio of the variation of the total pressure (see Figure IV.6). It should be noted that 1 °C is enough to justify the observed gap between the total and saturation pressures.

When the initial temperature of the water increases, the duration to the first stage of the process is shortened because the saturation pressure is higher. Besides, the undershoots of the vapour pressure are also higher, when compared with those of situations of lower initial temperature. It is also possible to see that, contrarily to what happens for the initial temperature of 22 °C, for higher temperatures the beginning of the FP occurs when the total pressure reaches the saturation pressure. It seems apparent that, for higher initial temperatures of the water the referred non-homogeneous distribution of the water temperature is not observed. In fact, while for the previous situation ( $T_{w,0} = 22\text{ °C}$ ) the water is almost in thermal equilibrium with the VC temperature, for the later situation ( $T_{w,0} = 34\text{ °C}$ ) there is no thermal equilibrium. This deviation from the thermal equilibrium tends to create convection currents within the bulk water that contribute for the homogenization of its temperature. For this reason, the FP will occur when the total pressure matches the saturation pressure and, once the whole mass of water is approximately in same conditions, a generalized (throughout the all volume of the liquid water) boiling phenomenon occurs with an increased vapour production.

The larger is the initial amount of the water, the sharper will tend to be the undershoot of the vapour pressure and higher will be the difference between the total pressure and the saturation pressure at the FP.



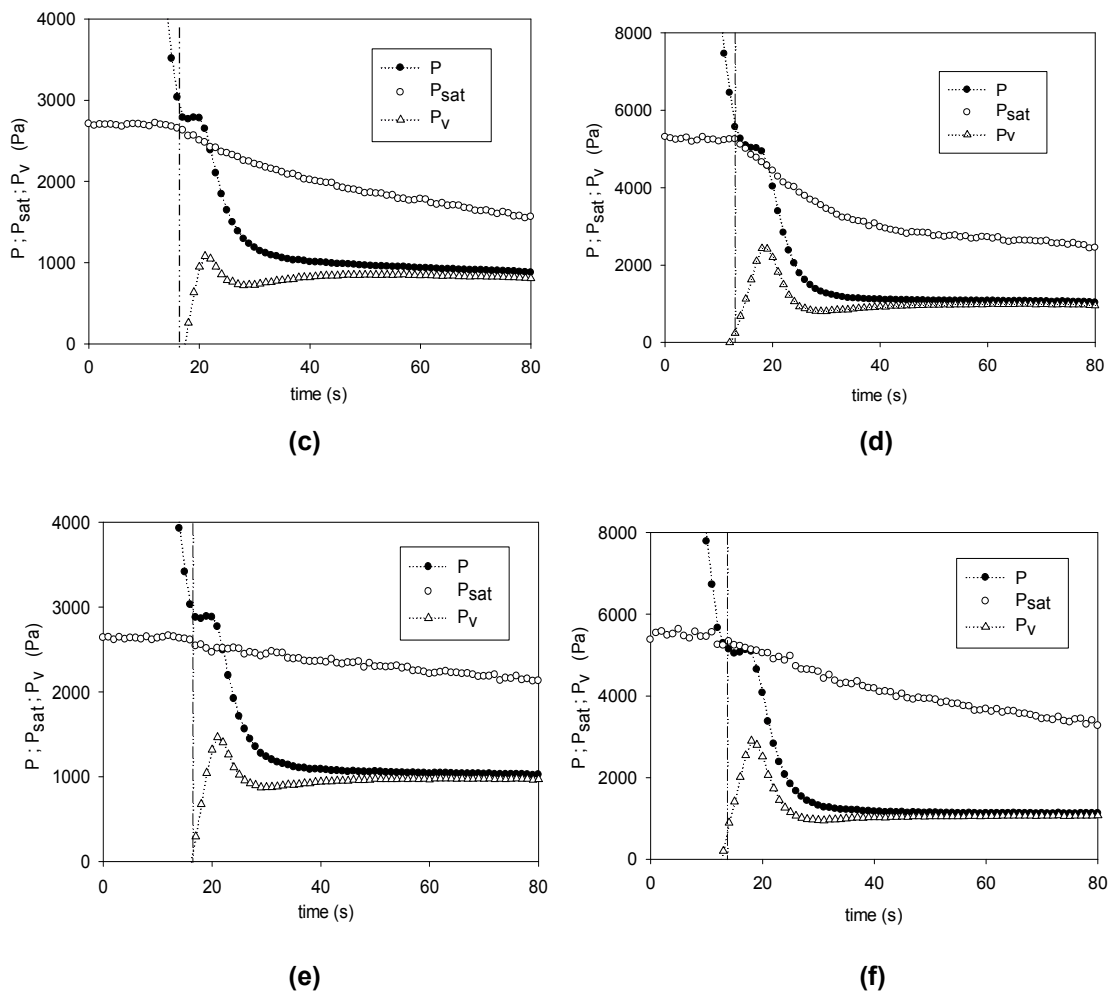


**Figure IV.6.** Evolutions of the total pressure, saturation pressure and vapour pressure for **(a)**  $V_{w,0} = 10$  ml,  $T_{w,0} = 22$  °C; **(b)**  $V_{w,0} = 10$  ml,  $T_{w,0} = 34$  °C; **(c)**  $V_{w,0} = 200$  ml,  $T_{w,0} = 22$  °C; **(d)**  $V_{w,0} = 200$  ml,  $T_{w,0} = 34$  °C; **(e)**  $V_{w,0} = 800$  ml,  $T_{w,0} = 22$  °C; **(f)**  $V_{w,0} = 800$  ml,  $T_{w,0} = 34$  °C (The vertical line (---) indicates the FP point).

### IV.3.2 Mass of the water vaporized in LPV

Within the wide range of applications where the LPV may be useful (see references cited in section 1), one of the most interesting characteristics of this process is the ability to increase the vaporization rate in comparison with normal thermally activated processes. Figure IV.7 shows the evolution of the cumulative mass of the vaporized water  $m_{w,v}(t)$  (as calculated with Eq.(IV.1)) for different initial volumes and temperatures of the water. Regardless the initial conditions, the cumulative vaporized water shows a logarithmic behaviour. It is also possible to see that the amount of water vaporized depends significantly on the initial volume (or mass) of water, increasing with it and being more pronounced for higher initial temperatures. This dependence is not,

however, proportional to the initial mass of water. While the initial mass of water increases eighty times (almost two orders of magnitude), the mass of water vaporized increases almost twenty times (typically one order of magnitude). The explanation of this behaviour can be made based on a single parameter: the superheating degree of the water. Note that the saturation pressure is evaluated from the water temperature and so, if  $P_{\text{sat}}$  is higher than  $P_v$ , the temperature of the water will be higher than the temperature that makes the saturation pressure equal to the vapour partial pressure, so it may be classified as superheated water. The superheating degree  $\phi$ , is defined as the difference between the saturation and the vapour pressures within the VC ( $\phi = P_{\text{sat}} - P_v$ ), and it is the driving force of the vaporization process. This means that the rate of vaporization is a function of the superheating degree. On the other hand,  $\phi$  is essentially determined by the pressure and temperature of the water, since the temperature determines the saturation pressure and the pressure is determined by the vapour and air partial pressures and by the height of the water column. For small initial volumes of water (also, small height of the water column), at each instant, the values of pressure and temperature, and so the value of  $\phi$ , are expected to be the same throughout all the water volume. However, for higher volumes (greater height of the water column), the vapour pressure variation due to the water column and the temperature variation due to differential vaporization rates may be significant. Thus, Saury et al.(2005) also reports, larger water volumes and increasing heights lead to smaller medium superheating degrees and, consequently, smaller water vaporization rates per unit of mass.

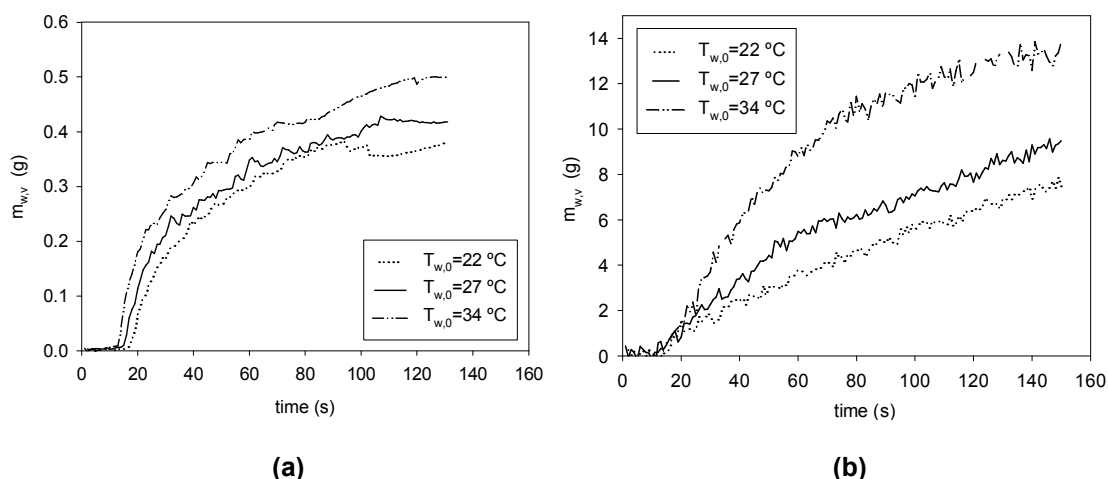


**Figure IV.7.** Evolution of the mass of water vaporized for several initial water temperatures and for **(a)**  $V_{w,0} = 10$  ml; **(b)**  $V_{w,0} = 800$  ml.

Nevertheless, the amount of water vaporized up to a certain moment of the process may be expressed as a function of the initial temperature and volume of the water. Figure IV.8 shows how the mass of water vaporized,  $m_{w,v}^f$  changes with  $T_{w,0}$  and  $V_{w,0}$  for two volume ranges studied. As can also be seen in Figure IV.8,  $m_{w,v}^f$  increases with both  $T_{w,0}$  and  $V_{w,0}$ , but more intensely with the latter. This situation was expected because, as it can clearly be seen from the graphs of Figure IV.6, the higher are  $T_{w,0}$  and  $V_{w,0}$ , the higher is the average superheating degree, and more vigorous is the boiling phenomena stimulating the vapour production.

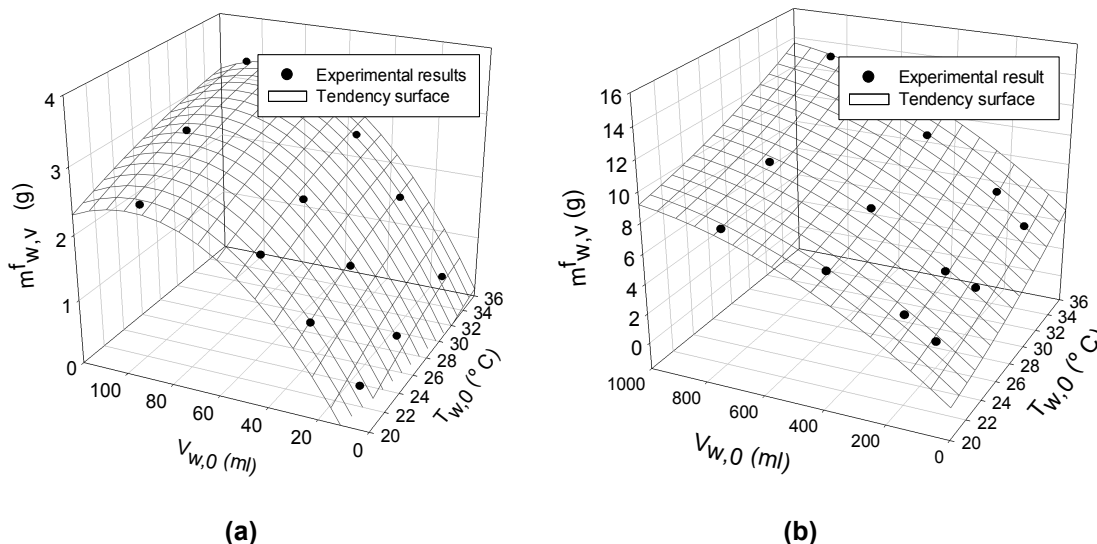


**Figure IV.8.** Plots and tendency surface of the variations with  $V_{w,0}$  and  $T_{w,0}$  of the total mass of water vaporized, for the sets of experiments in the lower and higher volume ranges, respectively:

(a) container C1; (b) container C2.

As described in sub-section IV.2.2, the experiments were carried out with two containers with different geometry and dimensions (free surface area vs. height), each one being used for a specific range of the initial water volume. However, both containers were used for the experiments performed with a particular common value of initial water volume:  $V_{w,0} = 100$  ml. The initial height of the water column for these two cases was 0.037 m and 0.017 m, for C1 and C2, respectively. The pressure of the water column above a certain value within the bulk liquid water works to reduce the superheating degree. Thus, for the same water volume, smaller container height lead to smaller average superheating degrees and to smaller vaporization rates and, consequently, to higher temperatures of the water along the LPV process. Figures IV.9 and IV.10 show,

respectively, the evolutions of the water temperature and of the total pressure in the VC for two different initial temperatures of the water and for each of the two containers used. The results corroborate the above proposed explanation.

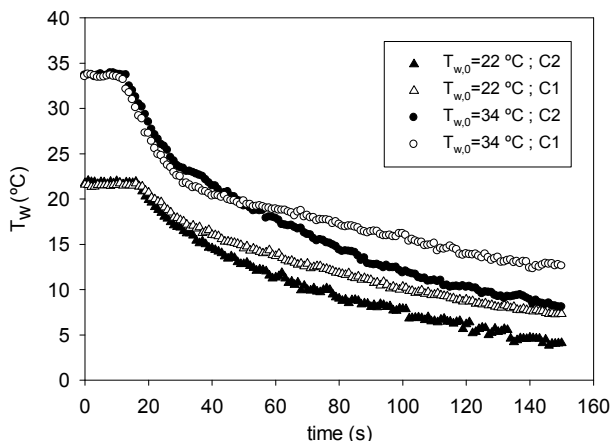


Figure IV.9. Water temperature evolution within the containers C1 and C2 for  $V_{w,0} = 100\text{ ml}$  and two initial water temperatures ( $T_{w,0} = 22$  and  $34\text{ °C}$ ).

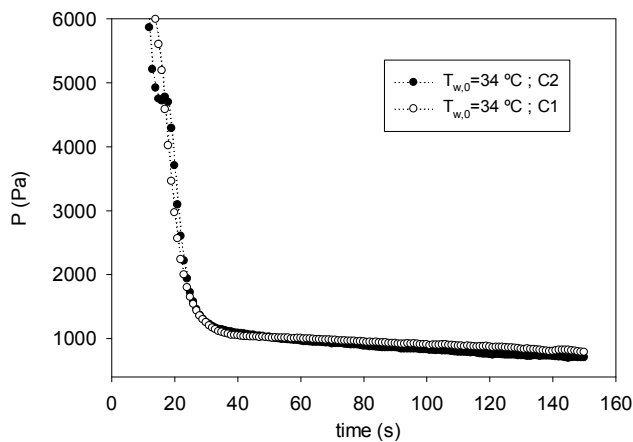


Figure IV.10. Total pressure evolution for the two containers C1 and C2,  $V_{w,0}=100\text{ ml}$  and  $T_{w,0} = 34\text{ °C}$ .

#### IV.4.Conclusion

An experimental study was performed of the influence of the initial volume ( $V_{w,0}$ ) and temperature ( $T_{w,0}$ ) of the water on the evolution and characteristics of the low-pressure-vaporization (LPV) process in order to understand its different stages and regimes.

The results show that  $V_{w,0}$  and  $T_{w,0}$  have great influences on the water temperature and pressure (total, saturation and vapour partial pressure) evolutions, as well as on the times for the stage and process changes ( $t_{FP}$ ,  $t_{RP}$ ). The main findings of this study are:

- The smaller is the initial volume and the higher is the initial temperature of the water, the sharper is the water temperature drop after the flash point (FP);
- The increase of both the initial temperature and the initial volume of water leads to a decreasing of  $t_{FP}$  and  $t_{RP}$ ;
- The initial volume of the water has much more influence on the temperature evolution than its initial temperature;
- The observed pressure evolution shows that the LPV process is divided in two stages, the second one being itself divided in two regimes. The first of these regimes is characterized by an intense boiling throughout the bulk liquid water and the second one is characterized by a much less pronounced boiling vaporization localized underneath the liquid free surface;
- The larger is the initial volume of the water, the higher is the superheating degree and likewise the rate of vapour production per unit of mass of water, and the steeper will be the change in the reduction trend of the total pressure.

It was also possible to verify that, the higher are  $V_{w,0}$  and  $T_{w,0}$ , the higher is the total mass of water vaporized up to a certain moment of the LPV process. For the same initial conditions, the evolutions of the water temperature and pressure as well as of the mass of vaporized water are affected by the height of the bulk liquid.

These findings are relevant in what refers to the several practical applications of the LPV process in order to tune the initial conditions towards specific process optimization on a physical basis.



---

## **V. Physical and experimental calibration of a mathematical model of the low-pressure-vaporization of free water**

---

This chapter reports the procedure used for the calibration of a model of the low-pressure-vaporization in free water previously developed by the authors. This calibration includes the determination of the time to the flash point, the time to the transition between the first and the second boiling regimes, the difference between the liquid-vapour interface pressure and the pressure experimentally measured in the free space of the vaporization chamber, which allowed the definition of the vaporization coefficient  $\varepsilon$ , and the volume of the vaporization layer. The influence of the initial volume and temperature of the water on these parameters is also determined. For this purpose, a set of multivariable functions were determined from a series of experiments, with different initial water temperatures and volumes.

The experimental set-up comprises two main components: the vaporization chamber (VC) and the depressurization system (DS). Part of the VC volume is occupied by an open container for the water, which was isolated from the VC walls. Two different containers were used having different surface areas and heights, both with a negligible heat capacity.

The results obtained show that the functions determined for all the referred parameters are in a good agreement with the experimental results.

*Keywords:* Low-pressure-vaporization; water vaporization modelling, model calibration, vaporization coefficient; vaporative layer, free surface vapour pressure.

## V.1. Introduction

---

As described in a previous work by the authors (Augusto et al., 2012) and in several others (Saury et al., 2005, 2002; Bouchama et al., 2003; Mutair and Ikegami, 2012), the low-pressure-vaporization (LPV) is a fast phase-change process with characteristics suitable for a wide variety of applications that demand for enhanced heat transfer and water vaporization processes. For example, Muthunayagam et al. (2005b) used the low-pressure-vaporization of saline water for the production of potable water achieving a significantly good yield. Gude and Nirmalakhandan (2009) focused their study on the development of a prototype for a new phase-change desalination process to produce potable water from impaired or saline waters and, in contrast with traditional phase-change processes, they have found that this can be operated in the range of 45–50°C. Other works put in evidence the applicability of the LPV in food and agriculture industry to dry and refrigerate different products (Bazyma et al., 2006; Nimmol et al., 2007a; Pimpaporn et al., 2007a, 2007b; Kingcam et al., 2008; Kristiawan et al., 2011). For example, the wine industry has been using the LPV to concentrate the wine and improve its quality (Sebastian and Nadeau, 2002; Tiat et al., 2008). LPV is also used for the improvement of the juice yield and quality, as referred by Paranjpe et al. (2012).

The deepening and the enlargement of the potential practical applications of the LPV is, however, dependent on the understanding and ability to model the phenomena and which have been the object of significant efforts of experimental and theoretical research during the last 10 years. For example, Saury et al. (2002) and Mutair and Ikegami (2009) have developed an extensive experimental work to identify and characterize the behaviour of the essential features of the LPV. Saury et al. (2002) have measured the time to the flashing point and the amount of water vaporized from layers of water, for different LPV conditions, and compared the results with those obtained for simple vaporization. They showed that the vaporization rate during the *flash evaporation* phase of the LPV is an order of magnitude higher than in simple vaporization and emphasized the importance of this feature for several practical applications.

Other authors as (Aoki, 2000; Wang and Sun, 2002a; Augusto et al., 2012) developed mathematical models to study the LPV evolution. For example, Aoki (2000) developed a detailed model for the *flash evaporation* of the water under low-pressure and studied the associated maximum heat flux, emphasizing its relevance to the aerospace technologies.

Despite of the relative success of the present models in the prediction of some characteristics of the LPV process, like the cooling capacity, most of them oversimplify its physical description due to the intrinsic complexity of the process. The consequences are normally an overestimation of the vaporization rates, which are then corrected with empirical coefficients that need to be calibrated. In most of the situations, the calibration process is done for a single coefficient and just for a certain initial condition, (see Dostal and Petera, 2004; Sun and Wang, 2004), neglecting that the LPV is on its essentially a transient process and, for this reason, extremely affected by those initial conditions, which justifies the use of non-constant, time dependent, calibration coefficients. Given so, a detailed simulation of the LPV process with such models for situations other than those of the calibration is thus impossible.

One of the most common simplifications made when modelling the LPV process consists of ignoring the initial vaporization stage (before the flash point) and of considering a single boiling regime for the second stage. The first stage, characterized by a diffusion vapour transport ruled the evaporative process, is often ignored because its consequences on the liquid water temperature are minimal. However, the consequences on the total time of the process are not negligible (Augusto et al., 2012). The duration of this first stage (i.e., the time to the flash point) is dependent on the characteristics of the depressurization system and of the vaporization chamber, but also on the initial volume and temperature of the water; and this dependence needs to be calibrated. It is also known that the second stage of the LPV is characterized by two different boiling regimes: a first regime of exuberant boiling (just after the flash point), followed by a second, weaker one. The time of transition of the LPV process from the first to the second regime depends also on the initial volume and temperature of the water and likely needs to be calibrated.

Another very common simplification is to assume that the vapour pressure in the vaporization chamber is homogeneous and in equilibrium with the liquid water phase present in the chamber (Augusto et al., 2012). Nevertheless, it is known that there is a vapour pressure gradient in the chamber above the water free surface of the water in the chamber (Eames et al., 1997; Saury et al., 2002). It is the vapour pressure at the interface (free surface vapour pressure) that is in equilibrium with the liquid phase and determines the rate of vaporization. This means that whenever this vapour pressure value, by the action of the depressurization system, decreases bellow the saturation pressure at the liquid water temperature a certain part of that liquid water vaporizes to bring the free surface vapour pressure to equilibrium with the saturation value. This

vapour pressure is known to decrease gradually along a layer (named vaporization layer) formed above the water free surface, down to a uniform value equal to the one experimentally measured. The thickness or volume of this layer and the magnitude of the difference between the free surface vapour pressure and the one effectively measured are thought to change with the process evolution and to be dependent on the initial conditions of the process; therefore they need to be calibrated.

The purpose of this work is to present the calibration procedure developed for the particular case of our model (described in Augusto et al. 2012) and experimental set-up, but easily adaptable to other LPV models and experimental installations. It includes the calibration of: i) the time to the flash point; ii) the time to the instant of transition from the first to the second regime of boiling in second stage; iii) the difference between the water-vapour interface pressure and the one experimentally measured and iv) the volume of the vaporization layer all of them as a function of the initial water volume and temperature.

With such calibration procedure the model will be able to cover all stages and regimes of the LPV process as well as a wide set of different initial temperature and volume conditions, providing an optimization tool for a large range of applications involving heat removal or temperature control in the food industry.

## **V.2. Mathematical model of the low-pressure-vaporization in free water**

---

The mathematical model to be calibrated in this work is a slightly different version of the one described in Augusto et al. (2012). In this model, the low-pressure-vaporization system is divided into two control volumes (CV): the CV1 that comprises the liquid water, considered with a uniform temperature throughout its volume and the CV2 that defines the region of the chamber above the liquid free surface. This CV2 also included the depressurization system (DS). In the original version of the model, the properties of the air and of the water vapour in this region (above the water free surface), during the second stage of the LPV process (after the flash point), were considered homogeneous. Both control volumes were considered adiabatic and assumed to be in equilibrium with each other. This means the assumption of thermodynamic equilibrium between gaseous and liquid phases of the water so that the two phases would be instantaneously at the same temperature. The model used the vapour pressure within the CV2 to determine the vaporization rate: whenever the vapour

pressure in CV2 drops below the saturation pressure, the water from the CV1 vaporizes, tending to raise the vapour pressure towards equilibrium with the saturation value. It is this vaporization process that removes the energy from the liquid phase and produces its temperature decrease.

Despite being a very common simplification and of being used by us in the original version of the LPV model, the authors found experimental evidences, like other researchers (Eames et al., 1997; Saury et al., 2002), that the vapour pressure is not homogeneous all over the VC and a vapour pressure gradient is developed above the water free surface, i.e., in the region here named vaporization layer, whose dimension depends on the initial conditions and will change with time. The pressure decreases from a maximum, at the liquid water free surface, where the phase equilibrium is established, to a significantly smaller value that coincides with the experimentally measured.

To describe the vapour pressure decay within the vaporization layer, a parameter named vaporization coefficient ( $\varepsilon$ ) is used. This coefficient establishes a relation between the vapour partial pressure within the vaporization layer  $P_v$  and the vapour partial pressure in the free layer  $P_{v,FL}$ , i.e. just above the vaporization layer, as defined in Eq.(V.1) and schematically represented in Figure V.1. The vaporization coefficient  $\varepsilon$  can be used to characterize the phase change in process; it accounts for deviations related with disregarding molecular collisions and the effects of polarity and molecular orientation, above all, with details in the experimental apparatus. It is inversely related with transfer resistances in the vaporization layer. So, the vaporization coefficient decreases from a value equal to unity at the upper limit of the vaporization layer to a minimum at the liquid-vapour interface, which depends on the surface temperature and specific properties of the water:

$$\varepsilon(z) = \frac{P_{v,FL}}{P_v(z)}. \quad (V.1)$$

Accordingly, in the second stage of the LPV process, the CV2 will be divided into two parts, as schematically represented in Figure V.1. The CV2' comprises the vaporization layer, where the vapour partial pressure ranges from the vapour pressure  $P_{v,FS}$  at the water free surface, to the vapour pressure in the free layer  $P_{v,FL}$ . The free layer, or CV2'', comprises all the space of CV2 beyond the vaporization layer, wherein

the vapour partial pressure takes a uniform value of  $P_{v,FL}$ . The volume of CV2' will be identified by  $V_{VL}$ , while the volume of CV2'' will be designated as  $V_{FL}$ .

In this upgraded model, the driving force for the vaporization is the difference between the free surface vapour pressure  $P_{v,FS}$  and the saturation pressure  $P_{sat}$  at the water temperature. However  $P_{v,FS}$ , depends on the  $P_{v,FL}$  through the vaporization coefficient at the liquid-vapour interface,  $\varepsilon_{z_0} = \varepsilon(z = 0)$ . This dependence is affected, as referred before, by the process initial conditions and time evolution, i.e.,  $\varepsilon_{z_0} = \varepsilon(t, V_{w,0}, T_{w,0})$  and needs to be calibrated.

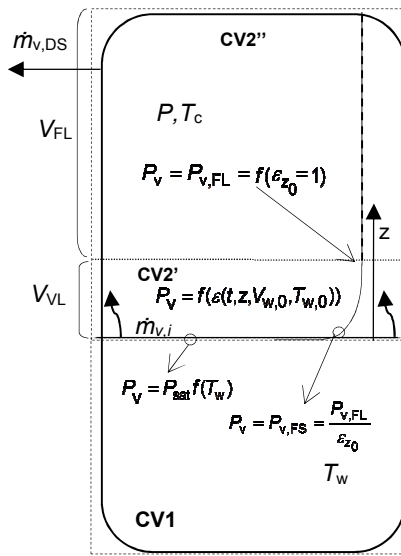


**Figure V.1.** Schematic representation of the physical model during second stage of the LPV in free water.

Like in the original model, ideal gas behaviour is assumed for each of the gaseous mixture components in the vaporization chamber. Thus total pressure  $P$  in the vaporization chamber is equal to the sum of the partial pressures of the air  $P_a$  and of the water vapour  $P_v$ :

$$P = P_a + P_v, \quad (V.2)$$

the rate of variation of the air partial pressure being given by:

$$\frac{dP_a}{dt} = -\frac{\dot{V}_e P_a}{V_{FL}}, \quad (V.3)$$

where,  $V_{FL}$  is the volume of the free layer the chamber and  $\dot{V}_e$  is the volume flow rate of the depressurization system, considered constant.

Similarly, the rate of variation of the vapour partial pressure is given by:

$$\frac{dP_v}{dt} = \frac{\dot{m}_v RT_c}{M_v V_{FL}}, \quad (V.4)$$

where  $M_v$  is the vapour molar mass,  $R$  the universal ideal gas constant,  $T_c$  the chamber temperature and  $\dot{m}_v$  the rate of change of the mass of water vapour, given by:

$$\dot{m}_v = \frac{dm_v}{dt} = \dot{m}_{v,i} - \dot{m}_{v,0}, \quad (V.5)$$

where  $\dot{m}_{v,0}$  is the mass flow rate of vapour extracted by the depressurization system, given by :

$$\dot{m}_{v,0} = \dot{m}_{v,DP} = \dot{V}_e \cdot \rho_v, \quad (V.6)$$

with,

$$\rho_v = \frac{P_v M_v}{R \cdot T_c}. \quad (V.7)$$

In the first stage of the LPV process, the vapour generation rate,  $\dot{m}_{v,i}$ , is a function of the water temperature and of the vapour partial pressure gradient above the water free surface given by (Mills, 1995),

$$\dot{m}_{v,i} = -AD \frac{M_v}{RT_w} \frac{\partial P_v}{\partial z}, \quad (V.8)$$

where  $A$  is the free-surface area and  $\partial P_v / \partial z$  is the gradient of vapour partial pressure at the water surface. The diffusion coefficient of water vapour in the air,  $D$ , is given by the Fuller-Schettler-Giddings equation (Quick et al., 2009).

For the second stage of the LPV process (after the flash point), the rate of vapour generation  $\dot{m}_{v,i}$  is mostly determined by the difference between the saturation pressure,  $P_{\text{sat}}$ , and the free surface vapour pressure,  $P_{v,\text{FS}}$ , in CV2', and, it is evaluated through the Antoine equation (Poling et al., 2001; see. Eq.(V.9)) at the liquid water temperature:

$$\dot{m}_{v,i} = \frac{d}{dt} \left[ \frac{(P_{\text{sat}} - P_{v,\text{FS}}) V_{\text{VL}} M_v}{RT_c} \right]. \quad (\text{V.9})$$

This difference ( $P_{\text{sat}} - P_{v,\text{FS}}$ ) is here named superheating degree,  $\phi$ , and can be considered as the driving force of the vaporization process. As referred above,  $P_{v,\text{FS}}$  is determined from Eq.(V.1) at the liquid-vapour interface ( $z=0$ ), i.e.,  $P_{v,\text{FS}} = P_{v,\text{FL}} / \varepsilon_{z_0}$ . The time evolution of the water temperature can be obtained from a thermal energy balance to the CV1:

$$m_{w,0} c_p \frac{dT_w}{dt} = -\dot{m}_{v,i} h_{\text{fg}}, \quad (\text{V.10})$$

where  $h_{\text{fg}}$  is the latent heat of vaporization of water. The specific heat capacity  $c_p$  is considered constant, as well as the mass of liquid water, because the total mass of vaporized water during the process is not significant compared with the initial mass of water ( $m_{w,0} = V_{w,0} \cdot \rho_w$ ), as it was experimentally verified.

### V.3. Experimental calibration methodology

---

#### V.3.1 Experimental details

The raw data needed for the calibration of the model are the initial conditions of each experiment and the time evolution of  $T_w$  and  $P$ . Thus, the experimental work plan involved the variation of the initial volume ( $V_{w,0}$ ) and temperature ( $T_{w,0}$ ) of water, as shown in Table V.1. In order to avoid great differences in the ratio of volume to free surface area of the water, two containers were used for the lower and higher water

volume levels, leading to water free surface areas of 0.0027 m<sup>2</sup> for container C1 and 0.0058 m<sup>2</sup> for container C2, respectively.

In each experiment the time evolutions of the water temperature  $T_w$  and of the total pressure  $P$  in the VC were directly measured. The partial vapour pressure in the VC,  $P_v$ , was obtained indirectly by performing a so-called reference dry experiment. In this test, the water was replaced by an equivalent volume of a solid plastic material. Considering that, for this latter experiment, the total pressure measured within the VC is equal to the partial pressure of the air in an experiment performed with water, the difference between the instantaneous values of the total pressures of both experiments (wet and dry) will retrieve the vapour partial pressure of the test with water. For each initial condition (cf. Table V.1), the experiments were run in triplicate, including the reference dry tests. The results correspond to the arithmetic mean of the instantaneous values of those three runs. The coefficient of variation of the triplicate experiments was found to be lower than 10 % for  $T_w$  and  $P$ .

**Table V.1.** Initial conditions used in the calibration experiments.

$T_{w,0}$ (°C)	$V_{w,0}$ (ml)	C1				C2			
		10	30	50	100	100	200	600	800
21		√	√	√	√	-	-	-	-
22		-	-	-	-	√	√	√	√
23		√	√	√	√	-	-	-	-
24		-	-	-	-	√	√	√	√
27		√	√	√	√	√	√	√	√
29		-	-	-	-	√	√	√	√
30		√	√	√	√	-	-	-	-
31		-	-	-	-	√	√	√	√
34		√	√	√	√	√	√	√	√

As sketched in Figure V.2, the experimental set-up used for the calibration of the model of the LPV process comprise, as main components, a vaporization chamber (VC) and a depressurization system (DS). The VC is a stainless steel cylindrical chamber with a volume of 0.017 m<sup>3</sup> ( $V_{vc}$ ). For the purpose of the present experiments, an open container (C) for the water is placed in the centre of the VC, and isolated from its walls. The DS consists of a vacuum pump with a volume flow rate capacity of 0.0033 m<sup>3</sup> s<sup>-1</sup>, which is constant for  $P > 100$  Pa according to the manufacturer data. The temperatures of the water in the container are measured by K-type thermocouples ( $\varnothing \approx 0.5$ mm; accuracy:  $\pm 1.5$  °C; response time: 100 ms) and the chamber pressure is measured with

an *Edwards™ ASG 1000 mbar* gauge (accuracy:  $\pm 2$  mbar). These sensors are connected through a *National Instruments™* data acquisition system to a personal computer, where the data are treated and saved using a *LabVIEW™ 8.6* based software.

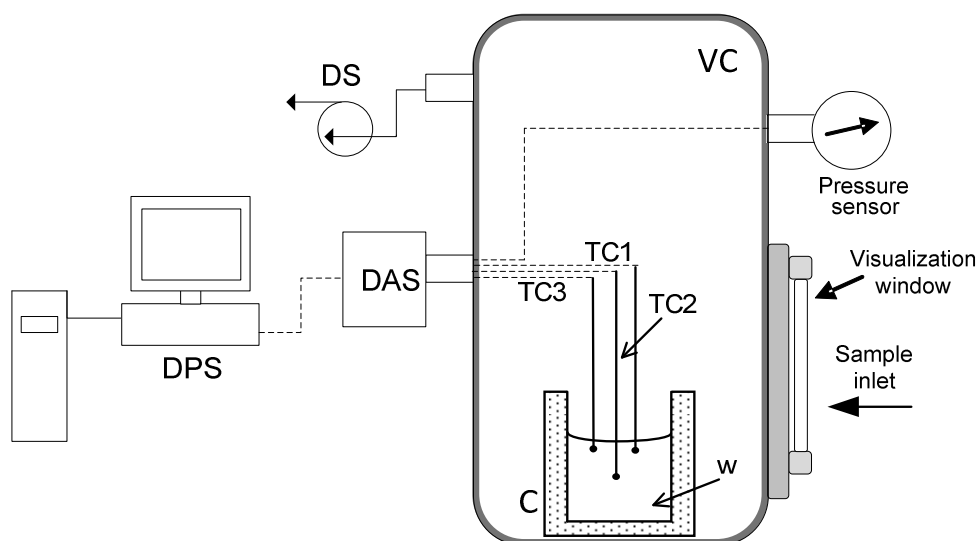


**Figure V.2.** Schematic diagram of the experimental set-up for the LPV process. (DS - depressurization system; DAS - data acquisition system; VC – vaporization chamber; C – container; W – water; DPS - Data processor and storage, TC – thermocouples).

### V.3.2 Calibration of the time to flash point and of the time of first-to-second boiling regime transition

As referred in section V.1, both the time to flash point  $t_{FP}$  and the time to the moment of transition from first to second boiling regime  $t_{RT}$  are functions of the initial conditions ( $T_{w,0}$  and  $V_{w,0}$ ) and need to be calibrated.

The flash point may be identified as the beginning of the sharp decrease of the water temperature and can be easily identified in the temperature time evolutions (see Figure V.3(a)). At this moment, the water vaporization changes suddenly from a diffusion ruled to a boiling phenomenon, with a consequent increase in the vaporization rate. The instant at which, in the second stage of the LPV process, the vaporization changes from the first to the second boiling regime is associated with an inversion in the vapour pressure evolution and can be clearly identified from vapour pressure time evolutions (see Figure V.3(b)).

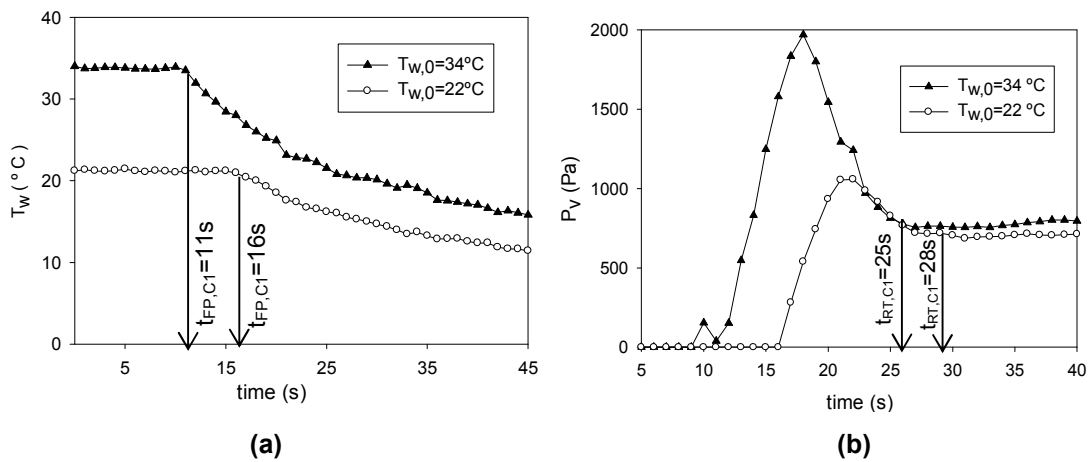


**Figure V.3.** Illustration of the (a) determination of the time to flash point and (b) determination of the time of transition the first-to-second regime of the LPV for C1.

The times  $t_{FP}$  and  $t_{RT}$  determined by this way, for the initial conditions specified in Table V.1, were then fitted by a second order polynomial function in  $T_{w,0}$  and  $V_{w,0}$ ,

$$t_{j,k} = a_1 + a_2 T_{w,0} + a_3 V_{w,0} + a_4 T_{w,0}^2 + a_5 V_{w,0}^2 \quad (V.11)$$

where  $j=\{FP;RT\}$  and  $k=\{C1;C2\}$ . The polynomial parameters are shown in Table V.2, and two examples of their graphic representation are given in Figure V.4(a) and V.4(b).

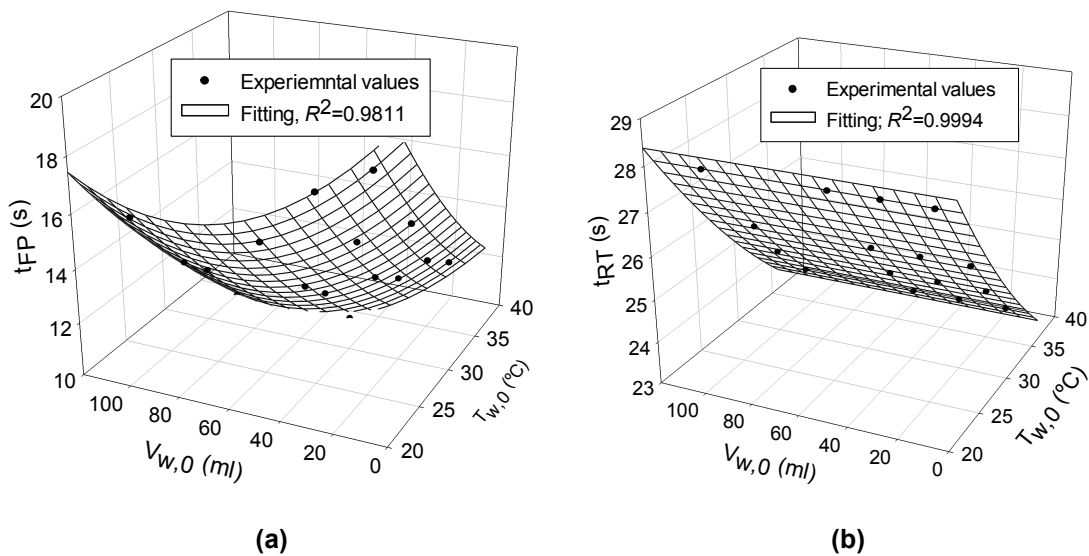


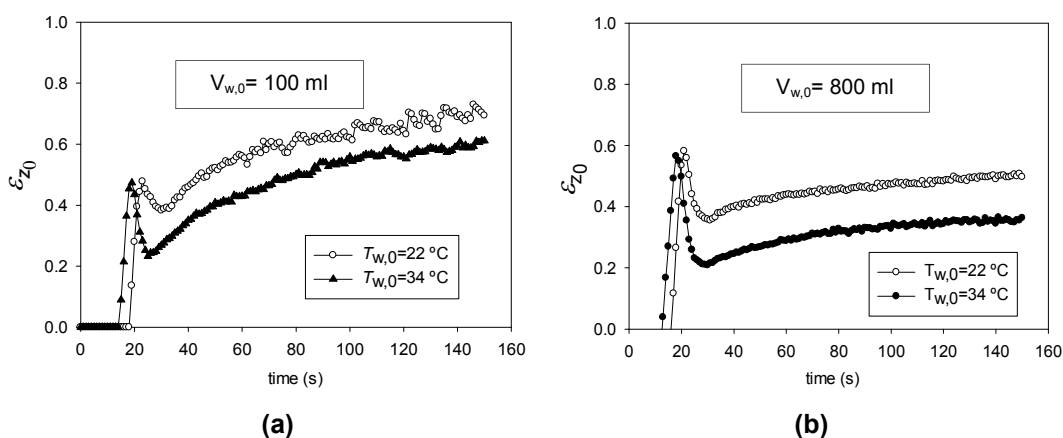
**Figure V.4.** Evolution of the (a) time to flash point and (b) time of transition of first-to-second regime of the LPV and fittings respective for C1.

**Table V.2.** Parameters values of the Eq.(V.11)

	$a_1$	$a_2$	$a_3$	$a_4$	$a_5$	$R^2$
$t_{FP,C1}$ (s)	34.8019	-0.8510	-0.1049	0.0070	0.0007	0.9811
$t_{FP,C2}$ (s)	29.8230	-0.9580	-0.0050	0.0142	2.7480E-6	0.7860
$t_{RT,C1}$ (s)	37.8554	4.7395E-14	-0.5673	-3.6605E-16	0.0047	0.9994
$t_{RT,C2}$ (s)	40.2254	-0.9000	-0.0048	0.0143	2.8627E-6	0.7307

### V.3.3 Determination of the vaporization coefficient and of the vaporization layer volume

The vaporization coefficient  $\varepsilon_{z_0}$  was experimentally determined for the several initial conditions specified in Table V.1 by measuring  $P_{v,FL}$ , as it was explain in section V.3.1, and by considering  $P_{v,FS}$  equal to  $P_{sat}$ , which is indirectly evaluated after the water temperature. The so determined values of  $\varepsilon_{z_0}$  are shown in Figures V.5(a) and (b) for two initial water volumes and two initial water temperatures. The first moments of the  $\varepsilon_{z_0}$  evolution correspond to the first stage of the LPV process, where the vaporization coefficient is almost zero. After this initial phase,  $\varepsilon_{z_0}$  increases rapidly to a maximum (absolute or local), this behaviour being associated with the characteristic onset of a strong boiling vaporization in the first regime of the second stage of the LPV process. The subsequent decrease of the  $\varepsilon_{z_0}$  values corresponds to the change from the first to the second regime. The second regime is characterized by smaller initial values of  $\varepsilon_{z_0}$ , when compared with the maximum reached during the first regime, increasing gradually with the time due to what is normally described as a weak boiling (Dostal and Petera, 2004; Wang and Sun, 2004; Augusto et al., 2012).

**Figure V.5.** Evolution of the vaporization coefficient for different initial water temperatures and volumes.

For both initial volumes, it is possible to verify that  $\varepsilon_0$  is higher for the lower initial water temperature. This is easily understandable since higher initial temperatures are expected to lead to higher vapour pressures above the liquid-water interface, i.e., to higher vapour pressures at the free surface, and so to lower  $\varepsilon_{z_0}$ .

The effect of the initial water volume on  $\varepsilon_{z_0}$  is not so clear. On the other hand, higher volumes show higher peak values during the first regime, on the other, smaller initial volumes show higher values of  $\varepsilon_{z_0}$  at the end of the LPV process. The lower temperatures of the liquid water at the end of the second regime, already expected for the smaller the initial volumes, are supposed to lead to smaller free surface vapour pressure. This may explain the higher  $\varepsilon_{z_0}$  values at the end. The higher initial  $\varepsilon_{z_0}$  peak values shown by the experiments performed with higher volumes can only be explained by an instantaneous disruption of the vaporization layer, due to the intensive boiling, which leads to an approximation between the free surface and the free layer vapour partial pressures. This disruption is expected to be greater for the experiments with higher initial volumes of water, since the ebullition is expected to be more pronounced.

The time evolutions of  $\varepsilon_{z_0}$  were found to be best fitted by a log-normal function with three-parameters, for the first boiling regime of the second stage:

$$\varepsilon_{z_0}(t^*) = \frac{a_1}{t^*} \cdot \exp \left\{ -0.5 \left[ \ln \left( \frac{t^*}{a_2} \right) / a_3 \right]^2 \right\}, \quad (t < t_{RT}) \quad (V.12)$$

and logarithmic function with three-parameters, for second boiling regime :

$$\varepsilon_{z_0}(t^*) = a_4 \cdot \ln(t^* - a_5) + a_6, \quad (t > t_{RT}). \quad (V.13)$$

The parameters  $a_i$  (with  $i=\{1$  to  $6\}$ ) in these equations depend on the initial temperature and initial volume of the water, in a way that was found to be well described by the polynomial function:

$$a_i(V^*, T^*) = X_{1i} + X_{2i}V^* + X_{3i}T^* + X_{4i}V^{*2} + X_{5i}T^{*2}, \quad i=\{1$$
 to  $6\} \quad (V.14)$

where the coefficients  $X_{ni}$  are in turn listed in Table V.3, and  $t^*$ ,  $T^*$  and  $V^*$ , respectively, are the time, the initial temperature and the initial volume of water, normalized as follows:

$$t^* = \frac{t - t_{\min}}{t_{\max} - t_{\min}}, \quad (V.15)$$

$$T^* = \frac{T_{w,0} - T_{w,0\min}}{T_{w,0\max} - T_{w,0\min}}, \quad (V.16)$$

$$V^* = \frac{V_{w,0} - V_{w,0\min}}{V_{w,0\max} - V_{w,0\min}}, \quad (V.17)$$

$T_{w,0\min}$  and  $T_{w,0\max}$  being the limit values of the range of initial temperatures considered in the experimental study, and likewise  $V_{w,0\min}$  and  $V_{w,0\max}$ , regarding the initial water volume;  $t_{\min}$  and  $t_{\max}$  are the limit values of the process time.

**Table V.3.** Values of the coefficients of the Eq.(V.12), Eq.(V.13) and Eq.(V.14).

	C1						C2					
	$t < t_{RT}$			$t > t_{RT}$			$t < t_{RT}$			$t > t_{RT}$		
	$a_1$	$a_2$	$a_3$	$a_4$	$a_5$	$a_6$	$a_1$	$a_2$	$a_3$	$a_4$	$a_5$	$a_6$
$X_{1i}$	0.0676	0.1704	0.1389	0.0860	0.1711	0.6424	0.0839	0.1562	0.1894	0.1295	0.1351	0.7217
$X_{2i}$	0.0577	-0.0185	0.0309	0.2299	-0.1158	0.768	-0.1258	-0.0241	0.0103	-0.2491	0.0097	-0.9432
$X_{3i}$	0.0034	-0.0150	0.0891	0.0130	0.0050	-0.0763	0.0132	-0.0115	-0.4203	0.0038	-0.0676	-0.1888
$X_{4i}$	-0.0513	-0.0047	0.0007	-0.1929	0.0678	-0.7562	0.1240	-0.0147	0.0248	0.1762	-0.0039	0.7091
$X_{5i}$	-0.0162	-0.0021	-0.0424	0.0046	-0.0410	-0.0623	-0.0210	-0.0153	0.3929	0.0045	0.0507	0.0773

Figure V.6 shows the fitting between the experimental and the calculated values (Eq.(V.12) and (V.13)) of the vaporization coefficient  $\varepsilon_{z_0}$  for four different initial volumes of water. The agreement between the calculated and experimental results is quite reasonable as the correlation factor ( $R^2$ ) is mostly beyond 0.9 and the average of the relative errors  $\overline{\varepsilon}_r$ , below 5 %.

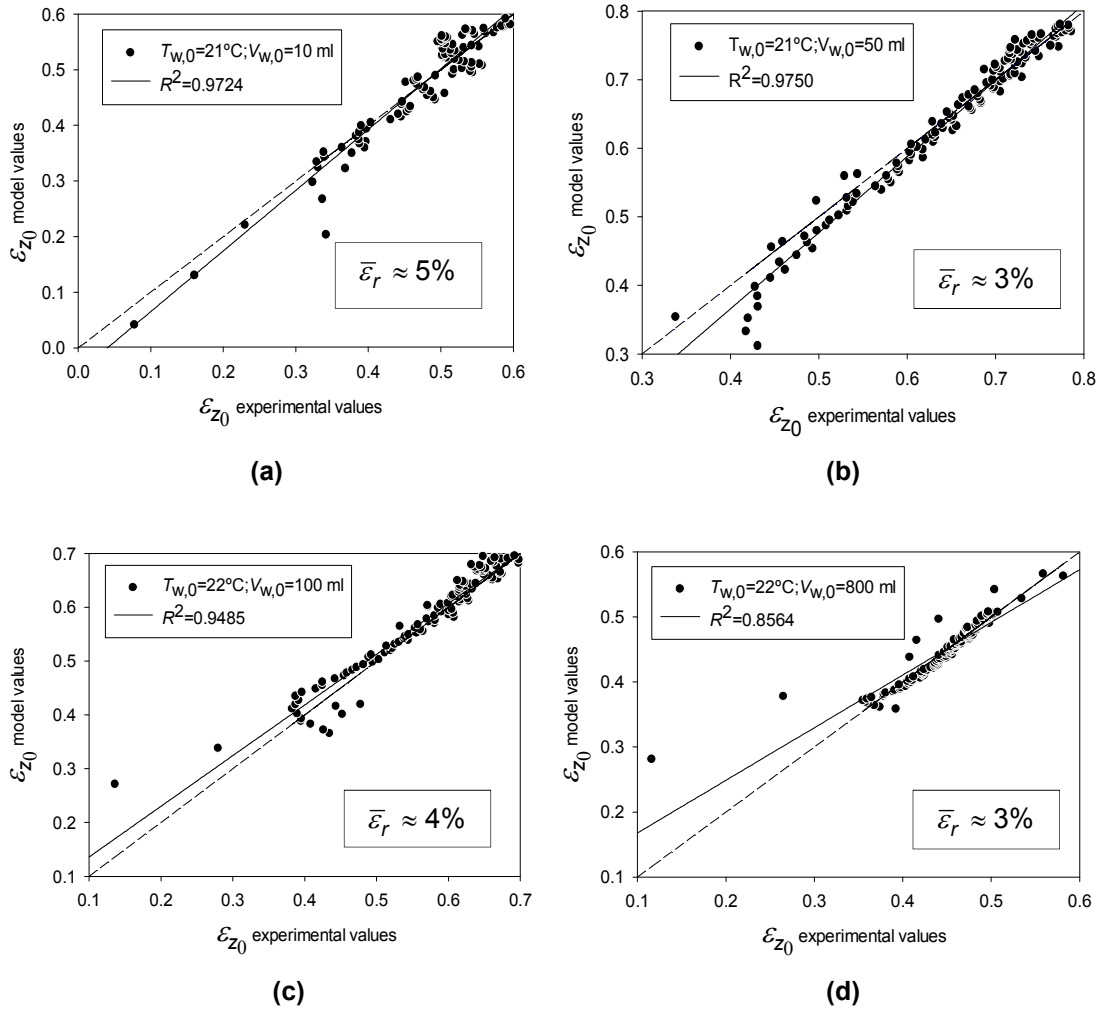


**Figure V.6.** Comparison between experimental and calibrated model values for  
**(a)**  $V_{w,0} = 10\text{ ml}$ ,  $T_{w,0} = 21^\circ\text{C}$ ; **(b)**  $V_{w,0} = 50\text{ ml}$ ,  $T_{w,0} = 21^\circ\text{C}$ ; **(c)**  $V_{w,0} = 100\text{ ml}$ ,  
 $T_{w,0} = 22^\circ\text{C}$ ; **(d)**  $V_{w,0} = 800\text{ ml}$ ,  $T_{w,0} = 22^\circ\text{C}$ .

As referred in section V.1, the volume of the vaporization layer changes with the process evolution and with the initial conditions. This volume is directly related with the vaporative transfer resistances and so it should be inversely proportional to the vaporization coefficient. Consequently, the volume of the free layer  $V_{FL}$ , complementary of  $V_{VL}$ , should be directly proportional to the vaporization coefficient and it should be possible to write:

$$V_{FL} = a_0 \cdot \varepsilon_{z_0} (t^*, V^*, T^*), \quad (\text{V.18})$$

$$V_{VL} = V_f - V_{FL}, \quad (\text{V.19})$$

where  $V_f (=V_{vc} - V_{w,0})$  is the initial free volume of the chamber. When the vaporization coefficient vanishes, the volume of the vaporization layer coincides with the initial free volume; when the vaporization coefficient increases, it is the volume of the vaporative layer that vanishes. In Eq.(V.18), the coefficient  $a_0$  needs to be calibrated. A sensitivity analysis about the  $a_0$  behaviour has shown that its value generally dependent on the initial values of the water volume and temperature as well as on the boiling regime. The determination of the optimal values of  $a_0$  for each initial condition referred in Table V.1 was made performing simulations of the process with several different values of  $a_0$  to find out which one minimize the error between the simulated and the experimental results. As a result, the variation of the calibrated  $a_0$  with the initial values of temperature and volume of the water is described by:

$$a_0 = a_1 + a_2 T_{w,0} + a_3 V_{w,0} + a_4 T_{w,0}^2 + a_5 V_{w,0}^2 \quad (V.20)$$

the coefficients being listed in Table V.4. For the lower range of the initial volume of the water (C1),  $a_0$  is independent of the initial temperature and volume in the first boiling regime, taking then a constant value.

**Table V.4.** Coefficients of Eq.(V.20).

	C1		C2	
	$t < t_{RT}$	$t > t_{RT}$	$t < t_{RT}$	$t > t_{RT}$
$a_1$	0.0159	0.0147	0.0232	0.0190
$a_2$	0.0000	0.0001	-0.0006	-0.0006
$a_3$	0.0000	8.3333E-5	-1.0037E-5	8.4309E-6
$a_4$	0.0000	1.1905E-6	5.9735E-6	1.1931E-5
$a_5$	0.0000	-3.7500E-6	6.2254E-9	-8.3041E-9

The so determined values of  $a_0$  were then used for the evaluation of the time evolutions of the volumes of the vaporization and free layers. Examples of those evolutions, for two very different initial volumes of water are shown in Figures V.7(a) and (b). As expected, the volume of the vaporization layer is symmetric to the free layer volume and to the vaporization coefficient. The reasons used to explain the vaporization coefficient behaviour with the initial values of the water temperature and volume are also valid for the behaviour of the volumes of the vaporization and of the free layers.

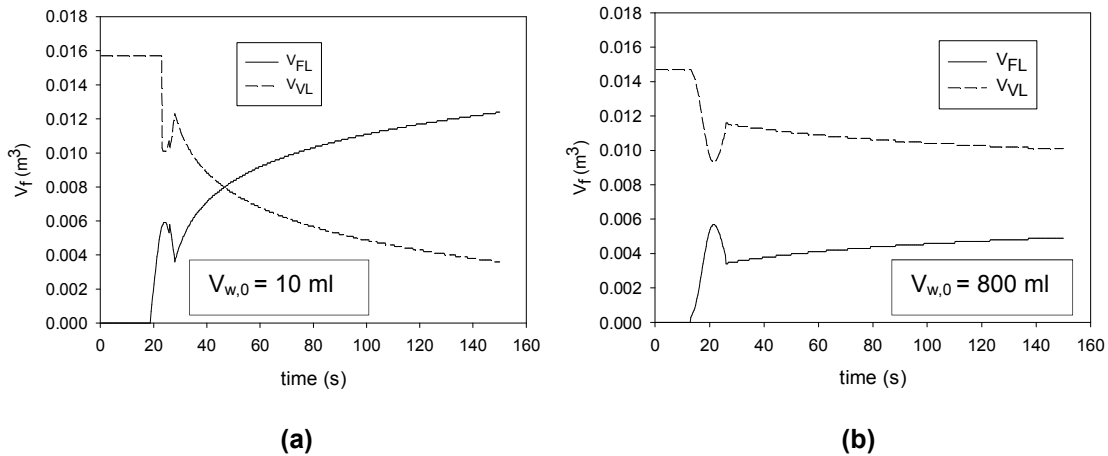


**Figure V.7.** Evolutions of the vaporization layer and free layer volumes, for  $T_{w,0} = 21$  °C, and for (a)  $V_{w,0} = 10$  ml and (b)  $V_{w,0} = 800$  ml

## V.4. Validation and insights of the calibrated model

### V.4.1 Model algorithm

The equations of the model were solved using the algorithm schematically shown in Figure V.8, implemented in *Microsoft Visual Basic 2010 Express*. The calculations are made in two steps: prior and after the flash point time,  $t_{FP}$ , the value of  $t_{FP}$  being determined for each initial condition from Eq.(V.11). The main difference between first and second stages lies on the equation used to calculate the rate of vapour generation. Eq.(V.8) is used for the first stage, assigning to the diffusion layer thickness,  $\Delta z$ , a value of 0.025 m (as discussed in Augusto et al., 2012) and Eq.(V.9) is used for the second stage. The calculations for the second stage were also divided in two steps: prior and after the boiling regime transition. The moment at which this transition occurs is given by Eq.(V.11). The transition of boiling regime implies changing the equations used for the calculation of the vaporization coefficient, from Eq.(V.12) to Eq.(V.13) and for the estimation of the calibration coefficient  $a_0$  used in the calculation of the volume of the vaporization layer (Eq.(V.20)). All the simulations were performed up to a process time of 150 seconds.

The validation of the calibration procedure was done through the comparison of the simulation results obtained using the calibrated model with the experimental results, regarding the water temperature evolutions. Besides the presentation of graphics with the direct comparison of the experimental and simulation results for some specific illustrative situations, the errors bands for 5 %, 10 % and 30 % are also shown.

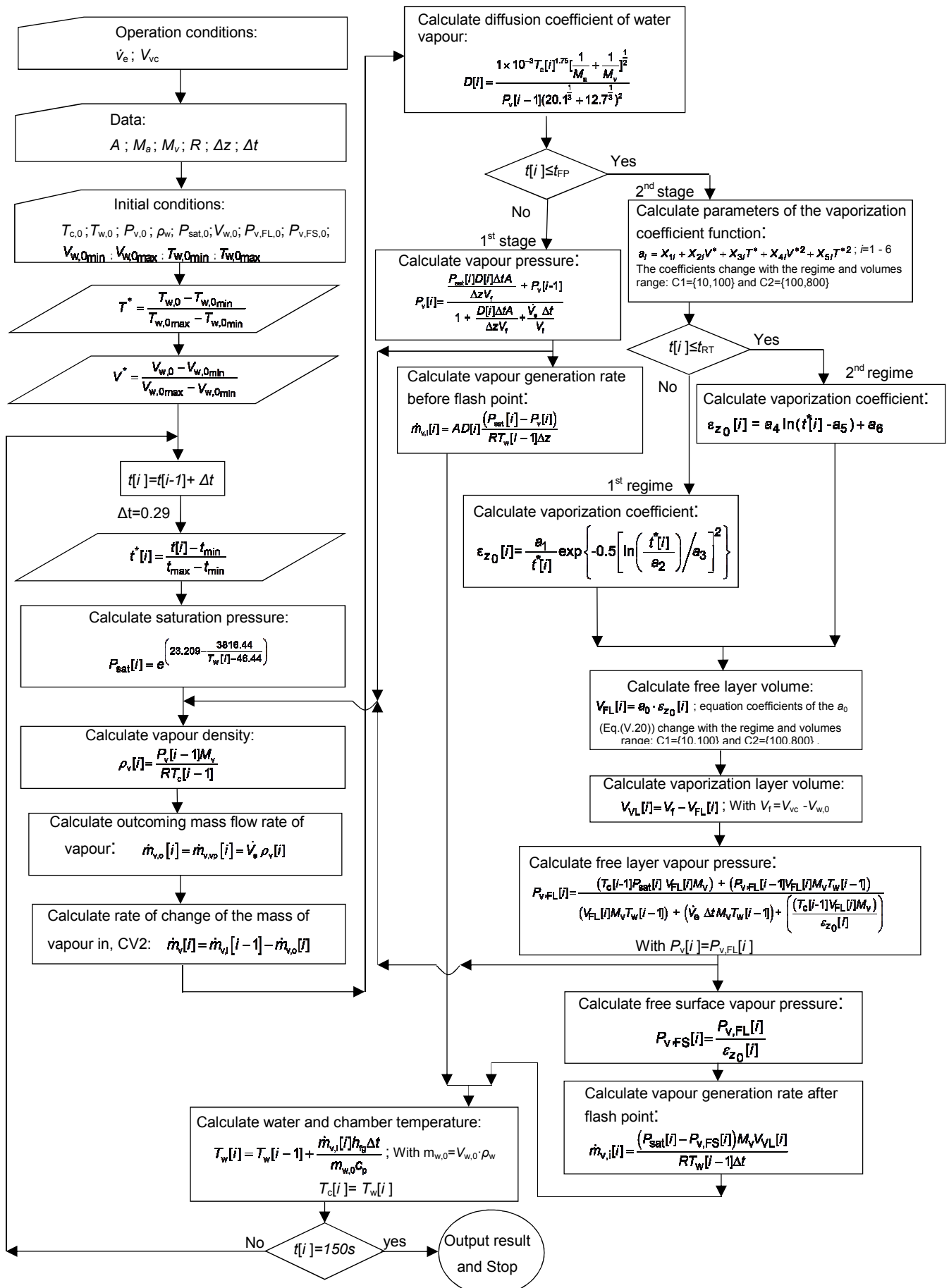
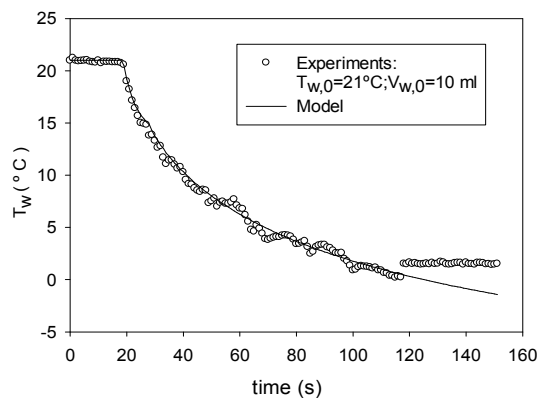
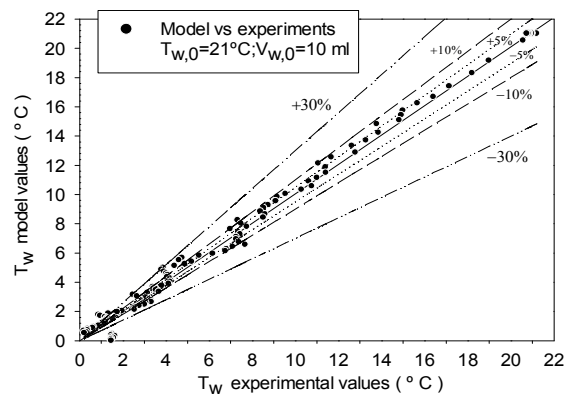


Figure V.8. Flow chart of the simulation program.

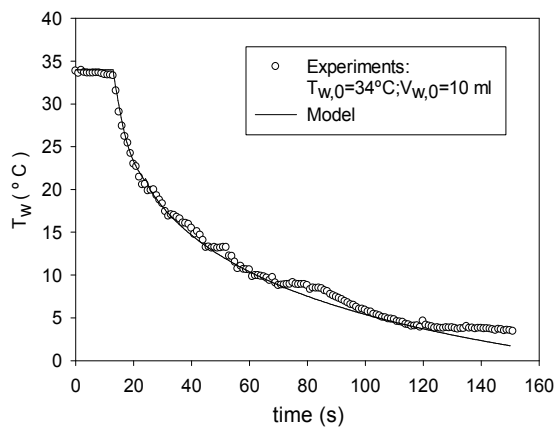
A direct comparison between experimental and simulated results of the temperature evolutions for four of the initial conditions studied in the lower range of initial volume of water (C1) is made in Figures V.9(a), (c), (e) and (g) the corresponding differences being report in Figures V.9(b), (d), (f) and (h). With the exception of the final part of the temperature decrease with an initial volume of 10 ml and an initial temperature of 21 °C (Figs. V.9(a) and (b)), and some other specific situations, the agreement between the experimental and calculated results is very good showing deviations within  $\pm 10\%$ .



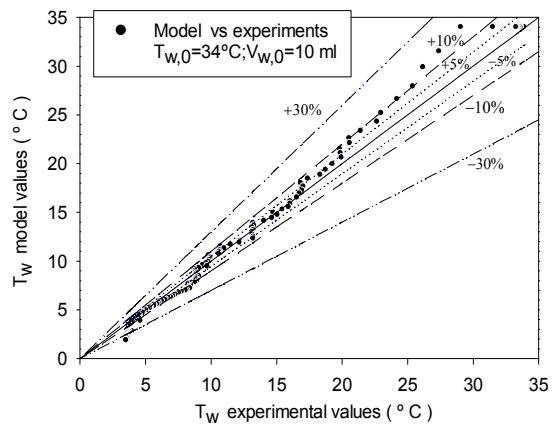
(a)



(b)



(c)



(d)

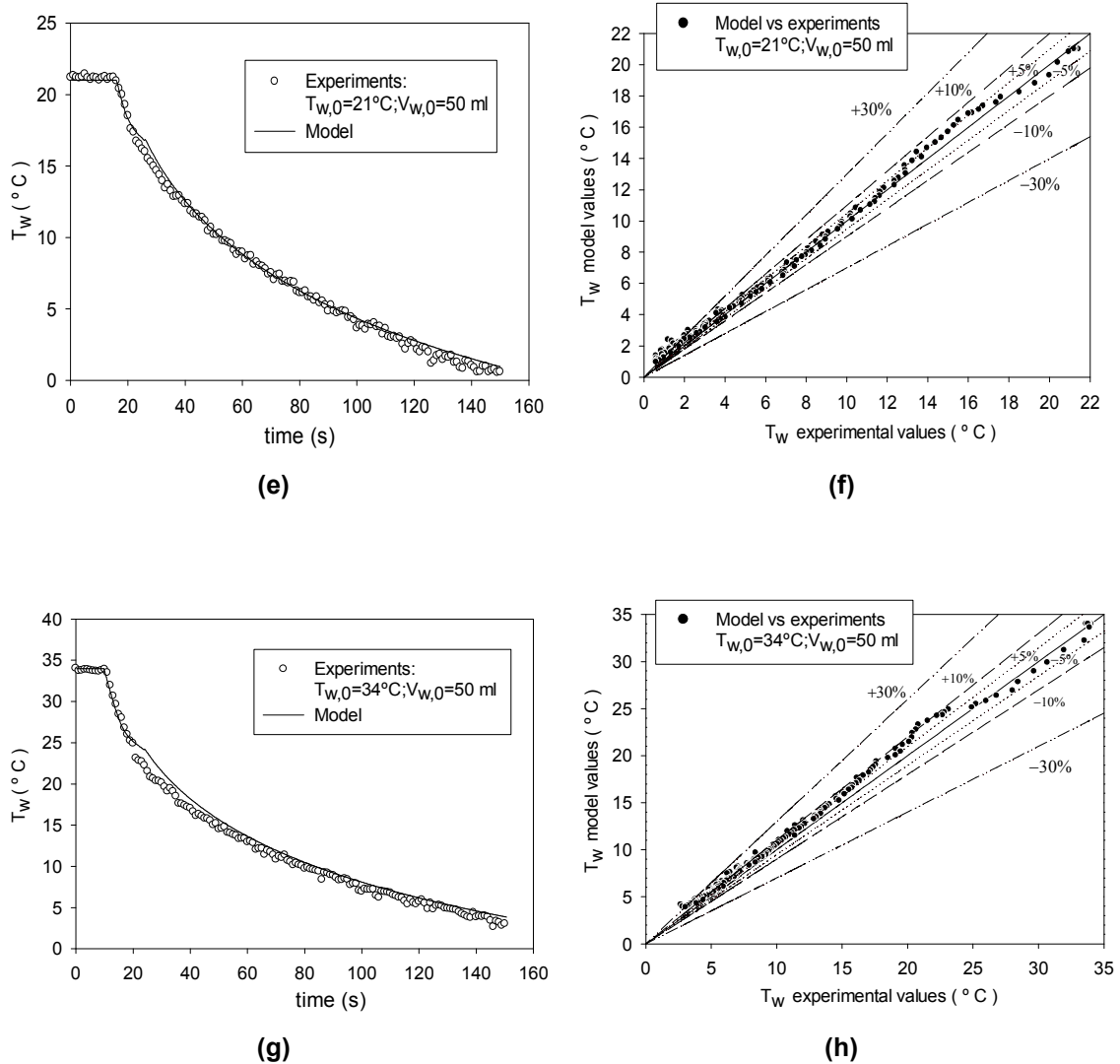
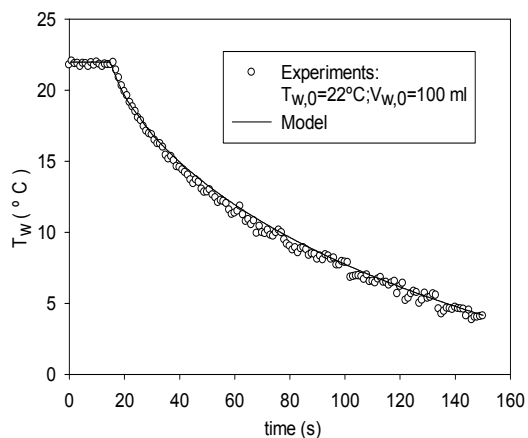
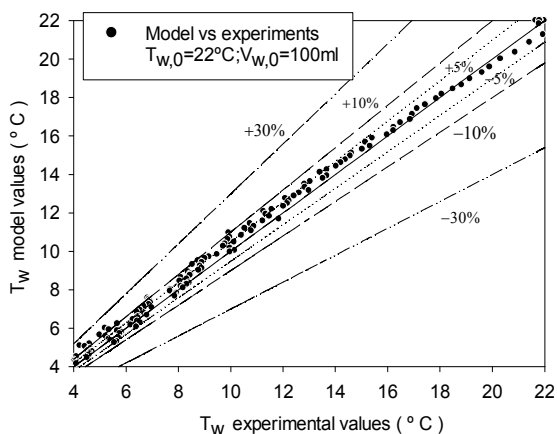


**Figure V.9.** Comparison between experimental and model results for different initial conditions of the volume range C1.

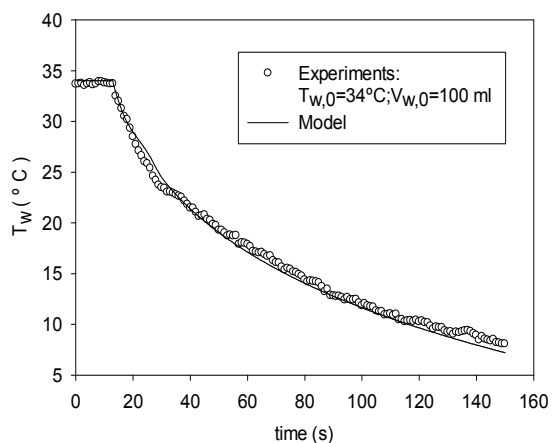
The comparison between the experimental and simulated results for the upper range of initial volume of water (C2) is made in Figures V.10(a), (c), (e), (g), (i) and (k). The corresponding differences are shown in Figures V.10(b), (d), (f), (h), (j) and (l). With the only exception of the final part of the water temperature evolution for an initial volume of 450 ml and an initial temperature of 34 °C (Figs. V.10(g) and (h)), the deviations between the experimental and calculated results are lower than  $\pm 5\%$ . The exceptional, abnormal deviation is attributed to random experimental errors.



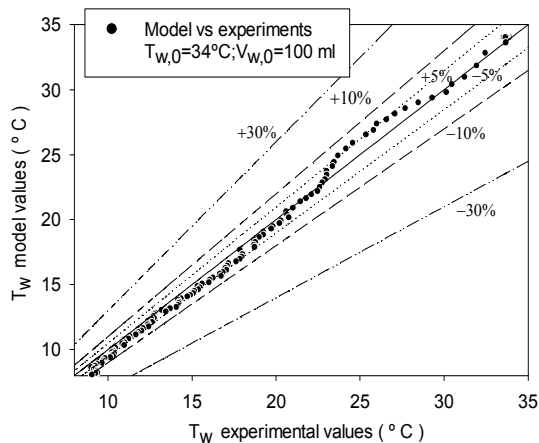
(a)



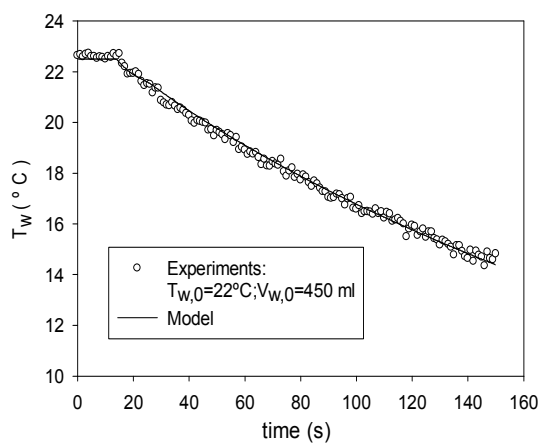
(b)



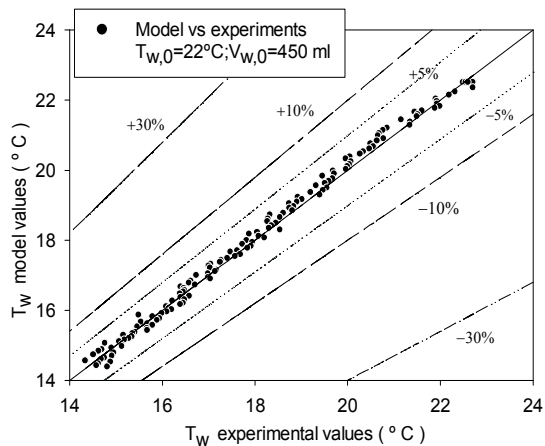
(c)



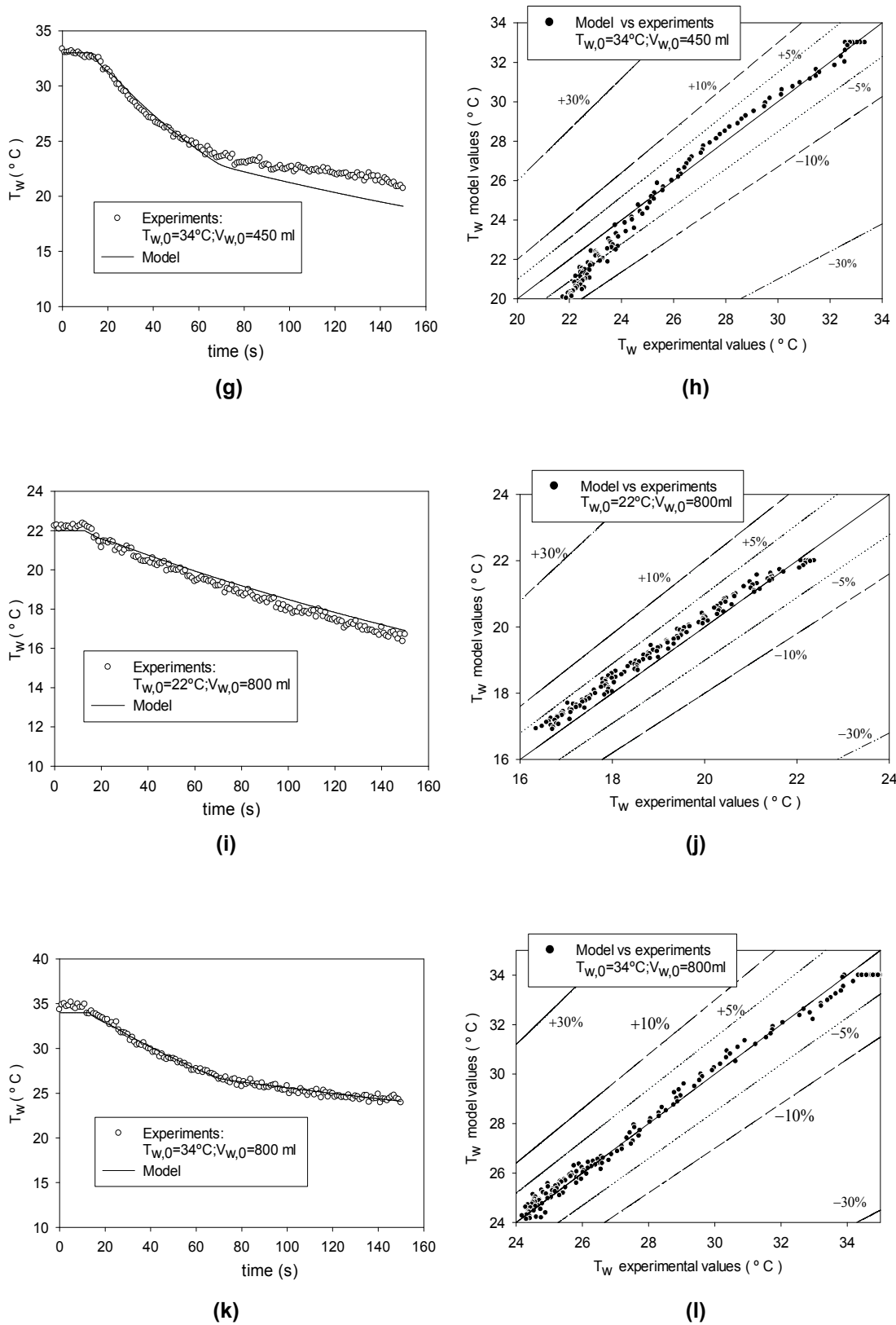
(d)



(e)



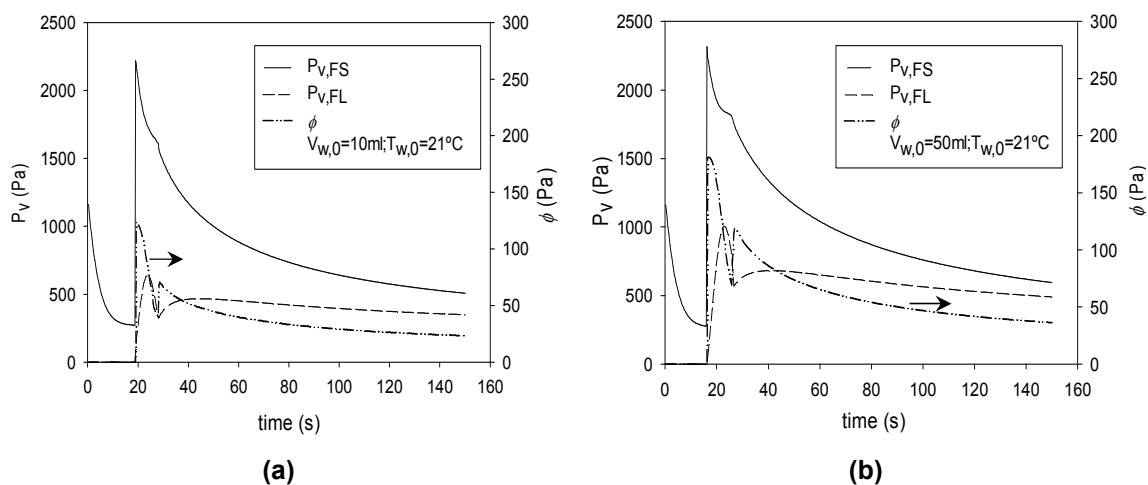
(f)



**Figure V.10.** Comparison between experimental and model results for different initial conditions of the volume range C2.

### V.4.2 Model insights

One of the essential features of the present model is its ability to calculate the vapour partial pressure above the water free surface, the so-called free surface partial vapour pressure,  $P_{v,FS}$ . The difference between this pressure and the saturation pressure at the liquid water temperature - the superheating degree  $\phi$  - is the driving force for the vaporization process and consequentially for the water temperature decrease. The value of the free surface vapour pressure is not calculated by the other known models and cannot be determined from the experimental results. The graphics of Figures V.11(a) to (d) show the time evolutions of the calculated  $P_{v,FS}$  and of the vapour partial pressure at the free layer,  $P_{v,FL}$ , as well as the superheating degree. The differences between  $P_{v,FL}$  and  $P_{v,FS}$  are evident and the shape similarity between the time evolutions of the free surface vapour pressure and the superheating degree emphasises the importance of the value of  $P_{v,FS}$  as an optimizing parameter of the LPV process, namely for the definition of the optimal regions of operation. Moreover, the analysis of the behaviour of the free surface vapour pressure variation, as a function of the initial conditions of the water temperature and volume, or others, may be used to deepen understanding of the low pressure vaporization process.



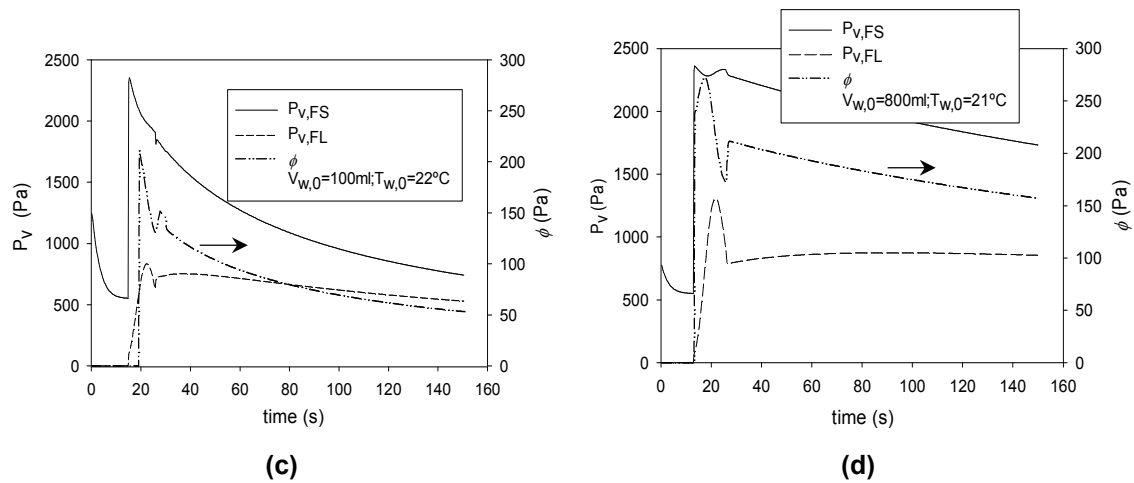


**Figure V.11.** Evolutions of the free surface and free layer vapour pressure, and of the superheat degree for several initial conditions.

## V.5. Conclusions

This chapter reports with detail the calibration procedure of an upgraded version of a previously developed mathematical model for low-pressure-vaporization in free water.

The calibration involved several important parameters:

- The time to the flash point and the time of transition from the first to the second boiling regime, which were described by a second order polynomial function in  $T_{w,0}$  and  $V_{w,0}$ , with correlation factors between 0.7 (for range C2) and 0.9 (for range C1);
- The difference between the pressure at the water-vapour interface and the pressure experimentally measured. This difference, that allowed the definition of the vaporization coefficient  $\varepsilon$ , is described through a log-normal function with three-parameters, for the first boiling regime, and a logarithmic function with three-parameters, for the second regime. The parameters of these functions were found to be dependent on  $T_{w,0}$  and  $V_{w,0}$  through a second order polynomial function. The results show that the vaporization coefficient varies strongly along the process stages and boiling regimes, and is affected by the initial temperature, and volume of water. The agreement between experimental and calculated values of  $\varepsilon_0$  shows correlation factors beyond 0.9 and the average of the relative errors below 5%;

- The volume of the vaporization layer, which changes with process evolution and initial condition, is directly related with the vaporative transfer resistance and inversely proportionally to the vaporization coefficient.

A good agreement between experimental and simulated values of the temperature evolutions is verified. The deviations between experimental and calculate results are generally 10% and 5%, respectively for range for the lower and higher ranges of the initial water volume. The present model allows the determination of important parameters, such as the free surface vapour pressure and the superheating degree, which may be used to deepen the understanding of the LPV process and so, to contribute for its application in several techniques of the specific industrial areas.

---

***Part C - Low-pressure-vaporization in porous media***

---



---

## **VI. Experimental study of the low-pressure-vaporization of water in different porous media**

---

The present chapter aims to evaluate the benefits of using porous media (PM) to enhance the rate of the low-pressure-vaporization (LPV) of water. An experimental characterization of the process of low-pressure-vaporization of water is presented considering four different types of porous media and different initial conditions. This characterization involves the measurement of the time evolution of the porous media temperature and of the total and the vapour pressure inside the vaporization chamber, as well as the indirect determination of the saturation pressure, the mass of water vaporized, its specific rate of vaporization and of the energy removed by this phenomenon. A direct comparison between the evolution of the LPV of water in porous media and the LPV of free water was also made for two selected situations. The results show that the evolution of the LPV parameters, namely the temperature decrease and the rate of energy removal, are strongly dependent on the volume of the water initially contained in the porous medium which in turn, depends essentially of the medium microstructure. The significant differences found between the evolution of the LPV parameters in free water and in porous media are related to different boiling onset mechanisms, which is strongly dependent on the surface tension of the liquid water in the whole LPV process in PM. The practical result of these effects is an increased vaporization rate and an enhanced surface heat transfer capability that justify the use of porous media in a wide variety of applications.

*Keywords:* Low-pressure-vaporization; experimental study; porous media; boiling regimes; vaporization rate

## VI.1. Introduction

---

Nowadays high capacity heat transfer techniques are quite required for non traditional industrial applications and scientific research such as nuclear power plants, solar energy concentration and conversion, freezing and refrigeration, temperature control in aviation and spaceflight and all sorts of energy conversion systems (Webb and Kim, 2005; Li et al., 2011). Some of these techniques are based on the liquid to vapour phase-change phenomenon. The low-pressure-vaporization (LPV) analysed in Augusto et al.(2012) is a very fast phase-change process, enhanced by a sharp pressure decrease and presents all the important characteristics that lead to high heat transfer rates.

As described by Mutair and Ikegami (2012), LPV is a combined heat and mass transfer phenomenon in which the liquid, initially in thermodynamic equilibrium, is exposed to a sudden pressure drop that brings it to a superheated state; i.e, with a temperature above the saturation value at that new pressure condition. In this situation the liquid is in a metastable stage and will begin to vaporize throughout all its extension to increase the total pressure over its free surface so that the phase equilibrium is again established. In this phenomenon the energy necessary for the liquid vaporization is taken from the liquid phase itself. Since the specific energy of vaporization is usually very high, the vaporization rate, essentially determined by the superheating degree which depends on the difference between the actual pressure and the saturation pressure at the temperature of the liquid phase, can also be very high, even for small pressure drops. Thus, this phenomenon can lead to high heat removal rates for which a wide range of interesting practical applications are envisaged. In chapter III (Augusto et al., 2012) the LPV process applied to free water systems (LPV-FW) was analysed, showing the LPV potential to enhance the water vaporization rate and consequently the rate of temperature decrease in the liquid water. The application of the LPV phenomenon to other situations beyond the simple temperature control of free liquid water was already envisaged as having even more potentially practical applications. As referred by Webb and Kim (2005), the application of LPV to moisture filled media applied over surfaces could be a way to overcome the problems associated with the low heat transfer coefficients in surface heat transfer processes and thus take advantage of the high heat removal rates related to the phase-change phenomenon. Webb and Kim (2005) concluded that significant improvements of the heat transfer coefficients have been achieved for specific surfaces, due to the promoted high performance nucleation of

the boiling process providing this way, an enhanced heat transfer coefficient. Porous media are a sort of material capable of promoting this enhanced boiling process. Several authors have studied the use of porous media (PM) as a way to increase the heat removal rate in several situations. For example, Figueiredo and Costa (2004) studied the use of porous media for thermal protection against high intensity heat fluxes (flames). Other authors (Meng and Hu, 2005; Zhao et al., 2008) analysed the application of porous media to temperature control in buildings. Zhao et al.(2008) investigated the heat and mass transfer properties of several different types of porous media considering its potential application in air-conditioning systems of buildings. Meng and Hu (2005) studied the possibilities of applying humid structures for the temperature control of roofs, in a process designated by passive water evaporation. For some naturally porous media, such as foodstuff (meat, vegetables and fruits) and fabrics, a few industrial applications have already been developed taking advantage from the improved heat removal rate associated with the enhanced surface boiling nucleation. The refrigeration of fruits (strawberries and melons), vegetables (lettuce, broccoli and mushrooms) and meat (ham and cooked beefs) or the quick drying of fabrics are probably the most typical examples of the technological application of this phenomenon (Mc Donald and Sun, 2000; Elustondo et al., 2002; Mc Donald et al., 2002; Bakhshi and Mobasher, 2011).

For this reason, details of the physical phenomenon associated with the water evaporation in porous media at sub-atmospheric pressures are being widely studied. For example, Elustondo et al.(2002) developed a model for moisture evaporation during drying under sub-atmospheric pressures, in which internal water is removed pushed by the movement of the solid structures of the porous media, making the vapour to flow towards the outer surface. On the other hand, Bakhshi and Mobasher (2011) conducted an experimental study of early-age drying of Portland cement paste in low pressure conditions to promote quick water evaporation. They consider that the majority of moisture transfer in porous media occurs by diffusion up to the free surface, where evaporation occurs.

However, in other published works (Udell, 1983; Yortsos and Stubos, 2001; Peng et al., 2002; Fang et al., 2004; Wang and Peng, 2004) the mechanisms behind the mass transfer are differently described: it is considered that the vaporization takes place within the pores and that the hydrodynamic movement of the water vapour within them is ruled by the pressure differences. Sun and Hu (2003) developed a computational fluid dynamics (CFD) model to simulate the heat and mass transfer within foods at low pressures, demonstrating the complexity and importance of the boiling vaporization in

pores. The studies of (Wang and Sun, 2002c; Jin and Xu, 2006a, 2006b) also focus on the importance of the dynamic of vaporization within the pores for the global process of the heat removal.

From the exposed above, the importance of the vaporization phenomena within porous media under sub-atmospheric conditions seems clear. This importance is reflected on the significant number of works trying to identifying the main characteristic parameters and the different stages of the vaporization process within porous media (Prat, 1998; Yortsos and Stubos, 2001; Peng et al., 2002; Mantle et al., 2003; Wang and Peng, 2004). Specifically, Wang and Peng (2004) presented the boiling vaporization heat transfer mode in porous media as an enhanced heat transfer technology, with a wide range of important practical applications. They referred that boiling is affected by the pore structure (pore scale and bead size), bubble growth and coalescence, pore variation and vibration. Furthermore, they highlighted the importance of surface tension on bubble shape and on the interface formation, as well as on the bubble growth. The surface tension affects the boiling phenomena and bubble growth parameters; when boiling is fully established, the number of nucleation points increases due to the decrease of surface tension. Since the rate of bubble formation is higher, the amount of water vaporized is also increased and thus the rate of heat removal (Chen et al., 2011). Yortsos and Stubos (2001) showed that the phase-change process in porous media occurs mainly within pores but is constrained by the solid boundaries of the porous media. The phase-change process is described as being affected by properties of the solid boundaries, like the roughness, and it is dependent on the equilibrium established between the confined fluid (liquid and vapour), the solid structure of the micropores and the capillary forces in meso and macropores while the mass and heat transport throughout the bulk porous media controls the bubble growth kinetics.

Given the above described characteristics of the low-pressure-vaporization process of free water and of the vaporization process in porous media, unequivocal heat transfer enhancement benefits are expected from the combination of these two processes. The ultimate objective of work of this chapter is experimentally to show the benefits of these combined contributes (low-pressure-vaporization process in porous media LPV-PM). Such achievement will involve not only the characterization of the LPV-PM through the direct measurement of the time evolution of the water temperature in the porous media and of the total pressure within the vaporization chamber, but also the determination of indirect parameters, such as the water vaporization rate, the total mass of water vaporized and the energy removed by vaporization at each instant, considering

four different porous media and several different initial water temperatures. A direct comparison of some of the above mentioned evolution and parameters is also made for the LPV in free water and in porous media.

## **VI.2.Experimental details**

---

### **VI.2.1 Low-pressure-vaporization in porous media – physical model**

The LPV is a complex physical phenomenon that results from a sharp pressure drop in a certain closed space where the water (or any other liquid) is initially in equilibrium with its vapour.

The LPV occurs in two distinct stages: in the initial one, while the total pressure in the closed space (chamber) is above the saturation pressure of the water, the vaporization is ruled by surface vaporization phenomena, namely diffusion of water vapour in the still air lying above the free surface of the liquid (Cioulachtjian et al., 2010) and bubble growth in a microlayer (Carey, 1992). When the total pressure within the chamber drops below the saturation pressure, the vaporization becomes ruled by the boiling process. Due to the hydrostatic pressure within the still liquid water, the superheating degree created by the pressure drop below the saturation pressure is not homogeneous throughout the liquid volume, as is not the vaporization rate. As consequence, the temperature spatial distribution within the liquid still water is also not homogeneous (Saury et al., 2002).

Such as in the LPV of free water (LPV-FW), it is believed that the LPV in porous media LPV-PM occurs in two distinct stages, with a first stage ruled by the diffusion of the water vapour in the still air and bubble growth in a microlayer. When the total pressure drops below the saturation pressure, a second phase begins with the vaporization process being ruled by the boiling process that will start at the higher temperature points in the porous medium, but it will quickly extend to the whole porous medium. It is commonly considered that the vaporization occurs in the pores and the transport phenomena are associated with the pressure-driven hydrodynamic flow of vapour towards the outer surface of the porous media (Udell, 1983; Yortsos and Stubos, 2001; Peng et al., 2002; Fang et al., 2004; Wang and Peng, 2004). The process is schematically represented in the Figure VI.1.

As the required energy for the vaporization is taken from the water itself and from the solid structure of the PM, the water and PM temperatures (and the saturation

pressure) decrease. The instant at which the water temperature experiences a sharp decrease, associated with the beginning of a boiling-ruled vaporization process, is designated by flash point, which signals the end of the first stage and the beginning of the second stage of the LPV-PM process. The second stage is usually divided into two regimes: in the first one, an intense boiling occurs throughout the whole water volume whilst; in the second regime, the vaporization occurs mainly near the outer surface with weak boiling.

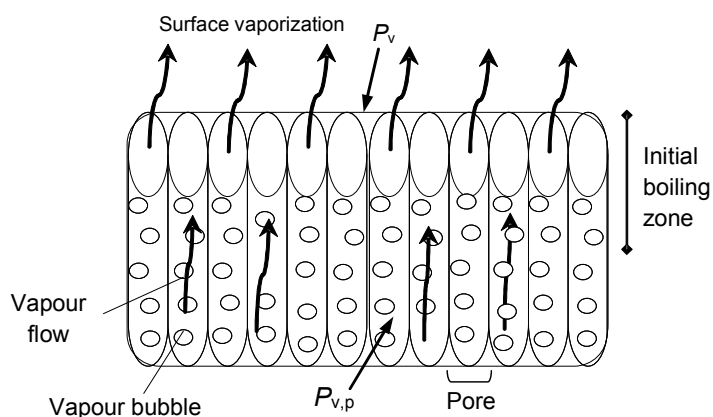


Figure VI.1. Schematic diagram of the vaporization phenomena in PM.

## VI.2.2 Experimental set-up and methodology

The objective of the experimental methodology described in this section is to characterize the low-pressure-vaporization process in porous media. As mentioned earlier, such achievement will involve the direct measurement of the evolution of the water temperature in the porous media, the total pressure within the vaporization chamber over the time, and the determination of indirect parameters like the water vaporization rate, total mass of water vaporized and the amount of energy removed by vaporization at each instant, for four different porous media and several different initial temperatures.

The experimental set-up comprises two main components: the vaporization chamber (VC) and the depressurization system (DS). The VC is a cylindrical stainless steel chamber with a volume of  $0.017 \text{ m}^3$ . The DS consists of a vacuum pump with a volume flow rate capacity of  $0.0033 \text{ m}^3 \text{ s}^{-1}$ . A schematic diagram of the experimental set-up is shown in Figure VI.2.

Process parameters, namely, the temperature of the water in the porous medium  $T_w$  and of the atmosphere within the VC were measured by K-type thermocouples (accuracy:  $\pm 1.5$  °C; response time: 100 ms;  $\varnothing \approx 0.5$  mm). The chamber pressure  $P$  was measured with an *Edwards ASG 1000 mbar* gauge (accuracy:  $\pm 2$  mbar). These sensors were connected through a *National Instruments*<sup>®</sup> data acquisition system to a personal computer and the signal was conditioned and saved using a *LabVIEW*<sup>®</sup> 8.6 based software.

The variation range of the studied parameters was chosen taking into consideration the potential use of this phenomenon for several applications and our particular experience. For each of the porous media (PM1 to PM4), four different initial temperatures (18, 21, 27 and 35 °C) were studied. In each test, the time evolution of the temperature in the porous media and of the total pressure  $P$  within the VC were measured. The saturation pressure evolution was calculated from the water temperature variation by the Antoine equation (Poling et al., 2001). The vapour partial pressure in the VC  $P_v$  was calculated from the total pressure  $P$  measured at the current experiment subtracting the total pressure in the VC obtained for a reference situation performed with a completely dry porous material. For each set of initial conditions (cf. Table VI.1), the experiments were run in triplicate and the arithmetic mean of the instantaneous measured values was considered. The time-average of the instantaneous coefficient of variation was always lower than 10 % for  $T_w$  and  $P$ . For example, for PM1 and  $T_0 = 27$ °C, the average coefficient of variation is 4% and 7.7 %, for  $T_w$  and  $P$ , respectively. To avoid heat entrapment from the surroundings, the PM is placed in an open container which is thermally insulated from the VC steel walls.

Besides the referred raw data, for each experiment the mass of water vaporized was also determined through an energy balance to the porous media. In the energy balance, it is assumed that the heat exchange between the PM and the surroundings may be neglected and that the liquid properties ( $h_{fg}$ ,  $c_{p,PM}$  and  $\rho_w$ ) are constant during the process (independent of temperature and of pressure). Thus, the mass of water vaporized up to a certain instant  $t$  is given by:

$$m_{w,v}(t) = \frac{m_t(t) c_{p,PM}}{h_{fg}} (T_w(t-\Delta t) - T_w(t)) + m_{w,v}(t-\Delta t), \quad (\text{VI.1})$$

where  $m_t(t)$  is the total mass of the porous medium ( $=m_w(t)+m_{PM}$ ).

In the LPV-PM process, the high amount of energy for the water vaporization is taken from the liquid water remaining within the PM. Thus, the expression for the energy required for the water vaporization up to instant  $t$  is given by:

$$E_v(t) = m_{w,v}(t) \cdot h_{fg}, \quad (\text{VI.2})$$

where  $m_{w,v}(t)$  is the mass of water vaporized up to the instant  $t$  (Eq.(VI.1)) and  $h_{fg}$  is the latent heat of vaporization of water.

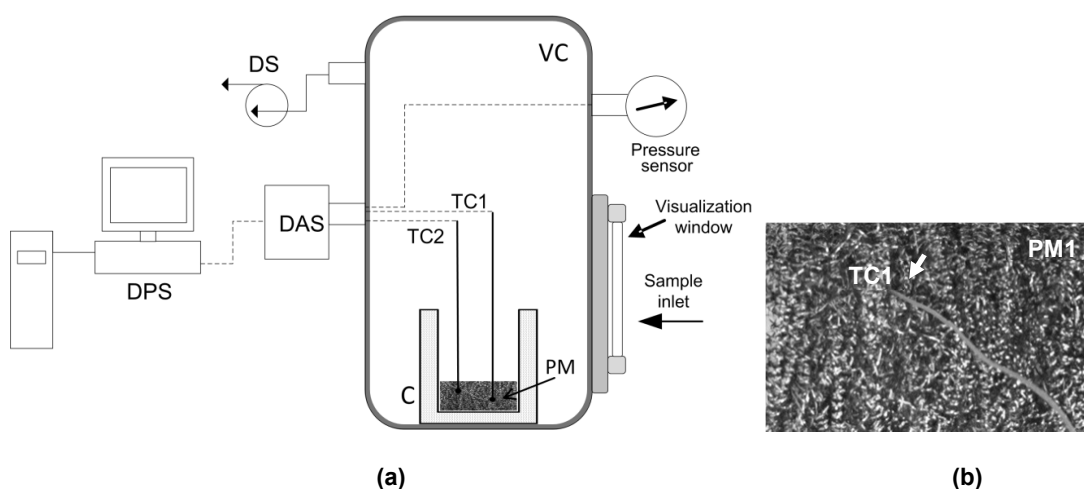


**Figure VI.2.** (a) Schematic diagram of the experimental set-up (DS - depressurization system; DAS - data acquisition system; VC – vaporization chamber; C – container; W – water; DPS - Data processor and storage). (b) Detailed view of the PM1 with the thermocouple TC1 located inside.

### VI.2.3 Characterization of the porous media

As referred in section VI.2.2, four different porous media (PM) have been considered in this work. In all the experiments performed, the PM presented a rectangular configuration, 165 mm long and 100 mm wide, with variable thickness. Table VI.1 lists the composition and the water absorption capacity of the considered PM, as well as the respective thickness.

Figure VI.3 contains photographs of the microstructure of each of the studied PM, performed with an optical microscope. PM1 (Figure VI.3(a)) presents a sparse microstructure made up of curly, thin, stainless steel fine strips with an irregular distribution of generally big-sized pores. The porous media from 2 to 4 show, at least compared with PM1, a much denser structure despite of the irregular pore distribution.

All of these PM2 to PM4 are made up of polymeric foams. PM2 presents a dense sponge-like microstructure, while PM3 and PM4 present mostly a fibrous microstructure, being PM3 denser than PM4. PM3 presents regions with irregular fibres, corresponding to viscose, and others not so fibrous, and apparently denser, more similar to polypropylene. PM4 is mainly composed by long cotton fibres surrounded by polyester fibres.

**Table VI.1.** Composition, thickness and water absorption capacity of the porous media.

	<b>Composition</b>	<b>Thickness (mm)</b>	<b>water absorption capacity or <math>V_{w,0}</math> (ml)</b>
<b>PM1</b>	100% stainless steel	10.1	$13.82 \pm 0.311^*$
<b>PM2</b>	30% cotton 70% cellulose	3.0	$73.35 \pm 0.008^*$
<b>PM3</b>	75% viscose 25% polypropylene	1.3	$27.23 \pm 0.282^*$
<b>PM4</b>	83.5% cotton 16.5% polyester	2.0	$21.31 \pm 0.159^*$

\* Standard deviation.

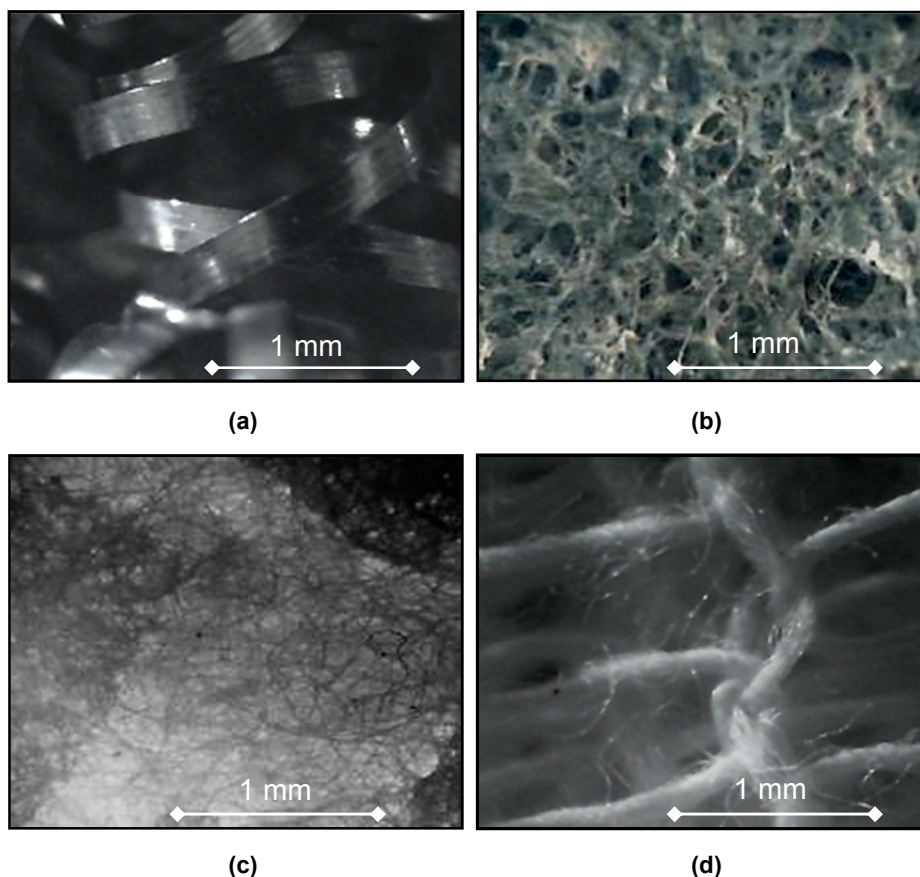


**Figure VI.3.** Photographs of the porous media, taken with a microscope Nikon Optiphot HFX-DX with a Nikon Fx-35 DX camera (objective M Plan 2.5/0.075): (a) PM1; (b) PM2; (c) PM3 and (d) PM4.

## VI.3. Results and discussion

---

### VI.3.1 Influence of the initial conditions on the LPV in different PM

In this section, the LPV process in four different types of porous media (LPV-PM) is analysed. The effect of the initial temperature  $T_{w,0}$ , and of the microstructure of the PM on the LPV-PM evolution is evaluated through the comparison of the following parameters: evolution of the temperature within the PM  $T_w$ , of the total pressure within the VC  $P$ , the saturation pressure of the water in the PM  $P_{sat}$  and the vapour partial pressure within the VC  $P_v$ .

Contrarily to the observations for the LPV-FW (chapter IV), there is a clear decrease in the temperature of the porous media during the first stage of the LPV-PM, as it can be seen in Figures VI.4(a)-(d). It is also possible to observe that the rate at which the temperature decreases in the porous medium varies with its nature. PM1 shows the highest rate of temperature decrease for all the initial temperatures. The temperature evolution for PM3 and PM4 are similar and not so different from the one observed for PM1. However, PM2 shows a significantly lower rate of temperature decrease and a much smaller temperature variation. Analysing the results of Figure VI.4(a) to (d), it is seen that, for all the PMs, the average rate of temperature variation is greater for higher initial temperatures. The observed behaviour can easily be understood based on the thermal inertia of each of the moistened porous media. Nevertheless, and since the thermal inertia depends on the initial amount of water absorbed, the far reason for the observed behaviour is related to the sparse structure with large cavities of the PM1 and to the structure of small sized pores of the PM2 (see. Table VI.1 and Figure VI.3), i.e., with the PM microstructures. Although presenting different fibre distributions, PM3 and PM4 show similar water absorption capacities and temperature variations.

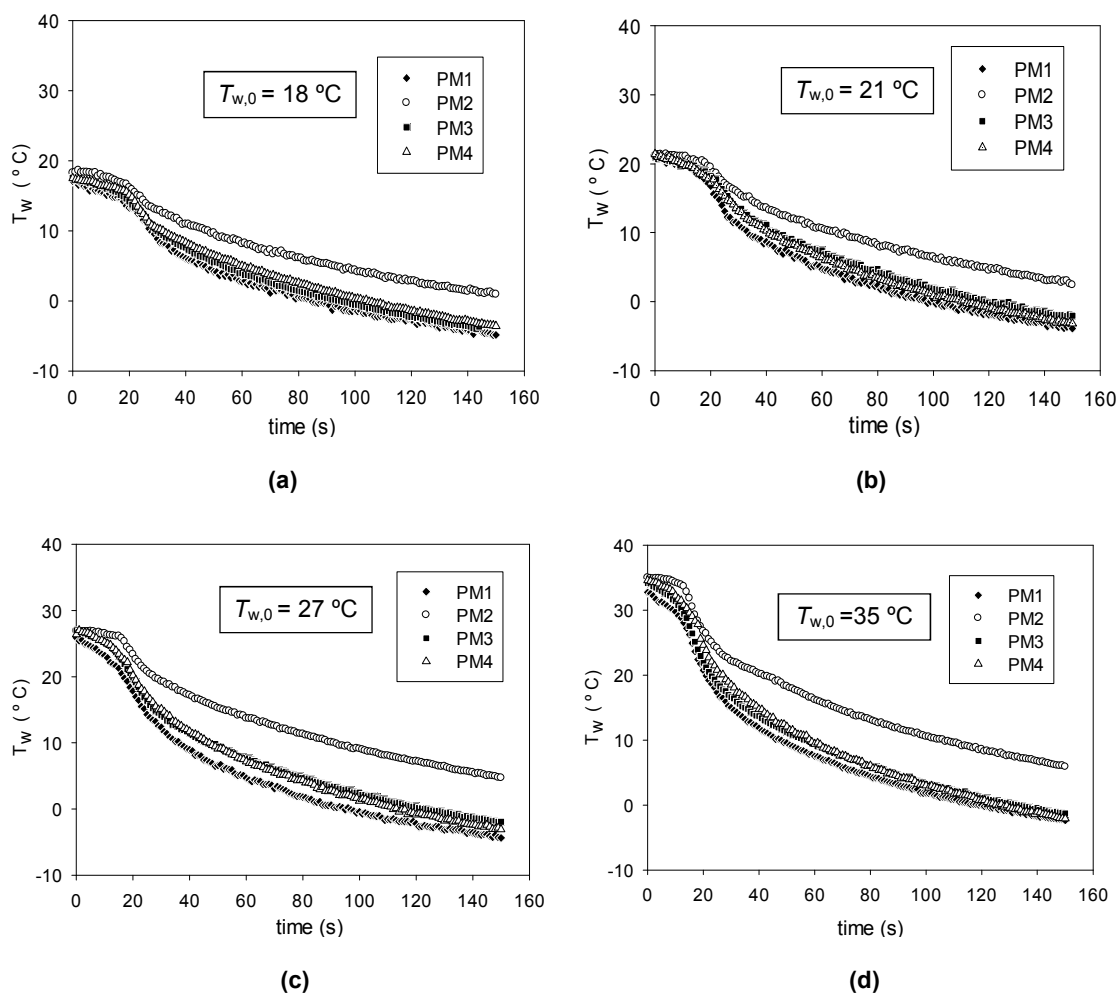


**Figure VI.4.** Water temperature evolutions in different porous media and for different initial temperatures.

It is evident in Figure VI.5 that the higher initial temperature, the higher the rate of the water decrease in both the first and the second stages of the process, and likewise the temperature drop at the flash point. In fact, the existence of two different profiles is clear (Figure VI.5): up to the FP, the evolution is pretty much linear, whilst in the second stage the temperature evolution of the porous media tends to an exponential function, being more pronounced to higher values of  $T_{w,0}$ .

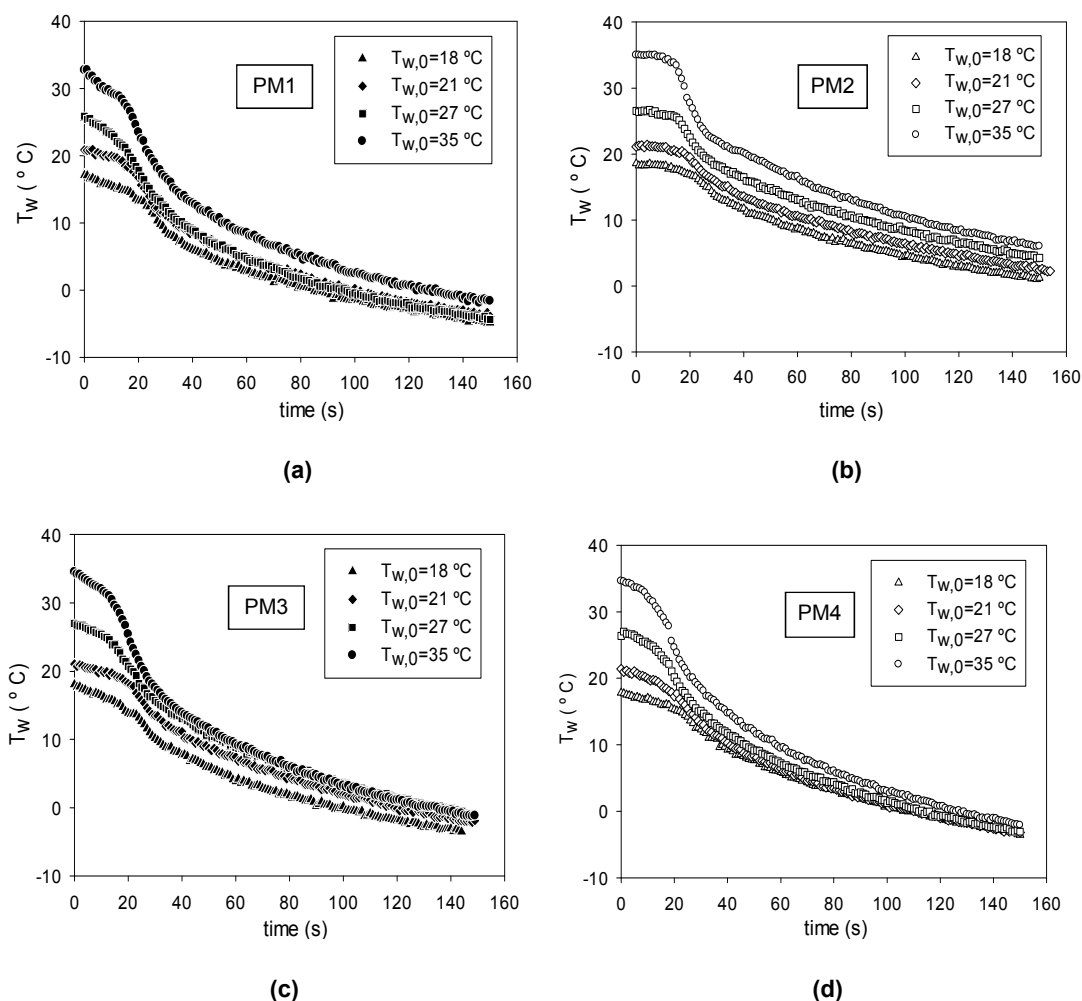


**Figure VI.5.** Water temperature evolutions for different initial water temperatures and in different porous media: (a) PM1; (b) PM2; (c) PM3 and (d) PM4.

This second stage (see section VI.2.1 and chapter IV) is still divided into two different vaporization regimes, as also described by several authors. The first of these regimes begins right after the FP and is described as a quite violent boiling process (Saury et al., 2002). The boiling front starts in the region of the porous medium with higher temperature and expands rapidly to the whole media. At this regime, the vapour bubble formation takes place throughout the whole volume of the pores. As referred by Wang and Peng (2004), the boiling phenomena include boiling nucleation and bubble dynamics, which in turn is divided into: bubble growth, bubble coalescence and departure from the pores. The departure corresponds to the movement of the vapour bubbles from the inner part of individual pores to their surface and is caused by differences between the partial pressure of the water vapour outside the pores (ruled by the depressurization system) and the partial pressure of the vapour within the pores.

The boiling phenomena and bubble growth are affected by different aspects related to the porous media microstructure, namely, pore size (micro, meso, macro and mega), pore roughness, surface tension, microlayer or bubble ((Marco et al., 2000; Yortsos and Stubos, 2001; Wang and Peng, 2004). For example, the surface tension has an important influence on nucleation and bubble formation parameters. When the nucleation is set, the boiling increases with the reduction in the surface tension, leading to high frequency bubble formation, high vapour generation and high heat removal. The second regime begins afterwards, when the rate of total pressure reduction decreases. This second regime is characterized by a decrease in the rate of bubble formation, and an increase in the importance of the diffusion-controlled evaporative phenomenon occurring at the free surface of the water (Augusto et al., 2012). The transition from the first to the second regime in the second stage, can be observed in Figures VI.6(a)-(b) at a time of about 30 s, when the total pressure reduction rate suddenly decreases to a very low value.

When the rate of vapour production is high (at least for the higher initial water volume) an inversion in the total pressure reduction trend can occur; this is known as the reaction point. This phenomenon is more visible in the results shown in Figure VI.6(b), obtained with PM2 – the porous medium with the highest water absorption capacity. The smaller the initial volume of water, the smaller will be the amount of superheated water, as will also be the vapour production and, likewise, the change in the decreasing trend of the total pressure. On the other hand, higher  $T_{w,0}$  leads to a higher superheating degree and a greater change in the reduction trend of the total pressure.

As consequence of the quick water vaporization, the temperature of the liquid decreases rapidly, the superheating degree decreases and the vapour production starts being localized just beneath the liquid free surface of the water within the porous medium. For that reason, after the RP, the total pressure recovers the initial trend of reduction (see Figure VI.6(b)). A while after that, the rate of the total pressure reduction decreases and the total pressure becomes approximately constant once there is equilibrium between the vapour generation and the rate of vapour removal by the depressurization system (Hahne and Barthau, 2000).

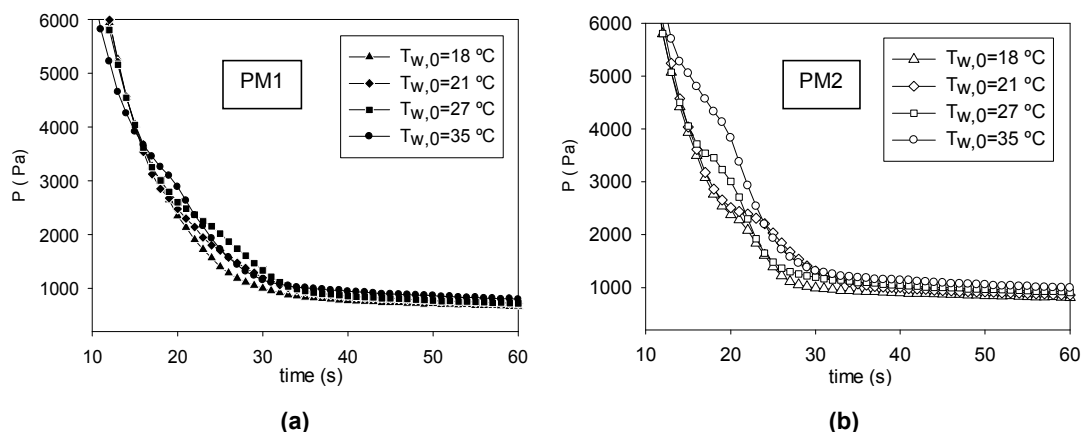
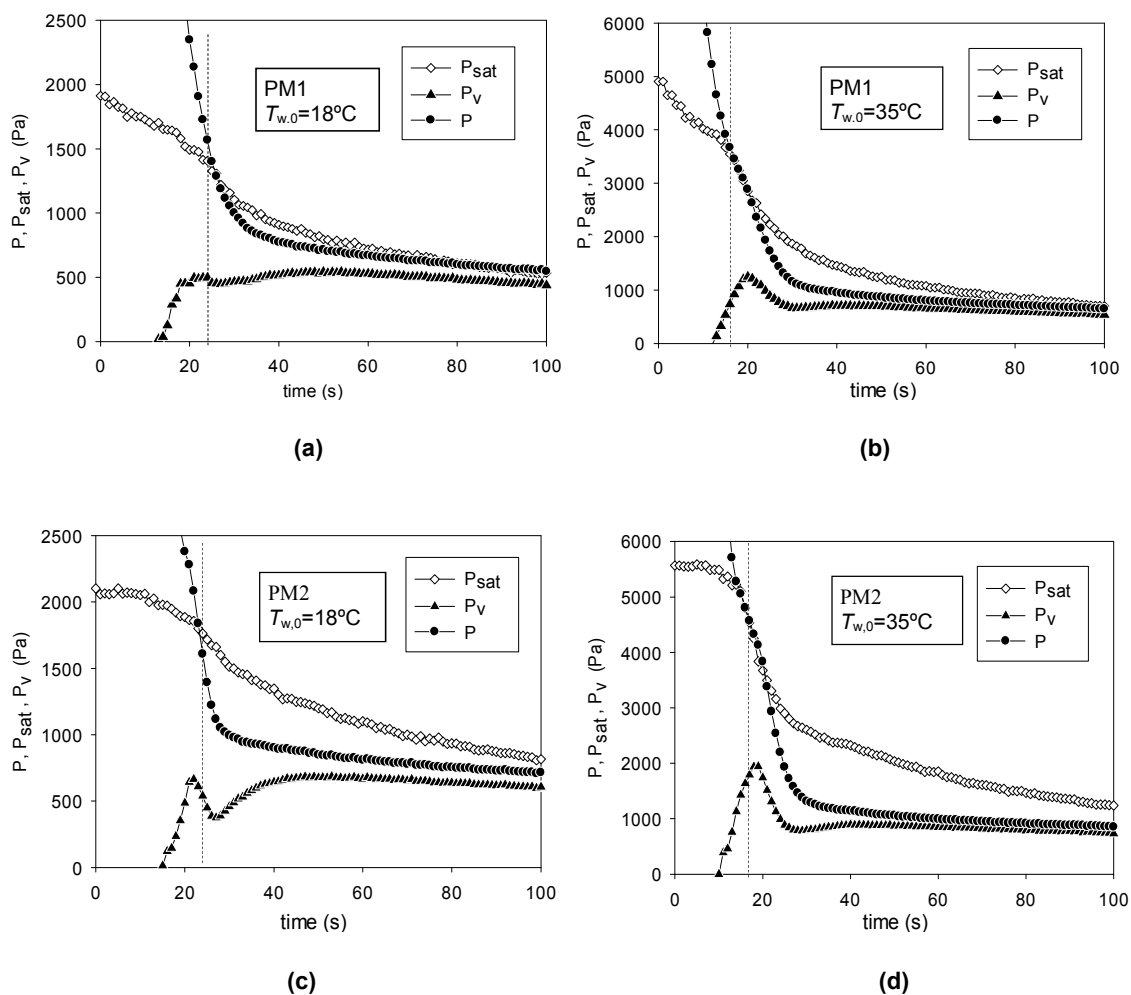


**Figure VI.6.** Total pressure evolutions in the vaporization chamber for different initial water temperatures and two different porous materials: **(a)** PM1 and **(b)** PM2.

As previously mentioned, in normal conditions the FP (the beginning of the sharp decrease of the temperature) corresponds to the instant at which the total pressure drops below the water saturation pressure. Usually after the FP, due to the great increase of vapour generation, an inversion of the total pressure reduction is observed (the reaction point). However, as it can be seen in Figure VI.7, this phenomenon does not always happen like that. For the lowest initial temperature ( $T_{w,0} = 18^{\circ}\text{C}$ , i.e., Figures VI.7(a), (c), (e) and (g)), the flash point corresponds to the instant at which the total pressure reaches down the water saturation pressure, leading to a sharper decrease rate of the temperature, but it does not correspond to the moment of the highest rate of vapour production. For the referred situation, the moment at which the rate of vapour production is greatest – the reaction point, corresponding to a local maximum of  $P_v$  – occurs before the FP, during the first stage of the process. Some time after the FP the vapour pressure increases again. However, at a lower rate than the one observed before the reaction point. Thus, coupling these results with the temperature evolution shown in Figures VI.4 and VI.5, one can conclude that the water temperature decrease in the first stage leads to an increase of the partial vapour pressure before FP, and to a decrease of the total pressure reduction. The change to the second stage occurs afterwards; the vapour pressure decreases until a local minimum value and then increases again due to FP. This happens because of lower initial temperatures. As the saturation pressure is lower, therefore it takes more time to be reached by the total pressure. Since there is a significant vapour production in the first stage, a maximum value of the vapour pressure is achieved, changing the normal evolution of the LVP process observed in free water. For higher initial temperatures the higher saturation

pressures of water are easily reached by the decreasing total pressure, which is an enhanced stimulation of the flash boiling and thus, shortens the duration of the first stage of the LPV process.

As already observed for the process of LPV in free water, Figure VI.7 also shows that the higher the initial temperature of the porous media, the higher the peak value of the vapour pressure characterizing the reaction point and, likewise, the final vapour pressure at the end of the LPV process. It is also possible to say that, at least for higher temperatures, there is a trend indicating that higher initial amounts of water in porous media lead to higher peak values of the vapour pressure.



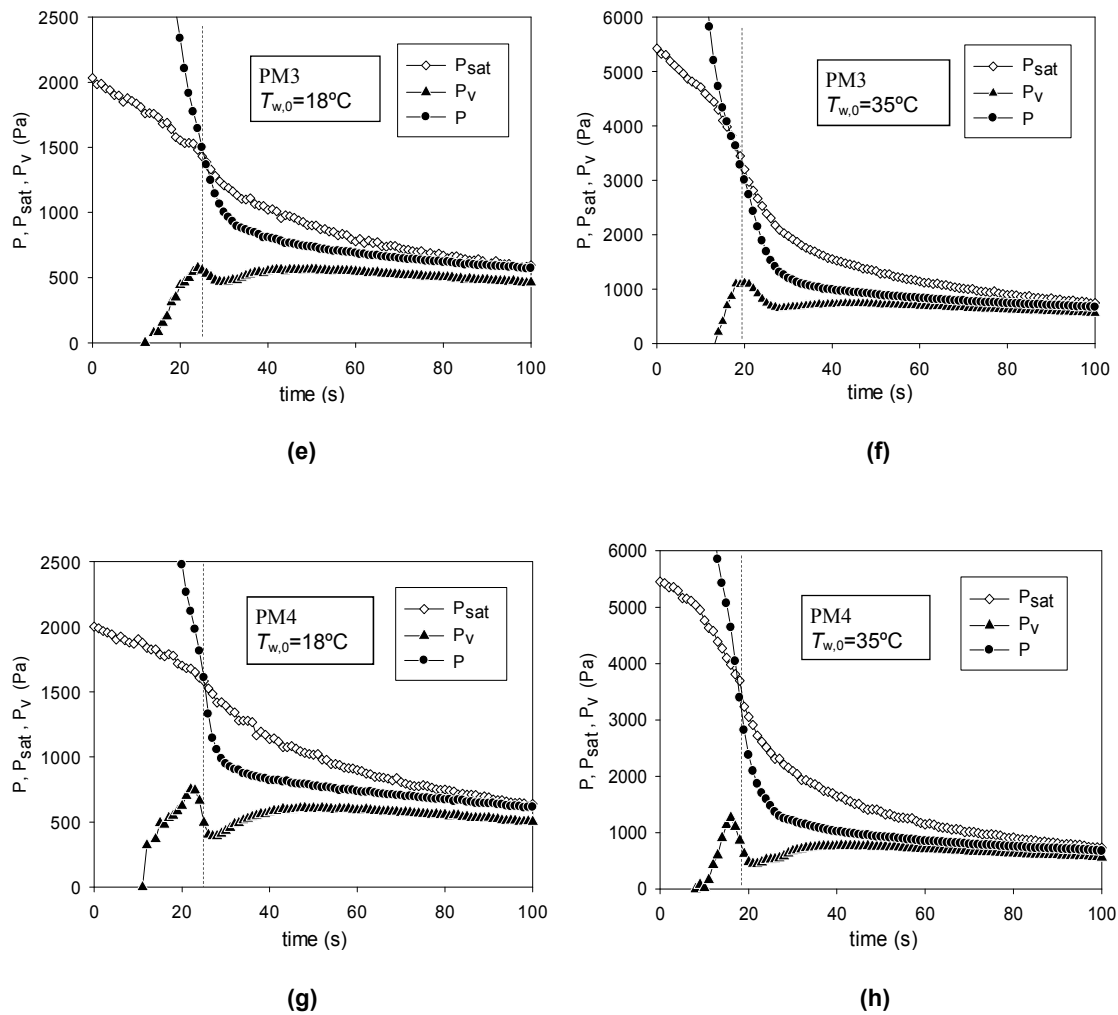


**Figure VI.7.** Comparison of the time evolutions of the total, the saturation and the vapour partial pressures during the LPV process, for the minimum and the maximum initial water temperatures, in each of the porous media tested. The dashed line indicates the flash point.

### VI.3.2 Mass of water vaporized on the LPV in porous media

As referred in the introduction section, the LPV in porous media is a good process to increase the water vaporization rate and consequently the rate of heat removal, with benefits for a large range of applications. The graph in Figure VI.8 shows the evolution of the mass of water vaporized,  $m_{w,v}(t)$ , as given by Eq.(VI.1), for PM1 and PM2, and two different initial temperatures. Despite the initial conditions, the cumulative mass of vaporized water shows a logarithmic behaviour that tends to a limit value (final mass vaporized for a specific process). It is also seen that the amount of water vaporized is extremely dependent on the initial volume of water contained in the porous

medium, a fact that is more pronounced if the process starts from higher initial temperature. However, the specific rate of vaporization (i.e., per unit of initial mass of water) is higher for lower initial water volumes, as shown in Figure VI.9 for PM1 and PM2. This behaviour can be understood if related to the superheating degree of water. The superheating degree  $\phi$  is defined as the difference between the interfacial  $P_{v,i}$  and the bulk vapour pressure  $P_v$  (cf. sketch in Figure VI.10), and corresponds to the driving force of the vaporization process (Carey, 1992; Zhang et al., 2001; Wang et al., 2004). This means that the specific rate of vaporization is a function of the superheating degree, i.e.,  $\dot{m}_{w,v}^* = f(\phi)$ . Contrarily to what happens in the LPV of free water,  $P_{v,i}$  is not equal to the saturation pressure of water. In the LPV in porous media, the liquid-vapour interface is concave, as sketched in Figure VI.10, and, due to the capillary effect, the pressure in the liquid phase is lower than the surrounding total pressure, according to the Young-Laplace equation (Webb and Kim, 2005). This circumstance offsets the flash point to a total pressure somewhat higher than the saturation pressure (evaluated by the temperature of the water in the porous media). As described by Udell (1983) and Carey (1992), assuming that at any point of the porous media the thermodynamic equilibrium prevails, characterized by a common temperature to all phases, the interfacial vapour pressure  $P_{v,i}$  and the liquid pressure  $P_w$  will be related at each instant by the Kelvin and Young-Laplace equations (Udell, 1983; Webb and Kim, 2005). Thus, the magnitude of this relation depends on the magnitude of the capillary effect described by the following parameters: pore radius  $r_p$ , surface tension,  $\gamma$ , and the contact angle  $\theta$ . Therefore, since PM1 has larger pore radius than PM2, this leads to higher superheating degree, and consequently, to higher vaporization rates. Besides the vaporization at the liquid-vapour interface in the pores, there is also some amount of water that vaporizes throughout the porous media solid walls (see Figure VI.10). For relatively high density porous structures, like PM2 with large fraction of solid material, the water absorption occurs in layers, and this kind of vaporization prevails over the vaporization within the pores. This situation reduces the capillary effect, eliminating the concave interface and approaching the LPV-PM to the LPV in a layer of the free liquid water, as it will be shown later in this chapter.

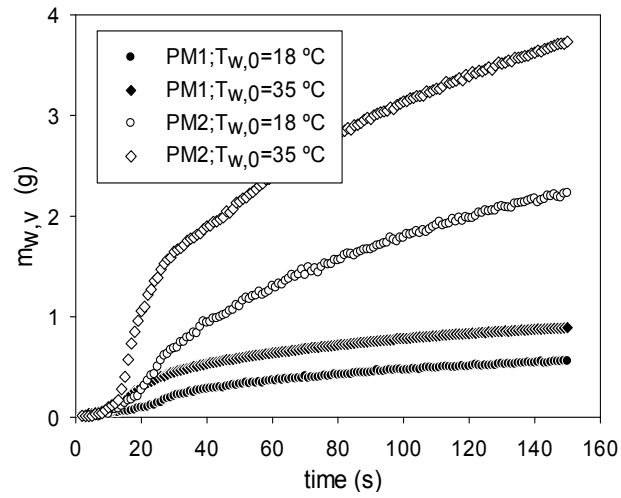


**Figure VI.8.** Evolution of the cumulative mass of vaporized water in the porous media PM1 and PM2, at two initial water temperatures,  $T_{w,0} = 18$  and  $35$  °C.

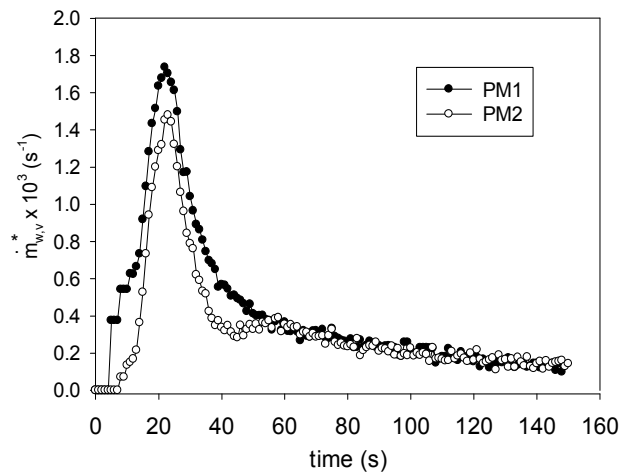


**Figure VI.9.** Evolutions of the specific rate of water vaporization in the porous media PM1 and PM2 for  $T_{w,0} = 35$  °C.

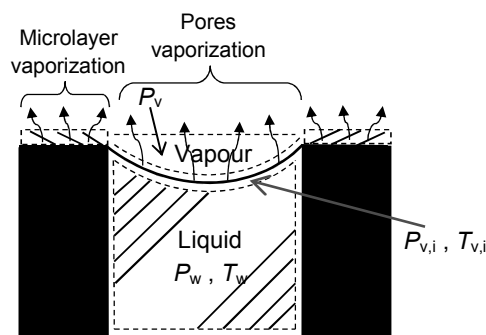


**Figure VI.10.** The schematically representation of the physical model of the vaporization in porous media.

As shown above, both the amount of water initially adsorbed by each PM and the initial temperature of each porous medium have a great influence on the mass of the water vaporized up to each instant of the process. Figure VI.11 represents the tendency of variation of the final mass of the water vaporized up to a certain instant  $t(=150\text{ s})$ ,  $m_{w,v}^f$ . It can be seen that it increases with both the initial temperatures  $T_{w,0}$  and the volume of the water initially contained in the PM,  $V_{w,0}$ . This was expected; the above analysis of Figure VI.7 shows that the higher values of  $T_{w,0}$  and  $V_{w,0}$ , the higher average superheating degree and the more vigorous is the boiling phenomena that stimulate the vapour production.

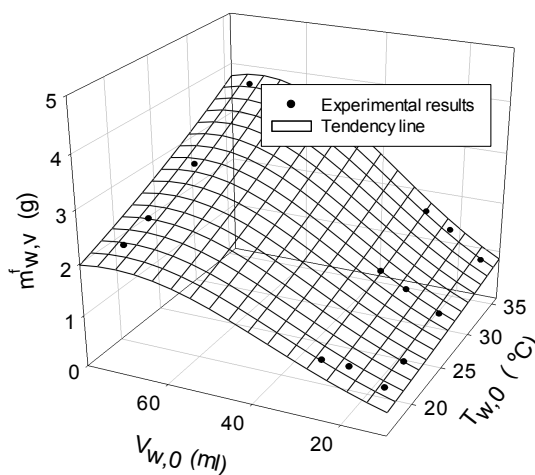


**Figure VI.11.** Variation trend of the final mass of water vaporized with  $V_{w,0}$  and  $T_{w,0}$ .

Assuming that all the energy necessary for the vaporization of the water is taken from the liquid phase remaining within the porous media, its value  $E_v$  can be estimated from the PM mass loss and from the enthalpy vaporization of water, as shown in Eq.(VI.2). The evolution of the rate of energy removal per unit of initial mass of water is shown in Figure VI.12(a). It can be seen that, during the first half of the process, the rate of energy removal is distinctly higher for the PM1 when compared with the PM2 (as it was expected, this evolution is similar to the evolution of the specific rate of water vaporization – Figure VI.9). Figure VI.12(b) presents the cumulative energy removed per unit of initial mass of water, showing for PM1 a value 15 % higher than for PM2 at the end of a 150 s period.

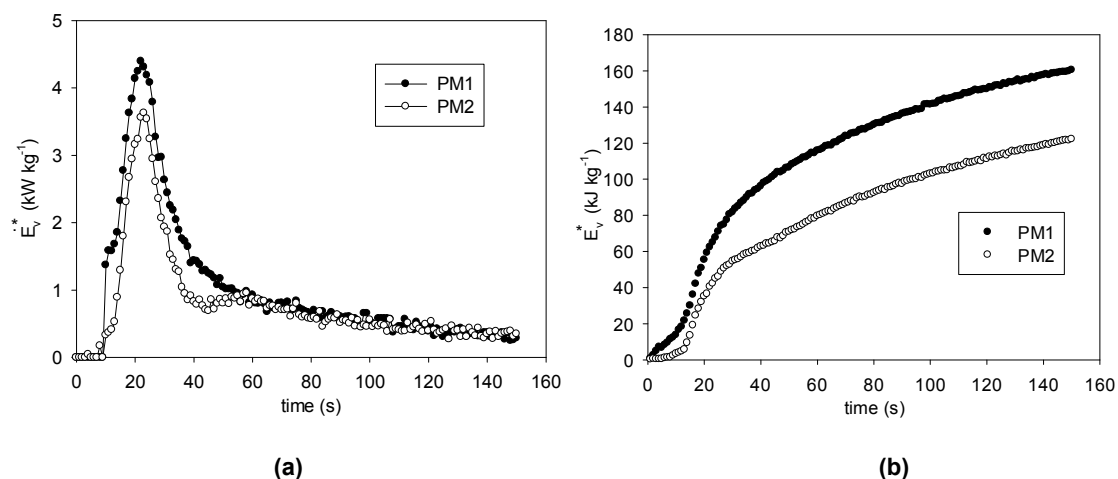


**Figure VI.12.** (a) Specific rate of energy removal and (b) specific energy removed by vaporization for PM1 and PM2, starting with  $T_{w,0} = 35$  °C.

### VI.3.3 Comparison of the LPV evolutions in porous media and of free water

In this section, a comparison is made between the results obtained for the LPV in porous media and those obtained for LPV of free water. The analysis will be based on the evolution of the temperature, the total pressure in the VC and the rate of water vaporization for the free water and for two porous media, PM1 and PM2. In this case, for each experiment, the initial amount of water, free or absorbed by the porous media, was the same and all the experiments were performed with an initial water temperature of 21 °C.

The comparison between the LPV of free water and in the PM1 is made in the graphics of the Figure VI.13. The main differences are observed for the temperature evolution (Figure VI.13(a)) at the beginning and the end of the process. In fact, while in PM1 the temperature starts to decrease immediately after the beginning of the process, the temperature of the free water only starts to decrease after the FP. At the end of the process, the temperature reduction for the free water stops at 0 °C, when the water at the free surface freezes. Contrarily, the temperature in the PM1 keeps on decreasing up to the end of the experiment, because the porous medium induces the *freezing-point depression* of the water, due to the decreasing in the chemical potential, and consequently, in the freezing point.

Regarding the total pressure evolution (Figure VI.13(b)), it can be seen that the reaction point (the inversion in reduction trend of the total pressure) is almost unnoticed for the process in PM1, while it is clearly observable for the LPV in free water. This happens because in the later case, the strong vapour production due to boiling, starts sudden and vigorously just after the FP, while for the process in the PM1, the boiling vapour production, for the reasons pointed in the last section, gradually increases since the beginning of the process, with no relevant disturbance on the decreasing total pressure within the VC.

The comparison between the LPV process in the PM2 and in free water is presented in the graphs of Figure VI.14. The results refer to the same amount of water (absorbed by the PM2 or freely deposited in the container within the VC). The differences between the temperature and the total pressure evolution for the LPV process in the PM2 and in the free water are negligible. This behaviour can be explained on the basis of the superheating degree,  $\phi$ . As described in the previous section,  $\phi$  is defined as the difference between the interfacial pressure  $P_{v,i}$  and the bulk vapour pressure  $P_v$ , and it is the main driving potential for the water vaporization. However, unlike in the free water LPV process, for which the interfacial pressure is equal (or very close) to the saturation pressure of the liquid water, in the LPV-PM the interfacial pressure depends on several PM properties, the most important being its microstructure. The differences in the microstructure are in fact the main reason for the differences found between the PM1 and PM2 behaviours when compared with the LPV in free water. While the microstructure of PM1 induces significant capillary effects, the microstructure of PM2 leads to a layered water deposition, with almost no concave interface and approaching the LPV in PM2 to that in a free water layer. This is corroborated by the similar vaporization rates during the LPV in PM2 and in the free water, plotted in Figure VI.15(b). The positive effect caused by the pores, leading to higher rates of vaporization and of temperature decrease, when compared with phenomena in free water as reflected for Figure VI.15(a).

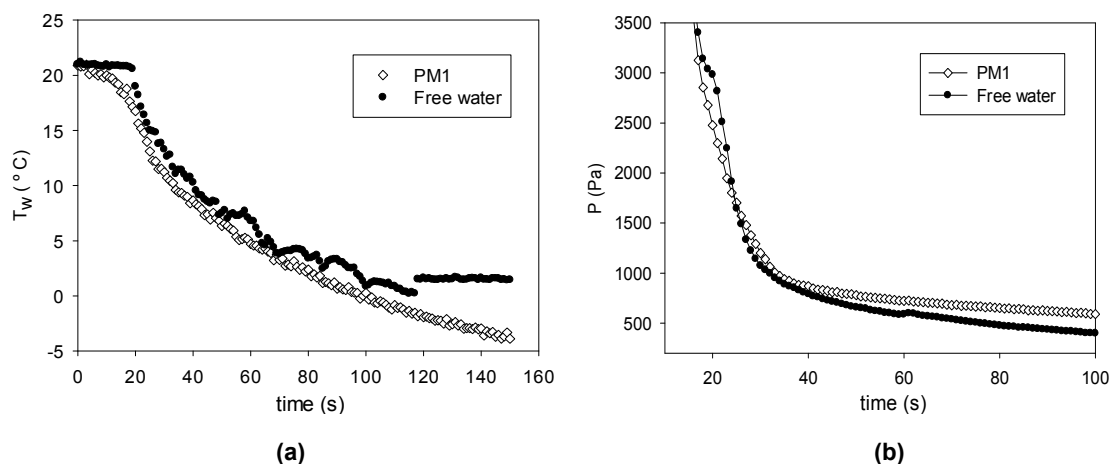


Figure VI.13. Time evolutions of (a) the water temperature and of (b) the total pressure for PM1 and free water.

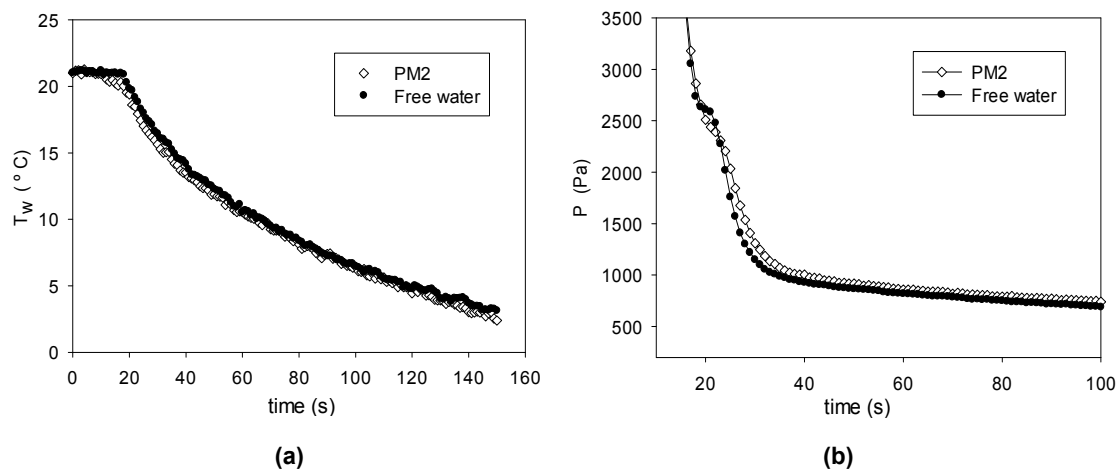


Figure VI.14. Evolutions of (a) the water temperature and of (b) the total pressure for PM2 and free water.

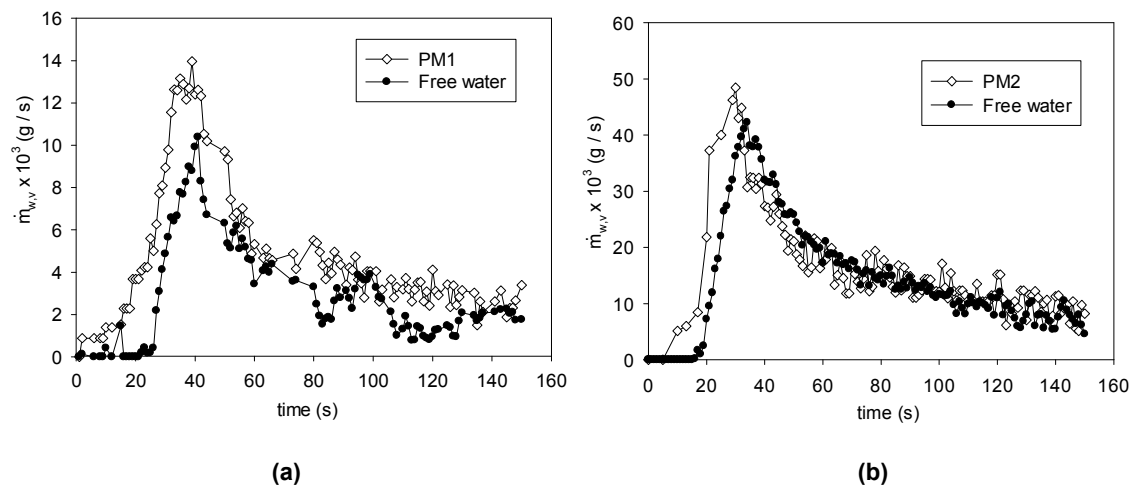


Figure VI.15. Comparisons of the water vaporization rates: (a) in PM1 and in free water and (b) in PM2 and in free water.

## VI.4. Conclusions

---

A detailed experimental study of the low-pressure-vaporization process of water in four different porous media was conducted. The main features of the vaporization process, such as the rate of temperature decrease and the rate of energy removal, showed to strongly depend on the total amount of water initially contained in the porous medium; this, in turn, depends on the porous medium microstructure. Significant differences were found for the process in porous media and in free water, the most relevant being a prompt beginning of the temperature decrease within the porous media. This behaviour was attributed to a gradual onset of boiling within the porous media, contrarily to a sudden boiling onset in a free water layer – at a well defined instant, the flash point, which is when the total pressure within the vaporization chamber reaches down the saturation pressure of water. For the porous media, due to the capillary effect, the onset of boiling occurs to a total pressure higher than the saturation pressure. The rate of energy removal by LVP in the porous media has revealed to be significantly higher than in free water. The results confirm the justifiable expectations on the use of porous media as a way to enhance surface heat transfer phenomena for a wide range of applications.



---

## VII. Development, calibration and validation of a mathematical model for the low-pressure-vaporization of the water in porous media

---

This chapter reports the development, calibration and validation of a mathematical model of the low-pressure-vaporization process in different types of porous media. This model aims to improve models developed by other authors in this area, namely by considering some aspects that have not been addressed, such as: the vapour pressure is not equal in all chambers; the interfacial vapour pressure is not equal to the saturation pressure; the surroundings have a significant influence in the vaporization phenomena in all zones of the porous media; and the first stage of the process is not characterized only by diffusion vaporization. For that purpose, an experimental calibration procedure was made involving the definition of several LPV parameters: vaporization coefficient of the porous medium  $\epsilon_{PM}$ , vaporization coefficient at the liquid-vapour interface within the porous medium  $\epsilon_{i,PM}$ , free surface vapour pressure  $P_{V,FS}$ , vapour pressure of the free layer  $P_{V,FL}$ , interfacial vapour pressure  $P_{V,i}$ , volume of the vaporization layer  $V_{VL}$  and volume of the free layer  $V_{FL}$ . These parameters were developed in a set of multivariable functions and determined from a series of experiments in different types of porous media, each one characterized by a different initial water temperature. Thus, in this work an enhanced physical model of the LPV in porous media is proposed, concerning two distinct stages.

The experimental set-up comprises two main components: the vacuum chamber (VC) and the depressurization system (DS). Part of the VC volume is occupied by an open container for porous media, which is insulated from the VC walls.

The results obtained show that the multivariable functions determined through the vaporization coefficient have a good agreement with experimental results (e.g.,  $R^2$  varies within 0.9581- 0.9903) and also that this parameter describes well all regimes of the second stage of the LPV process. The importance of the capillary effect and of the surface tension forces on the superheating degree and consequently, on the LPV evolution was demonstrated, as well as the effect of the amount of water initially contained in the porous medium.

From the validation based on the measured water temperature evolutions, deviations within  $\pm 5\%$  are found, which confirm the good agreement between experimental and simulated values. Thus, it is possible to conclude that the calibrated mathematical model describes well the experimental results and it is a good model of reference to various studies and applications.

*Keywords:* Low-pressure-vaporization; mathematical model; porous media, vaporization coefficient at the liquid-vapour interface; interfacial vapour pressure

## VII.1. Introduction

---

As referred in the previous chapter, enhanced heat transfer techniques are nowadays very required for industrial applications and scientific explorations such as nuclear power plants, solar energy concentration and conversion, high power cold production, temperature control and an all sorts of energy conversion systems (Webb and Kim, 2005; Li et al., 2011). As demonstrated in this chapter, it is unequivocal that heat transfer enhancement benefits from the combination of low-pressure-vaporization (LPV) and vaporization in porous media (PM). For this reason, significant experimental and theoretical efforts have been dedicated to understand the phenomena of both LPV and vaporization in porous media phenomena, and to assess their potential for practical applications. For example, Figueiredo and Costa (2004) studied the use of porous media for thermal protection against high intensity heat fluxes (flames). Other authors (Mc Donald et al., 2002; Meng and Hu, 2005; Zhao et al., 2008) analysed the application of porous media for the matter of temperature control in buildings. Zhao et al.(2008) investigated the heat and mass transfer properties of several different types of porous media considering the potential application in air-conditioning systems of buildings. Meng and Hu (2005) studied the possibilities of the application of humid structures for the temperature control of roofs, in a process designated as passive water evaporation. Webb. and Kim (2005) demonstrated that significant improvements of the heat transfer coefficients for specific surfaces have been achieved due to the promoted high performance nucleation of the boiling process and providing, by this way, an enhanced heat transfer rate.

Other authors (Prat, 1998; Yortsos and Stubos, 2001; Peng et al., 2002; Mantle et al., 2003; Wang and Peng, 2004; Augusto et al., 2012) have focused their works to identify the main characteristic parameters and the different stages of the vaporization process within porous media. As referred in the previous chapter, Wang and Peng (2004) and Yortsos and Stubos (2001) described the boiling vaporization heat transfer mechanism in porous media as an enhanced heat transfer technology, with a wide range of important practical applications. They emphasized the influences of the physical structure of the pores in the phase-change process and in the enhanced surface boiling nucleation.

By the reason appointed above, which is also demonstrated in chapter VI, details of the physical phenomenon associated with the water vaporization in porous media at sub-atmospheric pressures are being widely studied and modelled for a deeper and

more detailed knowledge, as it is reflected by the significant number of works (Elustondo et al., 2002; Wang and Sun, 2002b; Sun and Hu, 2003; Jin and Xu, 2006a, 2006b; Kim et al., 2007; Bakhshi and Mobasher, 2011). For example Elustondo et al.(2002) developed a model for moisture evaporation during foodstuffs drying under sub-atmospheric pressures in which internal water is pushed by the movement of the solid structures of the porous media, making the vapour to flow towards the outer surface. Sun and Hu (2003) developed a CDF model to simulate the heat and mass transfer within foods at low pressures, evidencing the complexity and importance of the boiling vaporization in pores. Wang and Sun (2002) developed a complete three-dimensional and transient model of the coupled mass and heat transfer of the cooked meat during low pressure and temperature. The model includes a sub-model describing the mass transfer in the inner vapour generation and another with heat transfer in the inner generation. However, these authors consider that the surface vapour pressure of the PM is only affected by a constant parameter that relates its pressure with the pressure in the chamber. As already demonstrated in our works, this can be a limitation of the model because the LPV process is sharply transient and the relation between all pressure changes as the stages and regimes change.

Despite the relative success of the recent models in the prediction of some characteristics of the low-pressure-vaporization process, most of them oversimplify the physical description of the process due to its intrinsic complexity, as already referred in chapter V, Part B. All of these works (Wang and Sun, 2002b; Sun and Hu, 2003; Jin and Xu, 2006a, 2006b) focused their study mainly in the phase change within pores and the vapour movement up to surface, despising the effect that the surroundings have on the surface vapour pressure of the pores and consequently, its effects in the vaporization phenomena within porous media. One of the most common simplifications made when modelling the LPV process is to assume that the vapour pressure in the vacuum chamber is homogeneous and in equilibrium with the liquid water phase present in the chamber (Jin and Xu, 2006a, 2006b; Augusto et al., 2012). Moreover, in general, the works that simulate the whole LPV process have considered that the interfacial vapour pressure is equal to the saturation pressure of the surface water, making a great simplification regarding the capillary effects on the vaporization phenomena, which are different for each porous medium. The consequences are, normally, an overestimation of the vaporization rates that are then corrected with empirical coefficients, equations that need to be calibrated, and neglecting that the LPV is essentially a transient process

and, for this reason, significantly affected by those initial conditions and their own evolution.

As also referred in chapter V, it is known that there is a vapour pressure gradient above the free surface of the water in the chamber (Eames et al., 1997; Saury et al., 2002). It is the vapour pressure at the free surface that is in equilibrium with the liquid phase and determines the rate of vaporization. This vapour pressure is known to decrease gradually along a layer formed above the free surface of the porous medium, down to a constant value that is equal to the vapour pressure in the free layer of the chamber. Thus, an experimental value relating these two pressures is needed as an evidence of its dependence with the initial conditions of the process and likewise with the process evolution itself. A correct definition of the interfacial vapour pressure is also needed, covering all surrounding effects and all contribution of the vapour generated inside the pores, in order to dispense the need for a detailed description of this production and, at the same time, to make a completely realistic model.

Therefore, in this work a mathematical model of the development of the LPV in the porous media integrated with experimental calibration is purposed, focusing all points described above and considered as weak points of the models in literature. The model developed is also validated with four different porous media. The present calibration methodology is made for the particular case of our model and experimental set-up, but easily adaptable to other LPV cases and experimental installations. Another improvement is the mathematical description of the first stage of the process, by not considering only the vaporization by diffusion.

For that purpose, the water temperature and total pressure evolutions were determined for a set of experiments, each one with a different initial water temperature  $T_{w,0}$  and in different types of porous media. This will allow developing a multivariable function for the vaporization coefficient in the porous medium, which relates the vapour pressure in the free layer of the chamber with free surface vapour pressure of the porous medium. This coefficient depends on the initial temperature, the initial total heat capacity of the porous medium and on the process evolution. A vaporization coefficient at the liquid-vapour interface in the porous medium is also determined, allowing the interfacial vapour pressure to be calculated from the traditional Kelvin equation (Zhang et al., 2001) and adjusted with experimental results. On the other hand, the calibrated mathematical model will be validated by several initial temperatures and four different types of porous media, and the respective error bands will also be determined.

Thus, it is possible to affirm that the present mathematical model developed for LPV in porous media is more complete and describes minutely all transport phenomena and phase-change processes, as well as the physics of the whole process comparatively to other models in the literature. Therefore, the present work could be of great importance to areas in which the LPV process is used as heat removal mechanism for temperature control, or to enhance the vaporization water in numerous procedures.

## VII.2. Experimental calibration methodology

The raw data needed for the development of the calibration procedures of the model are related with the initial conditions of each experiment and with the temporal evolution of the several parameters. Thus, the experimental work plan involved the variation of the types of porous media (characterized in chapter VI) and the variation of its initial temperature ( $T_{w,0}$ ), as shown in Table VII.1. In each experiment, the time evolution of the water temperature in the porous medium  $T_w$  and the total pressure in the vaporization chamber  $P$  were measured. The vapour pressure values in the VC  $P_v$  were experimentally obtained from the difference between the total pressures in the experiments performed with and without water. In the latter case, the total pressure is equal to the partial pressure of the air and a solid occupancy volume, equal to the initial volume of water, is used in the study. The experiments for each condition (see Table VII.1) were run in triplicate and the arithmetic mean of the results was considered. The mean value of the coefficient of variation between experiments was lower than 10 % in  $T_w$ . For example, for  $T_{w,0} = 27$  °C, the mean of the coefficient of variation is 4 % for PM1, and 4.4 % for PM4.

Some important initial conditions for the model simulation are presented in Table VII.1, such as the initial total mass  $m_{t,0}$  and heat capacity  $C_{PM,0}$  of the porous media, and the initial volume occupied by the porous media  $V_{PM,0}$ .

**Table VII.1.** Initial conditions of the experimental calibration tests.

$T_{w,0}$ (°C)	PM1	PM2	PM3	PM4
18, 21, 23, 27, 30, 35	√	√	√	√
$m_{t,0}$ (kg)	0.028820	0.084966	0.032027	0.026907
$C_{PM,0}$ (J K <sup>-1</sup> )	72	322	120	96
$V_{PM,0}$ (m <sup>3</sup> )	0.000167	0.000054	0.000025	0.000036

The experimental set-up for the LPV process is composed by two main components: the vaporization chamber (VC) and the depressurization system (DS), as sketched in Figure VI.2 of chapter VI. The VC is a stainless steel cylindrical chamber with an internal volume of  $0.017 \text{ m}^3$  ( $V_{vc}$ ). In the centre of the VC, and isolated from its walls, an open container (C) is placed for the porous medium. The DS consists of a vacuum pump with a volume flow rate capacity of  $0.0033 \text{ m}^3 \text{ s}^{-1}$ . The temperatures of the water in the container are measured by K-type thermocouples (accuracy:  $\pm 1.5 \text{ }^\circ\text{C}$ ; response time: 100 ms;  $\varnothing \approx 0.5 \text{ mm}$ ) and the chamber pressure is measured with an Edwards™ ASG 1000 mbar gauge (accuracy:  $\pm 2 \text{ mbar}$ ). These sensors are connected through a National Instruments™ data acquisition system to a personal computer where the signal is treated and saved using a LabVIEW™ 8.6 based software.

### VII.3. Development and calibration of the mathematical model

---

The physical system modelled for low-pressure-vaporization in porous media was also divided into two control volumes (CV), such as for the mathematical model of the low-pressure-vaporization in free water described in chapter III. However, the first one (CV1) comprises the porous medium with absorbed water – the water is considered ideally distributed with a uniform temperature throughout its pores volume. The CV2 defines the region of the vaporization chamber above the porous medium surface. The depressurization system (DS) is included in this CV2. Both control volumes are considered adiabatic and assumed to be in equilibrium with each other. This means assuming that there is thermodynamic equilibrium between gaseous and liquid phases, so that the two phases are instantaneously at the same temperature. The water temperature depends on the mass of water vaporized and it will be determined by applying coupled mass and energy balances to CV1. In turn, the vapour pressure within the CV2 is used to estimate the vaporization rate. This vaporization process takes out the energy from the water and the porous structure.

As referred in chapter V, the mathematical model described in chapter III is based on the assumption that above the surface the properties are taken as homogeneous and so, that the vapour pressure in CV2  $P_v$  is uniform in all vaporization chamber. However, according to our experimental results and other studies (Eames et al., 1997; Saury et al., 2002), it is concluded that, after the flash point, there is a gradient of vapour pressure developed above the free surface. Therefore the free surface vapour

pressure, which establishes the equilibrium with the saturation pressure of water, is not equal to the vapour pressure in all areas of the vaporization chamber. That vapour pressure gradient creates a vaporization layer (VL) above the water surface, with a volume  $V_{VL}$  that depends on the initial conditions. Thus, in the calibration methodology in chapter V, it was proposed a vaporization coefficient ( $\varepsilon$ ) that establishes the relation between the vapour pressure within the vaporization layer  $P_v$  and the vapour pressure in the free layer  $P_{v,FL}$  (above of the VL, see the Figure V.1 of chapter V). In the present case, this coefficient is designated by vaporization coefficient of the porous medium  $\varepsilon_{PM}$ , defined in Eq.(VII.1), and it can also be used to characterize the phase change of the process, as described in chapter V.

$$\varepsilon_{PM}(z) = \frac{P_{v,FL}}{P_v(z)}. \quad (\text{VII.1})$$

It is inversely related with the transfer resistances in the vaporization layer and accounts for differences values associated mainly with details in the experimental apparatus causing changes in the free surface of the porous media. So, the vaporization coefficient of the porous medium decreases from a value of unity at the upper limit of the VL to a minimum value, that depends on the surface temperature and the specific properties of the porous medium surface,  $\varepsilon_{z_0,PM} = \varepsilon_{PM}(z = 0)$  (see the Figure VII.1(b) ahead).

The first great difference between the model for LPV in porous media and the model developed in chapter III and calibrated in chapter V, and the LPV in free water is in the first stage of the process. As demonstrated in the preceding, there is a significant vaporization at this stage, however based on physical phenomena that are significantly different from the second stage. In the second stage, the great difference is the way of determining the rate of vaporization.

Once the vaporization phenomena are significantly different and the calibration methodology is based on experimental results for the sake of greater realism and robustness, the mathematical model developed comprises new formulations relatively to the model of the LPV in free water.

As described in chapter III the total pressure  $P$  in the vaporization chamber is the sum of the partial pressures of the air and of the water vapour, respectively  $P_a$  and  $P_v$ :

$$P = P_a + P_v, \quad (\text{VII.2})$$

the rate of variation of the partial pressure of air being derived from

$$\frac{dP_a}{dt} = -\frac{\dot{V}_e P_a}{V_{FL}}, \quad (\text{VII.3})$$

where  $V_{FL}$  is the volume of the free layer in the chamber and  $\dot{V}_e$  is the volume flow rate of the pump, considered constant and given in section VII.2.

Similarly, the variation rate of the vapour partial pressure is calculated by:

$$\frac{dP_v}{dt} = \frac{\dot{m}_v R T_c}{M_v V_{FL}}, \quad (\text{VII.4})$$

where  $M_v$  is the molar mass of the vapour,  $R$  is the universal ideal gas constant,  $T_c$  is the chamber temperature and  $\dot{m}_v$  is the rate of change of the mass of water vapour in the chamber, given by:

$$\dot{m}_v = \frac{dm_v}{dt} = \dot{m}_{v,i} - \dot{m}_{v,o}, \quad (\text{VII.5})$$

the mass flow rate of outgoing vapour ( $\dot{m}_{v,o}$ ) is given by:

$$\dot{m}_{v,o} = \dot{m}_{v,DS}, \quad (\text{VII.6})$$

where  $\dot{m}_{v,DS}$  is the mass flow rate of vapour extracted by the depressurization system, calculated by:

$$\dot{m}_{v,DS} = \dot{V}_e \cdot \rho_v, \quad (\text{VII.7})$$

where

$$\rho_v = \frac{P_v M_v}{R \cdot T_c}. \quad (\text{VII.8})$$

The incoming vapour generation rate from the liquid water  $\dot{m}_{v,i}$  is a function of the vapour partial pressure in the VL and the vapour partial pressure within the pores. As referred above and sketched in Figure VII.1, from the first to the second stage of the process, the physical configuration of the system changes. Thus,  $\dot{m}_{v,i}$  will be determined differently for the first and the second stages of the process.

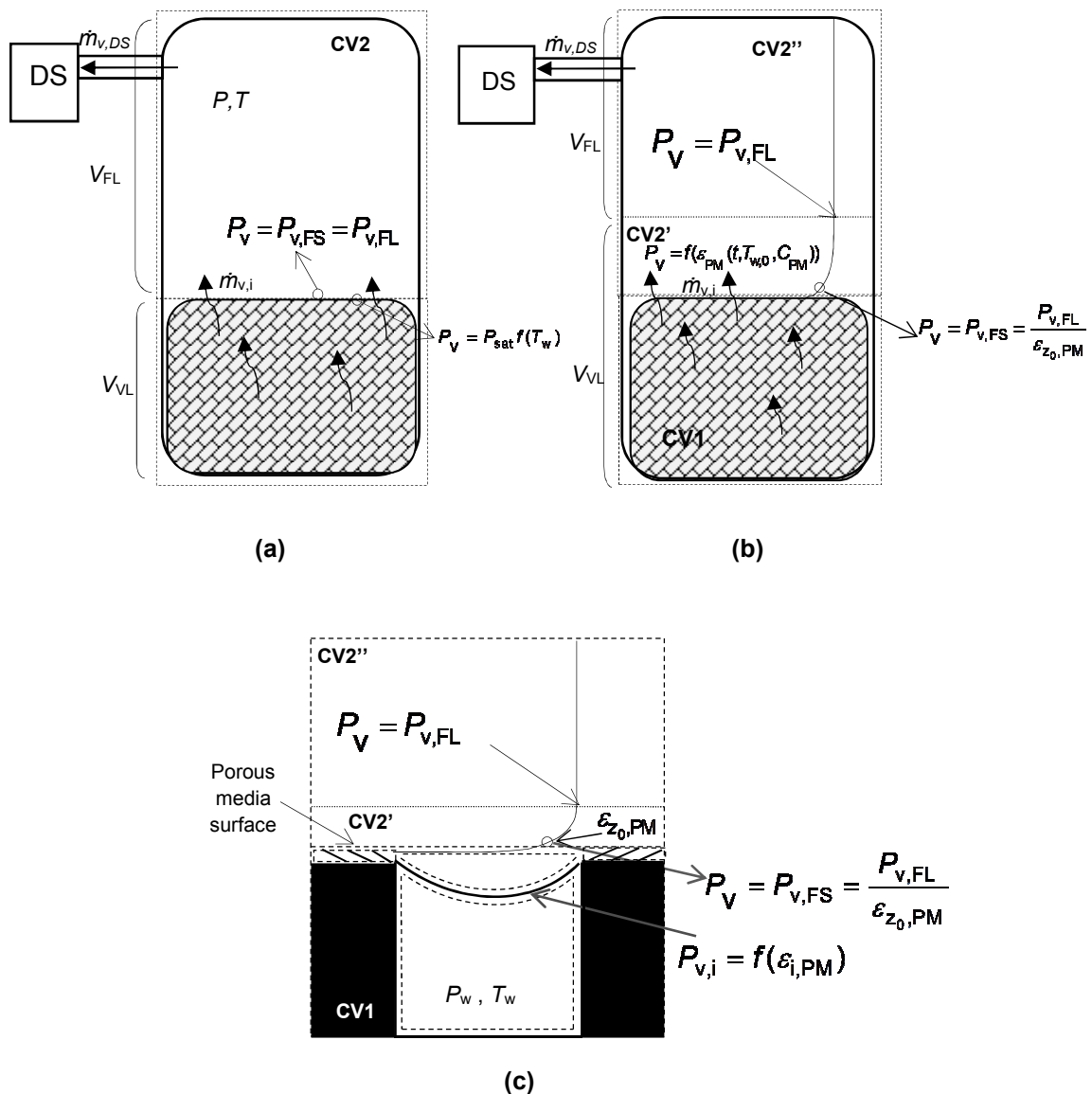


Figure VII.1. Schematic diagram of the physical model of (a) the first stage, (b) the second stage and (c) detail of the second stage of the LPV in porous media.

As described before, the first stage of the LPV in free water is characterized by diffusion only at the surface. Contrarily, in LPV in porous media, the vaporization is induced by capillary effects that decrease the surface tension, leading to an increase of the superheating degree in the whole volume of the pores. Consequently, there is a significant decrease of the temperature within the porous medium, which depends on the PM characteristics. The water temperature increases linearly since the beginning of the process, until the flash point, with no relevant disturbance on the decreasing total pressure within the VC, as also described in previous chapter. Thus, it is concluded that the free surface vapour pressure  $P_{v,FS}$  is equal to the vapour pressure in the free layer  $P_{v,FL}$ , as schematically represented in Figure VII.1(a). This happens because, at this stage, a small amount of vapour is generated and the rate of decrease in the pressure is high. This allows all the vapour generated being instantaneously removed. Thus the formation of a confined vaporization layer above the surface of the porous medium does not occur. The free spaces within the porous medium are considered vaporization zones. Thus at this stage there is not a vaporization coefficient above the surface of the porous medium. The pressure decrease in CV2 is responsible for the vaporization of water in CV1. The rate of vapour generation is mostly determined by the difference between the saturation pressure (at the liquid water temperature of porous medium) and the free surface vapour pressure  $P_{v,FS}$ , which is considered equal to vapour pressure in the free layer  $P_{v,FL}$  in CV2 – this difference is the driving force for the vaporization in first stage of the process). It may be represented by:

$$\dot{m}_{v,i} = \frac{d}{dt} \left[ \frac{(P_{sat} - P_{v,FS}) V_{VL} M_v}{RT_w} \right], \quad (VII.9)$$

where the water saturation pressure  $P_{sat}$  is estimated by the Antoine equation (Poling et al., 2001):

$$P_{sat} = e^{\left( \frac{23.209 - \frac{3816.44}{T_w - 46.44}}{T_w - 46.44} \right)}, \quad (VII.10)$$

and  $P_{v,FS}$  is calculated from Eq.(VII.4). The  $V_{FL} = V_f = V_{vc} - V_{PM,0}$  is the free layer volume,  $V_{vc}$  is the volume of the vaporization chamber and  $V_{PM,0}$  is the volume occupied by porous medium.

In the second stage of the process (after the flash point), as described in the preceding chapter, the water temperature evolution tends to an exponential function where the vaporization phenomena are much more complex. As demonstrated previously, this stage is divided in two vaporization regimes with different evolutions. The rate of vapour generation is determined from the difference between the interfacial  $P_{v,i}$  and free surface  $P_{v,FS}$  vapour pressure, considered as the driving force of vaporization (or as superheating degree  $\phi$ ) at this stage.

Contrarily to what happens in LPV of free water,  $P_{v,i}$  is not equal to the saturation pressure of water. In LPV in porous media, the liquid-vapour interface is concave, as sketched in Figure VII.1(c). Due to the capillary effect, the pressure in the liquid phase is lower than the surrounding total pressure according to the Young-Laplace equation (Carey, 1992). Thus, the rate of vapour generation is given by the following equation:

$$\dot{m}_{v,i} = \frac{d}{dt} \left[ \frac{(P_{v,i} - P_{v,FS}) V_{VL} M_v}{RT_w} \right]. \quad (\text{VII.11})$$

As described by Udell (1983) and Carey (1992), assuming that at any point of the porous medium the thermodynamic equilibrium prevails and is characterized by a common temperature to all phases, the interfacial vapour pressure  $P_{v,i}$  and the liquid pressure will be related at each instant by the Kelvin and Young-Laplace equations (Udell, 1983; Carey, 1992; Webb and Kim, 2005). The magnitude of this relation depends on the magnitude of the capillary effect stated through parameters as: the pore radius  $r_p$ , the surface tension  $\gamma$  and the contact angle  $\theta$ . For determining  $P_{v,i}$  in the present model, the Kelvin equation (Eq.(VII.12)) is correlated with experimentally determined parameters (vaporization coefficient), so that the  $P_{v,i}$  evolution covers all typical experimental deviations and the model keeps realistic and robust as possible. Thus, Zhang et al. (2001) considered that:

$$P_{v,FS} = P_{v,i} \cdot \exp \left( - \frac{2\gamma M_w}{r_p \rho_w RT_w} \right), \quad (\text{VII.12})$$

can be approximately expressed by the function:

$$\frac{P_{v,i} - P_{v,FS}}{P_{v,i}} = \frac{2\gamma M_w}{r_p \rho_w R T_w}, \quad (\text{VII.13})$$

or:

$$1 - \frac{P_{v,FS}}{P_{v,i}} = \frac{2\gamma M_w}{r_p \rho_w R T_w}. \quad (\text{VII.14})$$

Therefore, as an assumption, the relation  $P_{v,FL}/P_{v,FS}$  was considered approximately equal to  $\varepsilon_{z_0,PM} = \varepsilon_{PM}(z = 0)$  (see Figure VII.1(b)), and likewise the ratio

$P_{v,FS}/P_{v,i}$ :

$$\frac{P_{v,FS}}{P_{v,i}} \approx \varepsilon_{z_0,PM}. \quad (\text{VII.15})$$

With this assumption, Eq.(VII.14) now reads

$$1 - \varepsilon_{z_0,PM} = \frac{2\gamma M_w}{r_p \rho_w R T_w} \quad (\text{VII.16})$$

and Eq.(VII.12) turns:

$$P_{v,FS} = P_{v,i} \cdot \exp\left(-\left(1 - \varepsilon_{z_0,PM}\right)\right), \quad (\text{VII.17})$$

from which  $P_{v,i}$  can be determined. The  $P_{v,i}$  values thus calculated showed a little deviation from the above assumption expressed by Eq.(VII.15), which suggested the adoption of the following modified form:

$$\frac{P_{v,FS}}{P_{v,i}} = X \cdot \varepsilon_{z_0,PM}. \quad (\text{VII.18})$$

With the coefficient  $x$  determined from Eq.(VII.18), a vaporization coefficient at the interface is proposed,  $\varepsilon_{i,PM} = x \cdot \varepsilon_{z_0,PM}$ , so that  $P_{v,i}$  can be recalculated from the follow equation:

$$P_{v,i} = \frac{P_{v,FS}}{\exp\left(-\left(1 - \varepsilon_{i,PM}\right)\right)}. \quad (\text{VII.19})$$

The mean relative error between  $P_{v,i}$  obtained from the first approximation and the recalculated  $P_{v,i}$  was determined; for instance, a value of 4.3% was obtained for PM1 and  $T_{w,0} = 18$  °C. Thus, Eq.(VII.19) was considered a good proposal for the determination of  $P_{v,i}$  to model the LPV process in porous media.

From Eq.(VII.12) and with the  $P_{v,i}$  values, it is possible to determine the relation  $2\gamma/r_p$  representing the surface tension forces.

As referred above and sketched in Figures VII.1(b) and (c), contrarily to the first stage of the process, in the second stage there is a gradient of vapour pressure developed above the free surface of the porous medium which creates a vaporization layer (with a volume  $V_{VL}$  that depends on the initial conditions) and can be described by the vaporization coefficient of the porous medium  $\varepsilon_{PM}$ . At this stage the control volume CV2 is divided into two parts. CV2' comprises a part of the vaporization layer, just above the surface of the porous medium, where the vapour pressure ranges from the free surface values  $P_{v,FS}$  ( $z=0$ ) to the free layer vapour pressure values  $P_{v,FL}$ , that are taken as uniform throughout the whole CV2". The volume  $V_{VL}$  comprises the control volumes CV1 (free spaces within pores) and CV2' (vaporization layer above the surface). CV2" represents the volume of the free layer  $V_{FL}$  – above the vaporization layer (see the Figure VII.1(b)).

The free surface vapour pressure  $P_{v,FS}$  is determined from Eq.(VII.1), for  $z=0$ . As referred in chapter V, this dependence is affected by the initial conditions and by the process evolution,  $\varepsilon_{z_0,PM} = \varepsilon_{z_0,PM}(t, C_{PM}, T_{w,0})$ , and needs to be calibrated. The vapour pressure in the free layer  $P_{v,FL}$  is determined from Eq.(VII.4), however, considering the details of the second stage (see the Figure VII.1(b)).

The vaporization coefficient of the porous media at the surface  $\varepsilon_{z_0,PM}$  was experimentally determined considering several initial conditions represented in

Table VII.1. Thus, from the experimental time evolutions of  $\varepsilon_{z_0,PM}$  for each initial condition (shown in section VII.4.1), a best fitting procedure was conducted with the *Sigma Plot software* leading to a three-parameter log-normal function for the first regime of the second stage of the LPV process ( $t < t_{RT}$ ), and to a two-parameter logarithmic function for the second regime ( $t > t_{RT}$ ), as follows:

$$\varepsilon_{z_0,PM}(t^*) = \frac{a_1}{t^*} \cdot \exp \left\{ -0.5 \left[ \ln \left( \frac{t^*}{a_2} \right) / a_3 \right]^2 \right\}, \quad (t < t_{RT}) \quad (VII.20)$$

$$\varepsilon_{z_0,PM}(t^*) = a_4 \cdot \ln(t^* - a_5) + a_6, \quad (t > t_{RT}) \quad (VII.21)$$

The parameters  $a_i$  (with  $i=\{1 \text{ to } 6\}$ ) in these equations depend on the initial temperature and heat capacity of the porous medium, in a way that was found to be well described by the polynomial Eq.(VII.22<sub>i</sub>) and Eq.(VII.23<sub>i</sub>):

$$a_i(T^*, C_{PM,0}^*) = X_{1i} + X_{2i}C_{PM,0}^* + X_{3i}T^* + X_{4i}C_{PM,0}^{*2} + X_{5i}T^{*2}, \quad \text{with } i = \{1 \text{ to } 5\} \quad (VII.22)$$

$$a_i(T^*, C_{PM,0}^*) = X_{1i} + X_{2i}C_{PM,0}^* + X_{3i}T^*, \quad \text{with } i = 6 \quad (VII.23)$$

where the coefficients  $X_{ni}$  are in turn listed in Table VII.2, and  $t^*$ ,  $T^*$  and  $C_{PM}^*$ , respectively, are the time, the initial temperature and the initial heat capacity of the porous medium, normalized as follows:

$$t^* = \frac{t - t_{\min}}{t_{\max} - t_{\min}}, \quad (VII.24)$$

$$T^* = \frac{T_{w,0} - T_{w,0\min}}{T_{w,0\max} - T_{w,0\min}}, \quad (VII.25)$$

$$C_{PM,0}^* = \frac{C_{PM,0} - C_{PM,0\min}}{C_{PM,0\max} - C_{PM,0\min}}. \quad (VII.26)$$

$T_{w,0_{\min}}$  and  $T_{w,0_{\max}}$  are, respectively, the limit values of the range of initial temperatures considered in the experimental study, and likewise for  $C_{PM,0_{\min}}$  and  $C_{PM,0_{\max}}$  regarding the initial heat capacity of the porous media. This parameter is estimated as  $C_{PM,0} = m_{t,0} \cdot c_{p,PM}$ , where  $m_{t,0}$  is the initial total mass and  $c_{p,PM}$  is the mass-weighted initial specific heat of the water-saturated porous medium. The  $t_{\min}$  and  $t_{\max}$  are the limit values of the process time.

**Table VII.2.** Values of the coefficients for Eq.(VII.20), Eq.(VII.21), Eq.(VII.22) and Eq.(VII.23).

	$t < t_{RT}$			$t > t_{RT}$		
	$a_1$	$a_2$	$a_3$	$a_4$	$a_5$	$a_6$
$X_{1i}$	0.0774	0.1742	0.2156	0.1446	0.2139	0.9322
$X_{2i}$	-0.1385	-0.0557	0.0563	0.0717	-0.2511	-0.0679
$X_{3i}$	-0.0059	-0.0231	-0.0518	-0.0769	-0.1333	-0.1165
$X_{4i}$	0.1341	0.0453	-0.0667	-0.0443	0.1901	-
$X_{5i}$	-0.0130	-0.0057	-0.0003	0.1608	0.0144	-

From Eqs.(VII.20) and (VII.21), it is shown that the vaporization coefficient in the second stage of the LPV process is described by two different multivariable functions depending on the vaporization regime. The switch in the model from Eq.(VII.20) to Eq.(VII.21) is made at the time to regime transition  $t_{RT}$ , whose dependence on the initial conditions is reasonably represented by Eq.(VII.27) fitted to the experimental data using the *Sigma Plot software* ( $R^2=0.7550$ ):

$$t_{RT} = 27.8649 - 2.6316 C_{PM,0}^* - 2.2805 T^* \quad (\text{VII.27})$$

As in chapter V, in the present mathematical model, evolutions of  $V_{VL}$  and  $V_{FL}$  are considered transition from the first to the second stage of the process. At the first stage,  $V_{VL}$  is constant and assigned the value of the initial volume of each porous medium  $V_{PM,0}$  (Table VII.1), while  $V_{FL}=V_{vc}-V_{PM,0}$ . At the second stage of the process, both  $V_{VL}$  and  $V_{FL}$  change with the process evolution (regime change), with initial temperature and with the type of the porous medium. Therefore, according to the experimental results, equations for these two volumes are proposed, similarly to its development in chapter V:

$$V_{FL} = a_0 \cdot \varepsilon_{z_0,PM} \left( t^*, C_{PM,0}^*, T^* \right) \quad (VII.28)$$

$$V_{VL} = V_{vc} - V_{FL} \quad (VII.29)$$

The determination of coefficient  $a_0$  followed the same methodology of chapter V, where it was made a sensitivity analysis of  $a_0$  based on the mean relative error  $\bar{\varepsilon}_r$  between the simulated water temperature values and experimentally determined ones, in order to evaluate the best value of  $a_0$  for minimizing the relative error at each initial condition.

The time evolution of the water temperature in the porous media is estimated after an energy balance to the control volume CV1, expressed by:

$$m_{t,0} c_{p,PM} \frac{dT_w}{dt} = -\dot{m}_{v,i} h_{fg} \cdot \quad (VII.30)$$

The initial total mass  $m_{t,0}$  is assumed as being constant because the amount of water vaporized does not affect the process dynamics, as demonstrated in the previous chapter. The initial conditions considered in the model correspond to the experimental conditions described in section VII.2.

The model equations were solved using the algorithm schematically shown on Figure VII.2 and implemented in *Microsoft Visual Basic 2010 Express*, a computer program for numerically solving algebraic equations. The calculation is made in two stages according to the flash point time  $t_{FP}$  experimentally determined and represented in Eq.(VII.31) ( $R^2=0.8203$ ). The criterion to stop the simulation is the process limit time: 150s.

$$t_{FP} = 17.1733 - 3.4862 C_{PM,0}^* - 15.7509 T^* + 1.4866 C_{PM,0}^{*2} + 9.2766 T^{*2} \quad (VII.31)$$

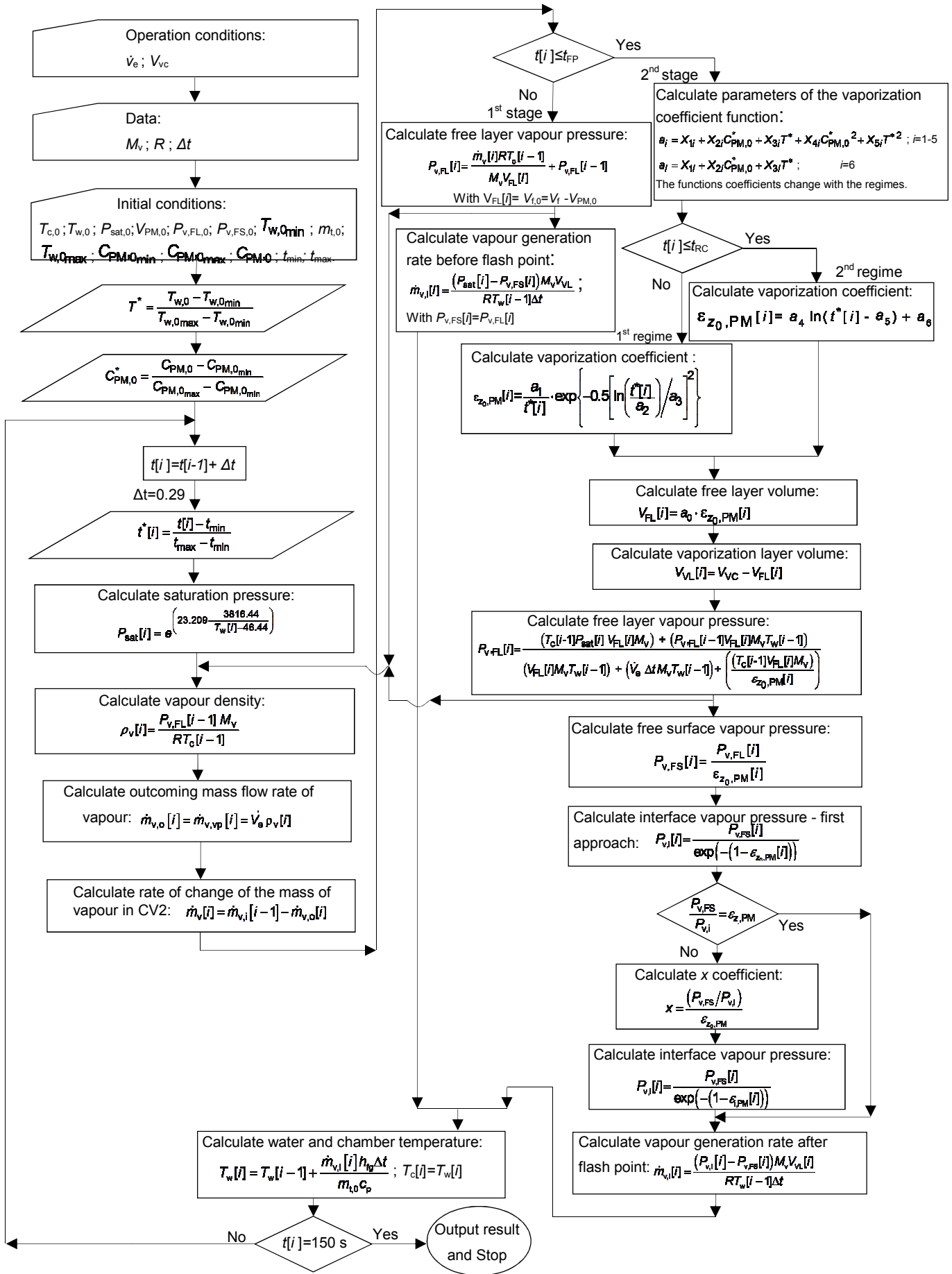
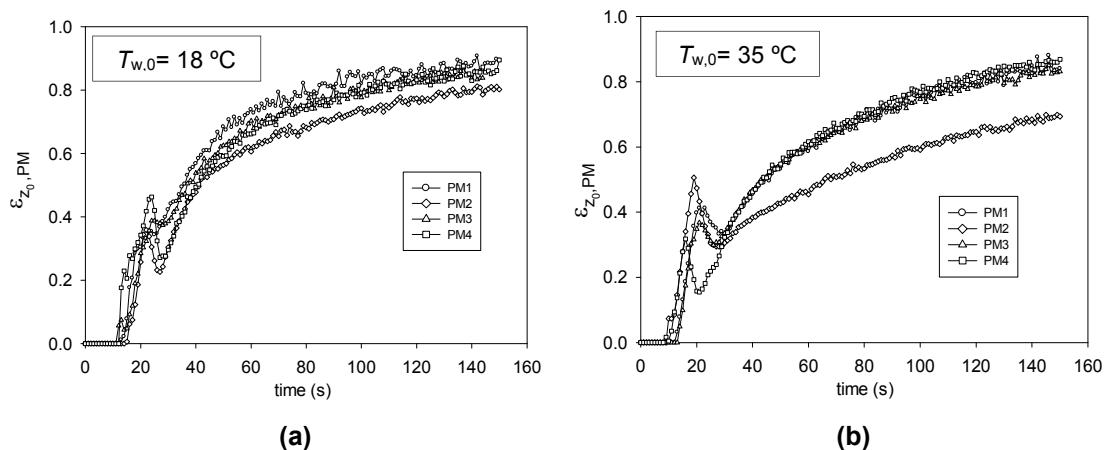


Figure VII.2. Flow chart of the simulation program.

## VII.4. Results and discussion

### VII.4.1. Features of development and calibration of the mathematical model

In Figures VII.3(a) and (b) the time evolutions of the vaporization coefficient is shown for two initial temperatures and for all porous media, as estimated by Eq.(VII.1) after the measured data. In all cases, the different regimes of the second stage of the LPV process are clearly identified. In the first regime, there is a sharp increase of  $\varepsilon_{z_0,PM}$  up to a peak value that corresponds to the point of maximum boiling rate. After a sharp drop, the second regime of the second stage begins with a second increase of  $\varepsilon_{z_0,PM}$ , now smoother as there is a weaker boiling. These results are in agreement with the description and characterization of the LPV in different porous media studied in chapter VI.



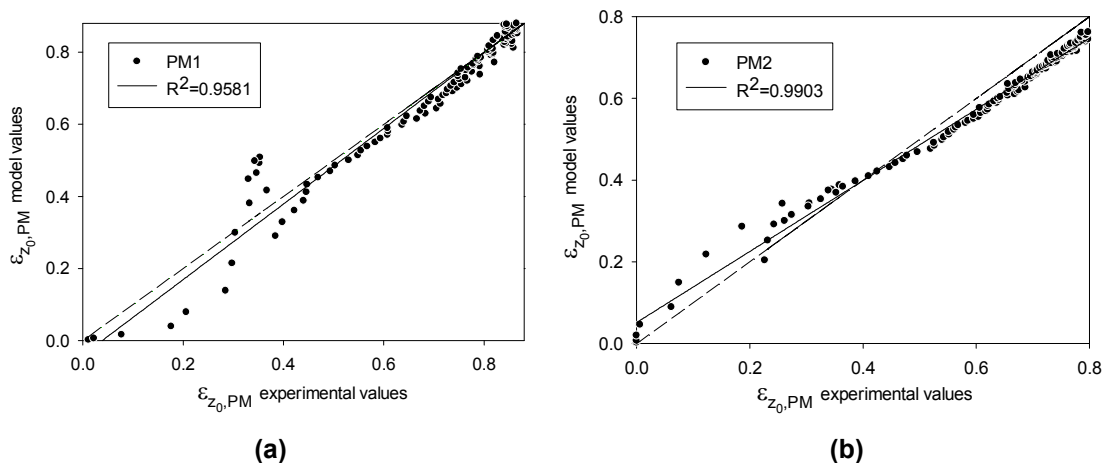
**Figure VII.3.** Time evolutions of the vaporization coefficient for the different porous media and two distinct initial temperatures.

For all porous media tested, it was verified that the vaporization coefficient is higher for lower initial water temperature (Figures VII.3(a)). As described in chapter V, this is related with the initial superheating degree  $\phi$ , which is lower for lower initial water temperature and thus induces a lower free surface vapour pressure ( $P_v(z \approx 0)$ ), leading to a higher vaporization coefficient (see Eq.(VII.1)). This influence of  $T_{w,0}$  is much more pronounced for the porous medium PM2, which exhibits for  $T_{w,0}=35$  °C a quite different evolution, with rather lower values of  $\varepsilon_{z_0,PM}$  in the second regime of the

second stage. This is another aspect of the different behaviour for PM2 already reported in chapter VI. In fact, PM2 has a greater amount of water initially absorbed, higher density in the porous structure and a larger fraction of solid material, leading to differences in the capillarity effects that make the vaporization phenomena to be significantly different in this medium.

With the remaining porous media, no significant differences are observed in the  $\varepsilon_{z_0,PM}$  evolutions in the second regime for  $T_{w,0} = 35\text{ }^\circ\text{C}$ . However, for  $T_{w,0} = 18\text{ }^\circ\text{C}$ , PM1 shows higher values, while PM3 and PM4 exhibit similar evolutions of the vaporization coefficient. Again, these results are related with the structure of the porous media. PM1 has less water absorbed and a sparse microstructure leading to a larger area for the vaporization to occur, i.e. a greater ratio of free surface area to volume of water absorbed. PM3 and PM4 have rather similar structures and likewise show similar vaporization coefficients.

Figure VII.4 shows the comparison between the experimental and the modelled values (by Eq.(VII.20) and (VII.21)) of  $\varepsilon_{z_0,PM}$  in different porous media and for  $T_{w,0} = 18\text{ }^\circ\text{C}$ . In all cases, a good agreement is observed, with correlation factors between 0.9581 and 0.9903. The higher differences between experimental and modelled values occur in the regime transition (around  $t_{RT}$ ), due to difficulties in defining the switching between Eq.(VII.20) and Eq.(VII.21). However, in a global way, it is possible to conclude that the multivariable functions determined for the vaporization coefficient represent satisfactorily the two regimes of the second stage of the process.



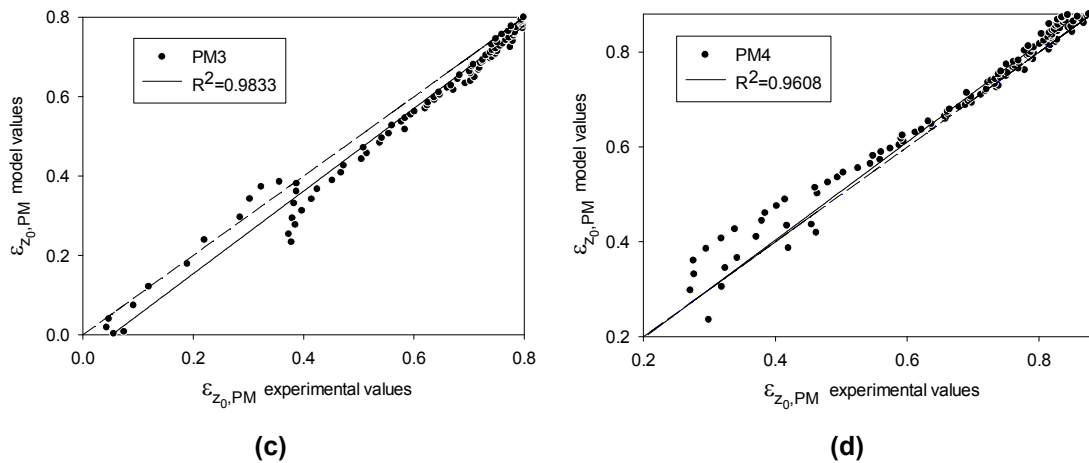


**Figure VII.4.** Comparison between experimental and simulated values of the vaporization coefficient in different porous media and for  $T_{w,0}=18$  °C.

In Figure VII.5 both coefficients can be seen following profiles with similar trends,  $\varepsilon_{i,PM}$  presenting higher values than  $\varepsilon_{z_0,PM}$ , as expected from their definitions.

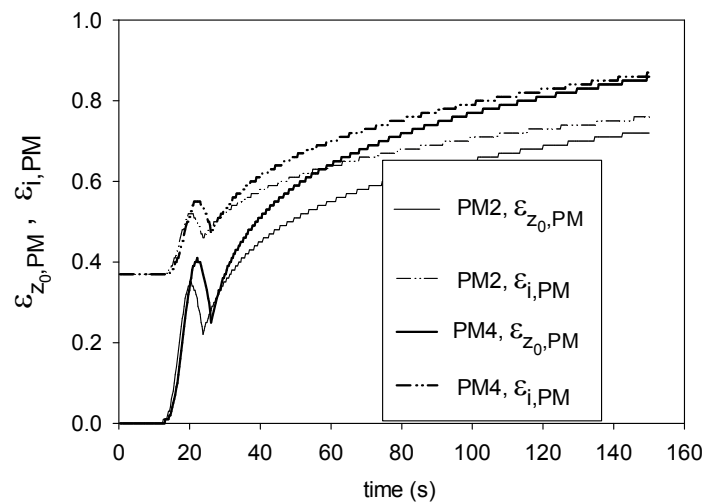


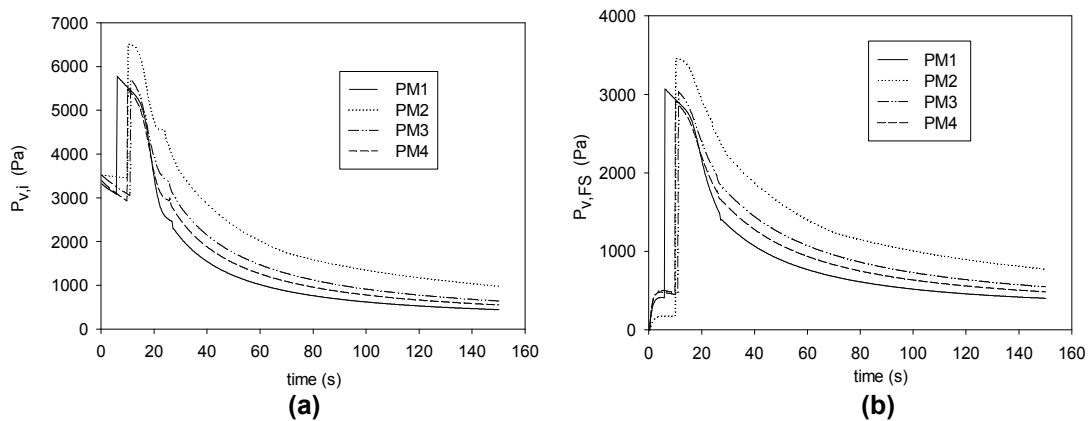
**Figure VII.5.** Evolution of the vaporization coefficients for two porous media and  $T_{w,0}=27$  °C.

As referred before, at the first stage of the process there is not a confined vaporization layer above the surface (see Figure VII.1(a)), and thus no vaporization coefficient is defined. However, it is seen in Figure VII.5 that  $\varepsilon_{i,PM}$  has a constant value during this stage, for both porous media. This value results from the proportional relation between  $P_{sat}$  and  $P_{v,FS}$  (driving force of the process) at the first stage. In

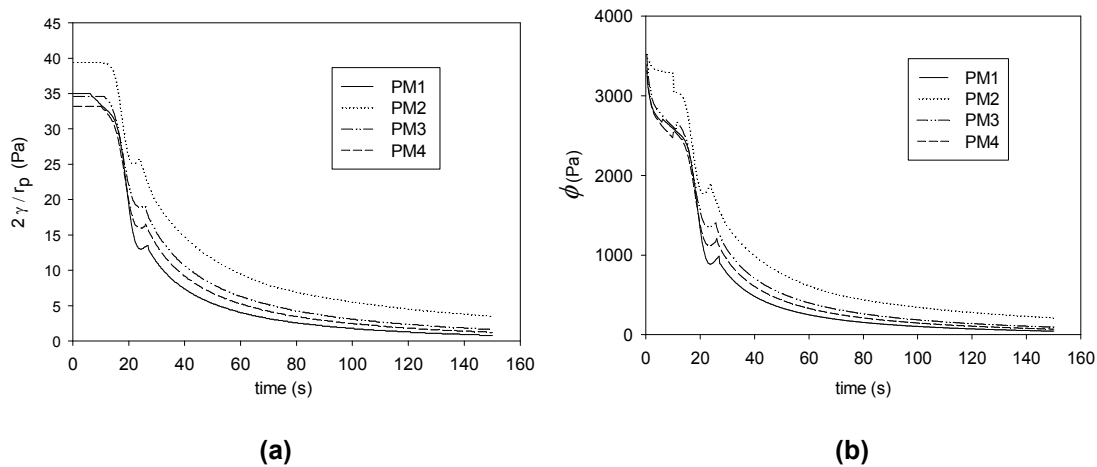
Figure VII.5 it is also verified that both vaporization coefficients present lower values for PM2 than for PM4.

In order to detail the LPV in porous media and to confirm the importance of the calibration methodology for the understanding and the characterization of the process, Figures VII.6 and VII.7 show the evolutions of a set of pressures representative of the vaporization phenomena, as predicted by the model.

The evolutions of  $P_{v,i}$  and  $P_{v,FS}$  presented in Figures VII.6(a) and (b), respectively, show clearly the differences between the two stages of the process. During the first stage,  $P_{v,FS}$  increases up to a threshold level where the flash point is reached. This level depends on the pump capacity (a constant, in this case) and the volume of the free layer. As it is seen in Figure VII.6(b), this value is lower for PM2 which is related with its much lower volume of the vaporization layer (see Table VII.1). This condition leads to a higher volume of free layer and, consequently, to a lower free surface vapour pressure. As referred in section VII.3, at this stage,  $P_{v,i}$  takes the value of the saturation pressure, thus decreasing with the liquid water temperature. The time of the flash point is clearly identified in both pressure evolutions for all porous media. Also in the second stage, PM2 shows a different behaviour, with higher values of  $P_{v,i}$  and  $P_{v,FS}$ . PM1 presents the lowest values, followed by PM4 and PM3. A similar relation is observed in Figure VII.7(a) between the values in the evolutions of the ratio  $2\gamma/r_p$ , that represents the capillary effect, indicating again the great influence of the medium microstructure and consequently of the initial amount of water absorbed. Contrarily to what was referred in chapter VI, Figure VII.7(b) allows to verify that PM2 has a higher superheating degree of water, together with higher values of  $P_{v,i}$  and  $P_{v,FS}$ .

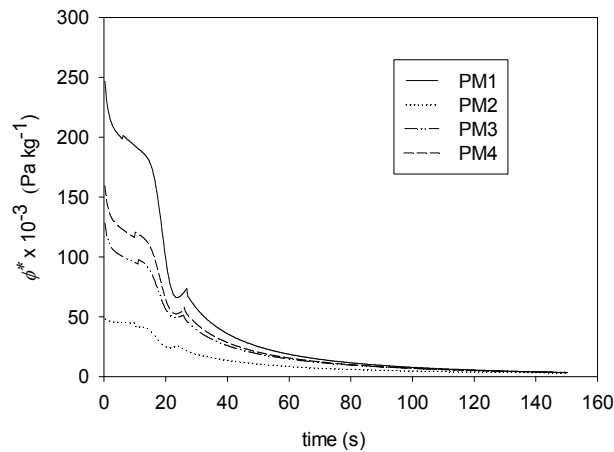


**Figure VII.6.** Evolutions of (a) the vapour pressure at the interface and (b) the free surface vapour pressure for four porous media and  $T_{w,0}=27^{\circ}\text{C}$ .



**Figure VII.7.** Evolutions of (a) the surface tension pressure  $2\gamma/r_p$  and (b) the superheating degree for different porous media and  $T_{w,0} = 27$  °C.

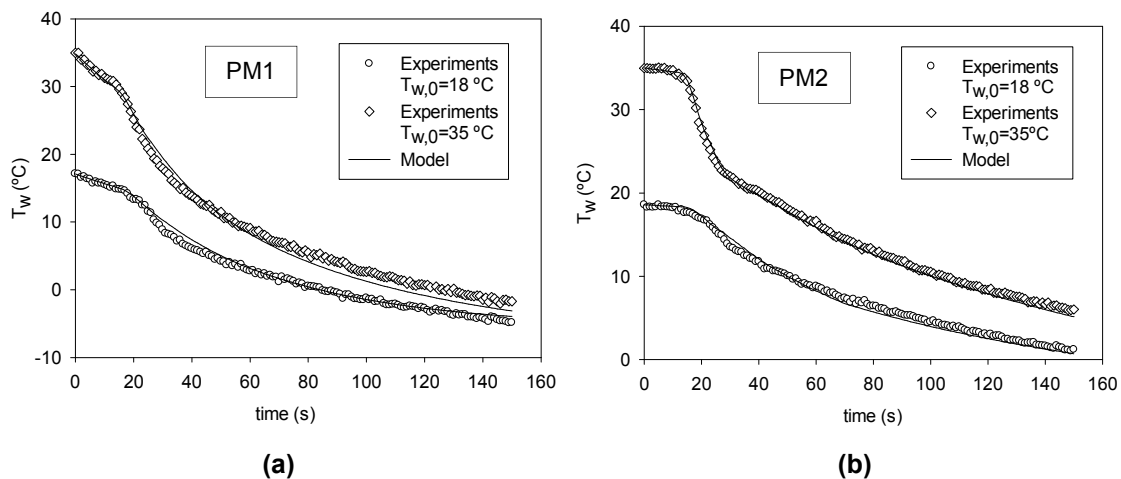
Comparing the results obtained in this chapter (shown ahead in section VII.4.2) with the experimental results for the water temperature evolution shown in the previous chapter, it is verified that a higher superheating degree does not correspond to a higher rate of decrease in temperature. This happens because the initial amount of water contained in the PM has a great influence in the LPV evolution, with a retarding effect on the water temperature evolution and indirect positive effect in the superheating degree (Figure VII.7(b)). So, the evolutions of the specific superheating degree  $\phi^*$  (i.e. per unit of initial mass of water) found for the different porous media are compared in Figure VII.8, showing higher  $\phi^*$  values for PM1 and lower for PM2, according to the evolution of the rate of decrease in the water temperature. These results confirm the same conclusion preliminarily presented in the previous chapter, where the PM1 shows a specific rate of water vaporization higher than PM2 (Figure VI.9, chapter VI). In cases where the porous medium has different properties with different capacity of absorbing water, the superheating degree is a characteristic parameter of the LPV process whose specific value should be determined in order to reproduce the process efficiency in terms of the temperature evolution.

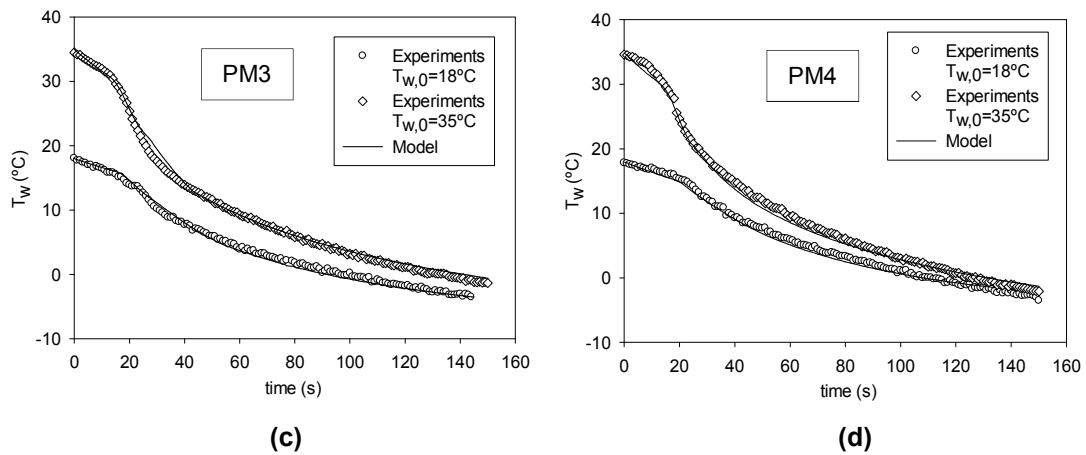


**Figure VII.8.** Evolutions of the specific superheating degree for different porous media and  $T_{w,0} = 27\text{ }^{\circ}\text{C}$ .

### VII.4.2 Validation of the mathematical model

As referred in the introduction of the present chapter, this work aims to develop and calibrate the mathematical model for LPV in porous media with experimental results. After the calibration activity (section VII.3), where the model calibration and its benefit for modelling the LPV phenomena are presented, an empirical validation was then used to assess the validity of the calibrated model to simulate the LPV process, taking the experimental data as a reference. The present section shows the comparison between the water temperature evolution predicted by the model and the measured data. The corresponding error bands for 5%, 10% and 20% are also determined. The good agreement obtained with the results for all porous media studied and for two different initial temperatures is evident in Figures VII.9(a)-(d).

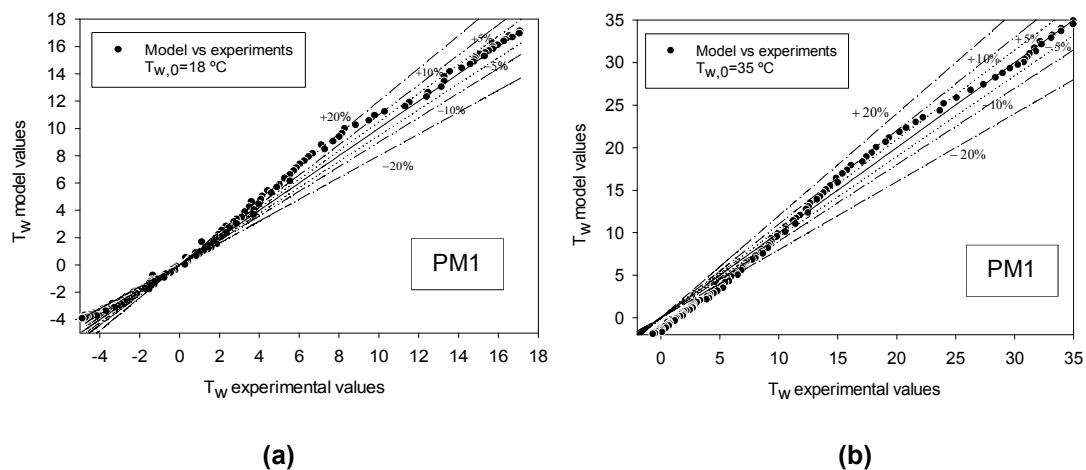


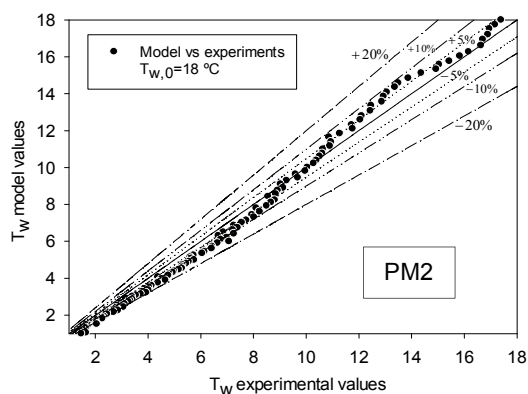


**Figure VII.9.** Comparison between experimental and predicted results of the water temperature evolution for different initial conditions.

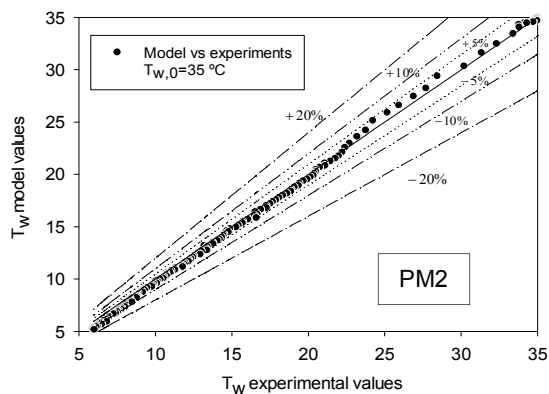
On the other hand, the determined error bands are represented in Figures VII.10(a)-(h), confirming the good agreement between measured and simulated values. Considering the cases presented in the overall, the majority of the predicted values of water temperature are within the range of the  $\pm 5\%$ , except for isolated cases in zones of regime or stage transition, where deviations reach  $\pm 10\%$ .

It is possible to conclude that the model developed and the calibration methodology for low-pressure-vaporization in porous media provides a good agreement with the experimental results, thus proving the reliability of the present model.

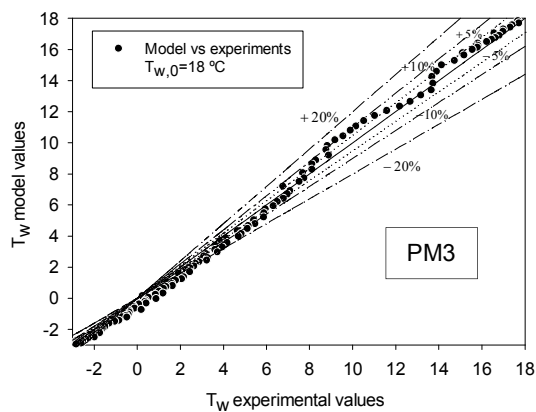




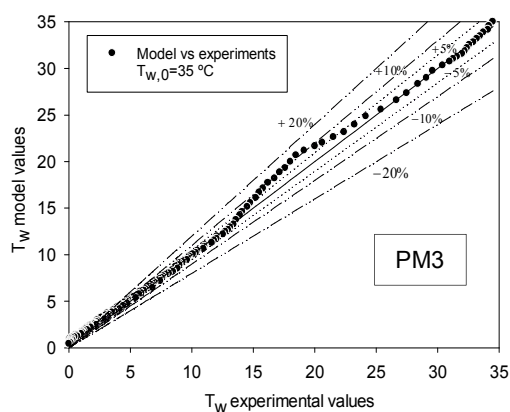
(c)



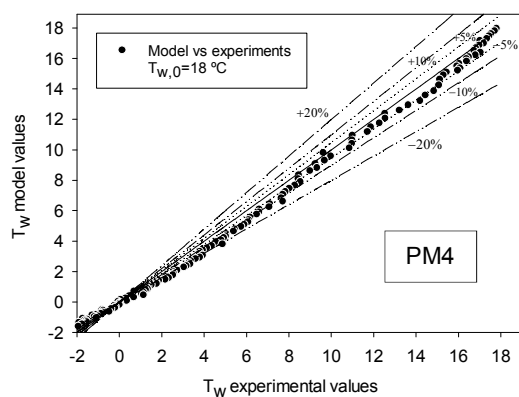
(d)



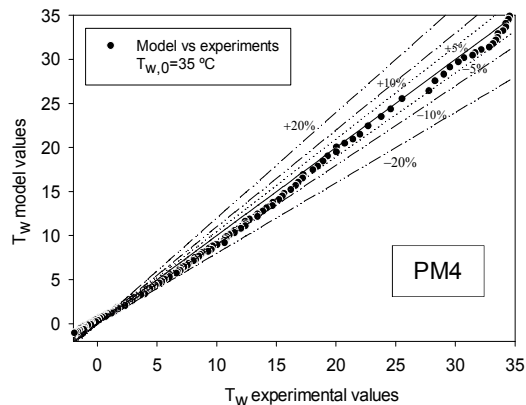
(e)



(f)



(g)



(h)

**Figure VII.10.** Comparison between experimental and modelled results for different PM and initial conditions.

## VII.5. Conclusions

---

The development and calibration of the mathematical model to predict the low-pressure-vaporization (LPV) process in porous media were performed, and the validation was made considering four different types of porous media. This work aimed to improve and fulfil most of the gaps found in models developed by other authors in this area, whose results confirmed the importance of the new considerations adopted.

The main findings of this study are:

- The vapour pressure is not uniform throughout the vaporization chamber – there is a vaporization layer above the free surface of the porous medium;
- In the vaporization layer, there is a gradient of pressure from the free surface vapour pressure to the vapour pressure in the free layer (where a uniform value is assumed);
- The interfacial vapour pressure is much higher than the saturation pressure;
- The surrounding has a significant influence on the vaporization phenomena in all zones of the porous medium – which is accounted for through the vaporization coefficient;
- The vaporization coefficient is described by two different multivariable functions, each one for each of the second stage regimes, which showed good agreement with experimental results;
- PM2 presents higher surface tension forces evolution, higher  $P_{v,i}$  and  $P_{v,FS}$  and, consequently, higher superheating degree;
- The specific superheating degree is higher for PM1 and lower for PM2 which showed that the initial water absorbed has a significant contribution in the LPV process and indirectly in the superheating degree;
- In studies with porous media with different properties and different water absorption capacities, the superheating degree can not be a representative parameter to describe the process efficiency in terms of the temperature evolution. However, it reproduces well the vaporization rate.
- The validation of the model showed a good agreement between measured and simulated values, with deviations lower than  $\pm 5\%$ .

Thus, it can be conclude that the calibrated mathematical model describes well the experimental results and is a good referential model to various studies and applications.



---

***Part D - Low-pressure-vaporization to enhance the heat transfer across surfaces***

---



---

## **VIII. Experimental study of ability of the low-pressure-vaporization in porous media to enhance the heat transfer across surfaces**

---

The present chapter aims to study the ability of the LPV to enhance the heat transfer across a container wall coated with free water (FW) or with a wet porous media (PM). For that purpose, an experimental study with six different coatings media: four porous media and two different volumes of free water, was carried out. On those experiments the temperature of the water within the container, whose outer surface was coated by either a porous media or free water, was measured.

The experimental set-up comprises two main components: the vacuum chamber (VC) and the depressurization system (DS). Part of the VC volume is occupied by a container coated with one of the previous referred media. This set of container and coating medium is insulated from the VC walls. When free water is used as coating medium, the initial volume of water influences the temperature drop within the coating as well as within the container, however, the differences arising from the initial volume of the water used as coating are much bigger for the temperature drop of the coating media than for the temperature of the water within the container. The rate of temperature decrease of the water for the standard LPV is smaller for the first regime and bigger for the second, after the flash point, when compared with the rate of the temperature decrease of the free water used as a coating media. On the other hand, when porous media are used as coating, the temperature evolution of the water within the PM is not directly correlated with the initial volume of the water absorbed and this non-correlating behaviour is also observed when the temperature of the water within the container is compared with the temperature of the coating media.

The main differences between the temperature of the PM in standard LPV process and in PM when is used as a coating media around a container, for all PM, are observed for the second regime of the second stage; the rate of temperature decrease is much higher for the standard LPV process than for the case where PM are used as coating media. These are even bigger if the initial temperature of the water is increased.

The results obtained in this chapter put in evidence, as it was shown in previous chapters, that the LPV process is a good technology to enhance heat removal and temperature control for several practical application.

*Keywords:* Low-pressure-vaporization; coated container; coating porous media; coating free water; bulk free water; bulk porous media

## VIII.1. Introduction

---

Throughout the years, the study of processes to enhanced heat transfer across, or from, surfaces has shown to be a very interesting subject with a wide variety of practical applications. The use of these enhancement heat transfer techniques, either active and/or passive have lead to quite a few procedural improvements in some industries. Several authors (Wen and Wang, 2002; Zhang and Shoji, 2003; Phan et al., 2009; Li et al., 2011; Nam et al., 2011; Dawidowicz and Cieśliński, 2012) have focused their works in the study of passive techniques for heat transfer enhancement. For example, Wen and Wang (2002) focused their studies on the influence of the fluid wettability on pool boiling heat transfer with three different surfactants. Small amounts of surfactants have shown to activate nucleation sites in bubble growth and so to increase the boiling heat transfer. Other authors, (Meng and Hu 2005; Zhao et al. 2008; Chen 2011) have analysed the application of passive techniques involving heat and mass exchange for temperature control in buildings. Zhao et al. (2008) have used several types of porous materials, considering their application with high heat and mass transfer potential in climate systems on buildings. Meng and Hu (2005) studied the possibility of application of humid porous media in temperature control of roofs, designating this process by passive water evaporation. In a similar way Figueiredo and Costa (2004) evaluated the use of porous media for thermal protection against high intensity heat fluxes (flames). On the other hand, the wetting surfaces (surfaces cover by free water) have also been used to enhance boiling heat transfer as a passive technique. Jo et al. (2011) focused their study in the analyse of the nucleate boiling heat transfer performance on wetting surfaces, emphasising the importance of this type of surfaces to increase the active nucleation sites that leads to the increase of the heat transfer. However, despite of all this research efforts it is known that a lot of work is to be done in this area and a gap in the knowledge needs to be fill.

Liquid to vapour phase change processes are known to present much higher heat transfer capability than single phase phenomena. As a way to quickly reach phase change condition, the low-pressure-vaporization, presents the important features to be considered an enhanced heat transfer process, as had been showed in previous chapters. In LPV, the liquid, initially in sub-cooled equilibrium state, when is exposed to a sudden pressure drop that takes its value bellow the saturation pressure at the liquid temperature, moves into a meta-stable phase and begins to vaporize throughout its bulk volume in order to reach a new state of equilibrium. In the LPV the great part of

the energy required for the vaporization of the liquid is taken from the liquid itself. Thus, once the referred process leads to vaporization rates, and consequently to heat removal capabilities, much higher than those obtained during non-ebullition vaporization (vaporization at normal conditions), an opportunity to use it within a enhance heat transfer technology can be envisaged.

The study of LPV process in free water (LPV-FW) and in different types of porous media (LPV-PM) has been described in previous chapters. In those chapters was shown that, for both media, free water and porous materials, the LPV is a good way to enhance the rate of vaporization and consequently the heat removal. Despite of this common ability it seems that the porous media present a slightly bigger potential to be used as a media in heat removal practical applications. In fact, as referred by Webb and Kim (2005), significant improvements of the heat transfer technologies have been established with the use of media that promote high nucleation boiling, such as porous materials, with different geometries and properties providing by this way an increase heat transfer coefficient. On the other hand, specific CFD simulations of the low pressure heat and mass transfer processes in porous food, performed by Sun and Hu (2003), have put in evidence the complexity and the relevance of the boiling vaporization in porous materials temperature control. Several other authors, like (Wang and Sun, 2002a; Jin and Xu, 2006a, 2006b) also focus the importance of the dynamics of the vaporization within pores for the global process of the heat removal. Given the predictable importance of the vaporization phenomena within porous media in enhanced heat transfer processes, mainly when that occurs at specific external conditions, as the case of low pressures, several researchers became focussed in the study of the dynamics of the vaporization process in the pores and on how the process is affected by the pores characteristics (Peng, Wang, and Lee 2002; Prat 1998; Fang, Peng et al. 2004; Yortsos and Stubos 2001; Mantle et al. 2003). Specifically, Fang et al. (2004) referred that boiling in porous medium is affected by pore structure (pore scale and bead size), bubble growth and coalescence, pore variation and vibration, as already referred in chapter VI. They highlight, beyond that, the importance of the surface tension in bubble shape and interface formation that has found to have a high contribution to the bubble growth.

Considering the enhancing heat transfer advantages (described above and in previous chapters) that are expected to arise from the association of the LPV process and the use of passive techniques, the main objective of this chapter is to study the

ability of the LPV to enhance the heat transfer across container wall coated with free water (FW) or wet porous media (PM).

In order to assess that ability for the different coating media an experimental study, with six different coatings: four types of the porous media, each one with different properties, and two different volumes of free water, were carryout. The comparison, for each one of the analysed media, of the LPV temperature evolutions when in contact with a closed container, or when isolated (vd. results of Chapter IV and VI), allows to take some conclusions about their ability to enhance the heat transfer across surfaces. Beyond that, the temperature of the water within the container whose outer surface was coated, was monitored. The evolution of this temperature allows to identify the coating media with better ability to enhance the heat transfer across the container wall.

## **VIII.2. Low-pressure-vaporization of a coated container – physical model**

---

As referred in the previous chapters, the LPV is a complex physical phenomenon which result from a sharp pressure drop in a closed space, where water (or any other liquid) is initially in equilibrium with its vapour at a pressure close to the atmospheric value (Saury et al., 2002; Augusto et al., 2012).

As described in chapter VI and chapter III both, the LPV-PM and the LPV-FW, occurs in two stages. Nevertheless, LPV in free water and in porous media have their own peculiarities that lead significant differences in the process evolution (e.g. temperature and pressures profiles). In initial stage of the LPV-FW, while the total pressure in the chamber is above the saturation pressure of water, the vaporization at its water surface is ruled by surface vaporization phenomena, which means, diffusion of the water vapour in the still air above it (Cioulachtjian et al., 2010). When the total pressure, by the action of the DS, drops below the saturation pressure, the vapour production begins to be governed by the boiling process. A boiling front is established, at the points where the temperature of the water is higher, that quickly extends to all water volume. In LPV-PM, the initial stage is ruled by the diffusion of the water vapour and bubble growth in microlayer with a much bigger significance than the similar phase in the free water. The vaporization occurs in the pores and the transport phenomena is associated with the pressure-driven hydrodynamic flow of vapour towards the outer surface of the porous media (Udell, 1983; Yortsos and Stubos, 2001; Peng et al., 2002;

Fang et al., 2004; Wang and Peng, 2004). Details of the different phases of the vaporization phenomena in porous media were given in previous chapters.

As described in section VIII.1, this work aim to study the LPV process of a coated container, either with FW (coating free water) or PM (coating porous media), to assess its ability to enhance the heat transfer across it. The surface used in this study is those from a closed glass container filled with water (volume=200ml), as showed in Figure VIII.1. Therefore, the energy necessary to vaporize water of the coating media (CM) is taken from the coating media itself, that includes the dry media and the water within it, and also from of the attached container (wall and content). Significant reductions of the temperature of the coating media and of the water within the close container are then reached during the LPV process. The instant where the water temperature of the coating has a sharp decrease, designated by flash point, is where the second stage of the LPV process starts. This second phase is normally divided in two regimes where the first is characterized by an intense boiling vaporization, throughout all the water volume while in the second regime, the vaporization occurs mainly near the outside layer of the coating media, with weak boiling, as refer in previous chapters.

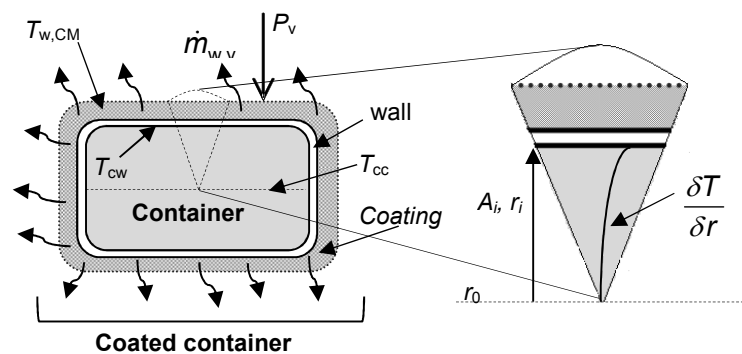


Figure VIII.1. Schematic diagram of the LPV phenomena in coated container.

### VIII.3. Experimental set-up and methodology

---

This section describe the experimental set-up and methodology used to study the low-pressure-vaporization process of a coated container with porous media (PM) or free water (FW). The parameters measured were the temperature of the coating media (coating free water (FW) or coating porous media (PM)), the temperature of the water within the close container at the centre of the container and nearby the wall and the total pressure within the vaporization chamber.

The experimental set-up used in this study comprises two main components: the vaporization chamber (VC) and the depressurization system (DS), as sketched in Figure VIII.2. The VC is a stainless steel cylindrical chamber with a volume of 0,017 m<sup>3</sup>. The DS consists of a vacuum pump with a volume flow rate capacity of 0.0033 m<sup>3</sup> s<sup>-1</sup>. The temperatures are measured by K-type thermocouples - TC1, TC2 and TC3 (accuracy: ±1.5 °C; response time:100 ms; Ø≈0.5mm), and the chamber pressure is measured with an Edwards™ ASG 1000 mbar gauge (accuracy: ±2 mbar). These sensors are connected through a National Instruments™ data acquisition system to a personal computer where the signal is treated and saved using a LabVIEW™ 8.6 based software.

In these experiments, beyond the analysis of the effect of the different type of coating media, porous media or free water, the effect of the initial temperature of the water on the coating media was also studied. Four types of the porous media (PM1, PM2, PM3 and PM4, described in detailed in Chapter VI) and two different water volumes ( $V_{w,0,1}=200$  ml and  $V_{w,0,2}=100$  ml) with three different initial water temperatures (19, 27 and 34 °C) were considered (see in Table VIII.1). At each experiment, the temporal evolution of the temperature in the coating media  $T_{w,CM}$ , of the temperature in the water inside the close container, at the center of the container  $T_{cc}$  and near by the container wall  $T_{cw}$  (Figure VIII.1) as well as the pressure in the VC was measured. The coating media is placed surrounding the close container, as showed in Figure VIII.1, and when the DS is turned-on and the pressure decreases, starting the process. For each set of initial conditions (cf. Table VIII.1), the experiments were run in duplicate, and the arithmetic mean of the instantaneous measured values was considered.

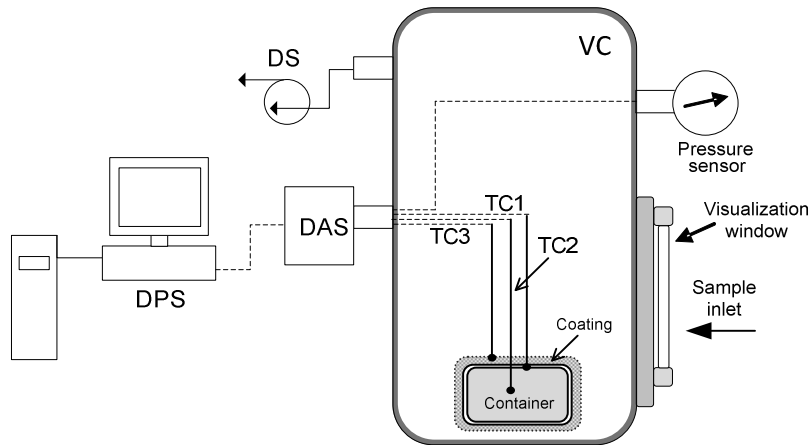


**Figure VIII.2.** Schematic diagram of the experimental set-up of the LPV process. (DS - depressurization system; DAS - data acquisition system; VC – vaporization chamber; DPS - Data processor and storage).

**Table VIII.1.** Initial conditions used in the experimental tests.

	PM				FW	
	PM1	PM2	PM3	PM4	$V_{w,01}$	$V_{w,02}$
	100% stainless steel	30% cotton 70% cellulose	75% viscose 25% polypropylene	83.5% cotton 16.5% polyester	100% water	100% water
$V_{w,0}$ (ml)	13.82	73.35	27.23	21.31	200	100
$T_0$ (°C)	19, 27, 34	✓	✓	✓	✓	✓

## VIII.4. Results and discussion

The methodology and the results presented in this section are those referred in section VIII.3. The results are presented separately for each one of the coating media and for each one of the initial conditions studied (both the initial volume of the water and its temperature were varied). The raw data, which mean the variation of the temperature with the process time for each one of the coating media (coating free water or coating porous media) in contact with the container - heat source surface, (see section VIII.2) will be compared with the variation of the temperature of the free water, or of the corresponding porous media, in a standard LPV process, in which the free water, or the porous media, is isolated from any heat source surface (see chapter IV and VI). The comparison between the time evolution of the total pressure within the VC for standard and a LPV processes where coatings media are used, will be also made.

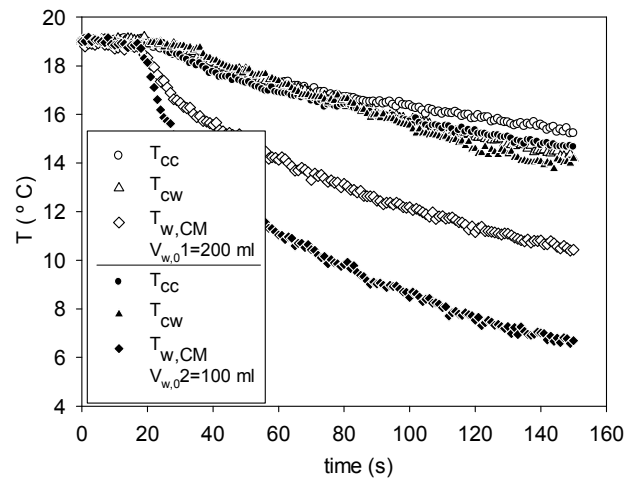
## VIII.4.1 Low-pressure-vaporization of a coated container with free water

### *Influence of the initial conditions*

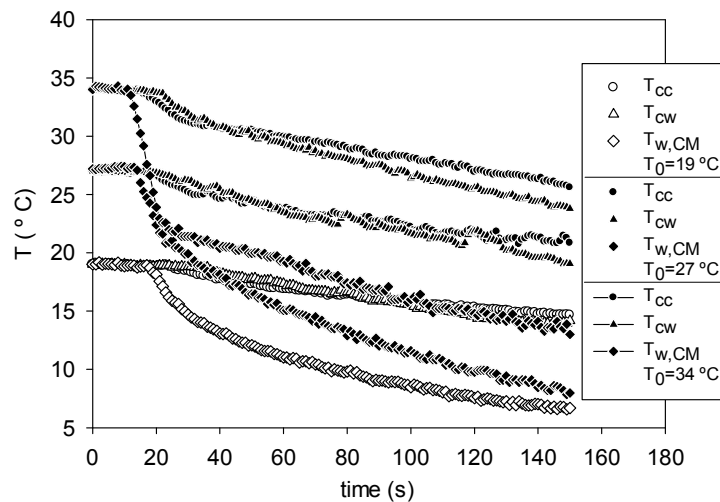
As presented in previous sections and reported in chapter III and IV, the LPV-FW process is divided in two stages. In the first one, the vaporization occurs at the water free surface and is ruled by the diffusion of the water vapour in the still air around it; it is commonly designated as evaporation. This initial stage is clearly apparent in Figures VIII.3 and VIII.4, lasting from the initiation of the process up to the flash point – the beginning of the sharp temperature decrease.

Figure VIII.3 shows the water temperature evolution within the coating, within the container, at the centre and nearby the wall, for experiments with same initial temperature and different initial volumes of the coating free water ( $V_{w,01}$  and  $V_{w,02}$ ). As it might be expected, as smaller is the initial volume of water, as sharper is the temperature drop of the coating free water after the flash point. Consequently, as sharper are the temperature drops of the water at the centre and nearby the wall of the container. However, these differences are not proportional, whereas the  $T_{w,CM}$  drop in  $V_{w,01}$  is two times bigger than those observed for the  $V_{w,02}$ , however, the  $T_{cw}$  and  $T_{cc}$  variation is less than one time.

In Figure VIII.4 can be seen that the temperature drop at the flash point of the water temperature of the coating is as more pronounced as higher is the  $T_0$ . As for the initial volume of the water used as coating media, the effect of the initial temperature on the temperature evolutions of the water within the container is perceptible but much weaker than that observed for the coating media itself. The thermal inertia of the water within the container and the heat transfer resistances across the container wall are supposed to be on the basis of this fading phenomenon.



**Figure VIII.3.** Evolution of the water temperature in coating, of the temperature in center and wall of the container, for two different free water volumes.



**Figure VIII.4.** Evolution of the water temperature in coating, of the temperature in center and wall of the container, for three different initial temperatures in  $V_{w,0.2}$ .

### **LPV performance – effect of free water as coating**

To study the capacity of the free water coating to enhance the heat transfer across the container wall a comparison between the results reported in this chapter and those of the evolution of the temperature of the water in a standard LPV process (bulk free water, reported in Chapter IV), where the water is in an isolated container with despicable heat capacity wall, was made. A similar comparison for the pressure evolution was also made. In both cases, and once as exposed in chapters III and IV,

the LPV-FW only show significant evolution in both the temperature and the pressure after the flash point; only this stage of the LPV is analyzed. As also is described in section VIII.2 of this chapter, the second stage of the LPV process begins at the flash point and is divided into two different vaporization regimes (see chapter IV, Saury et al., 2002 and Cioulachtjian et al., 2010). The first of these regimes begins exactly at the FP and is associated to a violent boiling phenomenon. The second regime is characterized by vapour bubble formation underneath the liquid free surface.

For all of the experimental situations shown in Figure VIII.5, but specially for the ones with initial higher temperatures, the rate of temperature decrease of the water for the standard LPV (bulk free water) is smaller in the first regime and larger for the second regime when compared with the rate of the temperature decrease of the free water in contact with the container (heat source surface or non-adiabatic surface). When the data related with the temperature are cross-checked with the data from the variation of the pressure (see Figure VIII.6) it is possible to see that the coating free water is kept on a saturation state while the bulk free water is on a superheated state. While the coating free water vaporizes cools down, and follows the saturation temperature, the bulk free water is unable to vaporize at the rate necessary to decrease the temperature to the saturation level. The higher intensity of the boiling process during the first regime of the second stage of the coating free water is thought to be mainly due to a much more extensive surface area when compared with the bulk free water. However, in second regime, the heat provided through the container wall, and the much bigger thermal inertia of the system, makes the rate of the temperature decrease smaller for the coating free water than for the bulk free water. This heat flux, nevertheless, favors the vaporization of the water and justifies a slightly bigger total pressure for this case in comparison with the bulk free water.

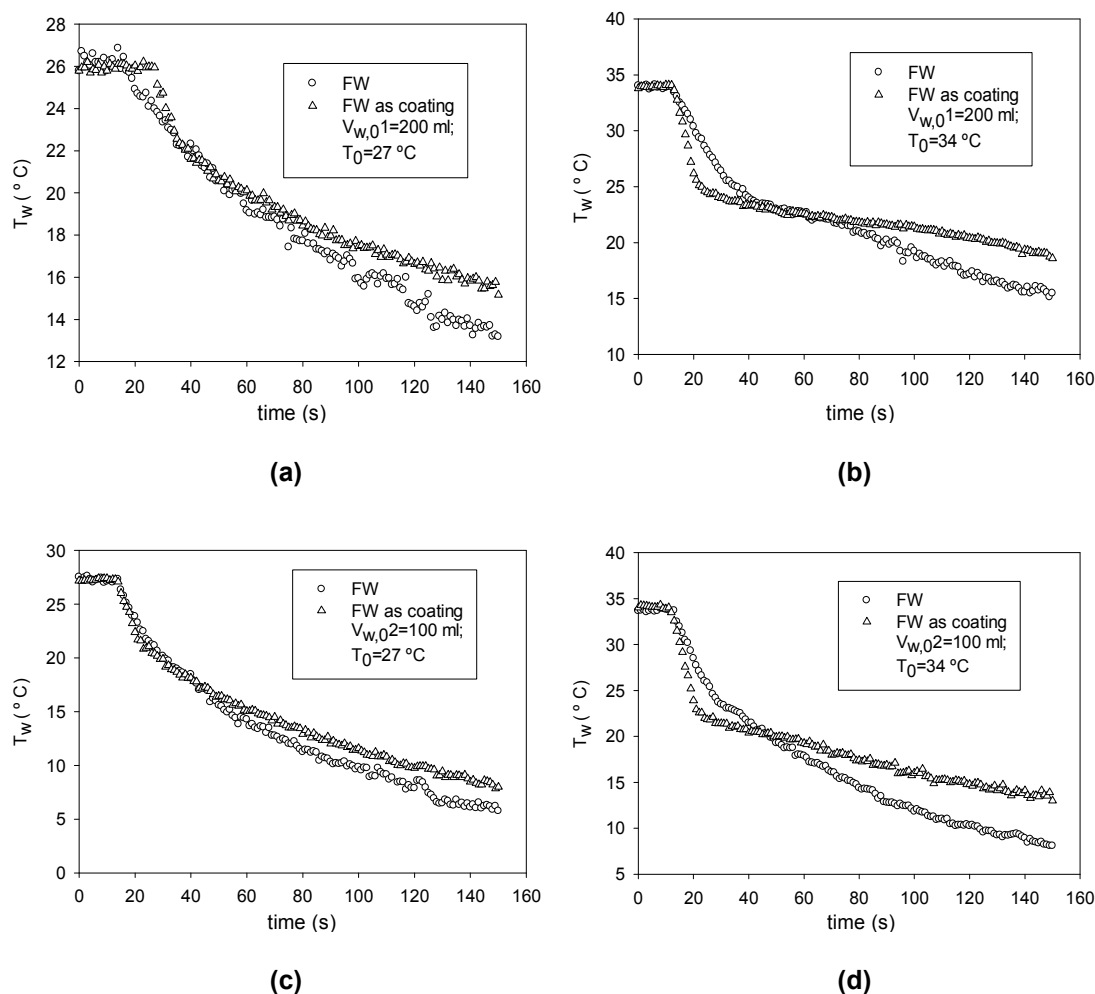


**Figure VIII.5.** Water temperature evolution in coating free water (FW as coating) and bulk free water (FW) for (a)  $V_{w,01}=200$  ml and  $T_0 = 27$  °C; (b)  $V_{w,01}=200$  ml and  $T_0 = 34$  °C; (c)  $V_{w,02}=100$  ml and  $T_0 = 27$  °C; (d)  $V_{w,02}=100$  ml and  $T_0 = 34$  °C.

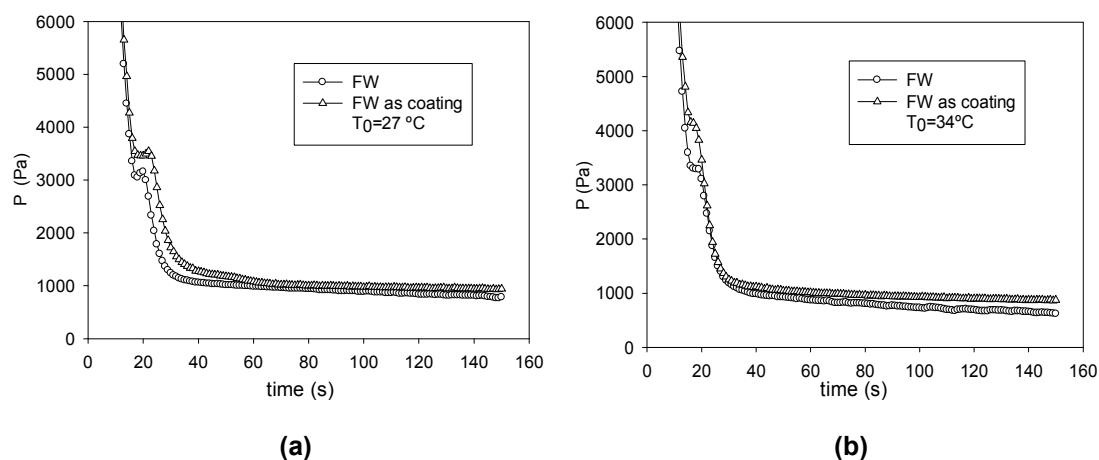


**Figure VIII.6.** Total pressure evolution in vaporization chamber using coating free water (FW as coating) or bulk free water (FW) for  $V_{w,01}$  (a)  $T_0 = 27$  °C and (b)  $T_0 = 34$  °C.

## VIII.4.2 Low-pressure-vaporization of a coated container with porous media

### *Influence of the initial conditions*

As described in the chapter VI and referred in the section VIII.2 of this chapter the LPV-PM process is divided in two stages: prior and after the flash point. However, and on the contrary to what is observed for the LPV-FW, due to a significant vaporization prior to the flash point, a non despicable temperature decrease of the water in the porous material is observed from the first moments of the process (cf. chapter IV).

The same kind of behaviour is observed when the porous media are used as coating media as can be seen in Figure VIII.7 (a). Nevertheless, contrarily to what happen when the free water is used in a LPV process as a coating media (cf. section VIII.4.1), the water temperature evolution of the PM is not inversely correlated with the initial volume of the water absorbed. For example, despite of showing the small initial water content (27.23 ml), it is not PM3 but PM2, that presents an initial water content of 73.35 ml, and that shows the sharper temperature drop. The same kind of non-correlating behaviour is also observed when  $T_{cc}$  and  $T_{cw}$  are compared with  $T_{w,CM}$ . The porous media for which the sharper variations of the  $T_{w,CM}$  were found are not the ones for which the sharper variations of  $T_{cc}$  and  $T_{cw}$  were found. Comparing the Figure VIII.7 (a), (b) and (c), it can be seen that PM1 has the higher decrease rate of  $T_{w,CM}$  while it is PM4 that causes the sharper drop in  $T_{cc}$  and  $T_{cw}$ . On the other hand, PM2, which do not show the smaller  $T_{w,CM}$  variation is the one showing the smaller drop in the water within the container. All this findings are considered to be due to the specific properties of the porous media (shown in Table VIII.1) and how these affect their ability to exchange heat with the container surface.

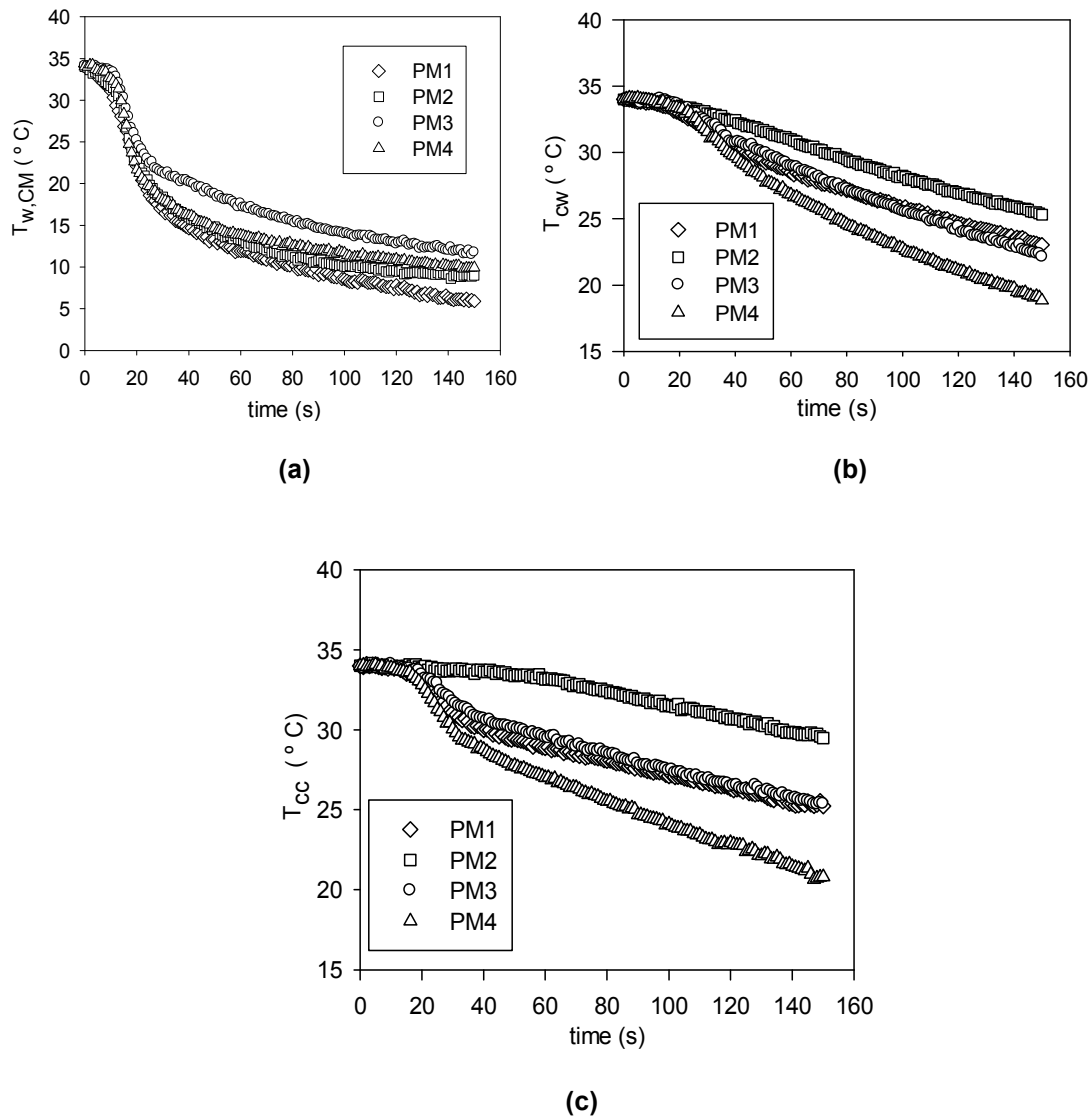


**Figure VIII.7.** Temperature evolution (a) of the water in coating (b) of the container wall and (c) of the container center using four different types of the PM as coating and  $T_0=34$  °C.

Figure VIII.8 shows the evolution of the  $T_{w,CM}$ ,  $T_{cc}$  and  $T_{cw}$  for three different values of the initial temperature ( $T_0 = 19, 27$  and  $34$  °C). Such as in the case where the FW is used as coating media it can be said that the temperature of the water drops within the PM is as steeper as higher is the  $T_0$ . Nevertheless, higher initial temperatures and steeper temperature drops do not have equal correspondence with the  $T_{cc}$  and  $T_{cw}$  variations that do not show any relevant difference arising from the initial temperature.

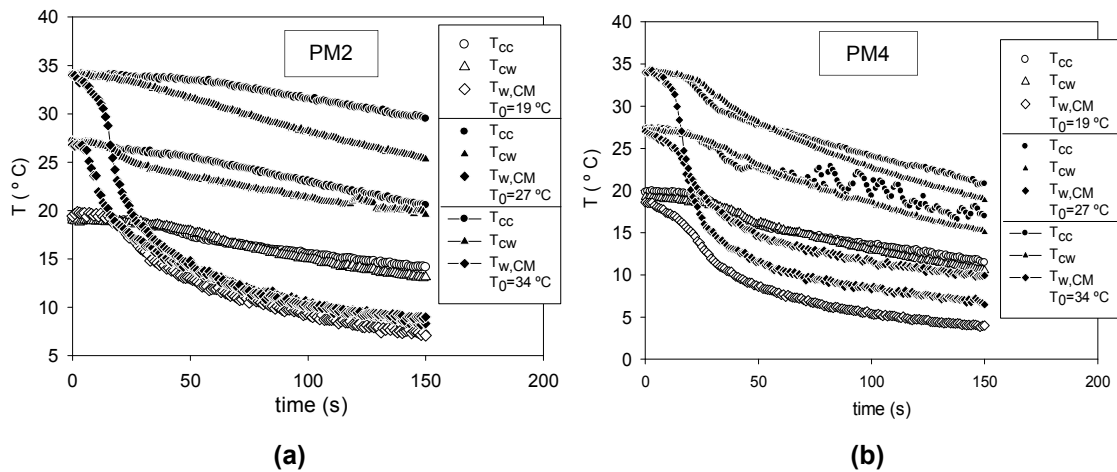
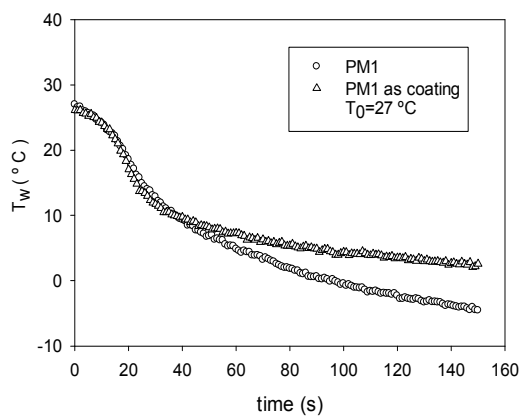


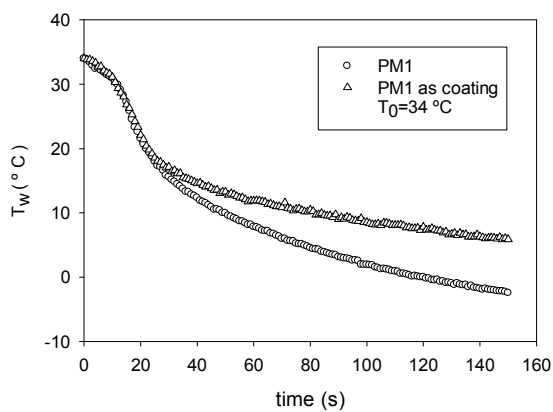
**Figure VIII.8.** Evolution of the water temperature in coating, of the temperature in center and wall of the container for PM2 and PM4 and for three different initial temperatures.

### ***LPV performance – effect of the porous media as coating***

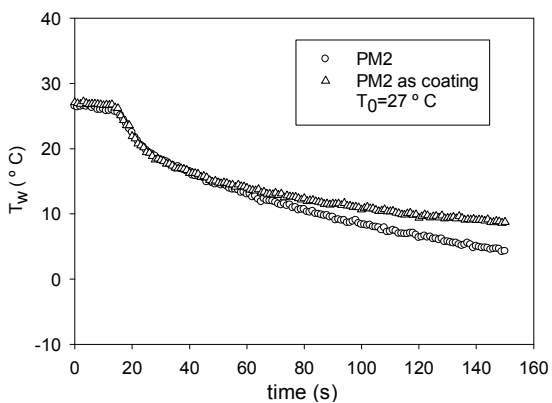
As it was done when the FW was used as coating media (cf. section VIII.4.1), to evaluate the effectiveness of the PM to enhance the heat exchange across the container wall, a comparison between the variation of the temperature of the PM in the standard LPV process (bulk porous media), for which the PM is considered adiabatic, and the LPV process where the PM are in contact with a container are shown in Figure VIII.9 (a) to (h). The main differences, for all the PM, are observed for the second regime of the second stage. All the results obtained for the situation in which the PM is used as coating show, for this regime, a smaller rate of temperature decrease. This is due to the bigger thermal inertia of the set PM-container, and reveals that heat is being removed through the container wall. Unless for the PM2, this behavior is dependent of the initial temperature. However, the differences between the rate of temperature decrease observed for the isolated PM or for the PM used as coating is emphasized with the increase of the initial temperature. The bigger temperature differences, that can be correlated with the bigger ability to enhance the heat exchange across the container wall was found for the PM4.



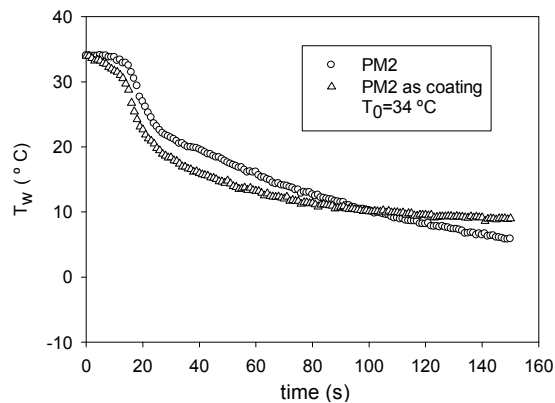
(a)



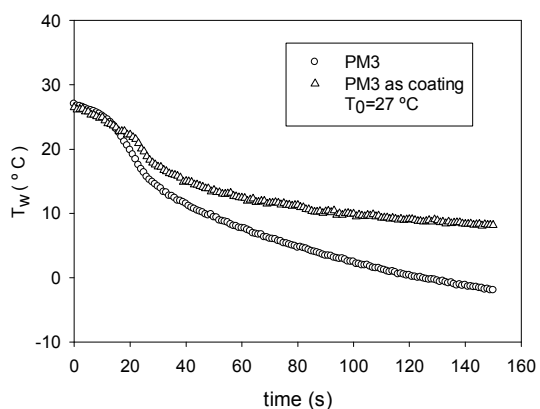
(b)



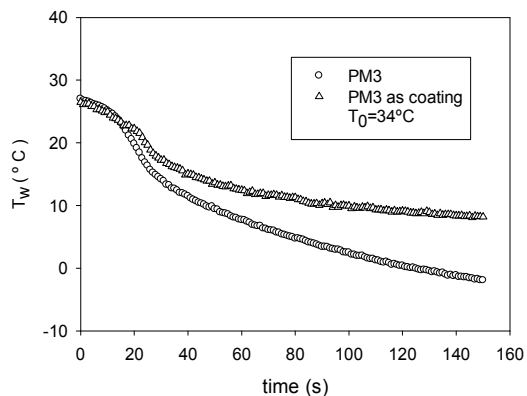
(c)



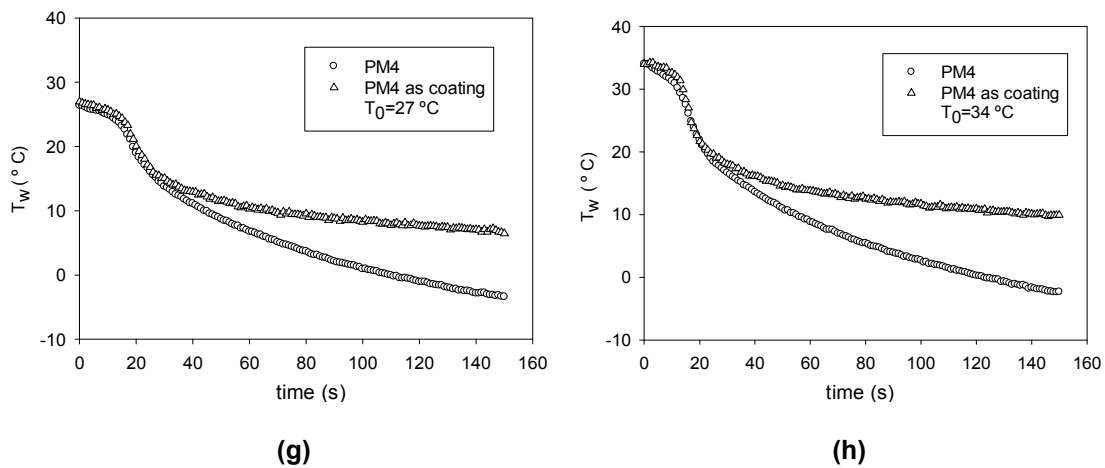
(d)



(e)

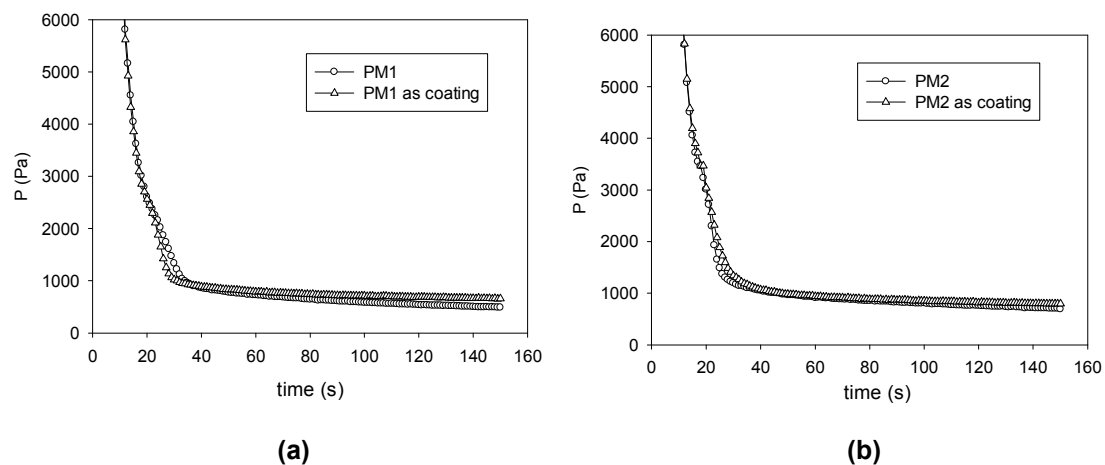


(f)



**Figure VIII.9.** Water temperature evolution for different types porous media used as coating (PM as coating) and as bulk porous media (PM) for  $T_0=27$  °C and  $T_0=34$  °C.

Beyond the comparison of the temperature variation for the coating and non-coating (adiabatic and non adiabatic) situations, the evaluation of the ability of the different PM to enhance the heat exchange across the container wall also includes the comparison of the variation of the total pressure within the VC. Those results are shown in Figure VIII.10. Slightly higher values of the total pressure are found for all the non-adiabatic situations. These points to a higher rate of vaporization that only do not have consequences at the PM temperature (that should be smaller for the cases presenting higher total pressures) due to the energy that crosses the container.



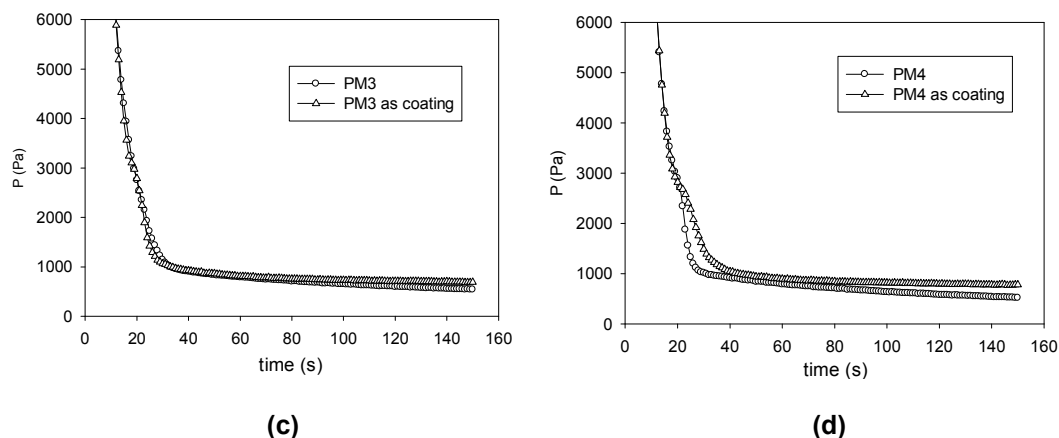


**Figure VIII.10.** Total pressure evolution in VC for  $T_0=27$  °C and for (a) PM1; (b) PM2; (c) PM3 and (d) PM4 used as coating (PM as coating) and as bulk porous media (PM).

## VIII.5. Conclusions

---

In this chapter an experimental work was realized to study the ability of the LPV to enhance the heat transfer across a container coated with free water (FW) or wet porous media (PM). Six different coatings media have been used: four types of the porous media, each one of it with their own characteristic properties, and two different volumes of free water.

The main findings of this study are:

- As smaller is the initial volume of water, as sharper is the temperature drop of the coating free water after the flash point and consequently, as sharper are the temperature drop of the water at the centre and nearby the wall of the container;
- The temperature within the coating media (either wet porous media or free water)  $T_{w,CM}$  drops in  $V_{w,0.1}$  is two times bigger than observed for the  $V_{w,0.2}$ . However, the variation induced by the changes in the volume of the free water in contact with the container wall, on the temperatures of the water within the container (for both the centre and wall temperatures) was found to be smaller;
- When the free water is used as coating media, the effect of the initial temperature on the temperature evolution of the water within the container is perceptible but much weaker than observed for the coating media itself. The thermal inertia of the water within the container and the heat transfer resistances across the container wall are supposed to be on the basis of this fading phenomenon;

- The rate of temperature decrease of the water for the standard LPV with bulk free water, is smaller for the first regime and bigger for the second regime when compared with the rate of the temperature decrease of the free water in contact with the container;
- When porous media are used as coating media the evolution of the water temperature within the PM is not directly correlated with the initial volume of the water absorbed. The same kind of behaviour is observed when  $T_{cc}$  and  $T_{cw}$  are compared with  $T_{w,CM}$  PM1 has the higher decrease rate of  $T_{w,CM}$  while it is PM4 that causes the sharper drop in  $T_{cc}$  and  $T_{cw}$ . This, are considered to be due to the specific properties of the porous media and how these affect their ability to exchange heat with the container surface;
- The main differences between the temperature of the PM in standard LPV process and the temperature of the PM when used as a coating media in contact with a container, for all the PM, are observed for the second regime of the second stage and the differences between the rate of temperature decrease is emphasized with the increase of the initial temperature;

Thus, from the work developed in this chapter, it is possible to conclude that LPV process of porous media in contact with surfaces show an interesting ability to enhance the heat transfer across surfaces and this may have a very high potential for practical use in a wide range of practical applications.



---

***Part E – Conclusions and forthcoming work***

---



---

## **IX. Conclusions and forthcoming work**

---

In this chapter, a general overview of the main results is presented, along with the most pertinent conclusions. At last, proposals for future work are recommended.

---

### **IX.1. General overview and conclusions**

---

Currently, a problem strongly studied, both in academic as industrial level, is the speed and efficiency of industrial processes related with the physical phenomena of heat and mass transfer in the procedural steps. In the present work the low-pressure-vaporization (LPV) process was studied in detail, in the perspective of a technology capable to improve and to control the heat and mass transfer, in stages of the several industrial areas. In this context, the present document was divided into five parts, each one with chapters which address the study of specific issues of the main goal. Part A was divided in two chapters that include an introduction, the motivation and aim of the work, as well as the description of the thesis structure. A concise state of the art was also presented, about vaporization phenomena, LPV phenomena and description of the main areas where the LPV is used as a technology to enhance the heat and mass transfer. Parts B, C and D are the core of the present thesis. Part B, composed by three chapters, reports the experimental study of the LPV process of free water, and the development and calibration of a first mathematical model. Part C contains two chapters, which were dedicated to the experimental study of the LPV in different types of porous media and to the development of a mathematical model which describes the LPV in porous media. Part D presents the study of the capability of the LPV in the enhancement of heat transfer across surfaces, using porous media and free water as coatings. Part E is dedicated to describe the most relevant conclusions and to present some recommendations for future work.

In Part B, the results of a preliminary mathematical model of the LPV process of free water, led to the conclusion that it is ruled by the time evolution of the partial vapour pressure in the chamber, which is influenced by the vacuum pump flow rate. It was shown that both the initial mass of water and the vacuum pump flow rate have influence on the time to the flash point, as well as on the final temperature of the water. Thus, it was concluded that the first stage of the process has an expressive contribution for the total process duration and can not be neglected, contrarily to previous statements of

other authors. In the experimental study of the LPV of free water it was shown that the initial volume and temperature have great influence on the water temperature and pressure evolutions, as well as on the times to the stage and regime transitions. Likewise, the water temperature and pressure evolutions, as well as the mass of vaporized water are also affected by the height of the bulk liquid. It was shown that the LPV process is divided into two stages, the second one being divided into two regimes. The first of these regimes is characterized by an intense boiling and the second one is characterized by a much smoother boiling localized underneath the liquid free surface. In the physical and experimental calibration of the preliminary mathematical model, the following parameters were defined and calibrated: the time to the flash point and the time to the regime transition; the magnitude of the difference between the water-vapour interface pressure and the experimentally measured was established, through the definition of the vaporization coefficient, as well as the free surface and free layer vapour pressures. The vaporization coefficient was described through a log-normal function, whose parameters were described by polynomial functions of the initial water temperature and volume. It was concluded that the vaporization coefficient is strongly affected by the evolution of the LPV stages and regimes, by the initial water temperature and volume. The volume of the vaporization layer was also calibrated, and changes with the process evolution and with the initial conditions, being inversely proportional to the vaporization coefficient. In the validation of the calibrated mathematical model, a good agreement between experimental and simulated values was verified. In Part C, in the experimental study of the LPV in four different porous media, it was concluded that the rate of temperature decrease and the rate of energy removal depend strongly on the total amount of water initially contained in the porous medium, and in turn depends on the porous medium microstructure. Significant differences were observed in LPV process between the porous media and the free water, the energy removal by LPV being higher in the former. Thus, this experimental activity confirms the importance of the porous media to enhance heat transfer for a wide range of applications. The results obtained in the development and calibration of the mathematical model of the LPV in porous media recognized the importance of the new considerations to improve the other authors' models and to determine parameters that are hard to obtain from the experimental research. It was shown that the surrounding has a significant influence on the vaporization phenomena in all zones of the porous medium and that the initial amount of water has a significant contribute to the LPV process and indirectly in the superheating degree. It was shown a good agreement between the measured and simulated values. The mathematical model developed for LPV in porous media could be a good reference to several studies and applications.

In Part D, it was concluded that the LPV process of free water and in porous media is able to enhance heat transfer across a coated surface and, consequently, to intensify the temperature decrease, particularly when porous media were used as coating.

Thus, it is possible to affirm that the proposed goal was achieved. From the whole work developed and presented in this thesis it was possible to assert that the low-pressure-vaporization is a process with great potential, capable to be used for different applications where the enhancement of the heat and mass transfer rate are crucial.

## **IX.2.Suggestions for forthcoming work**

---

The results of the present work reveal the importance of the low-pressure-vaporization process to improve the heat and mass transfer rate. However, it was demonstrated that LPV of water evolution change with the initial conditions, with the medium used and the surrounding. Thus, taking into account practical applications, it is proposed the implementation, in a laboratorial scale, the LPV for a concrete application, previously defined and selected, with the aim of a rapid heat removal, as well as for application in stages of the processing of products. For this purpose, the range of the initial conditions should be adjusted and the porous media structure should be selected and/or modified, as well as new porous media studied. In parallel, an improvement of the mathematical model adjusting it to the specific situation should be made, to obtain the most realistic results. It is also suggested to study new passive techniques to enhance heat transfer coupled to LPV, in view of the selected application, and comparing the performance with the one presently studied.

In this context – implementation of the LPV of water in specific applications, provision studies must be made to find a solution to capture the generated vapour, minimizing the vaporization layer formation, without being necessary to increase the vacuum pump flow rate. This solution should be tailored for a specific application, because for another configuration it may have to be adapted.

---

## X. References

---

- Aoki, I., 2000. Analysis of characteristics of water flash evaporation under low pressure conditions. *Heat Transfer—Asian Research* 29, 22–33.
- Augusto, C.M., Gaspar, A.R., Ribeiro, J.B., Ferreira, V.R., Costa, J.J., 2012. A mathematical model describing the two stages of low-pressure-vaporization of free water. *Journal of Food Engineering* 112, 274–281.
- Bakhshi, M., Mobasher, B., 2011. Experimental observations of early-age drying of Portland cement paste under low-pressure conditions. *Cement and Concrete Composites* 33, 474–484.
- Bakhshi, M., Mobasher, B., Soranakom, C., 2012. Moisture loss characteristics of cement-based materials under early-age drying and shrinkage conditions. *Construction and Building Materials* 30, 413–425.
- Barták, J., 1990. A study of the rapid depressurization of hot water and the dynamics of vapour bubble generation in superheated water. *International Journal of Multiphase Flow* 16, 789–798.
- Bazyma, L. A., Guskov, V.P., Basteev, A. V., Lyashenko, A.M., Lyakhno, V., Kutovoy, V. a., 2006. The investigation of low temperature vacuum drying processes of agricultural materials. *Journal of Food Engineering* 74, 410–415.
- Bouchama, A., Sebastian, P.S., Nadeau, J.-P., 2003. Flash evaporation: modelling and constraint formulation. *Trans IChemE* 81, 1250–1258.
- Carey, V.P., 1992. *Liquid-vapor phase-change phenomena—An introduction to the thermophysics of vaporization and condensation process in heat transfer equipment*. Hemisphere, Pub. Corp. Washington, D. C.
- Chen, R.-H., Phuoc, T.X., Martello, D., 2011. Surface tension of evaporating nanofluid droplets. *International Journal of Heat and Mass Transfer* 54, 2459–2466.
- Chen, W., 2011. Thermal analysis on the cooling performance of a wet porous evaporative plate for building. *Energy Conversion and Management* 52, 2217–2226.
- Cheng, H.-P., Lin, C.-T., 2007. The morphological visualization of the water in vacuum cooling and freezing process. *Journal of Food Engineering* 78, 569–576.
- Cioulachtjian, S., Launay, S., Boddaert, S., Lallemand, M., 2010. Experimental investigation of water drop evaporation under moist air or saturated vapour conditions. *International Journal of Thermal Sciences* 49, 859–866.

- Das, A.K., Das, P.K., Bhattacharyya, S., Saha, P., 2007. Nucleate boiling heat transfer from a structured surface – Effect of liquid intake. *International Journal of Heat and Mass Transfer* 50, 1577–1591.
- Dawidowicz, B., Cieśliński, J.T., 2012. Heat transfer and pressure drop during flow boiling of pure refrigerants and refrigerant/oil mixtures in tube with porous coating. *International Journal of Heat and Mass Transfer* 55, 2549–2558.
- Dostal, M., Petera, K., 2004. Vacuum cooling of liquids: mathematical model. *Journal of Food Engineering* 61, 533–539.
- Drummond, L., Sun, D.-W., 2008a. Temperature evolution and mass losses during immersion vacuum cooling of cooked beef joints - A finite difference model. *Meat science* 80, 885–91.
- Drummond, L., Sun, D.-W., 2008b. Immersion vacuum cooling of cooked beef - Safety and process considerations regarding beef joint size. *Meat science* 80, 738–43.
- Drummond, L., Sun, D.-W., 2012. Evaluation of the immersion vacuum cooling of cooked beef joints-mathematical simulation of variations in beef size and porosity and pressure reduction rates. *Innovative Food Science & Emerging Technologies* 16, 205–210.
- Drummond, L., Sun, D.-W., Vila, C.T., Scannell, A.G.M., 2009. Application of immersion vacuum cooling to water-cooked beef joints – Quality and safety assessment. *LWT - Food Science and Technology* 42, 332–337.
- Eames, I.W., Marr, N.J., Sabir, H., 1997. The evaporation coefficient of water: a review. *International Journal Heat and Mass Transfer* 40, 2963–2973.
- El-Dessouky, H., Ettouney, H., Al-Juwayhel, H., AL-Fulaij, F., 2004. Analysis of multistage flash - desalination flashing chambers. *ICChem- Chemical Engineering Research and Design* 82, 967–978.
- Elustondo, D., Elustondo, M.P., Urbicain, M.J., 2001. Mathematical modeling of moisture evaporation from foodstuffs exposed to subatmospheric pressure superheated steam. *Journal of Food Engineering* 49, 15–24.
- Elustondo, D., Elustondo, M.P., Urbicain, M.J., 2002. Drying with superheated steam: maximum drying rate as a linear function of pressure. *Chemical Engineering Journal* 86, 69–74.
- Erbil, H.Y., 2012. Evaporation of pure liquid sessile and spherical suspended drops: a review. *Advances in colloid and interface science* 170, 67–86.
- Fang, C., Peng, X.F., Yang, Z., 2004. Vapor Phase Transport of two-phase flow in porous media, in: Department of Thermal Engineering, T.U. (Ed.), ICAPM2004, Évora, Portugal.

- Figueiredo, A.R., Costa, J.J., 2004. Experimental analysis of the use of wet porous media for thermal protection against high intensity heat fluxes. *International Journal of Heat and Mass Transfer* 47, 11–19.
- Gude, V.G., Nirmalakhandan, N., 2009. Desalination at low temperatures and low pressures. *Desalination* 244, 239–247.
- Hahne, E., Barthau, G., 2000. Evaporation waves in flashing processes. *International Journal of Multiphase flow* 26, 531–547.
- He, S.-Y., Li, Y.-F., 2003. Theoretical simulation of vacuum cooling of spherical foods. *Applied Thermal Engineering* 23, 1489–1501.
- Houska, M., Podloucký, S., Zitný, R., Grée, R., Sesták, J., Dostal, M., Burfoot, D., 1996. Mathematical Model of the Vacuum Cooling of Liquids. *Journal of Food Engineering* 29, 339–348.
- Houska, M., Sun, D.-W., Landfeld, a., Zhang, Z., 2003. Experimental study of vacuum cooling of cooked beef in soup. *Journal of Food Engineering* 59, 105–110.
- Huang, M., Lai, F.C., 2010. Numerical study of EHD-enhanced water evaporation. *Journal of Electrostatics* 68, 364–370.
- Iguedjal, T., Louka, N., Allaf, K., 2008. Sorption isotherms of potato slices dried and texturized by controlled sudden decompression. *Journal of Food Engineering* 85, 180–190.
- Ikegami, Y., Sasaki, H., Gouda, T., Uehara, H., 2006. Experimental study on a spray flash desalination (influence of the direction of injection). *Desalination* 194, 81–89.
- Incropera, F.P., Dewitt, D.P., Bergman, T.L., Lavine, A.S., 2007. *Fundamentals of heat and mass transfer*, 6th ed. John Wiley & Sons, USA.
- Jin, T.X., 2007. Experimental investigation of the temperature variation in the vacuum chamber during vacuum cooling. *Journal of Food Engineering* 78, 333–339.
- Jin, T.X., Xu, L., 2006a. Numerical study on the performance of vacuum cooler and evaporation-boiling phenomena during vacuum cooling of cooked meat. *Energy Conversion and Management* 47, 1830-1842.
- Jin, T.X., Xu, L., 2006b. Development and validation of moisture movement model for vacuum cooling of cooked meat. *Journal of Food Engineering* 75, 333-339.
- Jo, H., Ahn, H.S., Kang, S., Kim, M.H., 2011. A study of nucleate boiling heat transfer on hydrophilic, hydrophobic and heterogeneous wetting surfaces. *International Journal of Heat and Mass Transfer* 54, 5643-5652.
- Jugjai, S., Polmart, N., 2003. Enhancement of evaporation and combustion of liquid fuels through porous media. *Experimental Thermal and Fluid Science* 27, 901-909.

- Kamal, I.M., Sobolik, V., Kristiawan, M., Mounir, S.M., Allaf, K., 2008. Structure expansion of green coffee beans using instantaneous controlled pressure drop process. *Innovative Food Science & Emerging Technologies* 9, 534-541.
- Kim, J., Huh, C., Kim, M.H., 2007. On the growth behavior of bubbles during saturated nucleate pool boiling at sub-atmospheric pressure. *International Journal of Heat and Mass Transfer* 50, 3695–3699.
- Kingcam, R., Devahastin, S., Chiewchan, N., 2008. Effect of starch retrogradation on texture of potato chips produced by low-pressure superheated steam drying. *Journal of Food Engineering* 89, 72–79.
- Klein, S.A., 2004. *Engineering Equation Solver (EES)*. F-Chart Software, Madison.
- Kristiawan, M., Sobolik, V., Al-Haddad, M., Allaf, K., 2008. Effect of pressure-drop rate on the isolation of cananga oil using instantaneous controlled pressure-drop process. *Chemical Engineering and Processing: Process Intensification* 47, 66–75.
- Kristiawan, M., Sobolik, V., Klíma, L., Allaf, K., 2011. Effect of expansion by instantaneous controlled pressure drop on dielectric properties of fruits and vegetables. *Journal of Food Engineering* 102, 361–368.
- Lai, F.C., Huang, M., Wong, D.S., 2004. EHD-Enhanced Water Evaporation. *Drying Technology* 22, 597–608.
- Li, C.H., Li, T., Hodgins, P., Hunter, C.N., Voevodin, A. a., Jones, J.G., Peterson, G.P., 2011. Comparison study of liquid replenishing impacts on critical heat flux and heat transfer coefficient of nucleate pool boiling on multiscale modulated porous structures. *International Journal of Heat and Mass Transfer* 54, 3146–3155.
- Li, X.-W., Zhang, X.-S., Quan, S., 2012. Evaporative supercooling method for ice production. *Applied Thermal Engineering* 37, 120–128.
- Liar, N., Chunga, R., Miyatakeb, O., 2002. Correlations (updated) for predicting the flow through MSF plant interstage orifices. *Desalination* 151, 209–216.
- Louka, N., Allaf, K., 2002. New Process for Texturizing Partially Dehydrated Biological Products Using Controlled Sudden Decompression to the Vacuum : Application on Potatoes. *Journal of Food Science* 67, 3033–3038.
- Louka, N., Allaf, K., 2004. Expansion ratio and color improvement of dried vegetables texturized by a new process “Controlled Sudden Decompression to the vacuum” Application to potatoes, carrots and onions. *Journal of Food Engineering* 65, 233–243.
- Mantle, M., Reis, N., Griffiths, R., Gladden, L., 2003. MRI studies of the evaporation of a single liquid droplet from porous surfaces. *Magnetic Resonance Imaging* 21, 293–297.

- Marco, P. Di, Grassi, W., Energetica, D., Pisa, U., 2000. Pool boiling in microgravity: assessed results and open issues, in: ETS (Ed.), Proceedings of the Third European Thermal-Sciences Conference. Pisa, Italy, 81–90.
- Maritza, A.-M., Sabah, M., Anaberta, C.-M., Montejano-Gaitán, J.G., Allaf, K., 2012. Comparative Study of Various Drying Processes at Physical and Chemical Properties of Strawberries (*Fragaria var. camarosa*). *Procedia Engineering* 42, 267–282.
- Mc Donald, K., Sun, D., 2001a. Effect of evacuation rate on the vacuum cooling process of a cooked beef product. *Journal of Food Engineering* 48, 195–202.
- Mc Donald, K., Sun, D.-W., 2000. Vacuum cooling technology for the food processing industry: a review. *Journal of Food Engineering* 45, 55–65.
- Mc Donald, K., Sun, D.-W., 2001b. The formation of pores and their effects in a cooked beef product on efficiency of vacuum cooling. *Journal of Food Engineering* 47, 175–183.
- Mc Donald, K., Sun, D.-W., Lyng, J.G., 2002. Effect of vacuum cooling on the thermophysical properties of a cooked beef product. *Journal of Food Engineering* 52, 167–176.
- McDonald, K., Sun, D.-W., Kenny, T., 2001. The effect of injection level on the quality of a rapid vacuum cooled beef product. *Journal of Food Engineering* 47, 139–147.
- Meng, Q., Hu, W., 2005. Roof cooling effect with humid porous medium. *Energy and Buildings* 37, 1–9.
- Mills, A.F., 1995. *Heat and Mass Transfer*. IRWIN, Eds., Los Angeles.
- Miyatake, O., Koito, Y., Tagawa, K., Maruta, Y., 2001. Transient characteristics and performance of a novel desalination system based on heat storage and spray flashing. *Desalination* 137, 157–166.
- Miyatake, O., Tagawa, K., 2001. Numerical and experimental analyses for RO desalination systems using a static pressure head. *Desalination* 136, 233–242.
- Miyatake, O., Tomimura, T., Ide, Y., Yuda, M., Fujii, T., 1981. Effect of liquid temperature on spray flash evaporation. *Desalination* 37, 351–366.
- Miyatake, O., Hashimoto, T., Li, N., 1993. The relationship between flow pattern and thermal non-equilibrium in the multi-stage flash evaporation process. *Desalination* 91, Pages 51–64.
- Mutair, S., Ikegami, Y., 2009. Experimental study on flash evaporation from superheated water jets: Influencing factors and formulation of correlation. *International Journal of Heat and Mass Transfer* 52, 5643–5651.

- Mutair, S., Ikegami, Y., 2010. Experimental investigation on the characteristics of flash evaporation from superheated water jets for desalination. *Desalination* 251, 103–111.
- Mutair, S., Ikegami, Y., 2012. On the evaporation of superheated water drops formed by flashing of liquid jets. *International Journal of Thermal Sciences* 57, 37–44.
- Muthunayagam, A.E., Ramamurthi, K., Paden, J.R., 2005a. Modelling and experiments on vaporization of saline water at low temperatures and reduced pressures. *Applied Thermal Engineering* 25, 941–952.
- Muthunayagam, A.E., Ramamurthi, K., Paden, J.R., 2005b. Low temperature flash vaporization for desalination. *Desalination* 180, 25–32.
- Nam, Y., Aktinol, E., Dhir, V.K., Ju, Y.S., 2011. Single bubble dynamics on a superhydrophilic surface with artificial nucleation sites. *International Journal of Heat and Mass Transfer* 54, 1572–1577.
- Nimmol, C., Devahastin, S., Swasdisevi, T., Soponronnarit, S., 2007a. Drying of banana slices using combined low-pressure superheated steam and far-infrared radiation. *Journal of Food Engineering* 81, 624–633.
- Nimmol, C., Devahastin, S., Swasdisevi, T., Soponronnarit, S., 2007b. Drying and heat transfer behavior of banana undergoing combined low-pressure superheated steam and far-infrared radiation drying. *Applied Thermal Engineering* 27, 2483–2494.
- Nutter, D.W., O'Neal, D.L., 1997. Experimental investigation of steel spheres as a passive enhancement technique for flash boiling of HCFC-22. *Experimental Thermal and Fluid Science* 15, 336–346.
- Miyatake, O., Hashimoto, T., H., 1992. The liquid flow in multi-stage flash evaporators. *International Journal of Heat and Mass Transfer* 35, Pages 3245–3257.
- Miyatake, O., 1994. Comparative study of flash evaporation rates. *Desalination Volume* 96, 163–171.
- Ozturk, H.M., Ozturk, H.K., 2009. Effect of pressure on the vacuum cooling of iceberg lettuce. *International Journal of Refrigeration* 32, 402–410.
- P. Brat, Olle, D., Reynes, M., Cogat, P.-O., Brillouet, J.-M., 2001. Preparation of Passion Fruit Puree by Flash Vacuum-Expansion. *Journal of Food Science* 66, 542–547.
- Paranjpe, S.S., Ferruzzi, M., Morgan, M.T., 2012. Effect of a flash vacuum expansion process on grape juice yield and quality. *LWT - Food Science and Technology* 48, 147–155.
- Peng, X.F., Wang, Z., Lee, D.J., 2002. Dynamic behavior of bubble interface during boiling. *Journal of Thermal Science* 11, 308–319.

- Phan, H.T., Caney, N., Marty, P., Colasson, S., Gavillet, J., 2009. Surface wettability control by nanocoating: The effects on pool boiling heat transfer and nucleation mechanism. *International Journal of Heat and Mass Transfer* 52, 5459–5471.
- Pimpaporn, P., Devahastin, S., Chiewchan, N., 2007a. Effects of combined pretreatments on drying kinetics and quality of potato chips undergoing low-pressure superheated steam drying. *Journal of Food Engineering* 81, 318–329.
- Pimpaporn, P., Devahastin, S., Chiewchan, N., 2007b. Effects of combined pretreatments on drying kinetics and quality of potato chips undergoing low-pressure superheated steam drying. *Journal of Food Engineering* 81 81, 318–329.
- Poling, B.E., Prausnitz, J.M., O'Connell, J.P., 2001. *The properties of gases and liquids*, 5th ed. New York;
- Prat, M., 1998. Discrete models of liquid-vapour phase change phenomena in porous media. *Revue générale de thermique* 954–961.
- Quick, C., Ritzinger, D., Lehnert, W., Hartnig, C., 2009. Characterization of water transport in gas diffusion media. *Journal of Power Sources* 190, 110–120.
- Rezzoug, S. a., Boutekedjiret, C., Allaf, K., 2005. Optimization of operating conditions of rosemary essential oil extraction by a fast controlled pressure drop process using response surface methodology. *Journal of Food Engineering* 71, 9–17.
- Rops, C.M., Lindken, R., Velthuis, J.F.M., Westerweel, J., 2009. Enhanced heat transfer in confined pool boiling. *International Journal of Heat and Fluid Flow* 30, 751–760.
- Sanya, E.A., Rezzoug, S., Allaf, K., 2003. A new method for drying waterlogged wooden artefacts: comparison of cyclical prssure drops with conventional methods. *Trans IChemE* 81, 0–6.
- Saury, D., Harmand, S., Siroux, M., 2002. Experimental study of flash evaporation of a water film. *International Journal of Heat and Mass Transfer* 45, 3447–3457.
- Saury, D., Harmand, S., Siroux, M., 2005. Flash evaporation from a water pool: Influence of the liquid height and of the depressurization rate. *International Journal of Thermal Sciences* 44, 953–965.
- Sebastian, P., Nadeau, J.P., 2002. Experiments and modeling of falling jet flash evaporators for vintage treatment. *International Journal of Thermal Sciences* 41, 269–280.
- Sebastian, P., Quirante, T., Tiat, V.H.K., Ledoux, Y., 2010. Multi-objective optimization of the design of two-stage flash evaporators: Part 2. Multi-objective optimization. *International Journal of Thermal Sciences* 49, 2459–2466.
- Stralen, S.J.D.V., Cole, R., Sluyter, W.M., Sohalt, M.S., 1975. Bubble growth rates in nucleation boiling of water at subatmospheric pressures. *International Journal of Heat and Mass Transfer* 18, 655–669.

- Sulfredge, C.D., Tagavi, K. a., Chow, L.C., 1996. Homogeneous nucleation of vapor by depressurization at constant volume. *International Journal of Heat and Mass Transfer* 39, 235–246.
- Sun, D., Hu, Z., 2003. CFD simulation of coupled heat and mass transfer through porous foods during vacuum cooling process. *International Journal of Refrigeration* 26, 19–27.
- Sun, D.-W., Wang, L., 2004. Experimental investigation of performance of vacuum cooling for commercial large cooked meat joints. *Journal of Food Engineering* 61, 527–532.
- Sun, D.-W., Zheng, L., 2006. Vacuum cooling technology for the agri-food industry: Past, present and future. *Journal of Food Engineering* 77, 203–214.
- Swasdisevi, T., Devahastin, S., Sa-Adchom, P., Soponronnarit, S., 2009. Mathematical modeling of combined far-infrared and vacuum drying banana slice. *Journal of Food Engineering* 92, 100–106.
- Tatemoto, Y., Tsunekawa, M., Yano, S., Takeshita, T., Noda, K., 2007. Drying characteristics of porous material immersed in a bed of hygroscopic porous particles fluidized under reduced pressure. *Chemical Engineering Science* 62, 2187–2197.
- Tatemoto, Y., Yano, S., Mawatari, Y., Noda, K., Komatsu, N., 2007. Drying characteristics of porous material immersed in a bed of glass beads fluidized by superheated steam under reduced pressure. *Chemical Engineering Science* 62, 471–480.
- Tiat, V.H.K., Sebastian, P., Nadeau, J.-P., 2008. Multicriteria-oriented preliminary design of a flash evaporation process for cooling in the wine-making process. *Journal of Food Engineering* 85, 491–508.
- Tiat, V.H.K., Sebastian, P., Quirante, T., 2010. Multiobjective optimization of the design of two-stage flash evaporators: Part 1. Process modeling. *International Journal of Thermal Sciences* 49, 2453–2458.
- Udell, K.S., 1983. Heat Transfer in Porous Media Heated From Above With Evaporation , Condensation , and Capillary Effects. *Journal of Heat Transfer* 105, 485–492.
- Wang, F., Peng, X.F., 2004. Pool boiling on a porous wire:Effect of pore size on bubble nucleation and dynamics, in: Department of Thermal Engineering, T.U. (Ed.), ICAPM2004, Évora, Portugal, pp. 279–284.
- Wang, J., Catton, I., 2001. Enhanced evaporation heat transfer in triangular grooves covered with a thin fine porous layer. *Applied Thermal Engineering* 21, 1721–1737.

- Wang, L., Sun, D., 2002a. Modelling vacuum cooling process of cooked meat - part 1 : analysis of vacuum cooling system. *International Journal of Refrigeration* 25, 854-861.
- Wang, L., Sun, D., 2002b. Modelling vacuum cooling process of cooked meat - part 2 : mass and heat transfer of cooked meat under vacuum pressure. *International Journal of Refrigeration* 25, 862–871.
- Wang, L., Sun, D., 2002c. Evaluation of performance of slow air ,air blast and water immersion cooling methods in the cooked meat industry by the finite element method. *Journal of Food Engineering* 51, 329–340.
- Wang, L., Sun, D.-W., 2004. Effect of operating conditions of a vacuum cooler on cooling performance for large cooked meat joints. *Journal of Food Engineering* 61, 231–240.
- Wang, Z., Peng, X.F., Ochterbeck, J.M., 2004. Dynamic bubble behavior during boiling in bead-packed structures. *International Journal of Heat and Mass Transfer* 47, 4771–4783.
- Webb, R.L., Kim, N.-H., 2005. *Principles of Enhanced Heat Transfer*, 2<sup>nd</sup> edition; ed. New York;
- Wen, D., Wang, B., 2002. Effects of surface wettability on nucleate pool boiling heat transfer for surfactant solutions. *International Journal of Heat and Mass Transfer* 45, 1739–1747.
- Yortsos, Y.C., Stubos, A.K., 2001. Phase change in porous media. *Current Opinion in Colloid & Interface Science* 6, 208–216.
- Zhang, J., Wang, B.X., Peng, X.F., 2001. Thermodynamic aspect of the shift of concave liquid-vapor interfacial phase equilibrium temperature and its effect on bubble formation. *International Journal of Heat and Mass Transfer* 44, 1681–1686.
- Zhang, L., Shoji, M., 2003. Nucleation site interaction in pool boiling on the artificial surface. *International Journal of Heat and Mass Transfer* 46, 513–522.
- Zhang, Z., Drummond, L., Sun, D.-W., 2013. Vacuum cooling in bulk of beef pieces of different sizes and shape – Evaluation and comparison to conventional cooling methods. *Journal of Food Engineering* 116, 581–587.
- Zhao, X., Liu, S., Riffat, S.B., 2008. Comparative study of heat and mass exchanging materials for indirect evaporative cooling systems. *Building and Environment* 43, 1902–1911.
- Zheng, L., Sun, D.-W., 2004. Vacuum cooling for the food industry—a review of recent research advances. *Trends in Food Science & Technology* 15, 555–568.
- Zotarelli, M.F., Porciuncula, B.D.A., Laurindo, J.B., 2012. A convective multi-flash drying process for producing dehydrated crispy fruits. *Journal of Food Engineering* 108, 523–531.